

An Ionospheric Mode Detection Sounder for
H.F. Data Communications

by

Peter Langdale Hayhurst

being a dissertation submitted to the Faculty of
Science, University of Leicester, in candidature
for the Degree of Philosophiae Doctor.

Department of Physics,
University of Leicester.
April, 1982.

UMI Number: U328106

All rights reserved

INFORMATION TO ALL USERS

The quality of this reproduction is dependent upon the quality of the copy submitted.

In the unlikely event that the author did not send a complete manuscript and there are missing pages, these will be noted. Also, if material had to be removed, a note will indicate the deletion.



UMI U328106

Published by ProQuest LLC 2015. Copyright in the Dissertation held by the Author.
Microform Edition © ProQuest LLC.

All rights reserved. This work is protected against
unauthorized copying under Title 17, United States Code.



ProQuest LLC
789 East Eisenhower Parkway
P.O. Box 1346
Ann Arbor, MI 48106-1346



THESIS
655416
30.11.82

x752931058

Acknowledgements

Firstly, I would like to thank Professor J.L. Beeby for the opportunity of working in the Physics Department of the University of Leicester.

I am particularly grateful to Dr B. Burgess and his staff, of the Royal Aircraft Establishment, Farnborough, for their support and interest. I would also like to thank the ionospheric physics technicians for their assistance in constructing equipment, and Mr M. Warrington for his help. I would especially like to thank my fiancée for her support and encouragement during the preparation of this thesis.

I would like to acknowledge the receipt of an S.R.C C.A.S.E. studentship for three years, and support from R.A.E. Farnborough for the loan of Equipment and for arranging field sites.

Finally I would like to thank Professor T.B. Jones for his constant guidance and helpful advice throughout the progress of the work.

CONTENTS

1	INTRODUCTION	1
1.1	The Ionosphere	1
1.2	Ionospheric Radio Propagation	14
1.3	Digital Communications	18
1.4	An Introduction to the Present Investigation	20
2	PREVIOUS WORK	26
2.1	HF Propagation	26
2.1.1	Predictions	26
2.1.2	Absorption	31
2.1.3	Radio Noise	31
2.1.4	Ionospheric Dispersion	32
2.1.5	Multipath Propagation	32
2.2	Ionospheric Sounding	34
2.2.1	Pulse Sounding	36
2.2.2	Oblique Pulse Sounding	38
2.2.3	Chirp Sounding	40
2.2.4	Backscatter	40
2.2.5	HF Doppler	43
2.2.6	Sounding in HF Communications	45
2.2.7	Pilot Tone	46
2.2.8	The Fadeogram	46
2.2.9	Performance Sensing and Channel Estimation	49
2.3	Data Communications	51
2.3.1	Frequency Selection	53
2.3.2	Diversity Operation	53

2.3.3 Adaptive Multipath Measurement	56
2.3.4 Steerable Antennas	61
2.3.5 Modulation Types	63
2.3.6 Soft Decisions	66
2.3.7 Coding	66
2.4 Conclusions	69
3 OUTLINE OF THE PRESENT INVESTIGATION	70
3.1 Pulse Sounding Format	70
3.2 Data Sounding Format	73
3.3 System Calibration	81
3.4 Development of the Experiment	86
4 EQUIPMENT	93
4.1 Hardware Overview	93
4.2 Programmable Sounder	94
4.3 Radio Transmitter	96
4.4 Radio Receiver	98
4.5 Simulator Hardware	102
4.6 Amplitude Detector	112
4.7 Phase Detector	112
4.8 FSK Detector	116
4.9 Analogue to Digital Converter	116
4.10 Project Computer	119
4.11 System Reliability	125
5 PROJECT SOFTWARE	128
5.0 Program Overview	128

5.1	Programmable Sounder	129
5.2	Receiver Control	134
5.3	Pulse Detection	135
5.4	Pseudo Random Data Detection	140
5.5	Data Logging	144
5.6	Data Dumping	147
5.7	Data Analysis	149
5.7.1	A Format	149
5.7.2	M Format	149
5.7.3	B Format	154
5.7.4	R Format	154
5.8	Summary	160
6	PULSE EXPERIMENTS	162
6.1	Ionospheric Models	162
6.2	Experimental Results	171
6.3	Rapid Mode Changes	181
6.4	Noise and Interference	186
6.5	Averaging Effects	191
6.6	Auroral Propagation	196
6.7	Computer Analysis	204
6.8	Summary	213
7	EVALUATION OF ERROR RATES	216
7.0	Introduction	216
7.1	Data Presentation	216
7.2	Results	222
7.2.1	Low Noise Conditions	223

7.2.2	Noisy Conditions	226
7.2.3	Timing Faults	231
7.2.4	Bandwidth Effects	231
7.2.5	Fading	234
7.2.6	Interference	238
7.3	The Effect of Ionospheric Propagation on PRS Data	245
7.3.1	Data Rate	247
7.3.2	Noise	250
7.3.3	Bandwidth	250
7.3.4	Fading	253
7.3.5	Time Stability	256
7.4	Pulse Sounding Predictions - PRS Data Correlation	261
8	SUMMARY AND CONCLUSIONS	271
8.1	Summary of the System Developed	271
8.2	Pulse Experiment, Conclusions	272
8.3	Data Experiment, Conclusions	274
8.4	Future Work	275
8.4.1	Practical Implementation	275
8.4.2	Develop Predictions	279
8.4.3	Pseudo Error	280
8.4.4	Range Finding	280
8.4.5	Phase	281

CHAPTER 1

INTRODUCTION

1.1 THE IONOSPHERE

The earth is surrounded by a layer of gas called the atmosphere, which can be sub- divided into layers by criteria based on composition ,temperature and ionisation.

At ground level the atmosphere is composed of molecules of Nitrogen (78%), Oxygen (21%) and smaller quantities of other constituents (Ar, He, CO₂, H₂O). Up to a height of about 100Km, these gases are constantly mixed by turbulence but above this height, the constitution changes under the influence of diffusive processes. This means the lighter atoms such as Hydrogen and Helium form a relatively larger proportion of the atmosphere as height increases (fig 1.1.1).

In terms of temperature the atmosphere is divided into five sub- layers as indicated in fig 1.1.2. The troposphere (0-10Km) contains a relatively large number of molecules such as H₂O and CO₂ which absorb and emit infra- red radiation. This leads to a decrease in temperature with height as the proportion of such large molecules decreases. The stratosphere (10-50Km) has an almost constant temperature of 220 degrees K over its height range. The Mesosphere (50-85Km) contains a greater proportion of ozone which absorbs a certain type of ultra- violet (UV) radiation leading to a heating of this

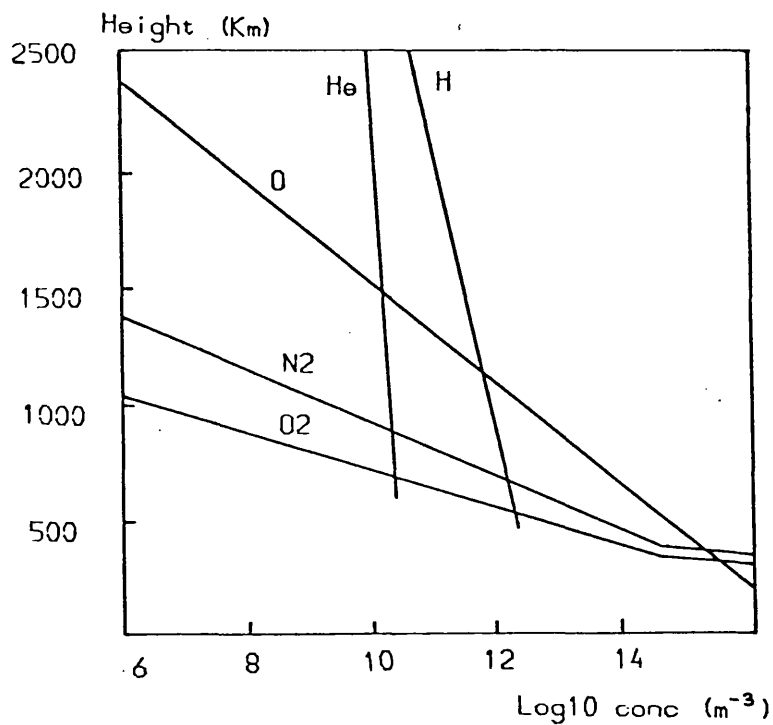


Fig 1.1.1 Atmospheric Composition
Day Time, Medium Sunspot No (C.I.R.A 1965)

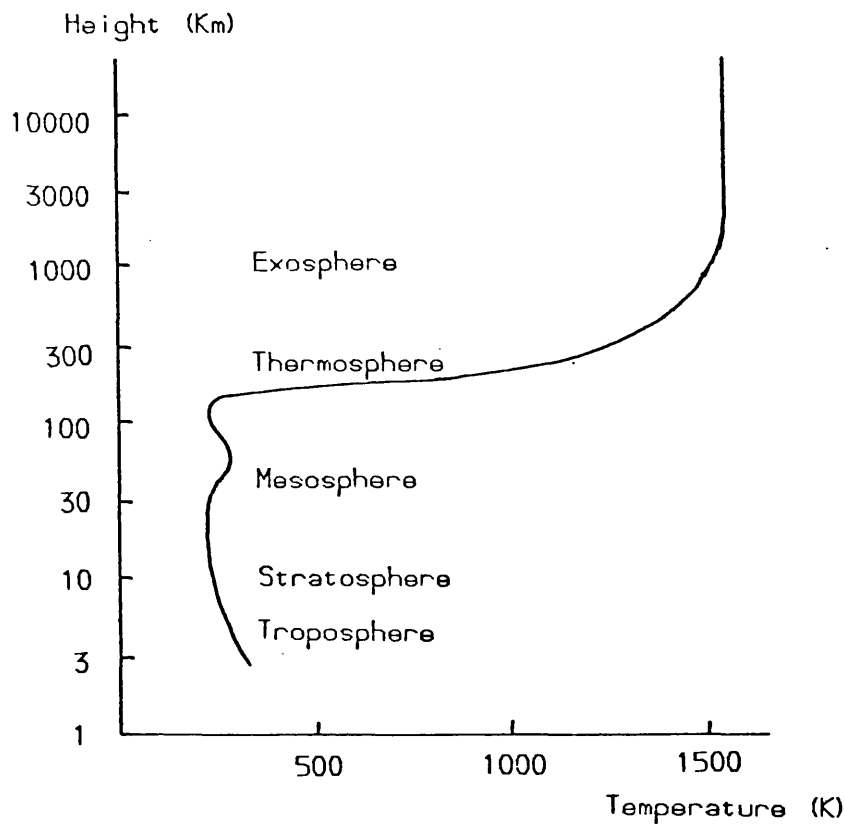
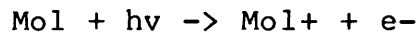


Fig 1.1.2 Atmospheric Variations of Temperature
(U.S. Standard Atmosphere)

region. The temperature in the thermosphere (90-300Km) increases with height due to the absorption of shorter wavelength UV solar radiation. Finally in the exosphere (1000-6000Km) the gas density is very low, therefore the thermal conductivity is very high and the temperature remains at an approximately constant value. Where ions are present in the atmosphere the neutral, ion and electron temperatures (T_n , T_i and T_e) are similar at night, but during the day T_e increases faster than T_i or T_n .

Ionisation occurs when an energetic photon from the sun collides with a neutral gas molecule.



The inverse process of recombination or electron loss also occurs. A state of equilibrium will be established when the rate of production equals the rate of loss. The changes in electron density (N_e) can be written :-

$$dN_e/dt = \text{production rate} - \text{loss rate}$$

In terms of ionisation the atmosphere is divided into three regions (fig 1.1.3). The ionosphere (50-1000Km) is the region where most of the effects on radio wave propagation due to the ionisation are noticed. Above this region is the magnetosphere where only VLF effects can be seen (eg whistlers) and below, the neutral ionosphere.

When an electromagnetic wave enters the ionosphere the electrons and ions are displaced by the oscillating electric field of the wave. The electron displacement is much greater than that of the ions as a consequence of the electron mass being about $1/2000$ of the ion mass. The equation of motion for

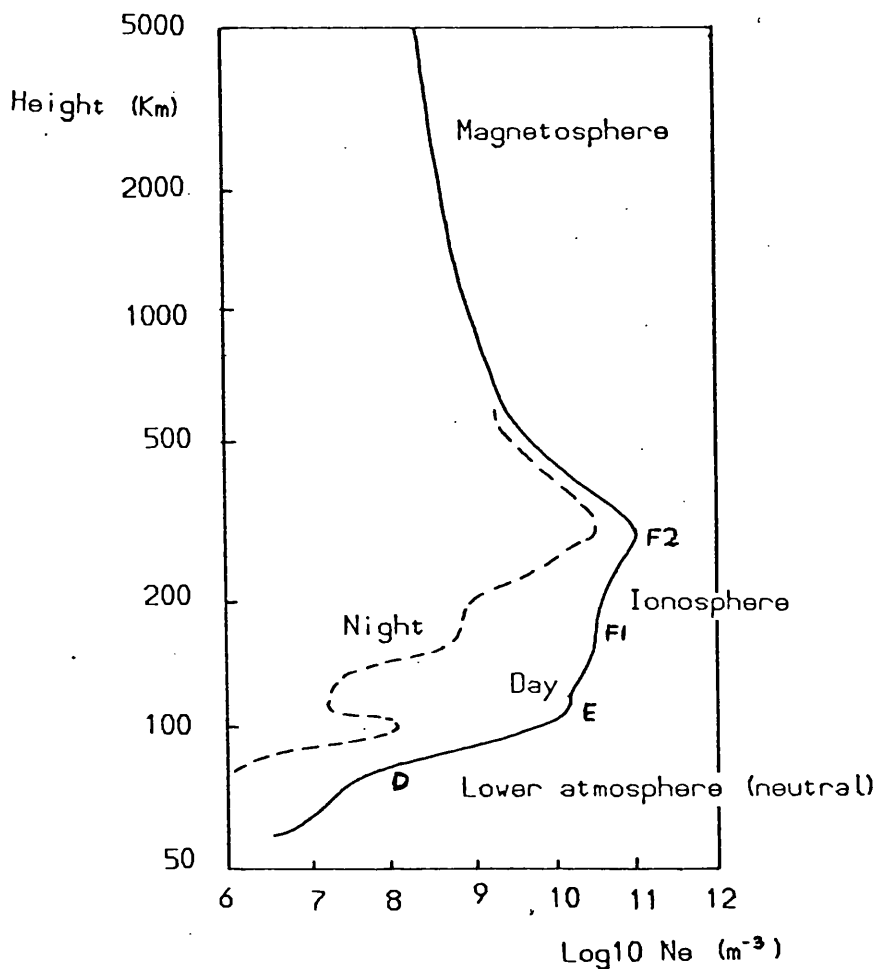


Fig 1.1.3 Ionospheric Electron Density Profile
(VanZandt - Knecht 1964 chap 6)

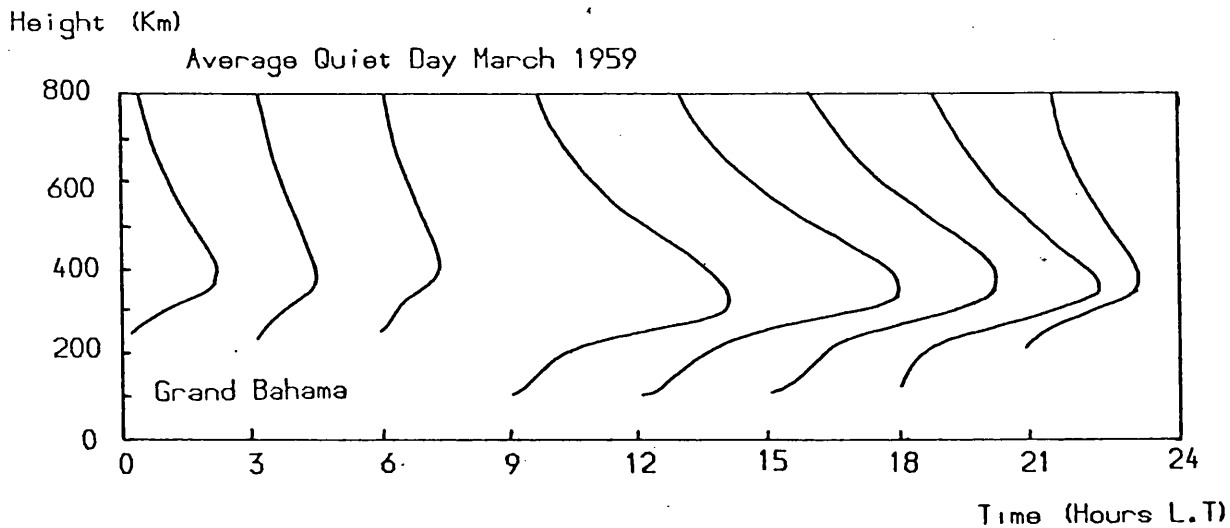


Fig 1.1.4 Diurnal Changes in Ionospheric Profiles
(after J.W. Wright, unpublished)

the electrons can be derived, and the displacement vector calculated as a function of the polarisability of the medium and the electric field strength of the wave. This leads to the definition of an equivalent dielectric constant for the ionosphere.

An expression for the refractive index of the medium for electromagnetic waves can be derived from Maxwells equations and the dielectric constant. The relationship between the refractive index and the wave frequency is known as the dispersion equation.

$$n^2 = 1 - (N e^2 / (\epsilon_0 m (2 \pi f)^2)) \quad -(1)$$

where n = refractive index

N = electron density

ϵ_0 = dielectric constant

m = electron mass

e = electron charge

f = radio wave frequency

For the radio wave to be reflected from the ionosphere the refractive index must go to zero. For this to occur :-

$$N = \epsilon_0 m (2 \pi f)^2 / e^2 \quad -(2)$$

$$\Rightarrow N_{\max} \propto f_p^2$$

where f_p = the plasma frequency

The highest frequency that an ionospheric layer can reflect, is obtained by writing the maximum value of the electron density of the layer (N_{\max}) into equation 2. If the radio wave is incident on the ionised layer at an angle (i) to the vertical, the dispersion equation modifies to :-

$$N = (\epsilon_0 4 \pi^2 m f^2 \cos^2(i)) / e^2 \quad -(3)$$

This shows that a given ionospheric layer can reflect larger frequencies at oblique incidences than at vertical incidence (Martyns theorem 1935).

Several other effects are important when considering the reflection of radio waves by the ionosphere. Firstly, over an oblique ionospheric path through any ionospheric layer there are two different angles of elevation from the transmitter which result in the signal reaching the receiver. These are known as the low angle ray and the high angle or Pederson ray respectively (Davies 1965, p195).

Secondly the motion of the oscillating ions and electrons will be damped by collisions with other particles. If n is close to unity this results in non deviative absorption.

$$K = (e^2 N v) / (2 \epsilon_0 m c \omega^2) \quad -(4)$$

where K = absorption coefficient

v = collision frequency

ω = angular frequency

If absorption is considered near to the reflection point where n is small the result is "deviative" absorption.

$$K = (v / 2 c) ((1 / n) - n) \quad -(5)$$

Both processes contribute to the attenuation of the wave reflected in the ionosphere.

The presence of the earths magnetic field causes the ionosphere to become anisotropic and two possible solutions are obtained for the refractive index.

$$n^2 = 1 - (N e^2 / (\epsilon_0 m (\omega \pm \omega_H)^2)) \quad -(6)$$

where ω_H = the gyro frequency = $e B / m$

Thus the ionosphere is birefractive and therefore two

distinct reflection conditions exist for the two ray paths, each having different polarisations. These two modes of propagation are referred to as the O (ordinary) and the X (extraordinary) modes respectively. In the northern hemisphere the X mode produces the greatest electron displacement and is therefore more strongly attenuated than the O mode.

The ionosphere is divided into three layers (fig 1.1.3) referred to as the D, E and F regions. The lowest of the three is the D layer which exists between 60 and 95 Km. Ne is of the order 10^{10} cm^{-3} and the collision frequency is in the order of 10^6 Hz. Therefore the layer is a strong absorber of electromagnetic waves and is only capable of reflecting low frequencies (i.e. $< 300\text{KHz}$). Since the layer recombines completely at night, more absorption occurs during the day than at night.

The E region extends from approximately 95 to 120Km. Ne is approximately 10^{11} cm^{-3} and the collision frequency is between 10^4 and 10^5 Hz. Under normal conditions the layer can reflect vertically incident waves in the frequency range 1.5 - 3.5 MHz. The layer has a strong solar dependence since it is produced by UV radiation. Under unusual conditions this layer develops into the so called sporadic E (Es) layer. This is a thin layer of intense ionisation embedded in the usual E layer. The Es electron density can exceed that of the normal E layer by a factor of four or more. The Es is able to reflect frequencies up to 50MHz at oblique incidence. The creation of this layer is intermittent and is related to the presence of strong wind shears which can exist at these heights in the atmosphere.

The highest layer of the ionosphere is the F layer (150-1000Km). This subdivides into the F1 and F2 layers in the summer. The F1 layer like the E layer, occurs only during the day and has a strong solar dependence. It exists between 150 and 250 Km and its behaviour can be quite accurately predicted as a result of this dependence.

The F2 layer is the most important layer from the point of view of HF propagation since it can support frequencies of up to 30MHz at oblique incidence. Unfortunately, this layer also displays the most anomalous behaviour which is difficult to predict.

Examples of the diurnal variation of the F2 layer are presented in fig 1.1.4. The electron density peak of the layer forms quickly after dawn decreasing gradually after dusk. The slow loss of ionisation after sunset is believed to result from the upward movement of the hot day- time plasma. The lower loss rate at these higher levels provides an effective store of ionisation during the night when no photo production takes place. Another factor influencing the maintenance of the F region at night is that winds in the neutral atmosphere cause the ionospheric plasma to move up the field lines in the evening so reducing the loss process. From fig 1.1.5 it is clear that the diurnal variation in the F2 peak is more pronounced in the winter months. This seasonal variation is due to the increased proportion of atomic oxygen in the atmosphere at this time which increases the rate at which ions are produced. Also the lower winter temperatures have a marked effect in slowing down one stage in the recombination process.

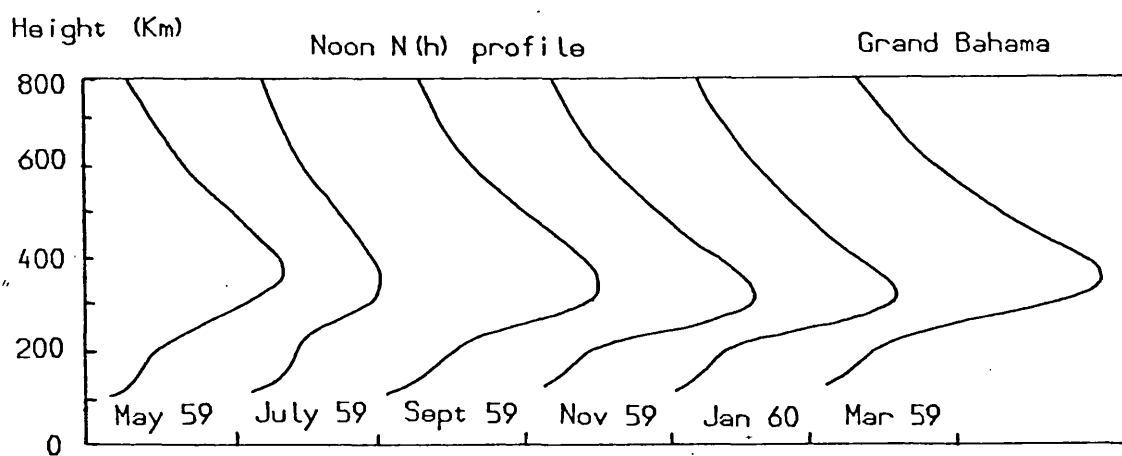
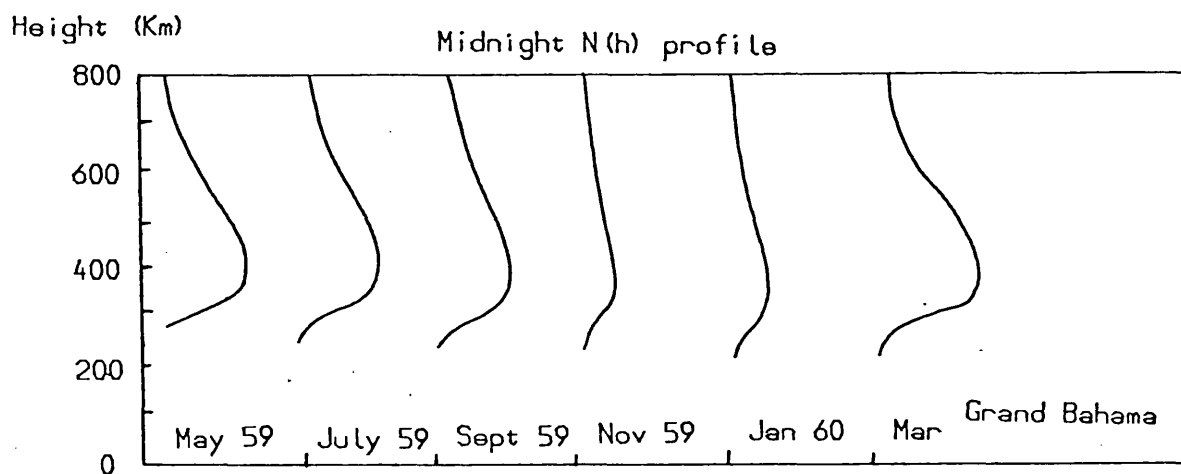


Fig 1.1.5 Seasonal Changes in Electron Density Profile
(after J.W. Wright, unpublished)

Both the diurnal and seasonal variations are apparent in the behaviour of FoF2 in fig 1.1.6.

The dependence of the F2 layer on the level of solar activity as indicated by the sunspot number is demonstrated in fig 1.1.7. An eight fold change in the maximum electron density occurs over the eleven year solar cycle. As before, the summer months exhibit a reduced level of F2 ionisation. Since electron density and critical frequency are related the solar cycle trend is repeated in fig 1.1.8.

During ionospheric storms the F2 layer electron density decreases while the D and E layer electron densities increase. The cause of this anomalous effect is believed to be an increase in the amount of molecular oxygen at F region heights which aids recombination hence decreasing the electron density and hence the critical frequency.

In addition to the critical frequency changes, the ionisation distribution can become disturbed and localised reflecting regions produced. When a radio pulse is reflected from this disturbed F layer, echos are returned from a wide range of apparent heights and hence the F layer is said to be "spread". The spread F layer can produce considerable disturbance in HF signals reflected during this condition. The occurrence of spread F seems fairly random but is most likely to occur at night or during the early evening in the summer months at low latitudes and in the winter months at high latitudes.

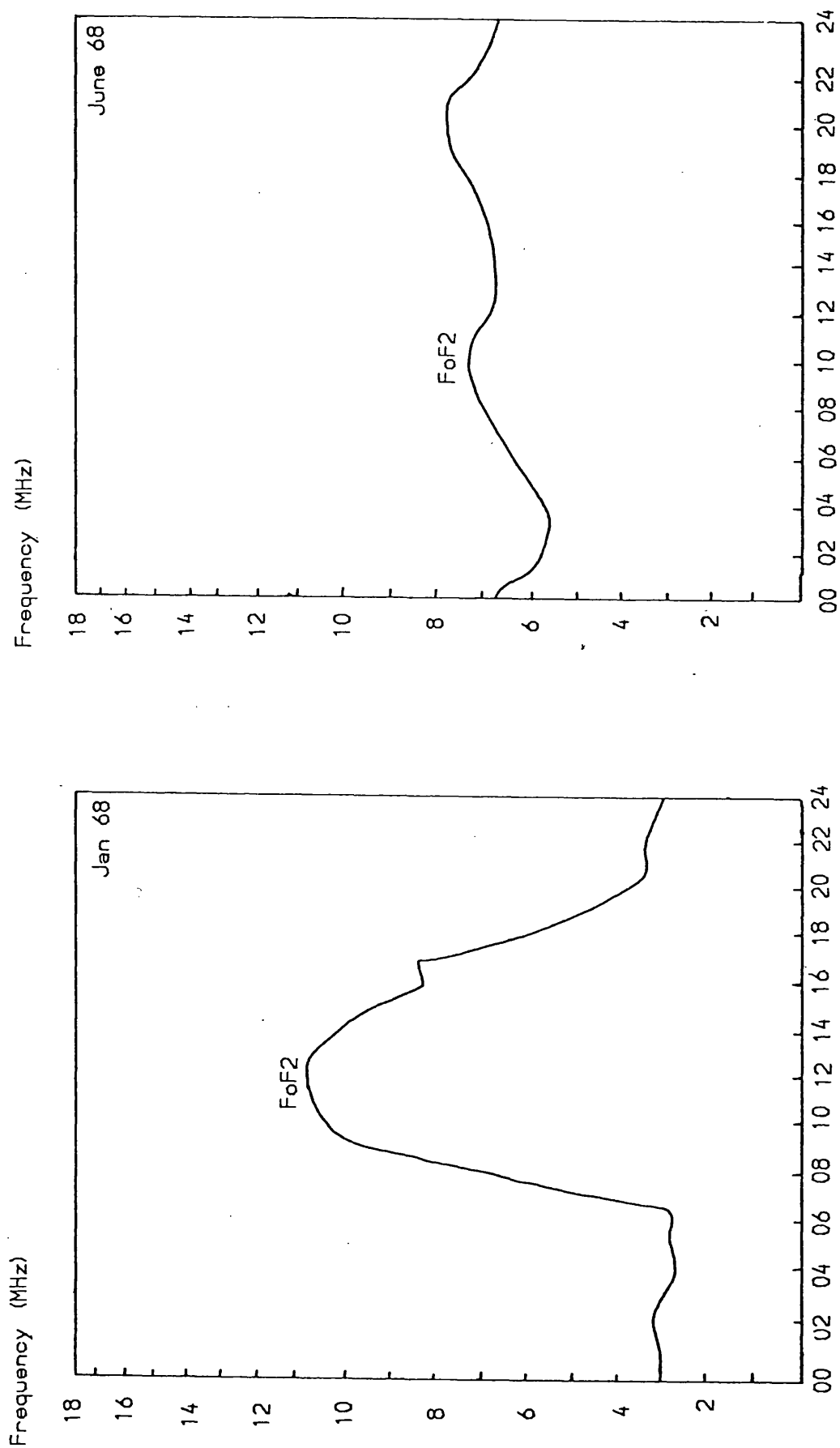


Fig 1.1.6 Daily and Seasonal variations in FoF2
(Slough Ionospheric Data 1968)

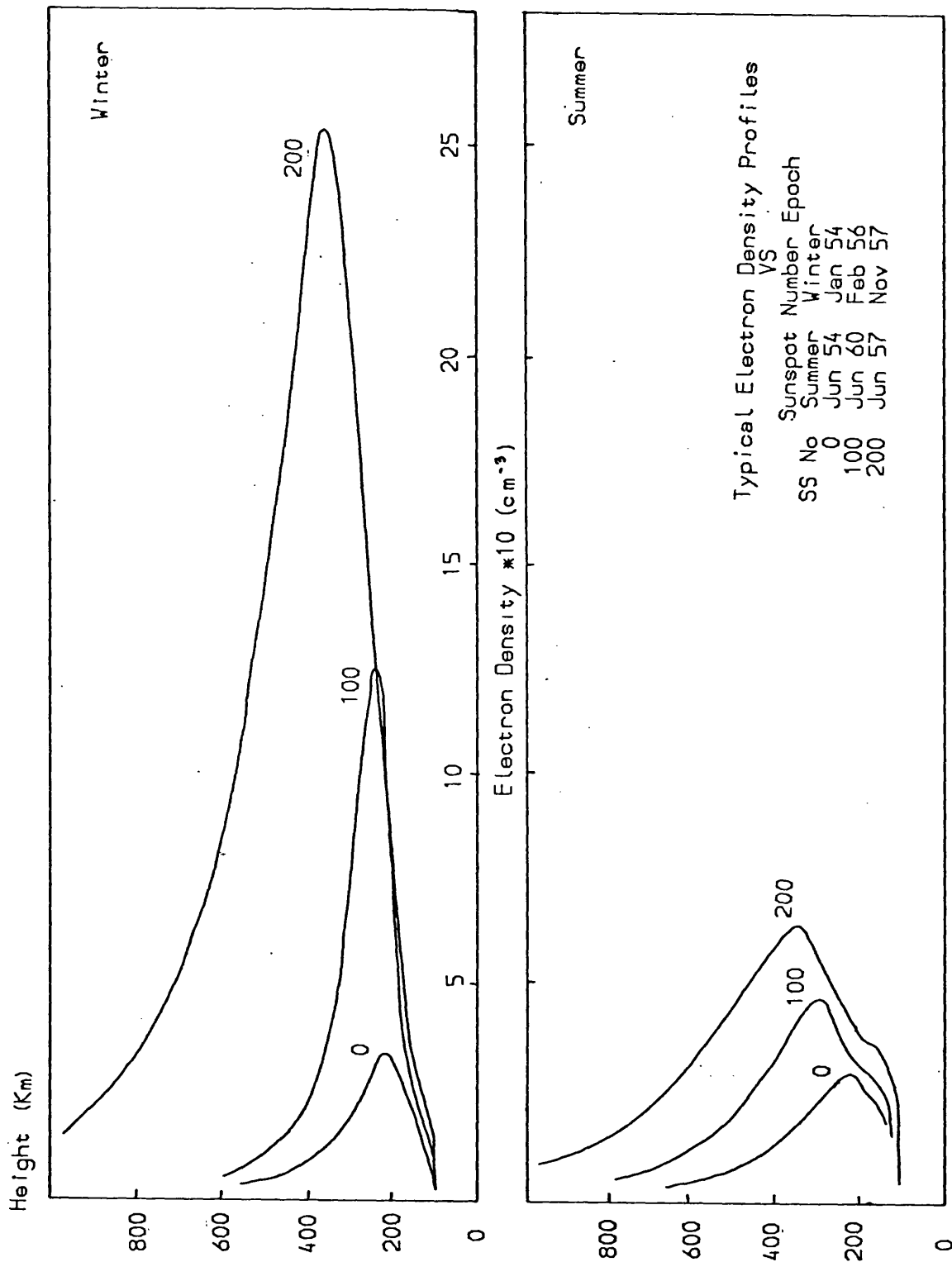


Fig 1.1.7 Solar Cycle Changes in Noon $N(h)$ Profiles
(after Wright 1962)

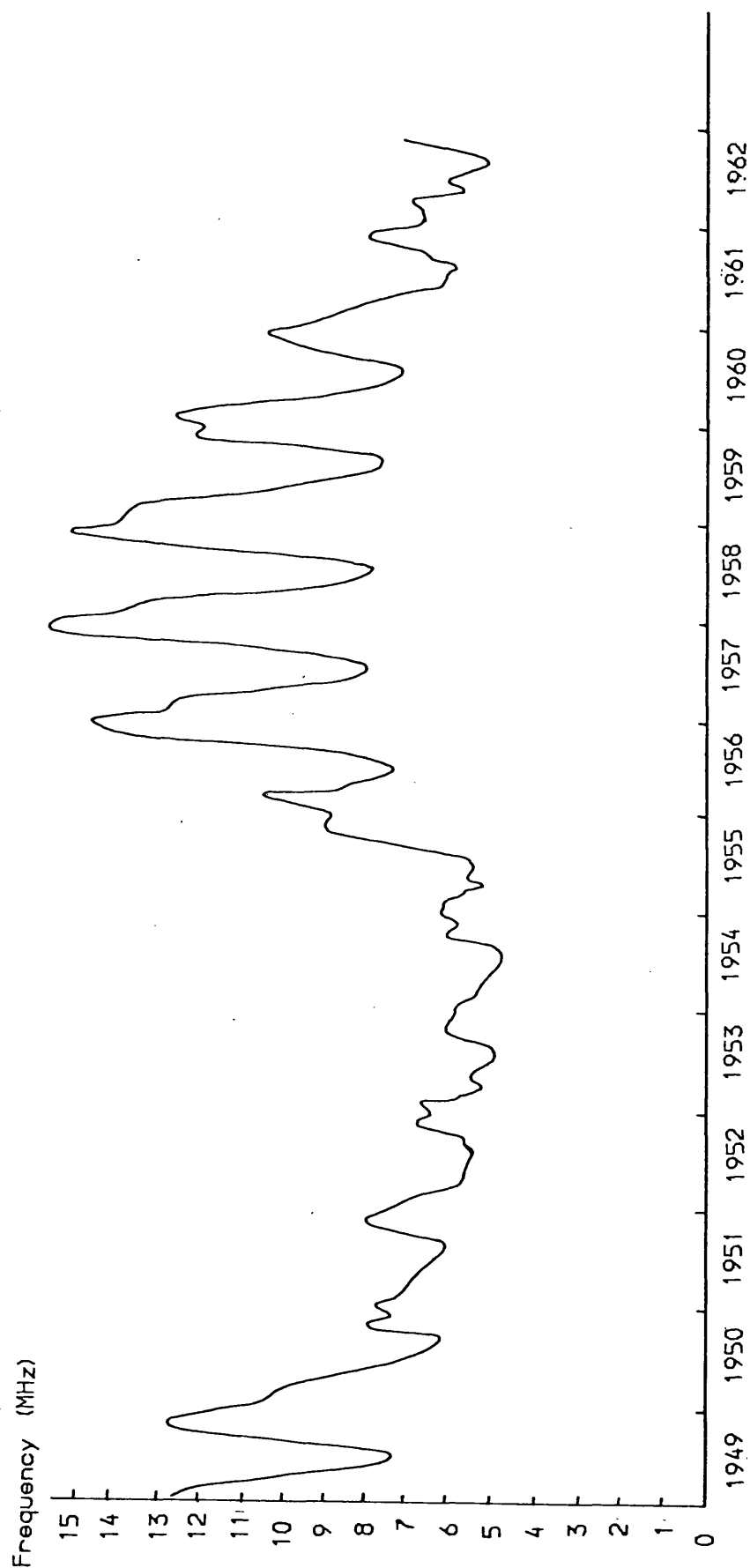


Fig 1.1.8 Monthly Mean Noon Critical Frequencies
(Slough Ionospheric Data)

1.2 IONOSPHERIC RADIO COMMUNICATION

Marconi (1901) transmitted the radio signal "S,S,S" across the Atlantic from Cornwall to Newfoundland. This was explained in terms of multiple scattering around the curvature of the earth's surface since the ionosphere was then unknown. However this process would have resulted in a much smaller signal at Newfoundland than was actually received. To account for this discrepancy Kennelly (1902) and Heaviside (1902) independently postulated the existence of a reflecting layer in the upper atmosphere.

In 1924 this layer was found experimentally by Appleton and Barnett (1925). In their experiment a radio transmitter and receiver were separated by approximately 100Km and the frequency of the radio transmitter varied. Interference beats in the received signal amplitude were recorded indicating that two paths for the radio propagation existed, along the ground and via the ionosphere. With this experiment the height of the ionosphere was determined by triangulation.

Radio developed rapidly for many purposes such as broadcasting, navigation, maritime, radio- telephones, police, amateur uses and the armed forces. Most of these services required long distance communication and initially frequencies in the LF and MF bands were employed (i.e. < 1MHz). In the 1930s the advantages of using higher frequencies became apparent and interest moved to the HF bands (2-30MHz), where it is possible to communicate over great distances with

relatively simple equipment if an appropriate frequency is chosen.

As described in the previous section the maximum usable frequency (MUF) for a given path and time of day is controlled by the electron density in the F region and the path geometry. The low frequency limit is caused by the absorption of radio wave energy by the D and E regions. Typical MUF and LUF curves are plotted in fig 1.2.1.

A major problem experienced in HF communications is that of fading. This is a reduction in the received signal due to destructive interference between components of the signal arriving at the receiver over different propagation paths. This can occur as a result of :-

- a) Multihop propagation.
- b) Multilayer propagation.
- c) In- mode interference.
- d) Two polarisation modes.
- e) Spread F (flutter fading)

These are summarised in fig 1.2.2

Modal interference is not a desirable feature in any communications system since it produces errors in digital data transmissions and greatly reduces the signal readability over voice links. The most effective way of avoiding the problem is to have a range of frequencies available to the operator so that if fading or interference is unacceptable on one channel an alternative clearer channel can be selected. As a general rule better frequency reliability is achieved by selecting a frequency just below the MUF (maximum usable frequency) for a

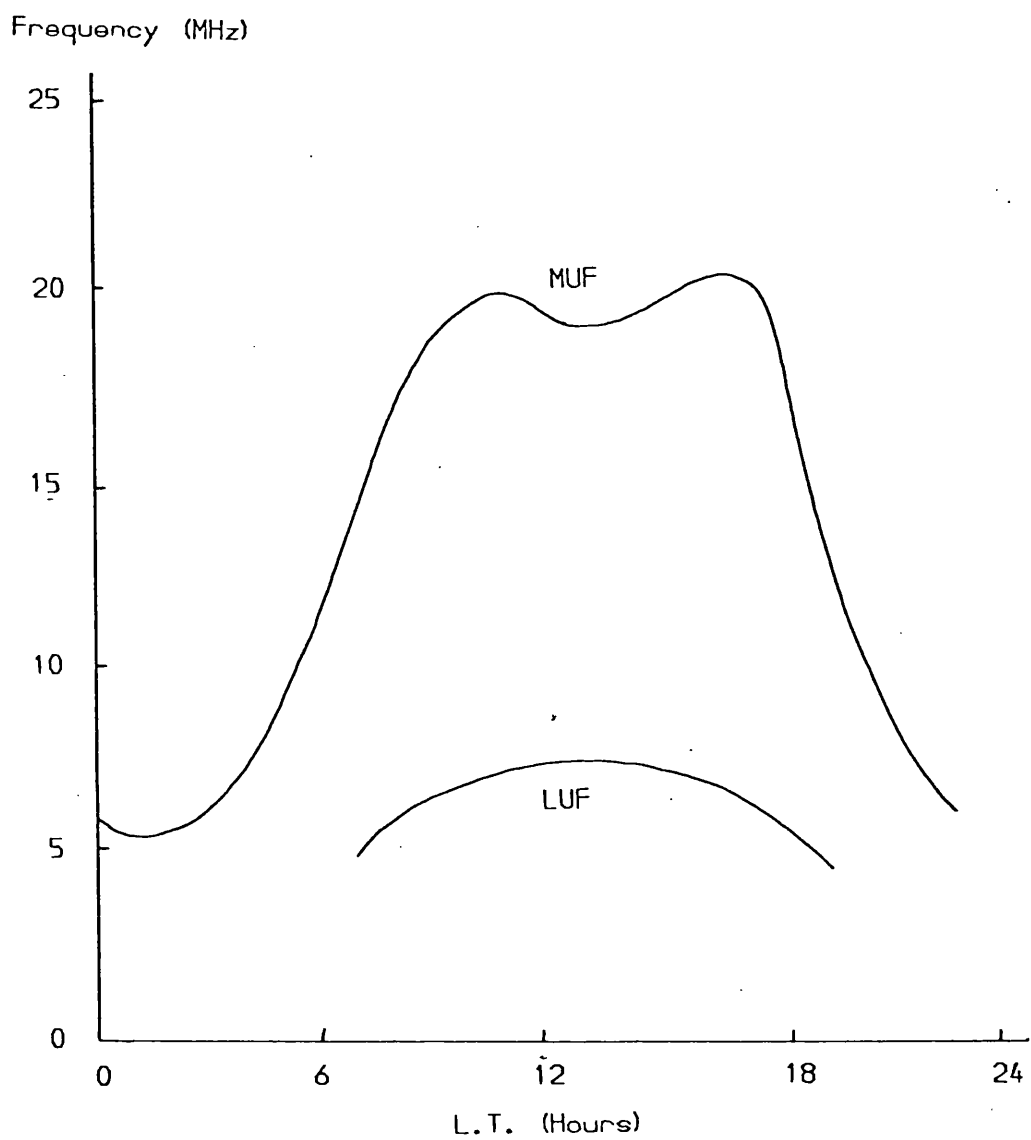
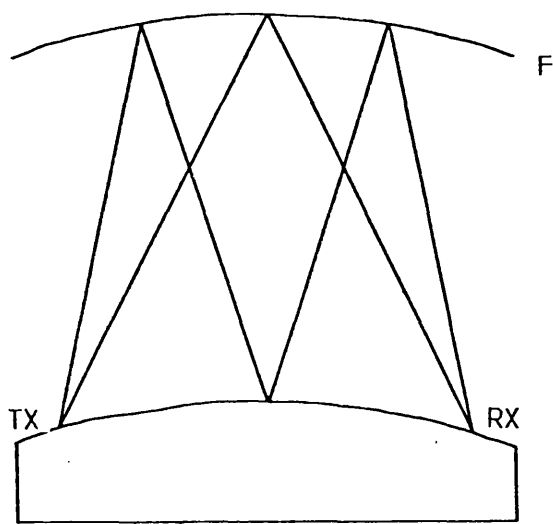
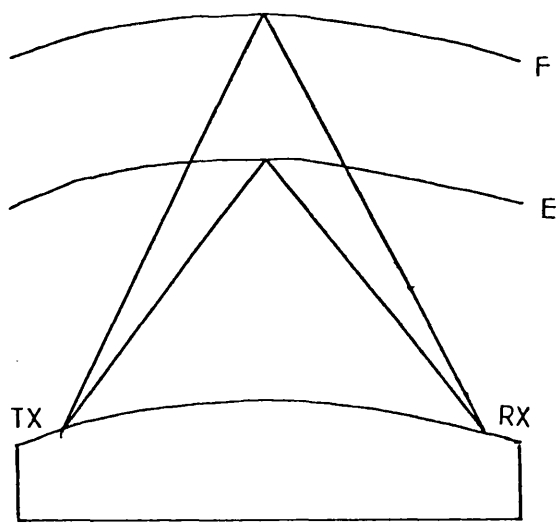


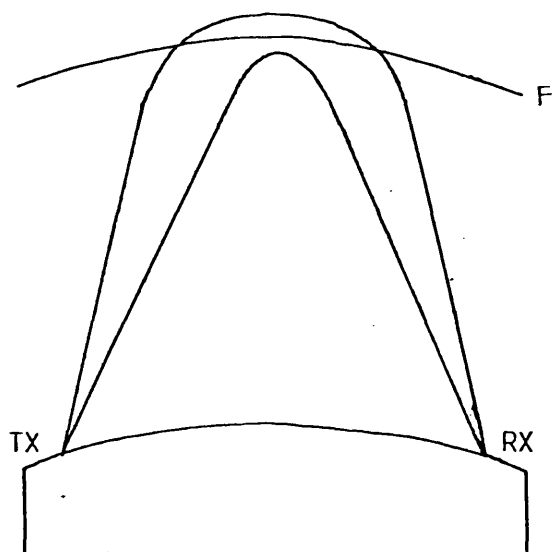
Fig 1.2.1 MUF and LUF Curves



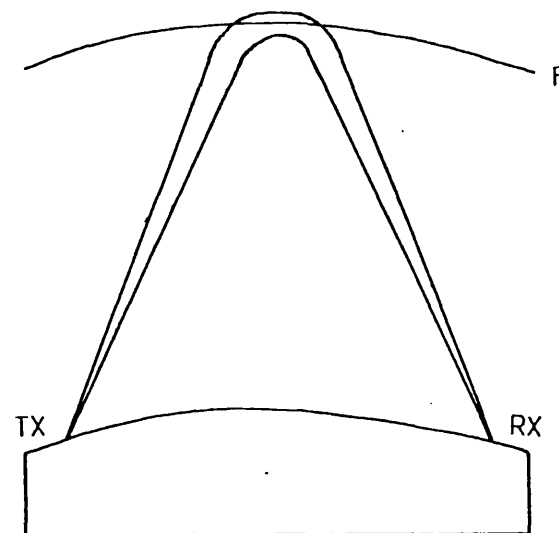
Multihop (1F and 2F)



Multilayer



High and low angle



O and X modes

Fig 1.2.2 Different Types of Multipath

given path. In this way the 1F ray will propagate but the 2F ray will not since it will penetrate the layer as a result of its smaller angle of incidence. This procedure also reduces D region absorption to a minimum. The use of a frequency very close to the MUF does however have several serious disadvantages, eg:-

- 1) For broadcast use frequency changes are not possible.
- 2) The HF band is already crowded so the allocation of several alternative frequencies to each operator is not desirable.
- 3) As ionospheric conditions vary from day to day it is difficult to schedule radio contacts in advance.
- 4) As the above strategy is popular the amount of co-channel interference can increase near the MUF.

An alternative approach is examined in this thesis.

1.3 DIGITAL COMMUNICATIONS

Information has been sent as digital data (in its most simple form binary 1's and 0's) for many years. As early as 1837 an electrical telegraph was capable of transmitting messages along a wire for considerable distances. The Morse code was generally employed in which letters and numbers are represented by a series of dots and dashes. The human element of this system limits the data rate to between 15 and 30 words per minute. To speed up communications the teleprinter was developed. The teleprinter usually employs the five bit international telegraph code no 5, more commonly referred to as

Baudot or Murray code. Using this code it was possible to raise the data rate to about 100 words per minute which was, at the time, the fastest speed at which the mechanical teleprinter could reliably operate.

The Morse code was also extensively used in high frequency radio communication for wireless telegraphy and is still employed for some purposes. A skilled operator is capable of identifying the code under conditions of severe noise, interference and even moderate fading without any dramatic reduction in either accuracy or data rate.

As with wire telegraphy, the use of the teleprinter followed Morse in HF radio transmission. The teleprinter is not as good as the human ear at recognising a signal sequence in the presence of a high general noise level, moreover with the higher data rate an interference fade out causes the receiver to miss more characters than with the slower Morse system. This thesis is largely concerned with measuring the errors received at normal data rates for HF communications and investigating how these errors can be reduced or at least predicted.

When Morse and Murray codes were first employed for radio communications the modulation system was interrupted carrier wave (ICW). For a mark or dot the transmitter was keyed on and for a space it was keyed off (ASK). The disadvantage of this system is that a signal fade out is not differentiable from a space. To solve this problem frequency shift keying (FSK) was introduced. A mark is transmitted as a known frequency shift in the carrier (1st tone) and a space as a different frequency shifts (2nd tone). The frequency shift being known. This system

enables the marks and the spaces to be distinguished from a fadeout resulting from a loss of signal. A further reduction in error rate is achieved by using the digitally coherent phase shift keying (DPSK) technique in which the phase difference between adjacent bits of carrier represents the binary information. The theoretical error rates for these systems are plotted out in fig 1.3.1. During the project described in this thesis ASK was used for transmitting the test data sequence. This choice was dictated by the equipment available for the experiment, however some of the results obtained using ASK can be applied to FSK and DPSK systems (see fig 1.3.1).

1.4 AN INTRODUCTION TO THE PRESENT INVESTIGATION

When dealing with high digital data rates the problem of multipath interference is a particularly serious one. It can manifest itself in two major forms. Firstly as the fading described in the previous section (fig 1.4.1). In this situation the multipath delay (t) is small when compared with the bit length (b). Therefore in the case of extreme destructive interference illustrated in fig 1.4.1, the mark bits are almost completely destroyed where the signals from the two different paths coincide. This leads to major errors.

The second effect of multipath interference (fig 1.4.2) occurs when t and b are approximately the same. In this example a mark from the longer ionospheric path arrives at the receiver at the same time as the following bit from the shorter path. Therefore the receiver has to interpret the following bit as a

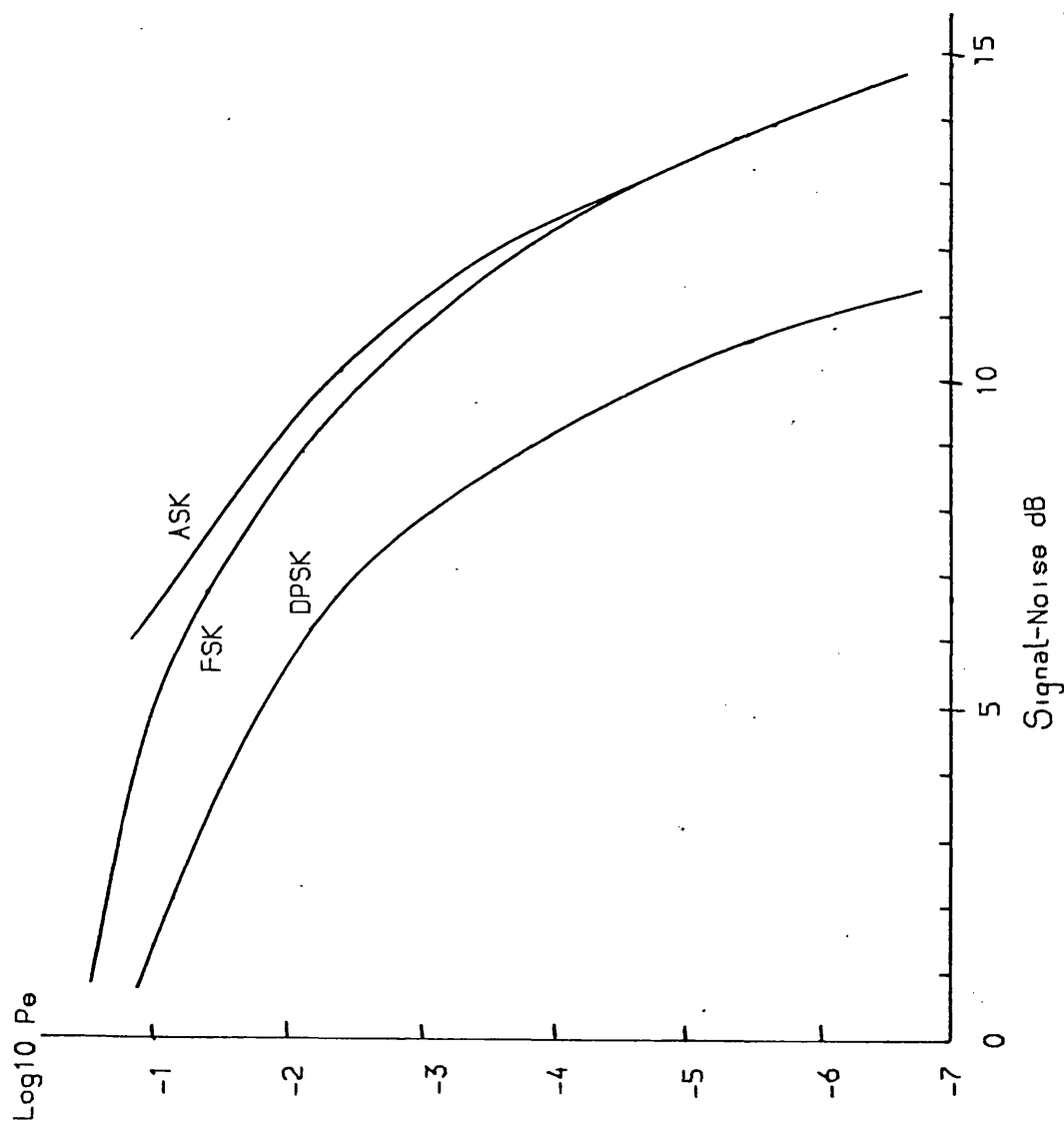


Fig 1.3.1 Error Probabilities for Binary Digital Modulation Systems (Carlson 1968)

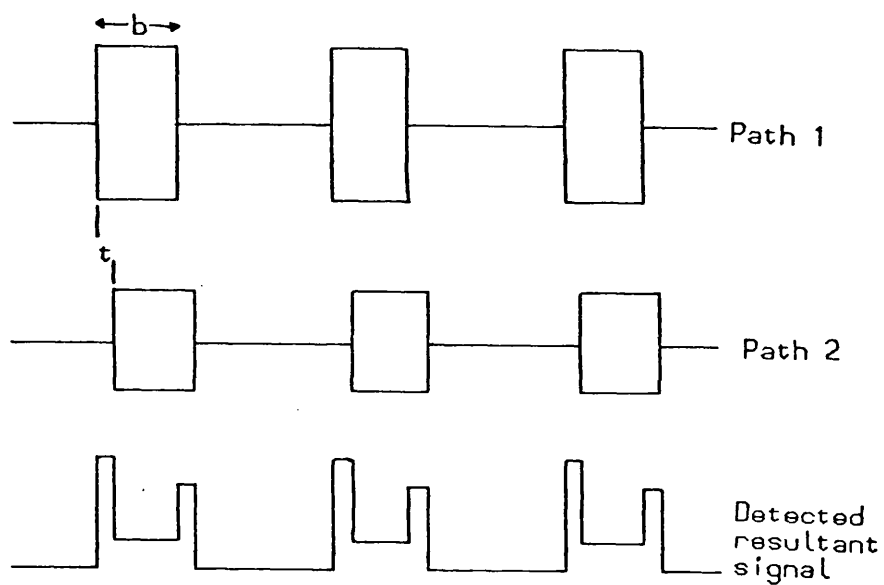


Fig 1.4.1 The Effect of Short Multipath Fading on Digital Data

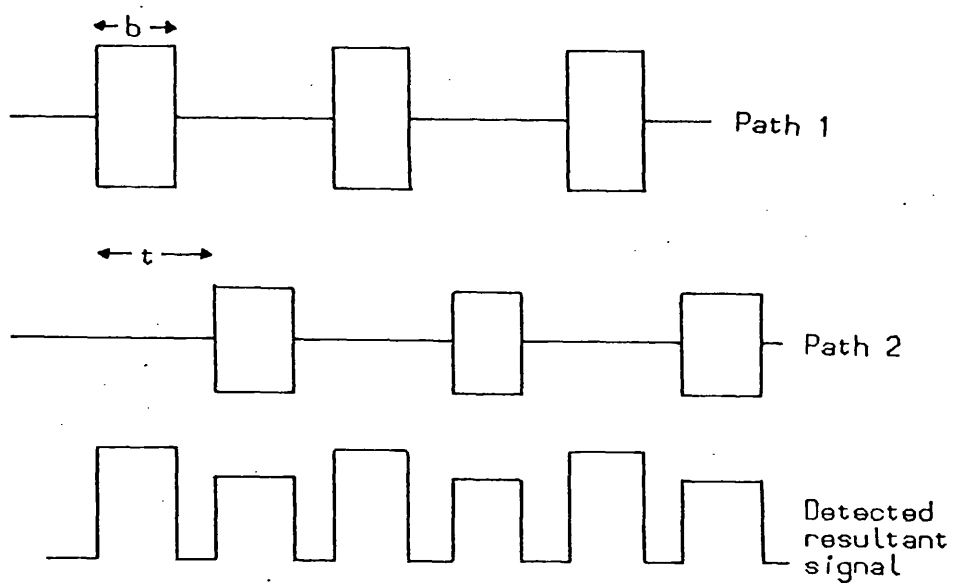


Fig 1.4.2 The Effect of Long Multipath Fading on Digital Data

mark rather than a space thus causing an error.

In order to transmit at high data rates the effect of multipath interference must be removed. A technique for achieving this has been proposed by the Royal Aircraft Establishment (RAE), of which the work in this project forms a part. This involves an elevation steerable antenna array (fig 1.4.3) to select the desired propagation mode.

The signals propagating over the different ray paths will arrive at the receiver at different elevation angles. If these angles are sufficiently spaced a null in the antenna polar diagram can be steered towards the unwanted path together with a maximum in the direction of the wanted component. This makes the received signal virtually single moded, and so reduces the modal interference and allows higher data rates. Even if the different ray paths are quite close in elevation angle of arrival an advantage over a conventional omnidirectional antenna can be gained by applying less gain in the direction of the unwanted mode.

In order to steer the antenna some real time knowledge of the active ionospheric paths is required. This is obtained by transmitting a sounding pulse signal over the path. Because the paths for the different propagating modes are of different length, the pulses propagating along the various paths arrive at different times at the receiver. This sounding signal yields information concerning the relative amplitudes and time delays of the active propagation modes.

Predictions of ionospheric behaviour provide an estimate of the likely modes of propagation for a given time, day and

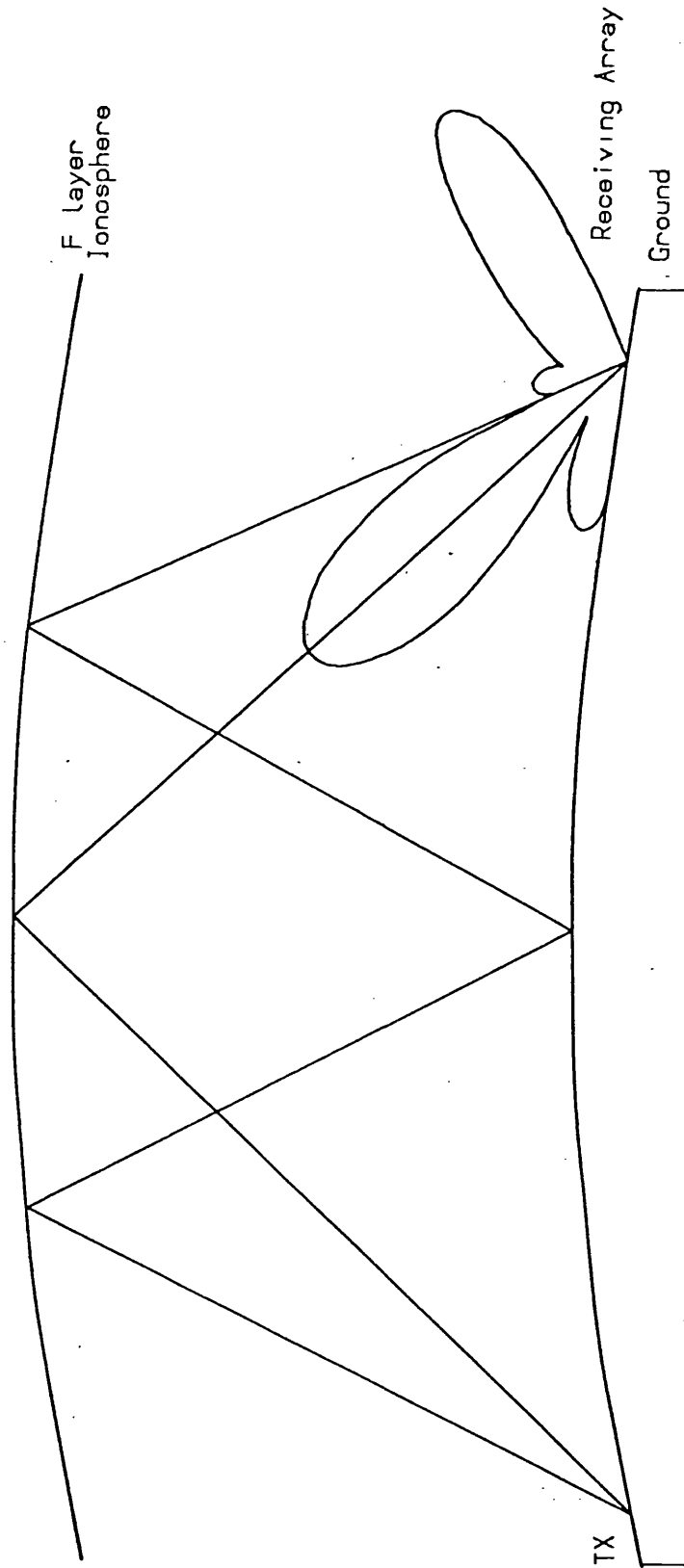


Fig 1.4.3 Maximum Array Sensitivity Steered
Towards the Required Path

path. If these predictions are compared with the measured results it is possible to decide which returned pulse echo corresponds to which ionospheric path. As the approximate angle of arrival can be predicted for these modes it is possible to use this knowledge to steer the antenna to increase the signal from the wanted mode and reduce those from the unwanted modes. The pulse sounding signal can then be used to optimise the antenna control around this initial position.

Due to development delays, the steerable antenna was not available during the course of this research project. Therefore the emphasis of the work shifted to a study of the effect of noise and multipath interference on the error rates for a digital communication link. The pulse sounding technique can acquire information regarding both the multipath content of a received radio signal and its signal to noise ratio. From this information it is possible to predict the number of received errors, which can in turn help an operator optimise the frequency, data rate and error protection coding.

CHAPTER 2

PREVIOUS WORK

2.1 HF PROPAGATION

Some of the features of HF propagation have already been mentioned in the previous chapter. In order to relate the present project to previous work in the field the published work is now briefly reviewed.

A short history of the subject has been presented by Booker (1975) which covers the period 1900 to 1950. A more general work which contains much greater detail was published by Davies (1965). Goldberg (1966) considers the subject of HF propagation and also discusses the subject of ionospheric reflection, maximum usable frequency (MUF), noise, multipath fading and data communications, before finally describing two adaptive methods of reducing the harmful effects of multipath. A highly mathematical approach to the subject of pulse sounding is presented by Malaga & McIntosh (1979). A more recent review by Rush (1981) provides an excellent summary of ionospheric HF propagation. This describes the properties of the ionospheric layers and how they vary in time and space. The consequent effects on an HF communications link are also discussed.

2.1.1 Predictions

Considerable attention has been given to the problem of

predicting propagation conditions for HF communication purposes. In general, predictions are made on a monthly mean basis of the MUF and LUF (section 1.2) for the required transmission path. Most prediction techniques are able to determine the various propagation modes likely to be active and to identify the dominant mode together with the expected relative strengths of the active modes. A historical review of the various types of early predictions of MUF, LUF, absorption etc, is given by Rawer (1975). Recent developments in prediction techniques are described by Bradley & Lockwood (1981) and Davies (1981)

Fig 2.1.1 gives an example of a the predicted daily variation of MUF and LUF based on a monthly mean model. It also illustrates how this information could be used by an operator, with three available allocated frequencies, to plan which frequency should be employed at any given time of day. Much work has been done, developing simple methods of predicting ionospheric parameters (Barclay 1970, Fricker 1981, Levine et al 1978). These methods are designed for applications where only a small amount of computing power is available. They all make certain simplifying assumptions which provide speed and portability for the calculations at the expense of a high degree of accuracy.

Where more accurate predictions are required and larger computers available (eg for service planning applications) more complex prediction programs can be utilised (Barclay 1973, Bradley 1975). These prediction methods in general follow the procedures outlined below.

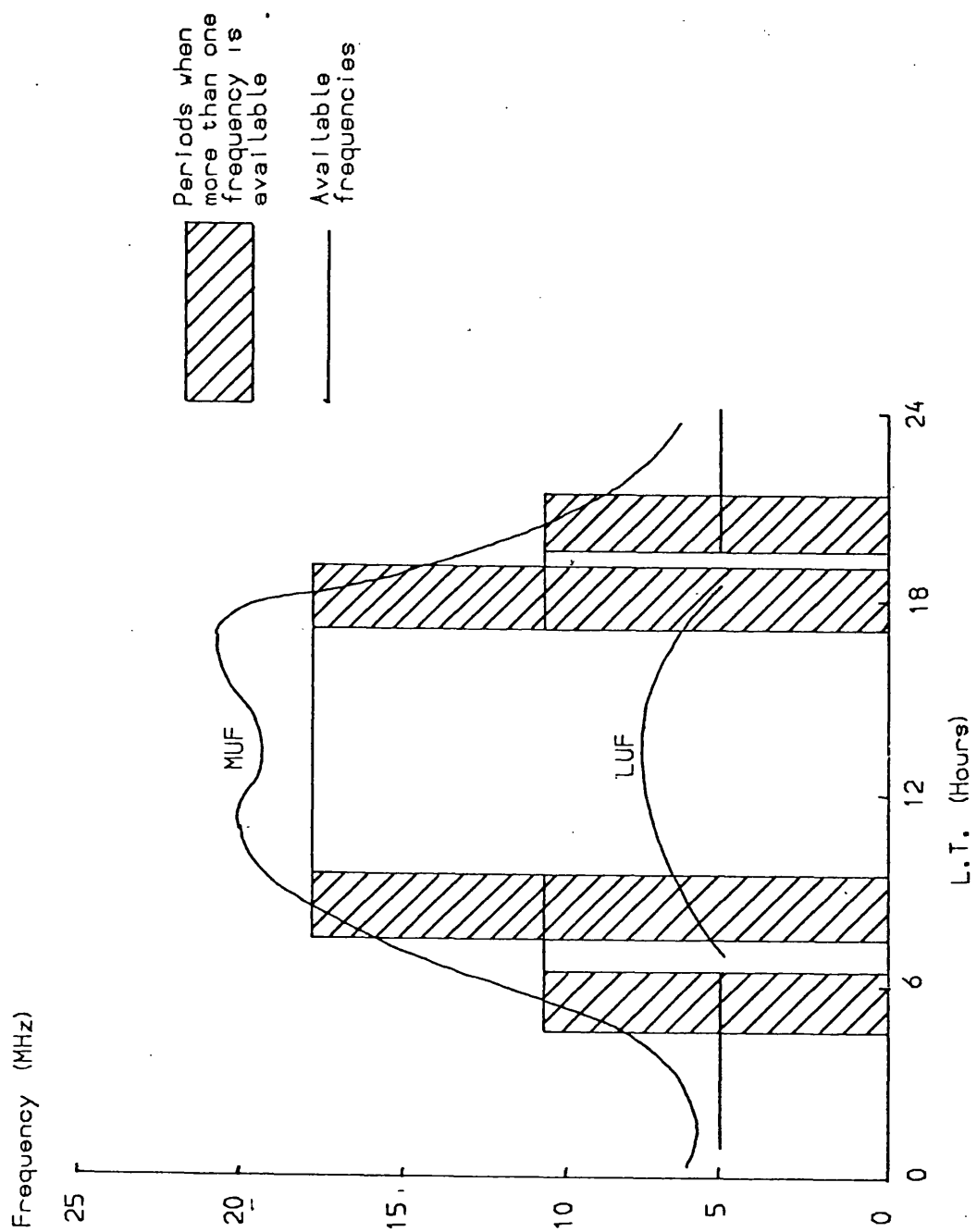


Fig 2.1.1.1 The Use of HF Predictions in Frequency Management (after Bradley 1981)

- 1) Estimating ionospheric characteristics along the propagation path eg f_oF_2 , $M(3000)F_2$.
- 2) Producing models of the vertical distributions of electron concentration.
- 3) Ray tracing to find transmitter launch and receiver arrival angles.
- 4) Estimating received signal strengths from propagation losses due to -
 - spatial attenuation (including ray focusing)
 - ionospheric absorption
 - polarisation- coupling losses
 - ground losses

(after Bradley 1975)

In this process a ray is traced through a model ionosphere. The ionospheric model consists of an electron density profile (eg fig 2.1.2) appropriate for the time and position for which the prediction is required. The actual parameters which control the model are usually taken from averages of ionogram records (section 2.2.1), and are usually available to the prediction program in the form of numerical maps of constant ionisation contours.

The results of a modern prediction program have been experimentally tested by Thrane & Bradley (1981) for a high latitude path. This study indicated that for longer paths predictions were generally accurate but for shorter paths (460 Km) the predictions were of little practical value. Some reasons for the variability of the ionosphere and hence of the prediction methods are presented by Jull (1967). The accuracy

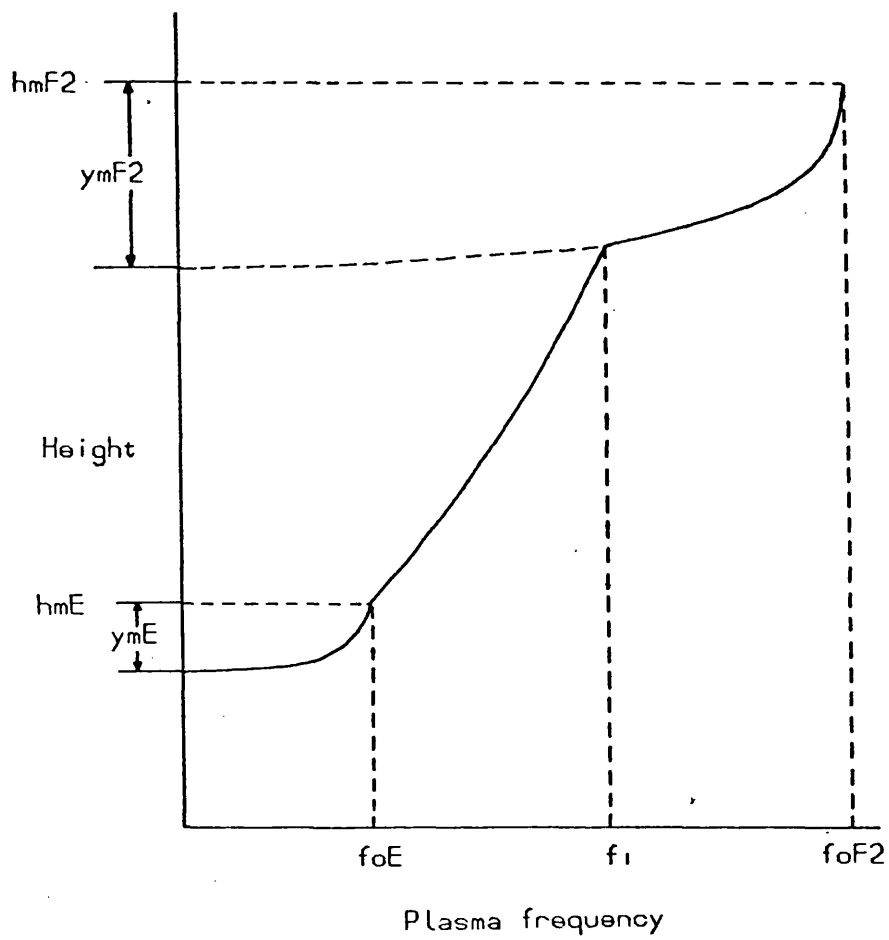


Fig 2.1.2 The Ionospheric Model
(after Bradley 1975)

of short term predictions can be improved by updating the program with real time data from ionospheric sounding or from monitoring broadcast stations (Dambolt 1979, Jones et al 1978).

While the sounding system described in this thesis employs very simple predictions to aid mode identification, it provides independent real time information regarding propagation conditions and therefore removes the need for any kind of detailed ionospheric prediction. Some of the factors that adversely affect the transmission of information over a typical HF communications channel are now considered.

2.1.2 Absorption

When an HF wave is reflected from the F layer of the ionosphere it passes through the lower ionosphere where some of the radio energy is absorbed. Rees & Jones (1979) describe how this absorption varies with place, time, season and frequency, and compare the observations with the theoretical predictions of this parameter. The relationship between vertical and oblique incidence absorption was discussed by George & Bradley (1973). The anomalously large absorption levels noted during the winter have been studied by many workers (eg Evans & Jones 1971).

2.1.3 Radio Noise

A further limitation on a data communications link is imposed by the signal to noise ratio for a given frequency at a

given time of day. HF noise is briefly discussed by Goldberg (1966) (see fig 2.1.3). A broader treatment is given by Fischer (1965) who surveys noise from 5Hz to 1GHz by combining the results of several earlier workers. Electronic simulators have been built (Bolton 1971) which employ digital circuitry to reproduce measured noise types in both LF and HF frequency bands.

Much HF radio noise is man made and a large part of this comes from other radio transmitters (see fig 2.1.3). Many modern communication systems (Cottrell 1979) are designed to monitor these noise levels and select the quietest available channels in order to reduce interference and improve the signal to noise ratio.

2.1.4 Ionospheric Dispersion

The ionosphere is a dispersive medium and as a result a square pulse of radio wave energy will be distorted as it travels through the medium. Inston (1969) gives a clear treatment of how pulse broadening is related to the dispersion. Hatton (1968) describes how dispersion can occur in both time and frequency domains. He also demonstrates how the dispersion influences various types of data transmission systems (CW, AM, suppressed carrier, SSB, FSK and DPSK).

2.1.5 Multipath Propagation

The multipath condition, which is of direct concern in

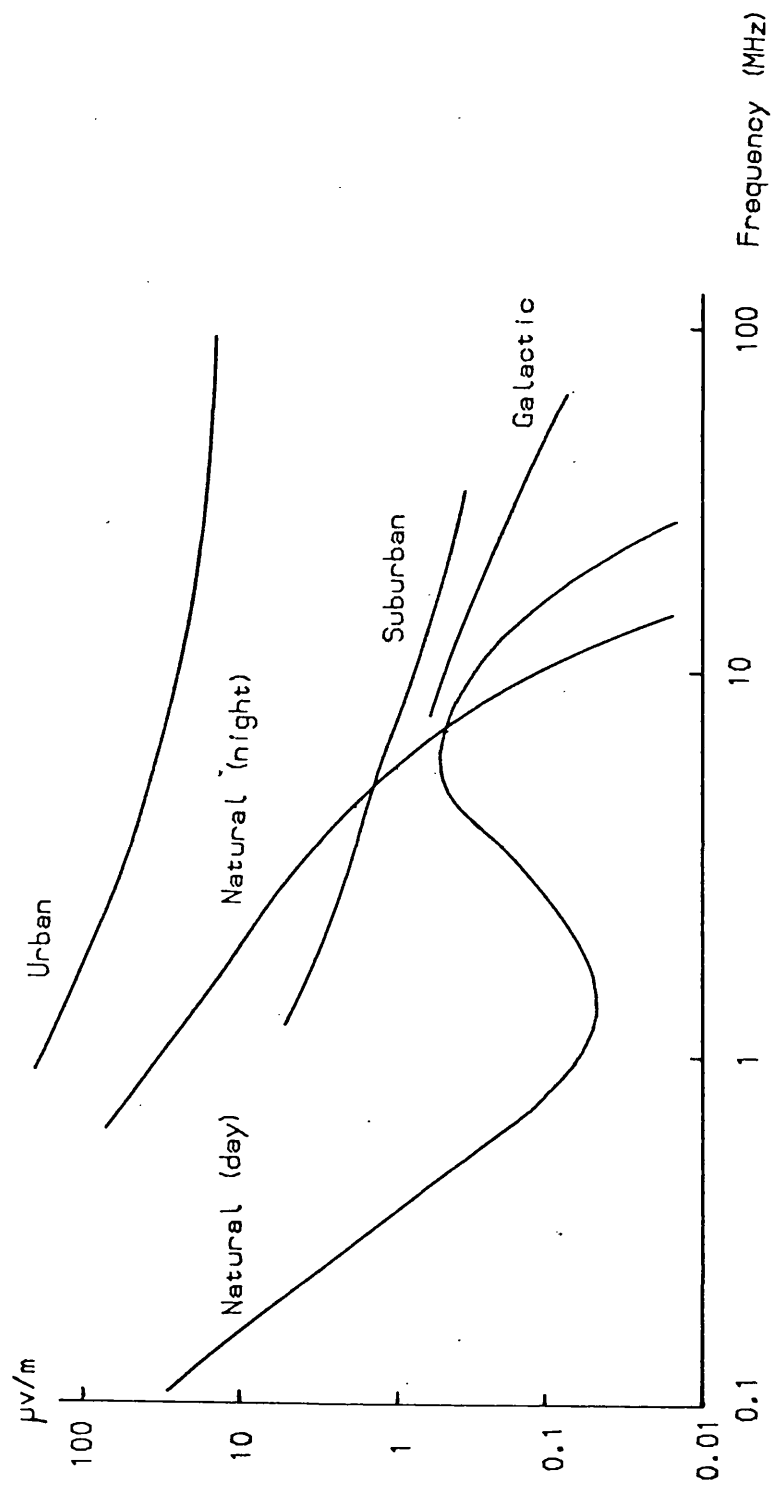


Fig 2.1.1.3 Noise Spectrum (after Goldberg 1966)

this thesis, is illustrated in fig 2.1.4. The diagram represents three possible paths whose amplitudes and phases can be changed in a controlled manner by means of weighting factors. This is the type of multipath simulation adopted in the project simulator hardware (section 4.5).

Much other work has been conducted into simulation of multipath propagation at HF. Simple two path simulators are described by Law et al 1957, Beck & Betts 1965 and Arrendo & Chriss 1973. These methods simulate both fading and random noise and are used for testing communications equipment under reproducible conditions. Simulators can also be employed to cut down the costly time spent on field trials.

More advanced versions of this basic type of simulator are described by Ralphs & Sladen (1976) and Mately & Bywater (1977). These incorporate such ionospheric properties as doppler shifts and more than two propagation modes. A computerised ionospheric simulation is described by Palmer (1974), in which the transmitter, ionospheric channel and the receiver are all simulated numerically.

In order to determine the correct weighting values a sounding or probing signal can be sent over a real link, and the link properties measured and recorded. This information is then employed to reconstruct an ionospheric path (Goldberg et al 1965, Bussgang et al 1974).

2.2 IONOSPHERIC SOUNDING

A short review is now presented of HF ionospheric sounding

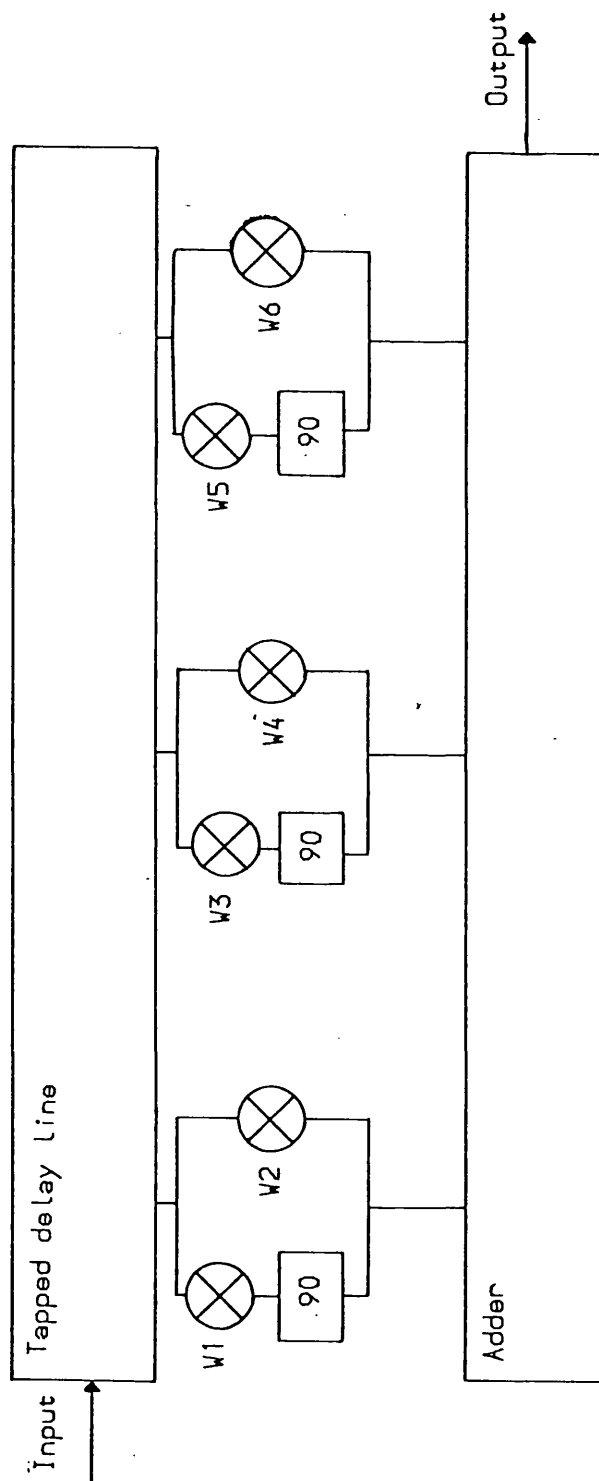


Fig 2.1.4 Multipath Propagation Model

techniques. The first five methods are intended to determine the properties of the ionosphere, whereas the remaining techniques are mainly employed to evaluate a communications channel.

2.2.1 Pulse Sounding

An ionosonde is an HF radar capable of sending pulses of radio wave energy into the ionosphere and of receiving and displaying the echos and times of flight. The radio frequency is swept over the range 1.5 to 20MHz and the resulting display of time of flight against frequency is referred to as an ionogram (fig 2.2.1). For vertical sounding the time of flight is related to the apparent or equivalent height of reflection h' where $h' = ct/2$. Pulse sounding experiments have been conducted for many years since the technique was first introduced by Briet & Tuve (1926). In fig 2.2.1 can be seen the effect of ionospheric reflections from the E, F₁ and F₂ layers in the ionosphere. Many improvements have recently been made to the conventional ionosonde, including such features as :-

- a) Digitising the control logic of a conventional ionosonde (Downing 1979)
- b) Digitising the display and recording facility as in the Digisonde (Bibl & Reinisch 1978), the Dynasonde and Kinesonde (Wright 1969)
- c) The use of a directional antenna to determine the angle of arrival of the various echos (Koehler 1976)
- d) The use of pulse synthesis techniques to gain better

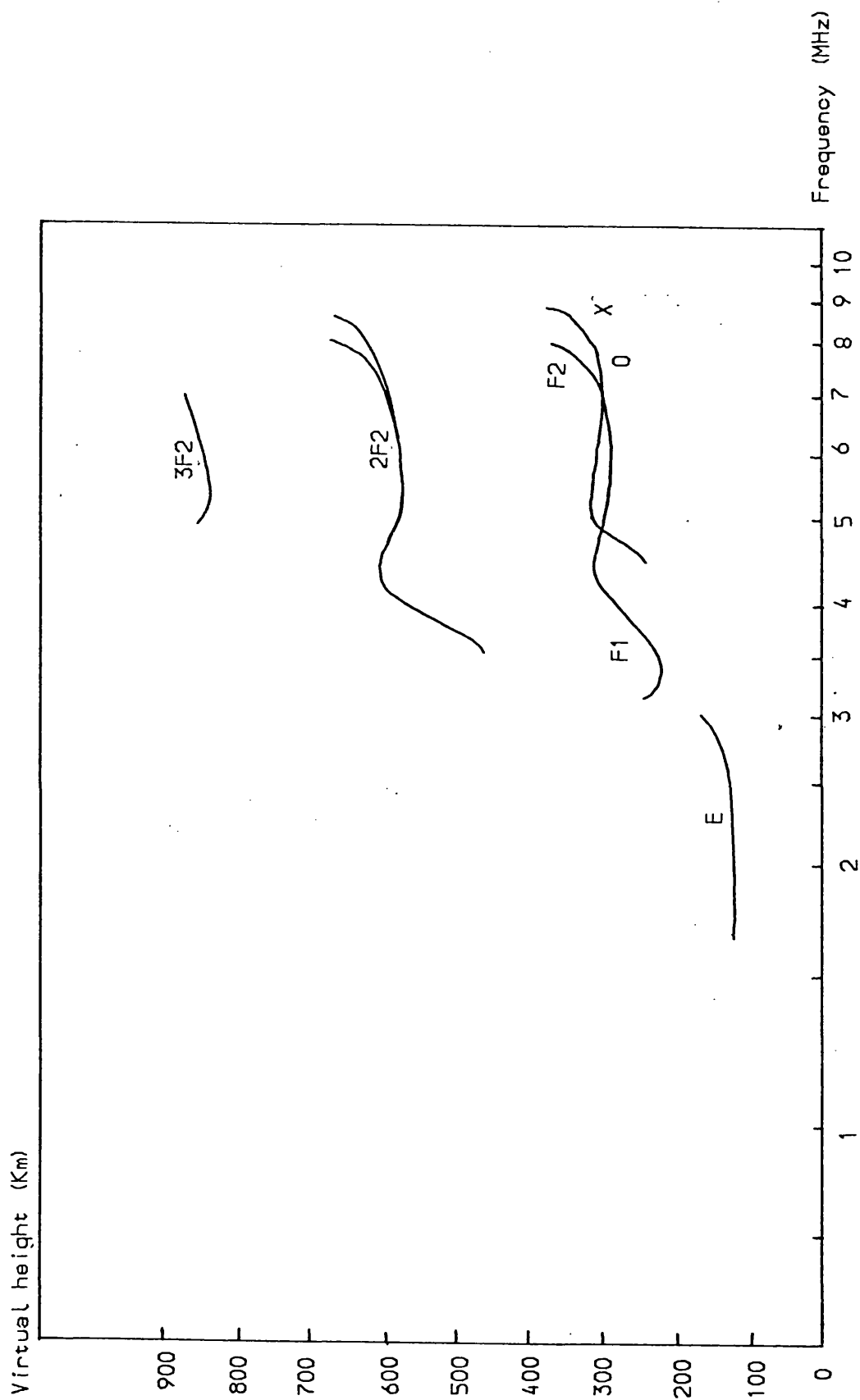


Fig 2.2.1 Typical Winter Day Ionogram (after N.B.S 1948)

height resolution (Delvin et al 1977, Coll & Storey 1964)

- e) A spaced antenna and phase information can give ionospheric drift velocities (Bibl & Reinisch 1978, Wright 1969)

2.2.2 Oblique Pulse Sounding

Radio communications take place over oblique ionospheric paths, therefore oblique sounding information is more appropriate than that obtained at vertical incidence. The earliest work on oblique pulse sounding was conducted by Farmer & Ratcliffe (1936) and produced recognisable oblique ionograms over the Cambridge to Edinburgh path. A typical example of the differences between a vertical and an oblique ionogram was given by Beynon (1948) in fig 2.2.2. A clear summary of the early work in this field is presented by Agy & Davies (1959). This paper also describes studies of observed MUF and the differences in the mode content of oblique and vertical incidence paths.

Many investigations of ionospheric propagation conditions have been undertaken with oblique sounders (Chapman et al 1955, Cox & Davies 1955, Sulzer 1955, Weider 1955, Doyle et al 1960, Jull 1962). Ames & Egan (1967) updated the technique by digitising the sounder and producing computerised short term HF predictions from the results. Finally oblique sounders have been employed to improve HF communications (Hatton 1961, Egan & Pratt 1963) allowing operators, for example to utilise sporadic E modes and thus make the best use of existing conditions.

Equivalent height (Km)

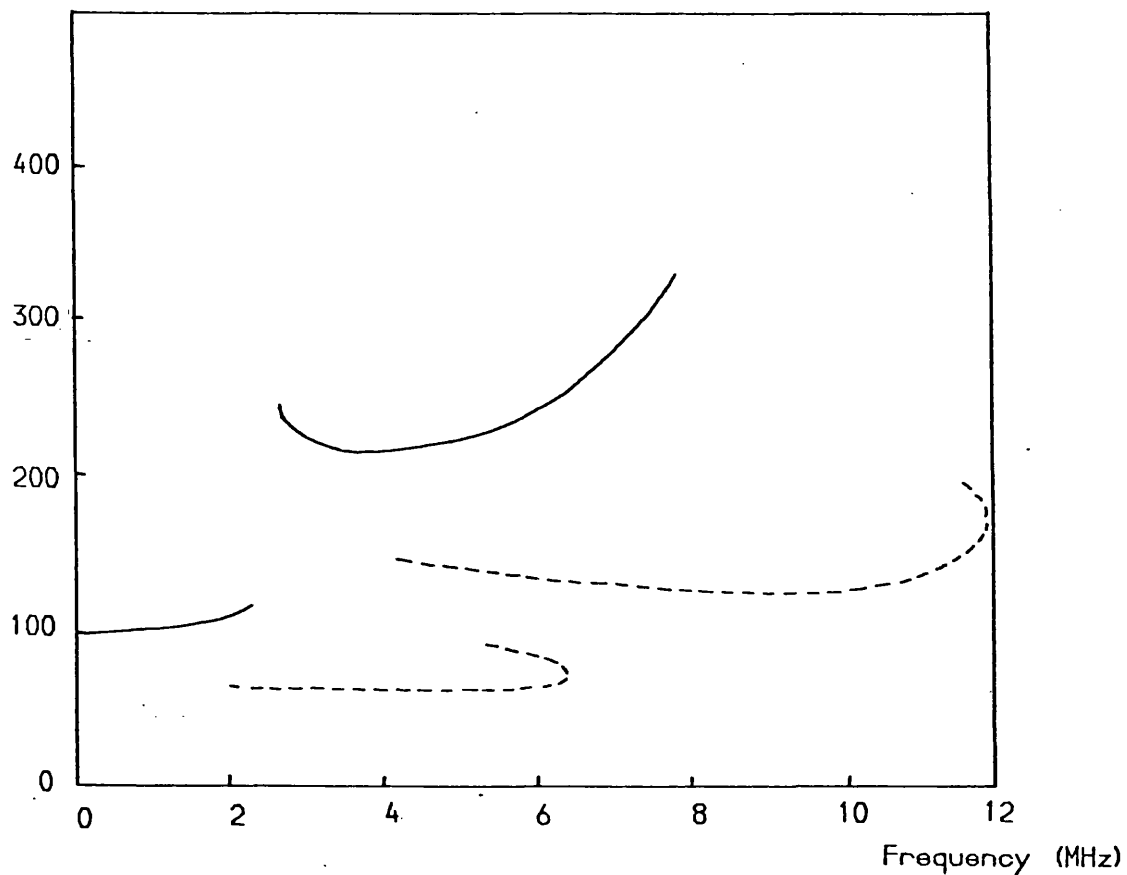
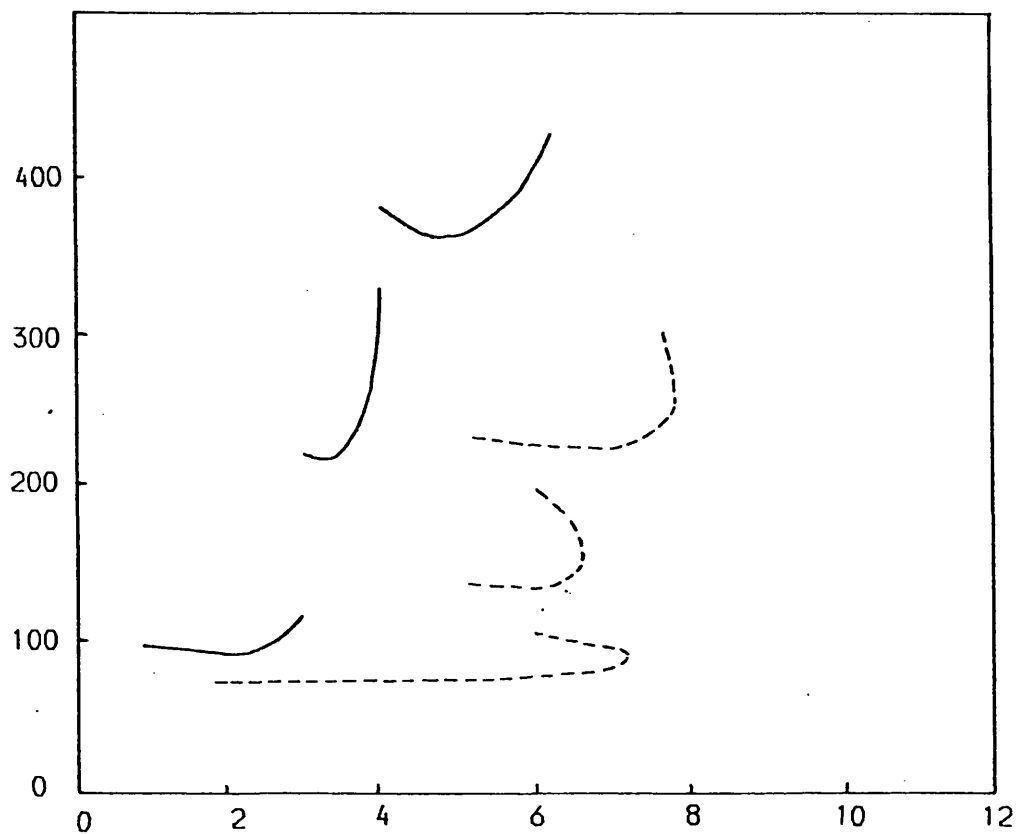


Fig 2.2.2 Oblique and Vertical Ionograms
(after Beynon 1948)

2.2.3 Chirp Sounding

The chirpsounder (Fenwick & Barry 1967) is an improved ionosonde generally employed on oblique paths. Instead of transmitting a pulsed sounding signal of stepped frequency, a continuous carrier is transmitted with a smoothly increasing frequency. At the receiver signals arrive with a frequency related to the time of travel (fig 2.2.3). The advantages of this technique are high noise immunity and low transmitter power. Practical examples of chirpsounder ionograms are presented by Fenwick & Barry (1967) and Fenwick & Woodhouse (1979) along with an assessment of the relative advantages and disadvantages of the method.

2.2.4 Backscatter

The backscatter technique employs a pulsed radio transmitter and a co-located receiver as would a conventional vertical incidence ionosonde. The signal is radiated obliquely and a small amount of energy is scattered at the ground in the direction of the downcoming signal. This travels along the return path back to the receiver (fig 2.2.4). Sounders of this type are described by Silberstein (1954), Shearman & Martin (1956) and Peterson et al (1959). An example of the results obtained from these sounders is given in fig 2.2.5, This shows the broad backscatter echo emerging from the two hop F trace on the familiar ionogram.

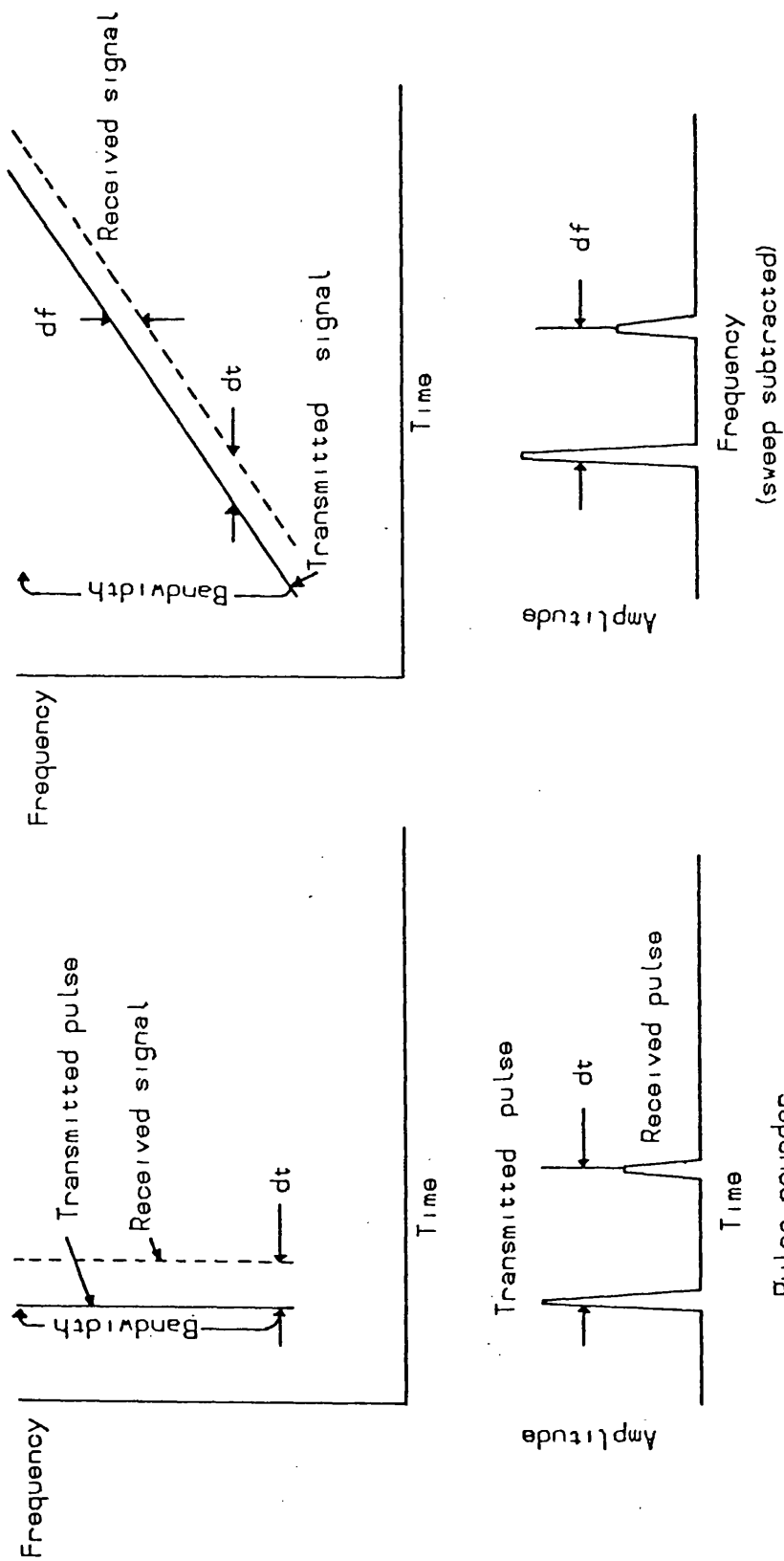


Fig 2.2.3 A Comparison of Pulse and Chirp Sounder Signals (after Fenwick 1966)

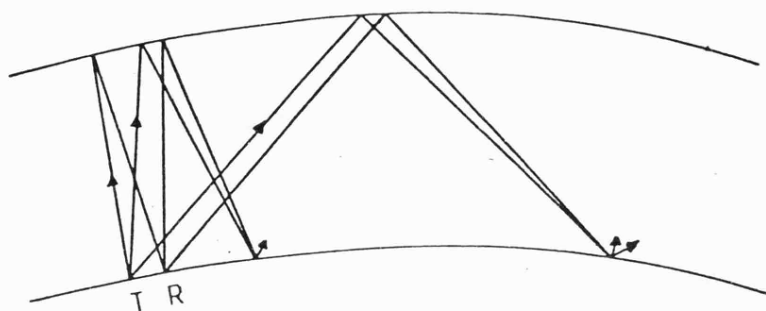


Fig 2.2.4 Geometry of Backscatter
(after Dieminger 1968)

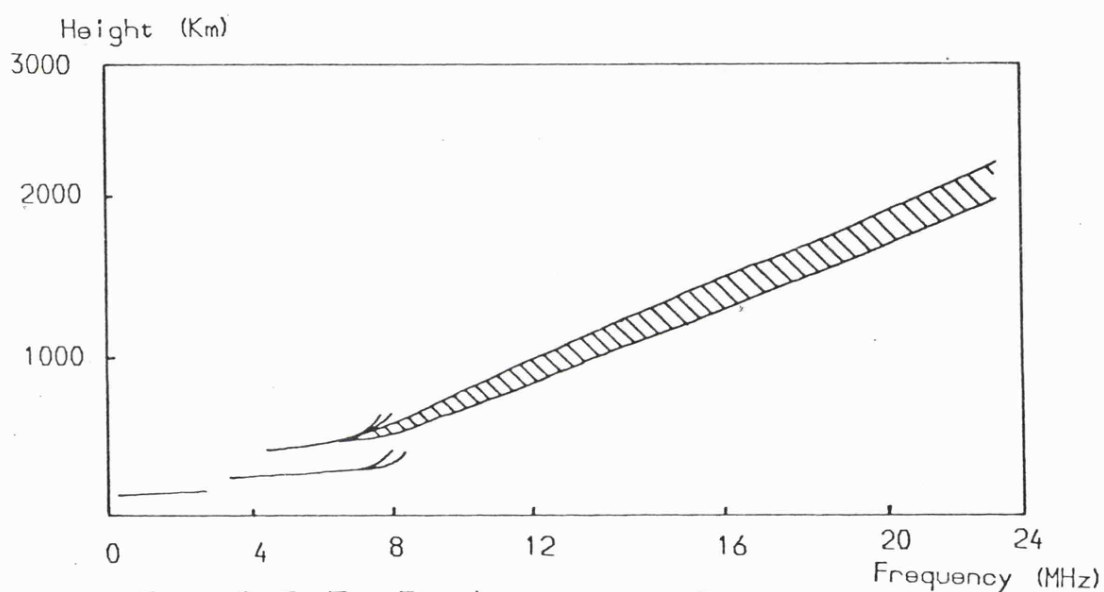


Fig 2.2.5 Backscatter Ionogram
(after Silberstein 1954)

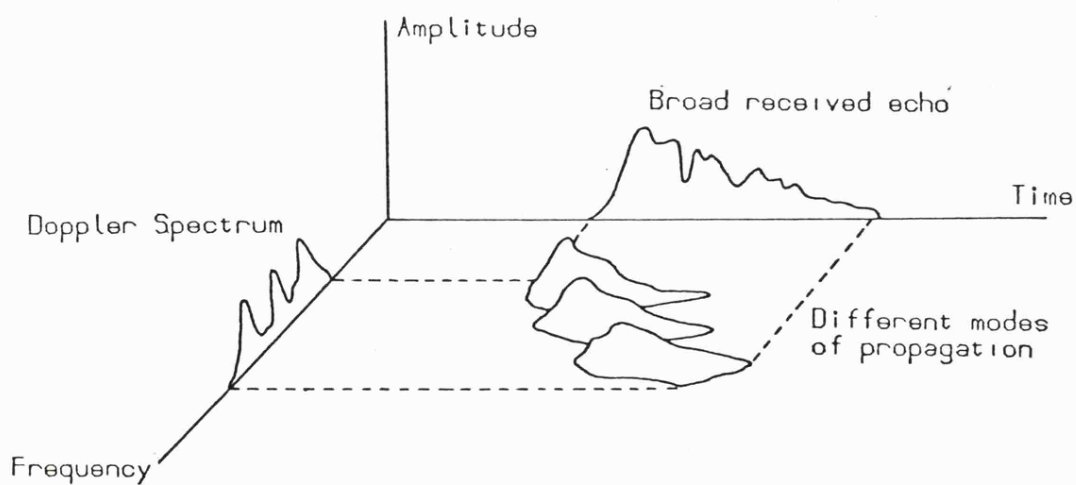


Fig 2.2.6 Mode Information from Backscatter
(after Goutelard 1977)

This powerful sounding technique can provide information regarding ground irregularities (eg mountains or sea state) in addition to ionospheric phenomena such as skip distances and travelling ionospheric disturbances (Tveten & Hunsucker 1969). More information can be obtained from the broad return pulse by subjecting it to frequency analysis. In this way different doppler shifts (section 2.2.5) induced by different ionospheric paths can be separated, thus giving mode content information about an oblique path from a single site sounder (fig 2.2.6).

2.2.5 HF Doppler

As mentioned in the previous section, radio waves reflected from the ionosphere can have a doppler shift imposed on them by the movement of the ionosphere at the reflection point (fig 2.2.7). In this way the movements of the ionosphere due to regular solar effects and disturbances can be measured. Early work of this type was carried out by Watts & Davies (1960) and Fenwick & Villard (1960). By monitoring three or four such paths, the movement of spaced reflection points can be measured simultaneously. From this information the speed and direction of any travelling disturbances can be determined by triangulation. The doppler spread introduced to a radio signal by the ionosphere is also of interest in HF communications applications and calculations of the magnitude of this effect are presented by Pickering (1975).

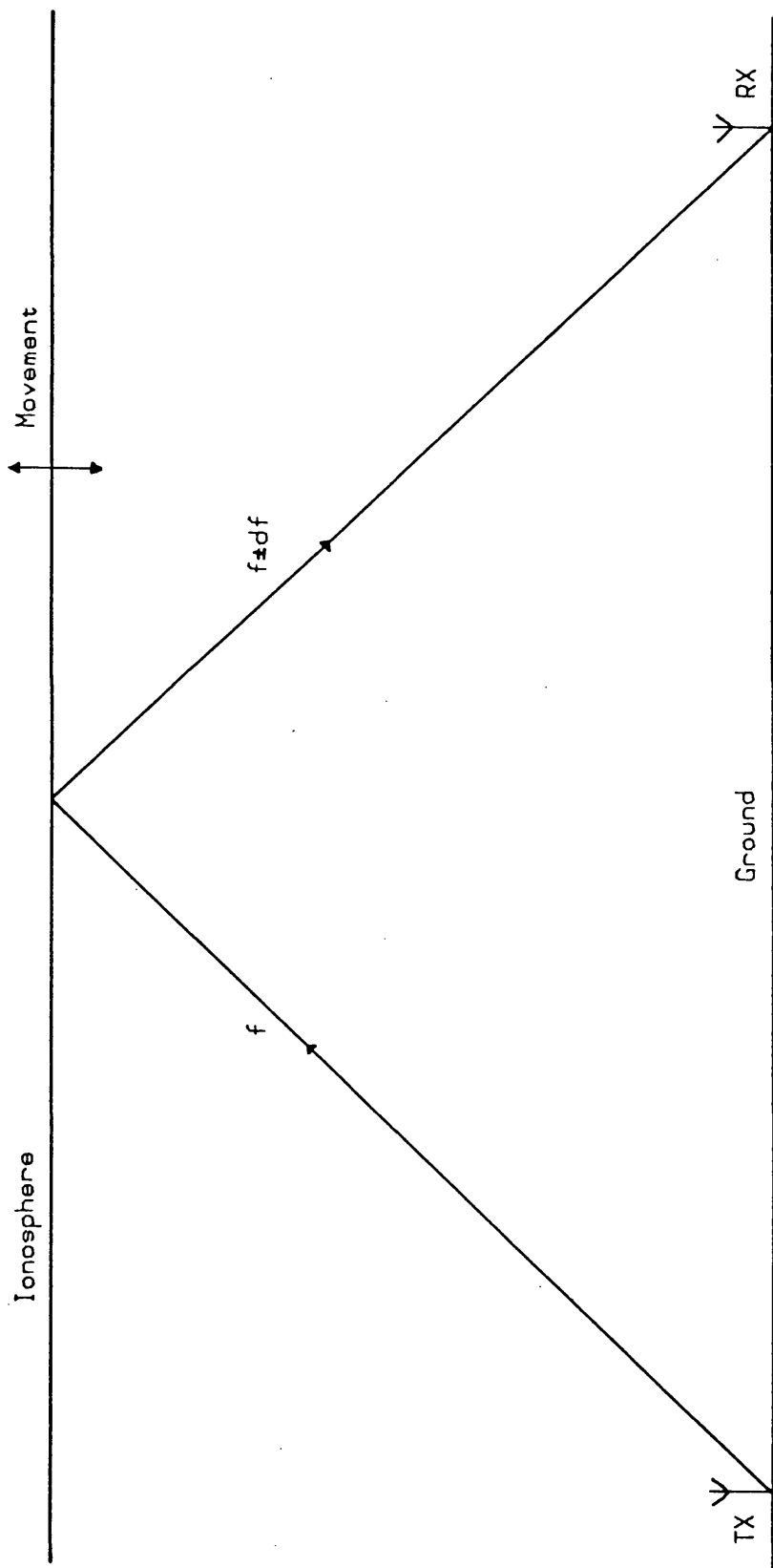


Fig 2.2.7 Movement of the Reflecting Layer Producing a Doppler Frequency Shift

2.2.6 Sounding in HF Communications

Sounding information has long been used to support radio communications. Monthly averages of ionospheric parameters provide the data base for long term predictions (section 2.1.1). Also real time sounding provides information regarding the conditions on a given path at a given time. To increase the benefits gained from this type of cooperation many modern communication systems incorporate a sounding element (eg Fenwick & Woodhouse 1979). A second example is the "Common User Radio Transmission Sounding" (CURTS) program (Probst 1968). In this work conducted by the Defense Communications Agency (DCA) a world-wide oblique sounder and noise monitoring network was set up covering the main HF trunk paths.

Information gathered by this equipment is digitised and sent to a central computer for analysis. The central computer then considers the frequency availability, path availability, resources required and the relative priority of the services, and outputs recommendations concerning the frequency allocations in order to optimise the continuity of the communications system.

Another sounding technique, this time developed for base to mobile rather than global trunk communications, is "Channel evaluation and calling" (CHEC) described by Stevens (1968). In this base station monitors local noise levels for a given channel and transmits this information to the mobile unit. This process is repeated for up to 16 allocated channels. The

strength and content of the received signal informs the mobile of the most suitable frequency for communication. A call facility is built into the system which allows any station to employ the sounding format to alert the other of an approaching transmission.

2.2.7 Pilot Tone

A typical example of a pilot tone sounding method was developed by J A Betts as a low cost in band sounding system capable of estimating data errors (Betts & Darnell 1975). A low power sounding tone is positioned in a gap in the normal signal baseband (fig 2.2.8). At the receiver this signal is extracted by a narrow filter and compared with a reference oscillator. The difference in phase between the two is detected and displayed as the phase error (fig 2.2.9). A close correlation exists between the phase error and the FSK data error. Other standby channels are also evaluated enabling the system to select the optimum frequency for communication and also predict the error rate for that frequency.

2.2.8 The Fadeogram

A Fadeogram (Filter et al 1978) is a method for displaying information regarding an ionospheric communications channel. Data is transmitted within the 3KHz channel bandwidth as 16 110Hz wide sub-channels of equal power (fig 2.2.10a). If selective fading takes place across the channel the received

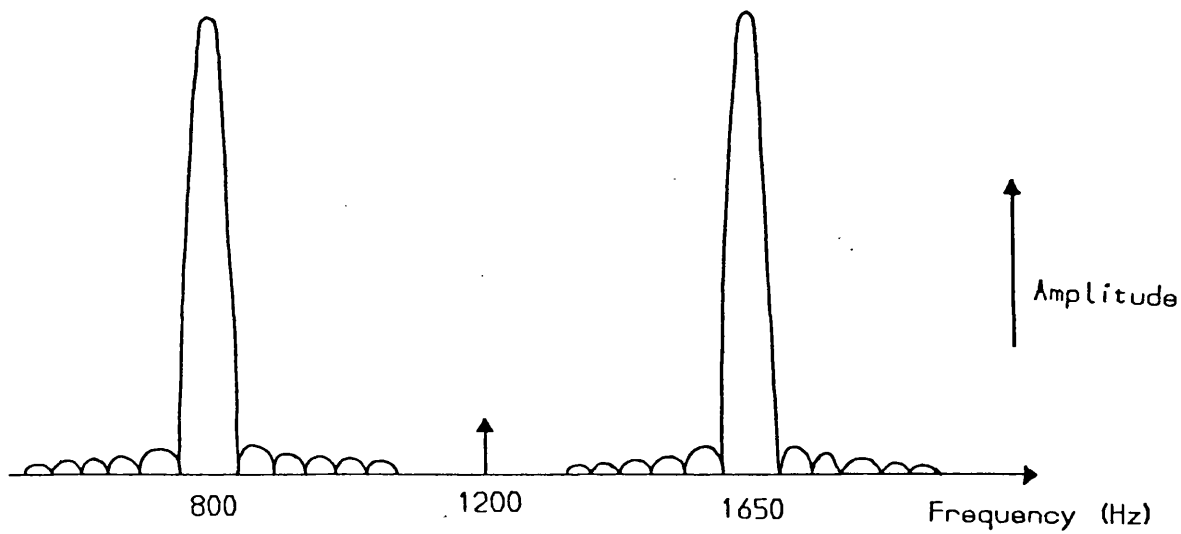


Fig 2.2.8 Baseband Spectrum of FSK Signal with Pilot Tone (after Betts 1975)

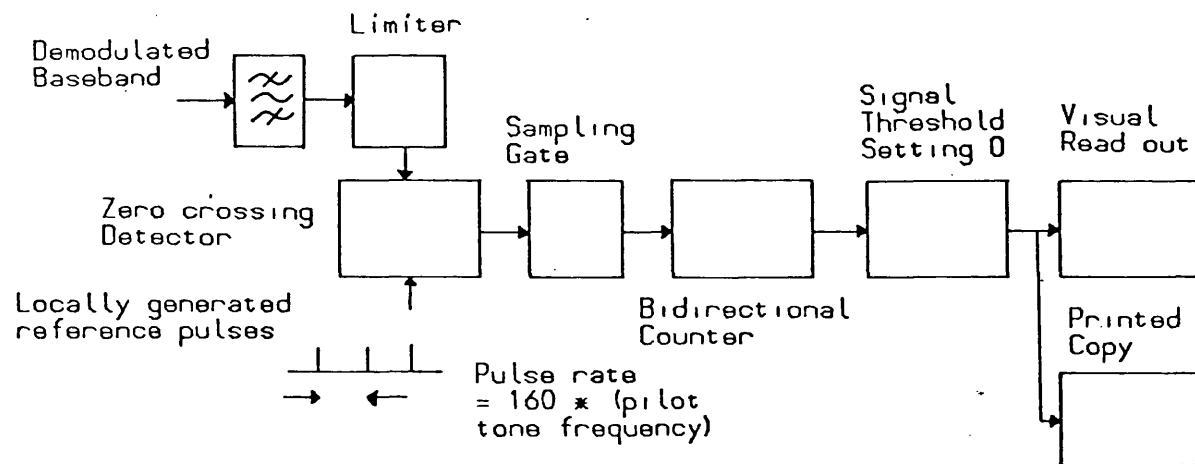


Fig 2.2.9 Pilot Tone Decoding Hardware (after Betts 1975)

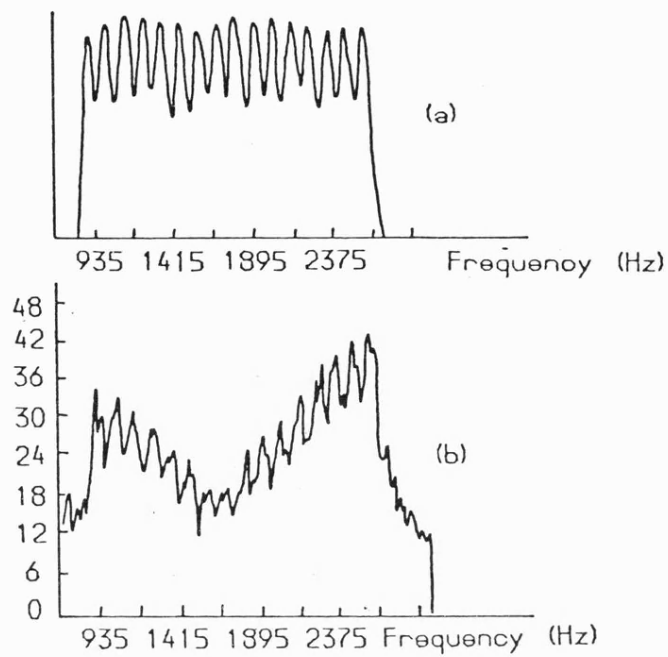


Fig 2.2.10 (a) Transmitted Signal
(b) Received Signal (after Filter 1978)

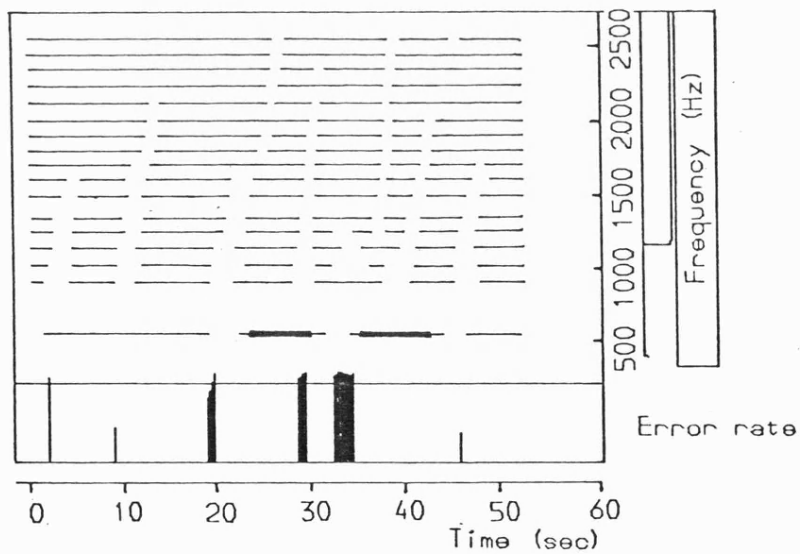


Fig 2.2.11 A Fadeogram (after Thompson 1979)

signal could be represented by fig 2.2.10b. In a fadeogram (fig 2.2.11) this selective fading is plotted against time to give a sonogram type display. This display can then be correlated against the error rate recorded by a modem data test set. This technique is particularly useful in recognising different types of fading.

2.2.9 Performance Sensing and Channel Estimation

Performance sensing is a method of estimating the quality of a received data transmission by monitoring the signal itself. Gooding (1968) developed a performance monitor unit (PMU) which could, without interrupting the data transmission, produce a pseudo error rate which was related to the actual error rate. This pseudo error rate was based on the measured confidence that could be attached to a decision made by a mark/ space threshold detector. The closer a decision is made to the threshold, the more likely it is to be in error. In this way a prediction of the actual error rate could be obtained.

Humphrey (1979) developed this idea further as part of an experiment to monitor factors connected with errors in data communication, such as noise and signal levels (fig 2.2.12). This leads onto the more general concept of "Real Time Channel Estimation" or RTCE (Darnell 1975a, Darnell 1979b). RTCE brings together all the sounding techniques already described in this section in addition to the types of information mentioned in fig 2.2.12. This provides a broader picture of the communications channel and the ionosphere in general. Darnell

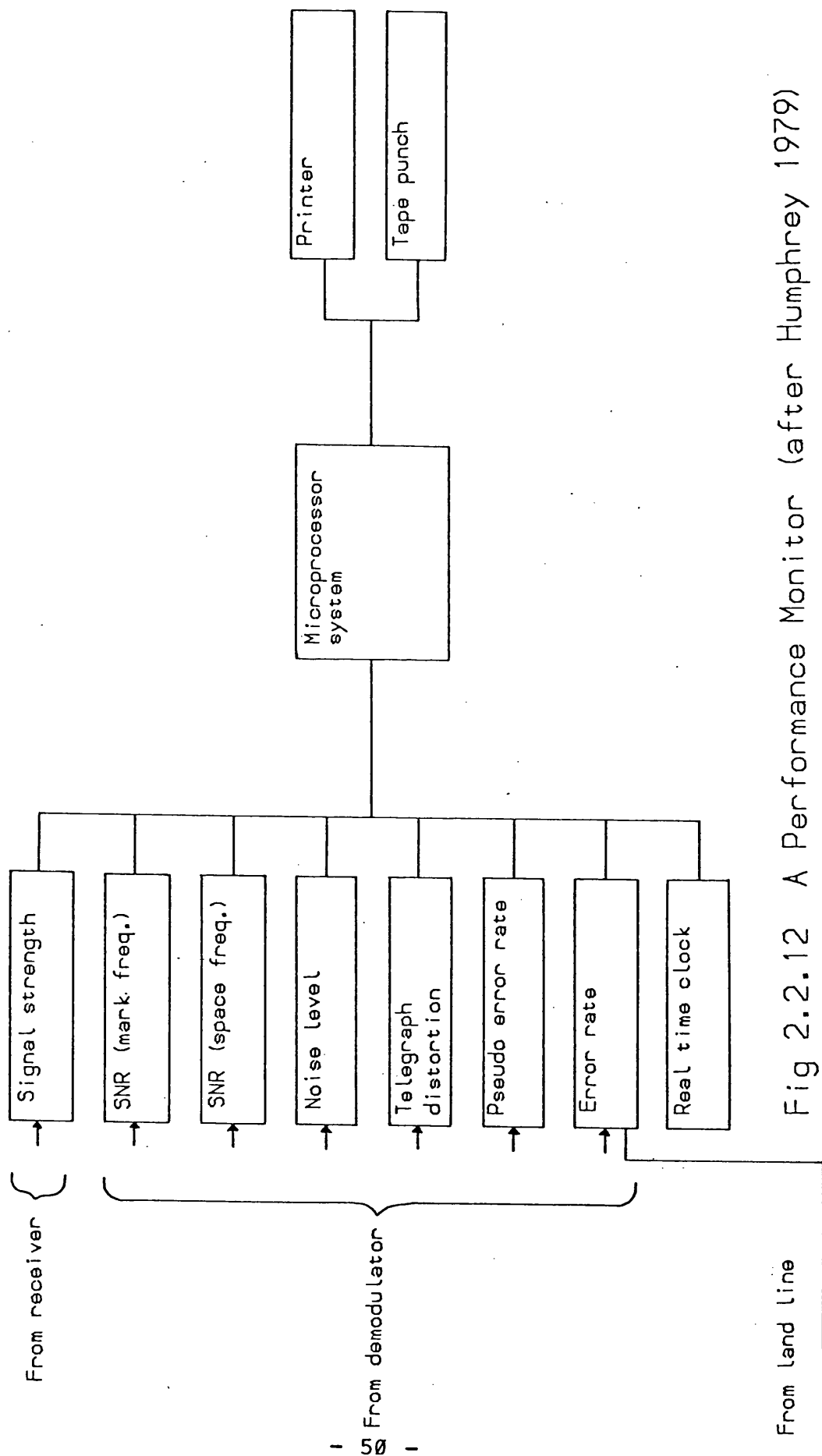


Fig 2.2.12 A Performance Monitor (after Humphrey 1979)

(1979b) presents a review of the available techniques, assesses the most useful ones for data communications, and lists the many obvious advantages of RTCE over a conventional prediction based system.

2.3 DATA COMMUNICATIONS

HF data communications via the ionosphere have always been subject to errors. These are caused by such factors as noise, absorption, multipath and doppler spread. The aim of the communications engineer is to reduce the errors caused by such effects to a minimum. This section describes some of the methods devised to achieve this aim.

A block diagram of a generalised communications link is presented in fig 2.3.1, and the sources of error or noise in such a link are indicated. Maslin (1979) calculates how these sources affect the reliability of the link. Many workers have studied the general problem of how to reduce error rates and improve reliability, outlining possible solutions (Knudtson 1968, Darnell 1975b, Darnell 1979a, Sloggett 1979). These solutions usually fall under the general headings of techniques to improve the propagation of the signal (eg frequency selection and antenna optimisation) or techniques which increase the immunity of the signal to ionospheric effects (eg modulation or coding). The remainder of this chapter is devoted to combinations of these two types of approach to improving system performance.

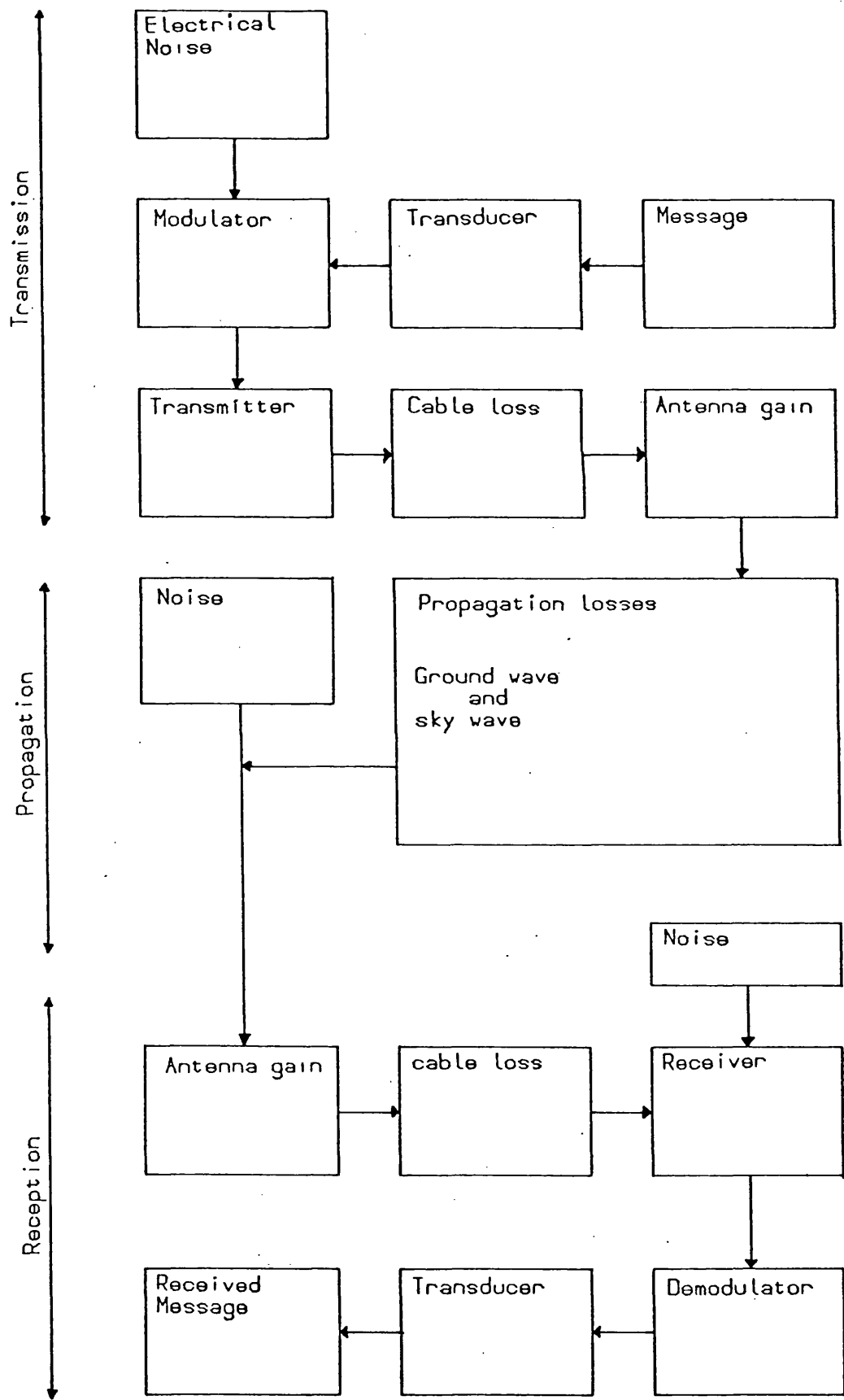


Fig 2.3.1 Schematic Diagram of a Communications Link (after Maslin 1979)

2.3.1 Frequency Selection

During an average day the optimum frequency for radio communication over any given link will vary with solar zenith angle, thus making a change in frequency essential (fig 2.1.1). Ideally a station should operate close to the predicted MUF to reduce both multipath and absorption effects to a minimum. The possibility of multipath interference is reduced by operating close to the MUF because only one propagation mode is then active. The factor that relates multipath to the operating frequency is the multipath reduction factor or MRF (Bailey 1959). The factor required to provide protection against multipath in excess of 2ms for a given path length is plotted in fig 2.3.2. This concept has been extended by Salaman (1962) and Pickering (1975). Pickering's work introduces a similar concept for protection against doppler shift. The MRF sets a lower limit on the operating frequency for data communications for a given data transmission rate.

The optimum procedure for choosing the operating frequency is by means of real time sounding (Darnell 1979b). In this way it is possible to take advantage of conditions on a given day to reduce multipath to a minimum (eg fig 2.3.3) rather than rely on less accurate predictions (section 2.1.1) based on average conditions.

2.3.2 Diversity Operation

A well tried method of reducing the effect of multipath

MRF = Operating frequency/MUF

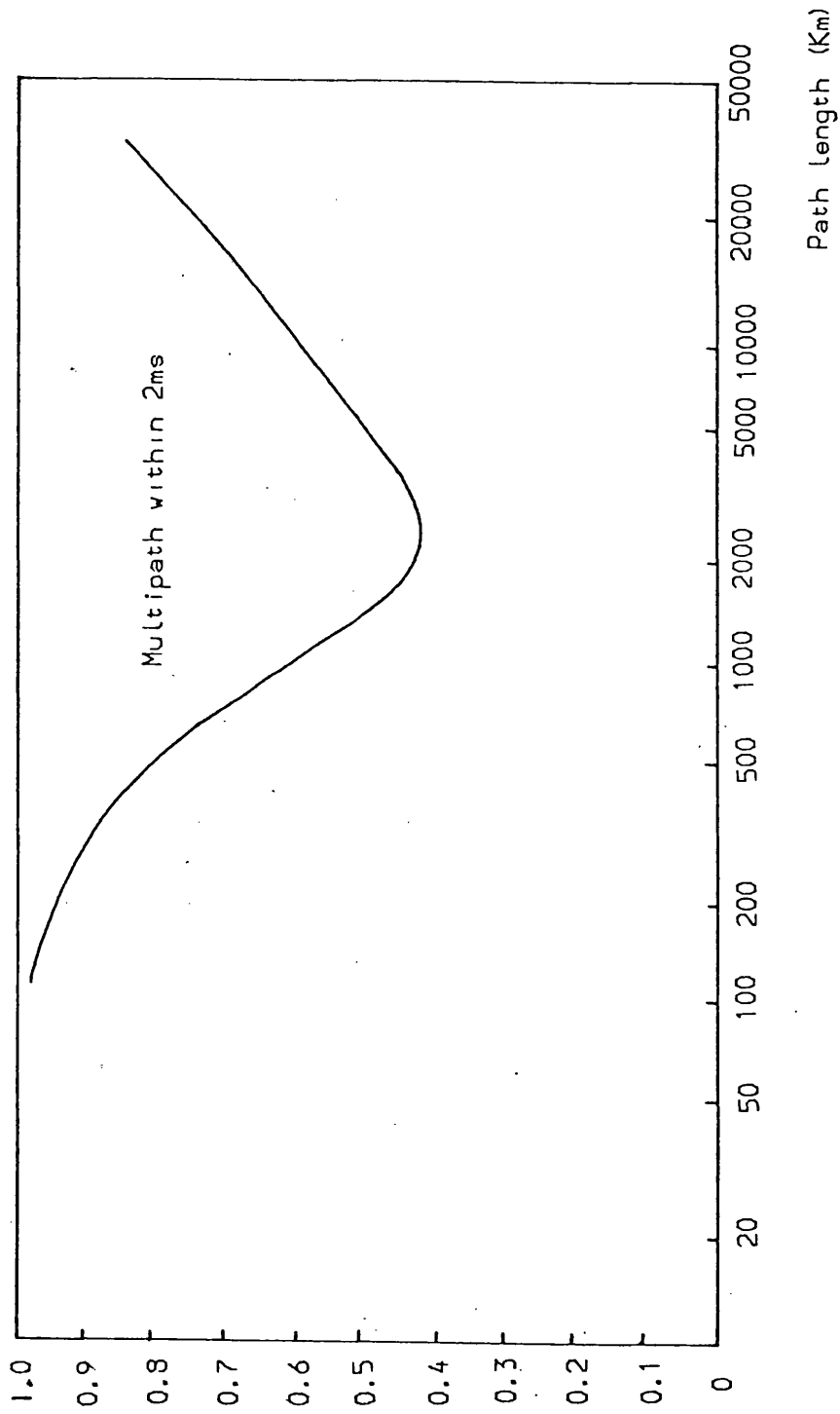


Fig 2.3.2.2 Multipath Reduction Factor (after Bailey 1959)

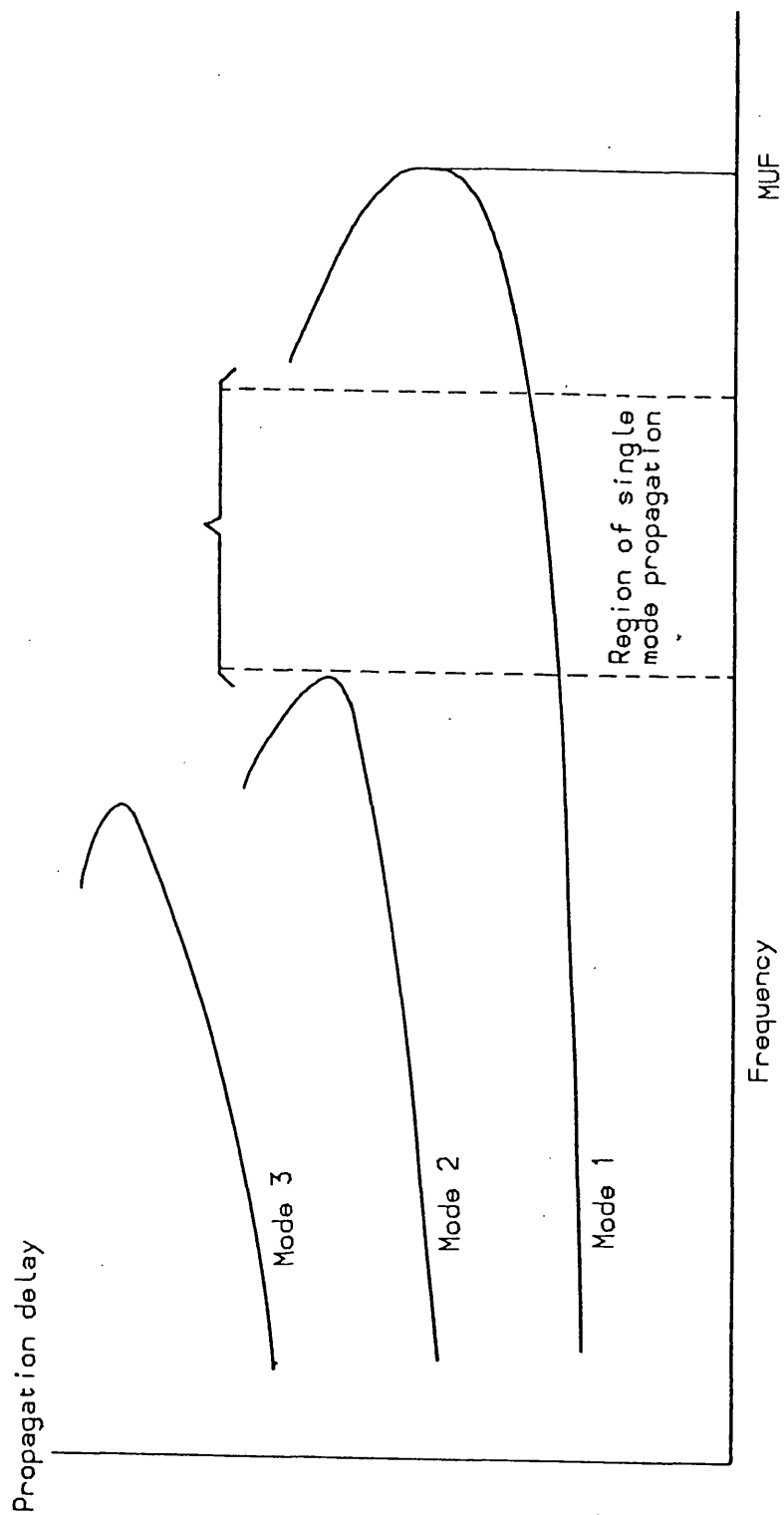


Fig 2.3.3.3 Single Moded Conditions (after Darnell 1977)

fading is that of diversity reception (Bond 1957). This technique relies on the change of relative phase of signal over relatively short distances on the ground, so if two antennas are spaced 100m apart, a fade-out is unlikely to occur simultaneously on both. The actual recommended spacing varies from 10 to 20 wavelengths with an absolute minimum of 4 (HMSO 1938). The method of combining the signals from both antennas has been the subject of much research. A standard technique is the so called equal gain combiner in which each antenna is connected to a different receiver, the outputs of the receivers are combined at baseband and the amplitude of the combined signal drives a common AGC on both diversity receivers. Thus the stronger of the two signals will be heard and the noise will be reduced. Improved combiners are available for particular situations such as unequal strength antenna arms (Barrow 1963), HF interference (Gott & Dutta 1979) and frequency selective fading (Susans 1979).

2.3.3 Adaptive Multipath Measurement

If the communications link is to operate on a fixed frequency and diversity techniques can not be applied, some other technique for improving performance is required. Such an alternative approach is to determine the mode content of the received signal and then by adaptively adjusting some system element, reduce the unwanted modes so the wanted mode is dominant. In this way fading and hence data errors are reduced. A typical example of such a system is RAKE (Price & Green

1958). A block diagram of RAKE (fig 2.3.4) demonstrates the important elements of the system. Mark and Space bits are sent by transmitting one of two broadband reference signals. After transmission via the ionosphere and reception, all the signals from the different paths are fed into a tapped delay line. The tap outputs are then compared with mark and space references identical to those generated at the transmitter. When a good correlation is achieved a mark or space is said to have been received at that tap. The correlation pattern along the line will represent the time dispersion of the ionospheric channel (eg if only taps 1 and 3 showed good correlation then two moded propagation would be deduced). As the multipath arrival time pattern is known, the signals from the shorter ionospheric paths can be delayed by the line to arrive at the detector at the same time as those from the longer paths, thus utilising all the signal components for a good decision. This system works well but is very complex, costly, uses much bandwidth and as a result is badly affected by noise.

Other more recent examples of this type of approach are presented by Coll (1968) and Morgan (1978). Both employ tapped delay lines (fig 2.3.5) but rather than deriving the tap multiplication factors from what is essentially an in built sounding signal, uses an iterative search process, a simple example of which is given in fig 2.3.6. Tests (Morgan 1978) indicate that the process is capable of removing the multipath errors with data rates as high as 2.5 kbaud.

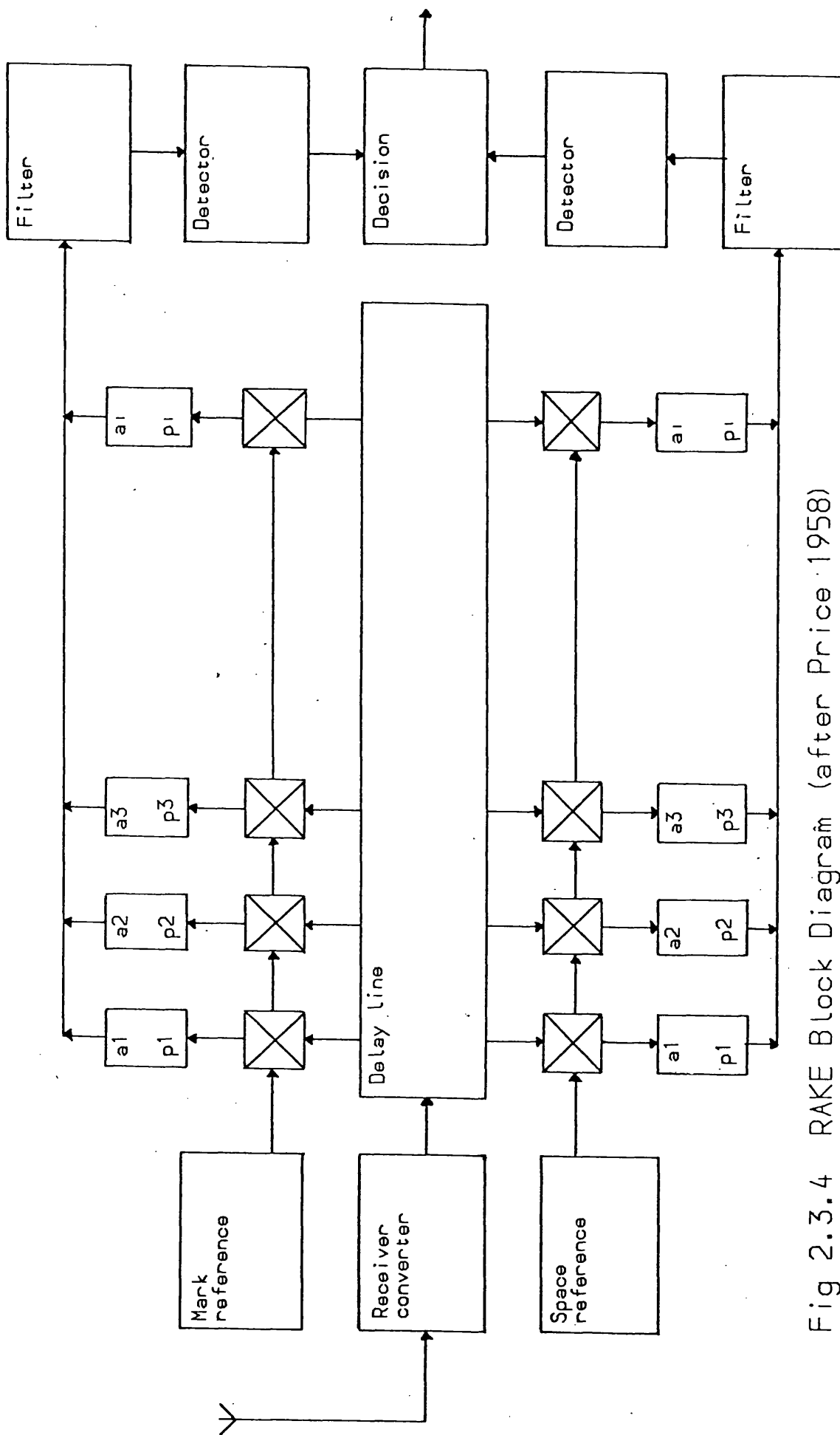


Fig 2.3.4 RAKE Block Diagram (after Price 1958)

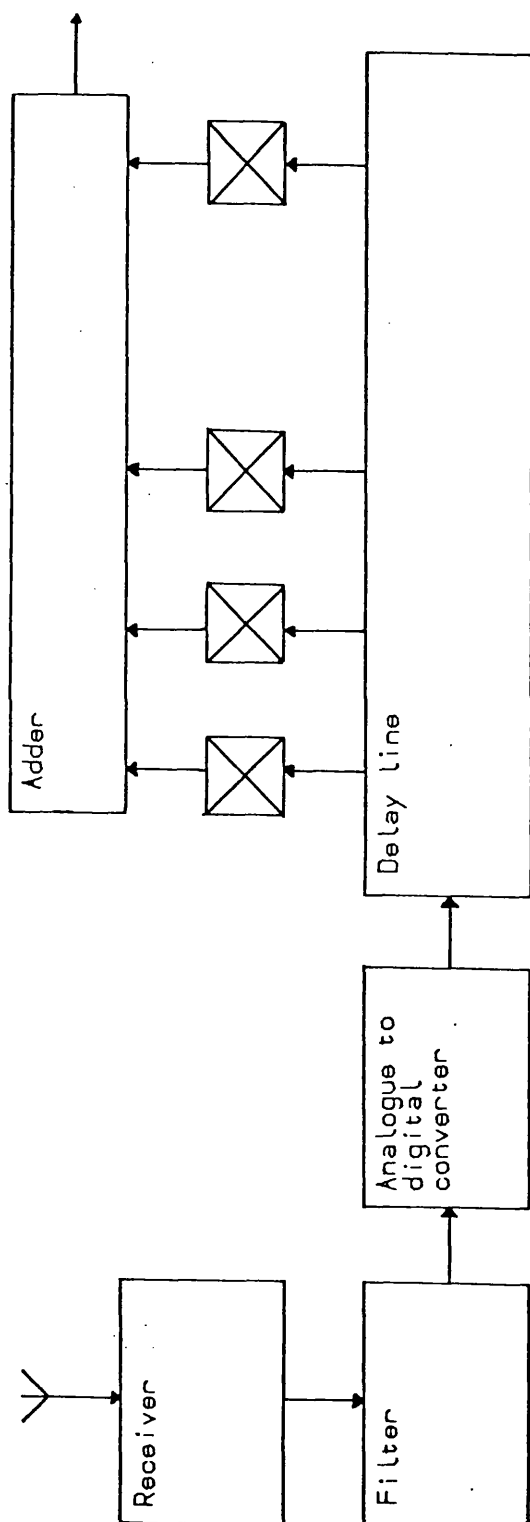


Fig 2.3.5 Adaptive Receiver (after Coll 1968)

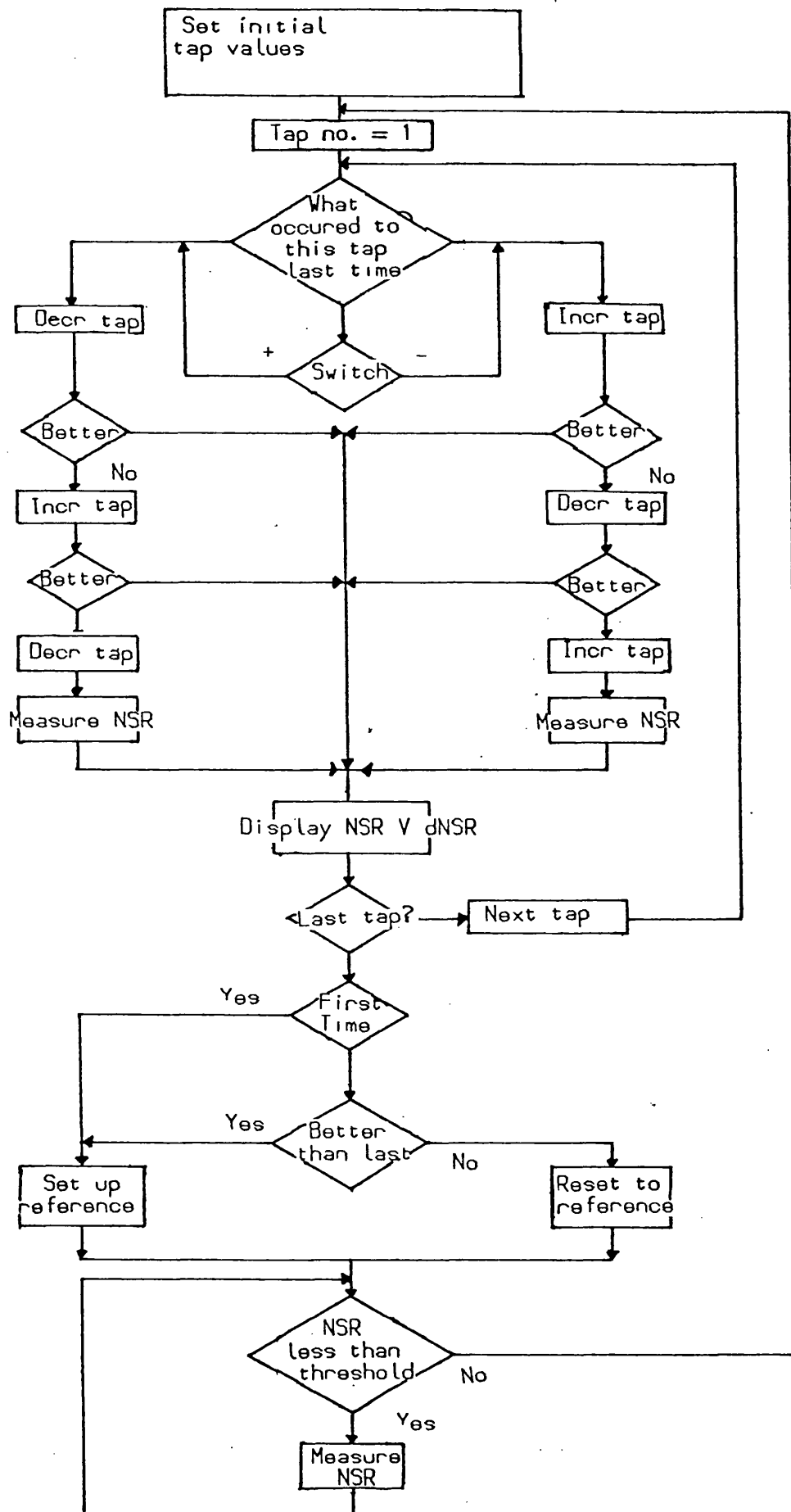


Fig 2.3.6. Flow Chart of Simple Search Procedure (after Coll 1968)

2.3.4 Steerable Antennas

When radio waves travel through the ionosphere over several different paths, the arrival angles of these paths at the receiver are different. Multipath interference can therefore be reduced by selecting a particular mode by means of an antenna having a steerable maximum in elevation angle.

Early work (Bruce 1931) describes a phased array of antennas which could be steered in this manner. This idea was further developed (Friis et al 1934, Friis & Feldman 1937) by investigating the arrival angle of the various modes by means of a pulsed sounding signal. This was first undertaken with fixed antennas of known radiation pattern but later with a MUSA (multiple unit steerable antenna) as reproduced in fig 2.3.7. These studies were conducted during 1935, 1936 and demonstrated that the system worked well but was very costly to implement. The work described in this thesis will eventually form part of a modernised version of such a system which will be capable of operating automatically under computer control.

Considerable attention has been given to the problem of determining arrival angle in both azimuth and elevation because of their importance in direction finding and range estimation (Gething 1969, Baulch & Butcher 1978, Clarke & Tibble 1978). Vertical and horizontal antenna arrays have been developed which can detect the various elevation angles of the received components of a multipath signal. Clarke & Tibble (1978) examine the possibility of reducing the effect of multipath

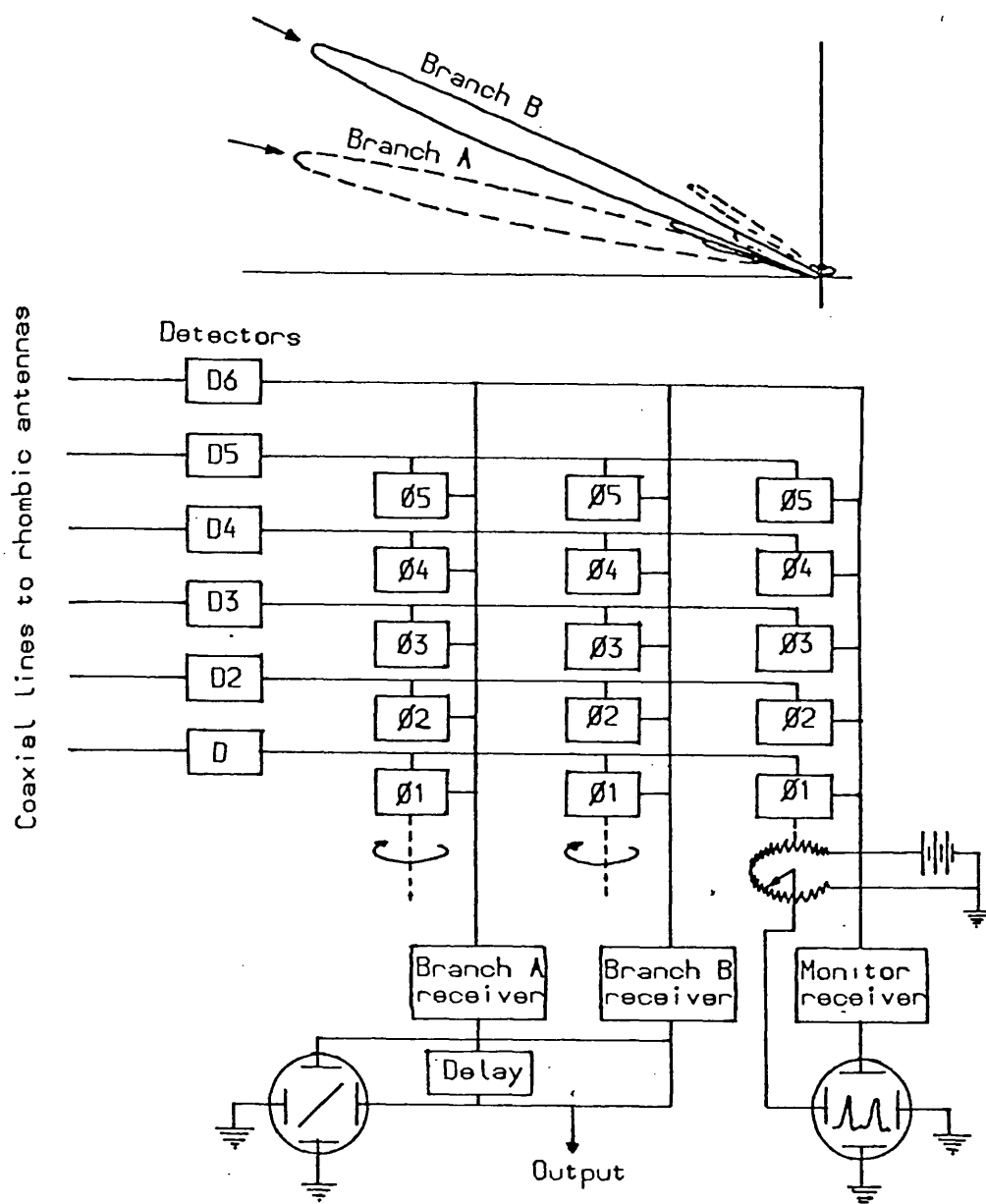


Fig 2.3.7a Schematic Diagram of the Experimental MUSA Receiver (after Friis 1937)

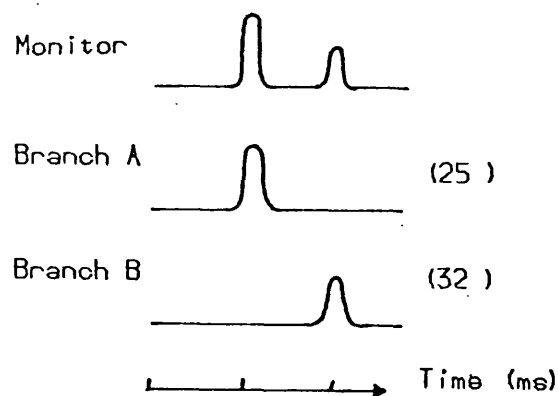


Fig 2.3.7b Results for Rugby Holmdel Path Showing Separation (after Friis 1937)

interference by means of a steerable antenna and conclude that improvements can be achieved for multimode conditions but not for in mode fading. The time of flight and elevation angle differences for the wave components responsible for in mode fading are so small that they cannot be resolved by the antenna pattern. An introduction to the subject of beam forming and null steering is presented by Gabriel (1976).

2.3.5 Modulation Types

As mentioned briefly in section 1.3 there are many different methods of transmitting data in digital form over an HF radio link. For slow speed transmission the earliest method was on- off keying of the carrier wave using the Morse code. This provides a slow, reliable, narrow bandwidth (and hence high noise immunity) communications link. As a consequence of the need for faster communications the teletype was developed and FSK modulation introduced. A rather large frequency shift of 850Hz was originally employed compared with the more narrow band systems currently available.

Multiple frequency shift keying or MFSK (Darnell 1979a) increases the number of tones (one for each character). The signal is decoded by means of quenched resonators. The best known example of this type of system is "Piccolo" (Robin et al 1963, Bayley & Ralphs 1972) designed to provide 75 baud data transmission. Due to the slow (10Hz) signal rate and the quenched resonator method of detection, the system is very tolerant to noise, being more reliable than even a skilled

Morse operator under severe noise conditions.

"Phase shift keying", PSK (Voelcker 1960) or "differential phase shift keying" DPSK (Darnell 1979a) offers many advantages over FSK. Here the difference between a mark and a space is indicated by a phase shift in the received signal of 90 or 180 degrees and therefore requires only a modest bandwidth. This leads to higher noise immunity and lower band congestion. Jones(1968) compares the effect of multipath reception on both FSK and DPSK modulation schemes. Error rates measured with these techniques are described by Ames (1969) for FSK and Goldberg (1961) for DPSK. Many methods have been developed to reduce system errors, some typical examples of these are now presented.

If a two way communications link is employed, an answer back feature can be built into the system. Thus, if a block of bits is received in error (detected by coding) the feedback link can request retransmission until the errors are eliminated. In a more advanced version of this method (Darnell 1981), several different data rates are sent simultaneously and the feedback link is used to inform the transmitter of the highest data rate correctly received which in turn controls the starting point of the next block in the message.

Under multipath conditions, a high baudrate may cause errors due to the multipath delay being of the same order of magnitude as the bit length. This problem is further discussed in section 2.3.1. This type of multipath induced error is reduced in most modern systems by splitting the 3KHz channel into sub- channels. Thus several slow speed signals can be sent

simultaneously in the same channel to give high overall baudrate. Within the sub- channels either DPSK or PSK modulation schemes can be employed. The relative benefits of the various modulation methods are discussed by Ridout & Wheeler (1963) and Dripps & Rosie (1979). When interference is present all of the sub- channels can not be employed simultaneously (Gott & Stainforth 1978). Darnell (1979c) describes an in band sub-carrier selection procedure which identifies the least noisy sub- channels and communication then takes place on these.

An example of a commercial multi- channel modem is provided by Kineplex (Doelz et al 1957). The 3KHz voice channel is split up into 20 tones, each working at 75 baud giving a total of 3000 baud. As in the Piccolo system the resonator method of detection is employed for good noise resistance. A second example is provided by the AN/GSC-10 or Kathryn modem (Zimmerman & Kirsch 1967). In this system 34 sub- channels are provided within the normal 3KHz voice band working up to a total data rate of 2550 baud. Its advantage over the previous example being greater flexibility, allowing many different data rates and containing a RAKE type channel monitoring capability. The effect of selective fading on this modem are discussed by Bello (1965). The high data rates allowed by these multichannel modems enable both teletype messages and digitised speech to be sent through the same system (Strassman 1961). A comparison of the modems mentioned above and several other commercial units is given by Strussynski & Gott (1970).

2.3.6 Soft Decisions

In a normal data demodulator a hard decision process is employed and a bit is defined as a '0' or a '1'. This process inherently discards information present in the received signal which could improve system reliability. To make use of this information a soft decision decoder is required (Darnell 1975b, Farrell & Monday 1979). The output of such a decoder is illustrated in fig 2.3.8 for a simple amplitude modulation scheme. A confidence factor or soft decision distance (number of confidence thresholds between the measured and maximum confidence) can thus be defined for a given bit. This information is of considerable value in real time channel evaluation techniques (Darnell 1979b).

When the confidence factor is combined with a coding scheme, data error correction is possible (Goodman et al 1979, Farrell 1979). For example, if an error detecting code recognises that two bit errors are present in a given block of data then the two bits with the maximum soft decision distance (nearest to the decision threshold) are taken to be in error and are therefore corrected. This gives an error correction ability not available with the hard decision decoder unless a higher level of coding is adopted.

2.3.7 Coding

When data is transmitted over a communications link it is important to know how many of the data bits are in error. This

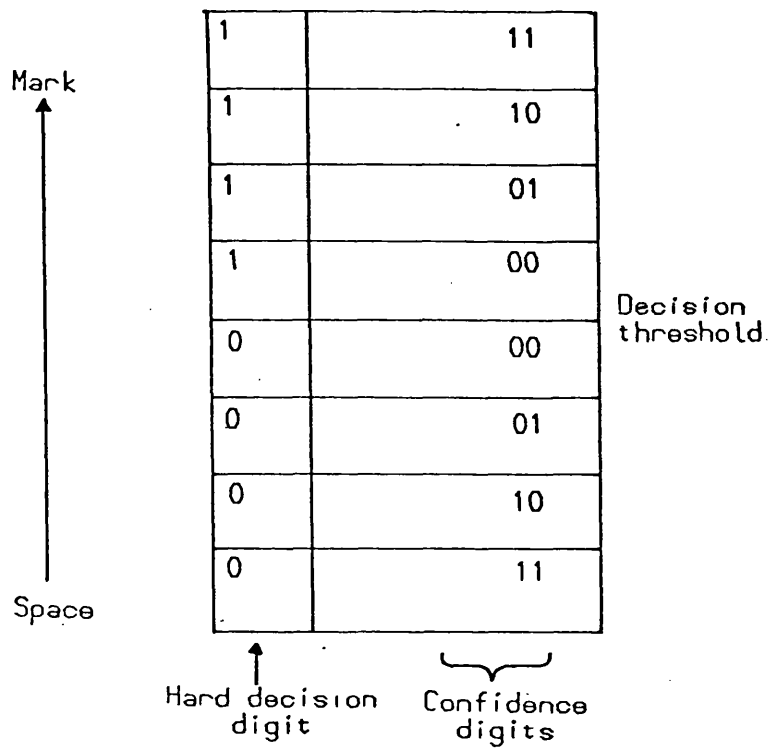


Fig 2.3.8 Eight Region Soft Decision Quantisation (after Farrell 1979)

can be achieved by introducing some redundancy into the message in the form of a test code. The simplest form of such coding is known as parity checking. An extra bit is added to each data word to make the number of '1's in a word even or odd, depending on the type of parity employed. At the receiver the word is checked and if the parity is incorrect at least one bit (or any odd number of bits) in the word is known to be in error. This code is only suitable for very low error rates as an even number of errors can not be detected.

To overcome these deficiencies more complex codes were developed such as the Hamming code or the block code. Block codes take the parity idea further by combining several data words into a block, then calculating parity sums across the rows and down the columns. With this matrix like format it is possible to correct data errors. Chase (1972) describes how block codes and soft decision information can be combined to yield more reliable data.

The degree of coding required to recognise errors under given conditions varies with those conditions. Goodman & Farrell (1975) describes a method for varying the redundancy to adapt to the changes in conditions and hence maintain efficiency.

Under normal HF conditions data errors tend to arrive in bursts, thus defeating a normal error detecting code. To overcome this the interleaving process was developed in which several coded blocks of data are sent bit by bit in rotation. This ensures that the burst of data errors is spread out over several coded blocks allowing easier decoding. Examples of work

employing this technique are presented by Fritchman & Leonard (1965), Brayer & Cardinale (1967) and Pennington (1979).

To achieve high immunity and fast data rates, many advanced coding schemes have been developed (eg Galager, Massey, Goulay and BCH) and have been reviewed by Brayer (1971). It is worth noting that under noisy conditions error correcting codes, however complex, may not be the best solution for the removal of data errors. An evaluation of error rates in the presence of noise and fading by Ralphs (1971) indicated that a conventional FSK modulation link with advanced error detection codes was outperformed by a simple unprotected Piccolo MFSK modulation system (Robin et al 1963).

2.4 CONCLUSIONS

Several methods are available for improving HF communications system performance. These include frequency selection, diversity, multipath canceling, steerable antennas, coding and soft decision techniques. For optimum communications on a given path some combination of these methods would be required, typically frequency agility, error correcting codes and some form of mode selection.

Channel estimation experiments show that there is a dependence between the correct mode selection and a reduction in the recorded error rates. This is what is to be exploited in the present study.

CHAPTER 3

OUTLINE OF THE PRESENT INVESTIGATION

3.1 PULSE SOUNDING FORMAT

The pulse sounding signal briefly mentioned in chapter 1 was developed by the Royal Aircraft Establishment (RAE) as part of a test facility for an elevation steerable antenna. Its purpose is to allow the operator to determine which modes of propagation are present in a received signal and thus to evaluate the influence of a particular antenna radiation pattern on the mode content. The aim is to select a single optimum mode of the received signal to reduce multipath modal interference to a minimum.

The format of the pulse sounding signal is reproduced in fig 3.1.1a. It consists of a sounding pulse 0.7ms long in the centre of a break in the carrier of 21.8ms. The entire sequence is repeated every 90ms. The pulse is of this length so that it can be contained within a normal voice communications channel (3KHz) bandwidth. The sounding pulse is made as short as possible to facilitate the resolution of the modes by measuring the times of flight of each mode. If the pulse was shorter it would spread over a greater bandwidth or it would be filtered out by a normal communications transmitter. The exact length of the pulse results from the availability of a commercial crystal whose frequency was a convenient multiple of that required

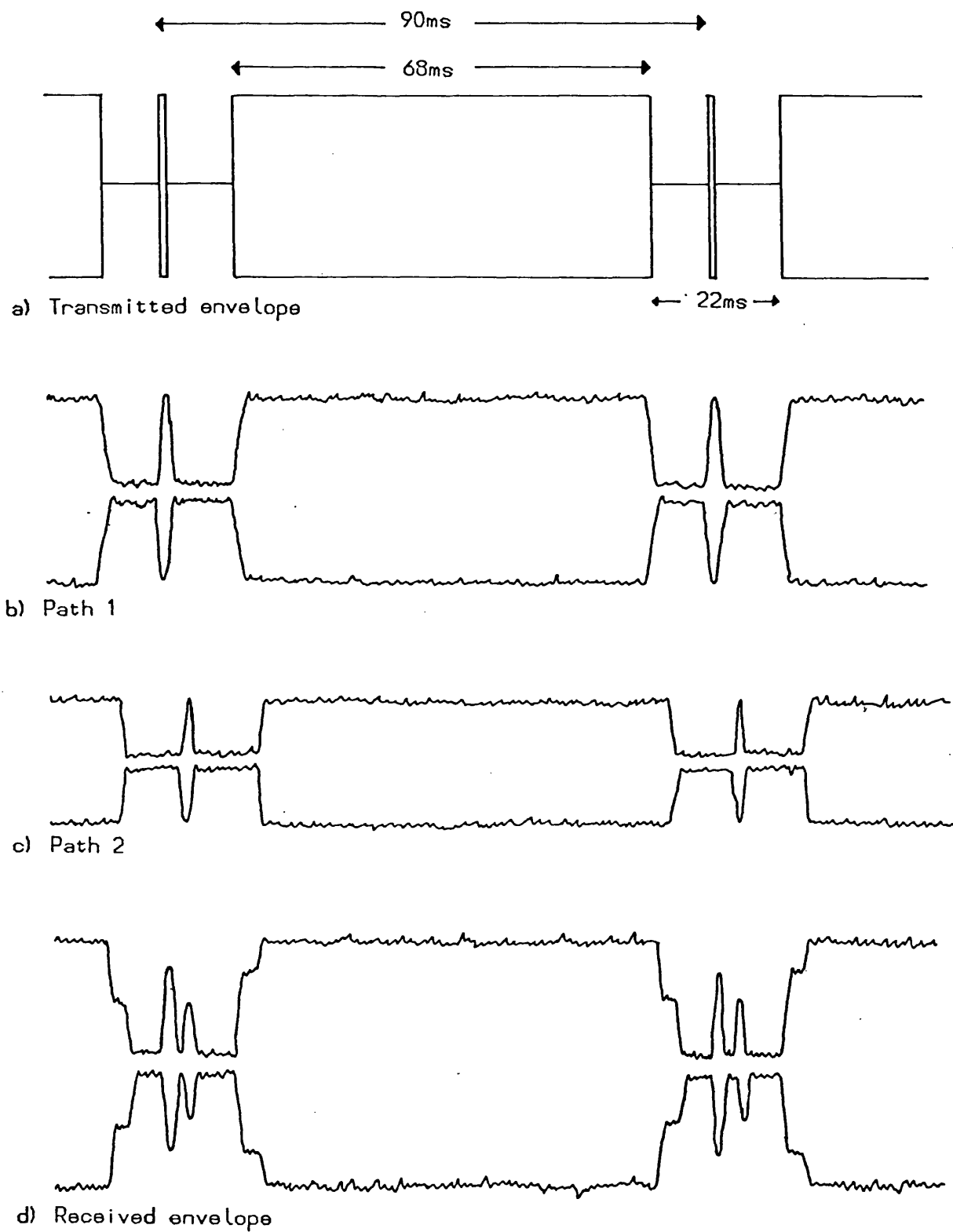


Fig 3.1.1 Pulse Sounding Envelopes

(section 4.5). The duration of the gap surrounding the sounding pulse corresponds to the original estimate of the maximum possible observable delays between modes in a multimode situation (ie a difference of 11ms between the longest and shortest time of flight. The 11ms gap ensures that the sounding pulses are not confused with the large blocks of carrier. The blocks of carrier keep the automatic gain control (AGC) of a standard radio receiver down so the sounding pulses are clearly visible and the receiver does not limit. The exact lengths of both the gap and the carrier block are again selected for convenience, being 31 and 97 times the length of the sounding pulse respectively ($31+97=128$).

When the sounding signal is transmitted via the ionosphere (fig 1.4.3) more than one propagation path is usually possible. In the figure 1 hop F and 2 hop F propagation paths are indicated. These will result in the sounding signal arriving at the receiver at different times and with different amplitudes and phases (fig 3.1.1b and 3.1.1c). With a normal omnidirectional antenna these two waveforms would be added vectorially to give fig 3.1.1d which contains sounding pulses from both modes. In this instance the two blocks of carrier add constructively but this is not always the case and cancellation could equally well occur. One of the main aims of this research project is to detect and resolve this combined signal automatically.

As indicated in fig 3.1.1 the transmitted pulse is dispersed by the process of propagation and probably to an even greater extent by the transmitting and receiving equipment.

This process leads to a deterioration in the ability to resolve pulses with closely similar times of flight.

3.2 DATA SOUNDING FORMAT

To make a quantitative assessment of how successful the steerable antenna is at reducing multipath interference, a test data sequence was developed. This enables the reduction in error rate observed by employing the steerable array to be quantitatively determined. The construction of the steerable antenna was considerably delayed and unfortunately it was not available during the period of the project. As an alternative the test data sequence has been used to examine the correlation between the mode content of the signal as determined by the pulse injection sounding technique and the error rate.

The data sequence itself consists of 1125 bits of on/off keying, a 33 bit Barker code for synchronisation, and finally a 1023 bit pseudo random sequence (PRS) over which the error rate is measured (fig 3.2.1). In the RAE sounding system the data was sent as 75 baud FSK. Due to equipment limitations the transmissions observed in this thesis were all sent as CW, carrier on or off. By employing a micro-computer to generate the PRS, different data rates could easily be generated. Of these the most common were 50, 75 and 600 baud.

The 1125 bit on/off keying at the start of the test sequence is used for bit synchronisation. This length gives the receiving equipment time to be sure of locking on to the sequence. It consists of alternate '1' and '0' bits providing

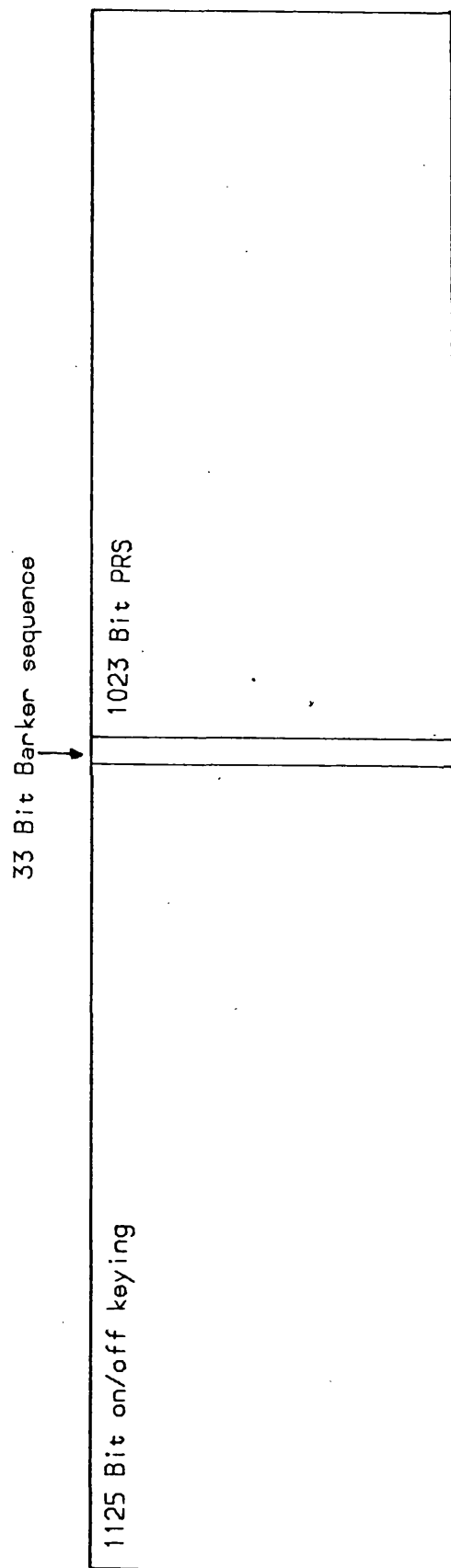


Fig 3.2.1 Data Sequence Format

as many transitions as possible. A transition defines the boundary between one bit and the next, therefore it is vital to know when one arrives in order that the exact arrival times of the following bits of information can be accurately predicted.

The next part of the test data sequence defines the bit that starts the PRS itself. This is achieved by inserting a Barker code synchronising block (Barker 1953) before the start of the PRS. A Barker sequence is a set of '1' and '0' bits which when correlated with itself produces a maximum when the sequence has been recognised and a value of 1 or 0 at all other times.

Barker sequences are found to obey the following rules :-

- 1) The number of digits must be one less than an integral multiple of four.
- 2) If the digits are paired counting from both ends, the odd pairs must be different and the even pairs alike.

The simplest patterns are :-

110

1110010

11100010010

Longer patterns have not been found and it is considered unlikely that they exist although this has not been proved. The auto- correlation functions for the 3 bit and 7 bit codes are given in fig 3.2.2. The auto- correlation function is defined as the sum of all the bit comparison results. A bit comparison results in a '1' if the bits are alike and a '-1' if they are different. This provides an excellent method for synchronising the start of the data as it does not depend on detecting all

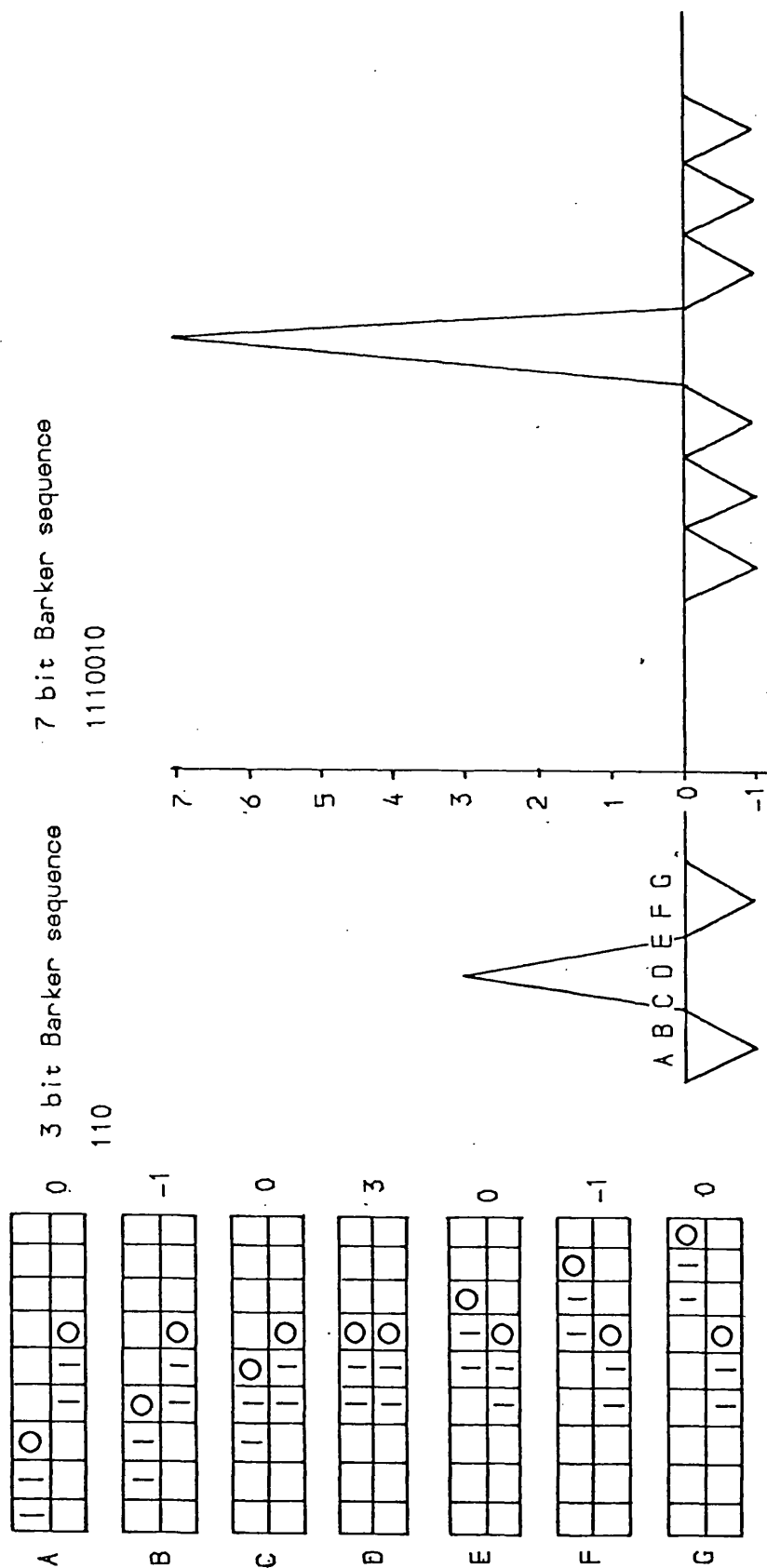


Fig 3.2.2 Barker Sequence Auto Correlation

the bits and has therefore a certain noise immunity.

For the longer sequences, the sync pulse is more distinct than for the shorter sequences, therefore as long a sequence as possible is desirable to ensure synchronisation. The upper limit on the length is governed by the time taken for the computer to carry out the correlation.

Although the longest known Barker sequence is only 11 bits long, sequences with similar properties can be found by combining several Barker sequences in the following way: Take a true Barker sequence and replace every '1' in it with a second Barker sequence and every '0' with the inverse of the second sequence. An example of this method utilising two 3 bit sequences can be seen in fig 3.2.3. The sequence adopted for the test data format combines a 3 bit and an 11 bit sequence to give a 33 bit sequence. This has a very distinct peak which enables the start of the data to be easily recognised (fig 3.2.4).

After the Barker code is the 1023 bit PRS, which is produced as follows: A ten bit shift register (fig 3.2.5) is initialised with all bits high. When the shift register is clocked the first bit is filled with the result of an exclusive OR of the previous bits 5 and 10. The output of the PRS generator is taken from the tenth element of the shift register. For an N bit shift register the length of the sequence produced is L.

$$L = (2^{*N}) - 1$$

In the present case leads to a length of 1023 bits before repeating. This type of sequence was chosen since it is easy

A nine bit sequence is constructed from two three bit sequences followed by an inverted three bit sequence.

110 110 001

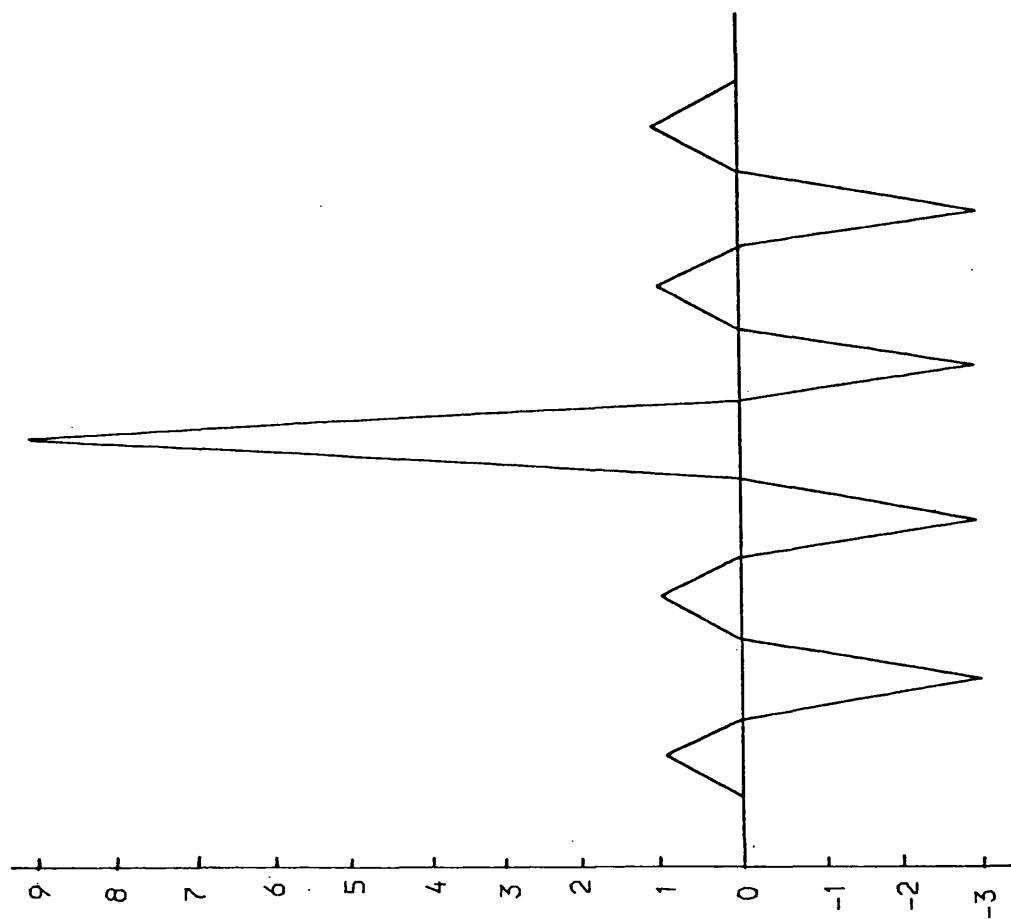


Fig 3.2.3 Composite Barker Sequence

A 33 bit composite Barker sequence

11100010010 11100010010 00011101101

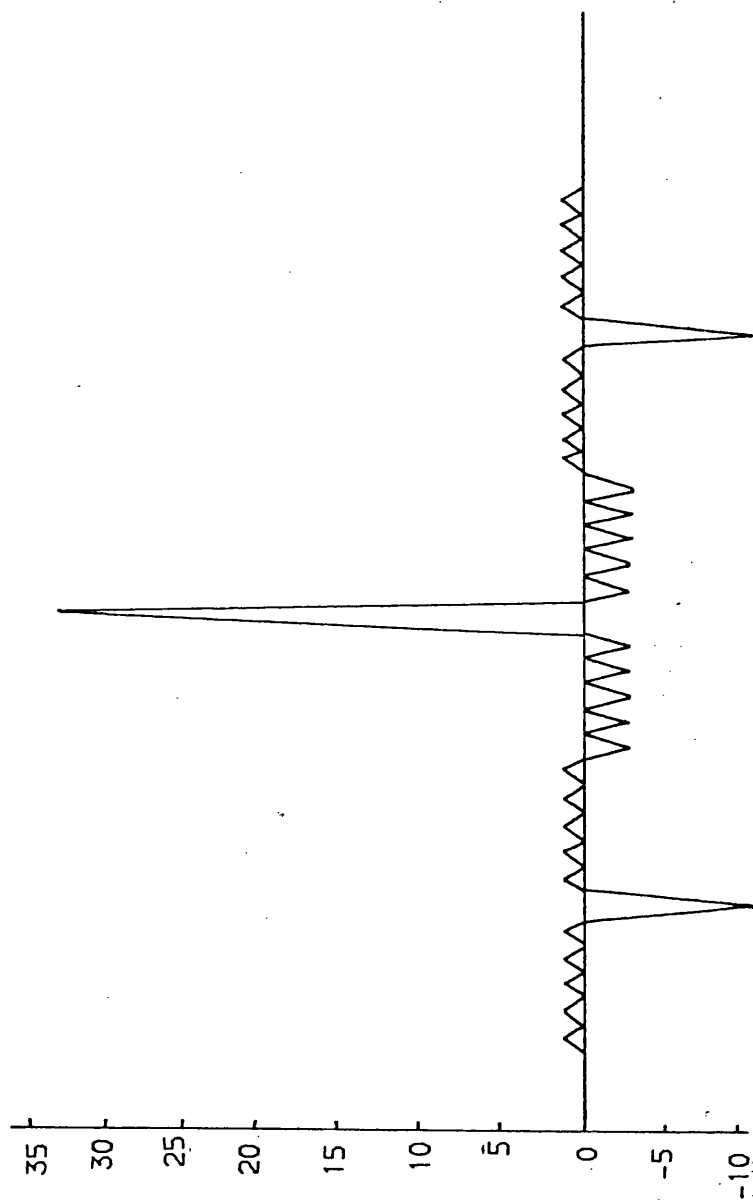


Fig 3.2.4 Synchronising Barker Sequence

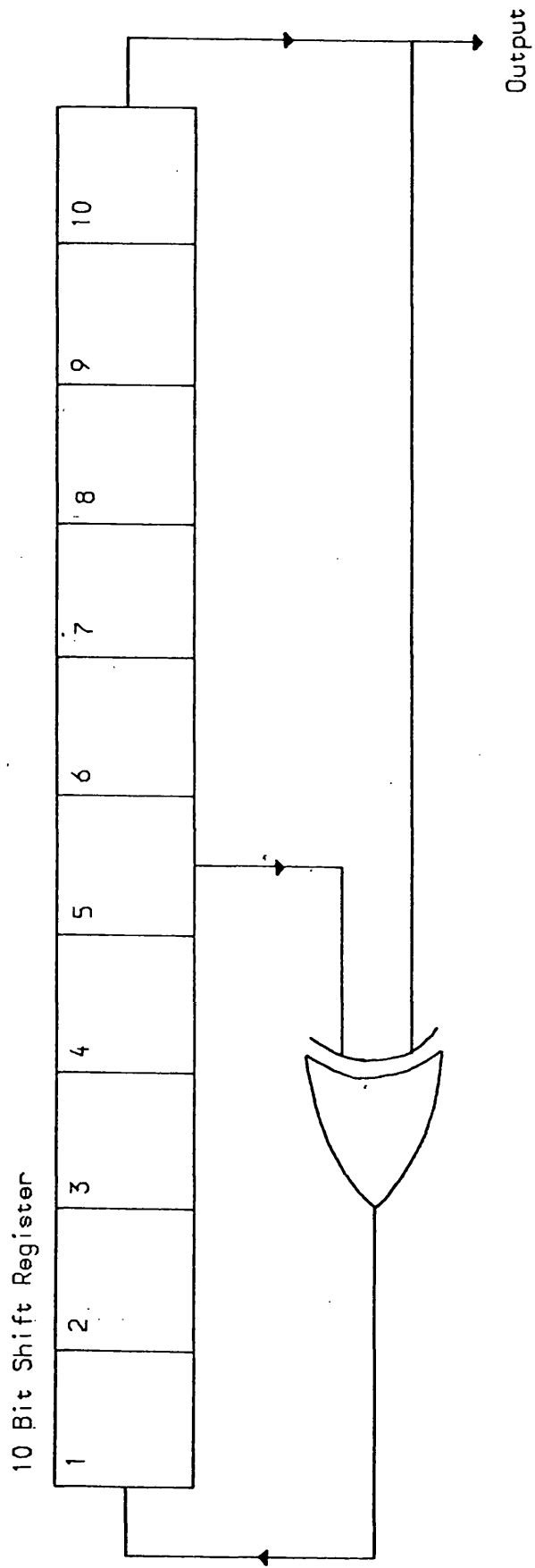


Fig 3.2.5 PRS Generator

and inexpensive to produce and also it provides a fairly typical random data message. The message is sent as non return to zero (NRZ) and is continuous. The data sequence is written out in hexadecimal in fig 3.2.6. Normally the entire data set including the on/off keying and the Barker code is sent twice with an intervening gap of 0.9 seconds where plain carrier is sent.

3.3 SYSTEM CALIBRATION

To check the linearity of the equipment, the entire system was calibrated. First the detector and the ADC board were checked for linearity with the experimental arrangement shown in fig 3.3.1. The 100KHz generator was fed through a stepped attenuator and then into the detector and the ADC to the computer. The computer was running a very small program that took the data from the input port and simply displayed it on the screen of the VDU, so enabling the operator to read the voltage measured by the ADC.

The input voltage was set at 3.5V and decremented by the attenuator. The results obtained are reproduced in fig 3.3.2. The equipment linearity is satisfactory until very low input voltages are reached. This results from the failure of the bias on the detector under these conditions. To avoid non linearities the experiment was arranged so that the pulse detection was carried out above this critical level.

The experimental configuration for the receiver calibration process is outlined in fig 3.3.3. The signal

FF C7 13 B2 BB D4 7A 54
17 FA AB D0 E9 19 6B 3D
63 3F 2A 99 94 FA 70 8D
91 4D EE AE 67 77 3A 9D
07 B7 0C 4A 59 A2 2D 2E
98 B0 29 2F BC 63 76 1E
4E 58 86 FE 71 A9 42 12
DF 5C 5C 87 DA A2 F6 73
E0 E4 AC BC B8 2B 66 1A
DD 15 FA 39 B9 46 81 92
20 9B 4F 35 61 76 8C 27
F7 1E 07 6C 51 32 DD 27
BE 2A D0 A0 2D BC F1 1F
B1 D6 A1 9B 06 01 B6 BA
F0 A9 0B 26 08 90 20 09
26 9A F9 8F 91 DF 87 01

Fig 3.2.6 PRS Listing

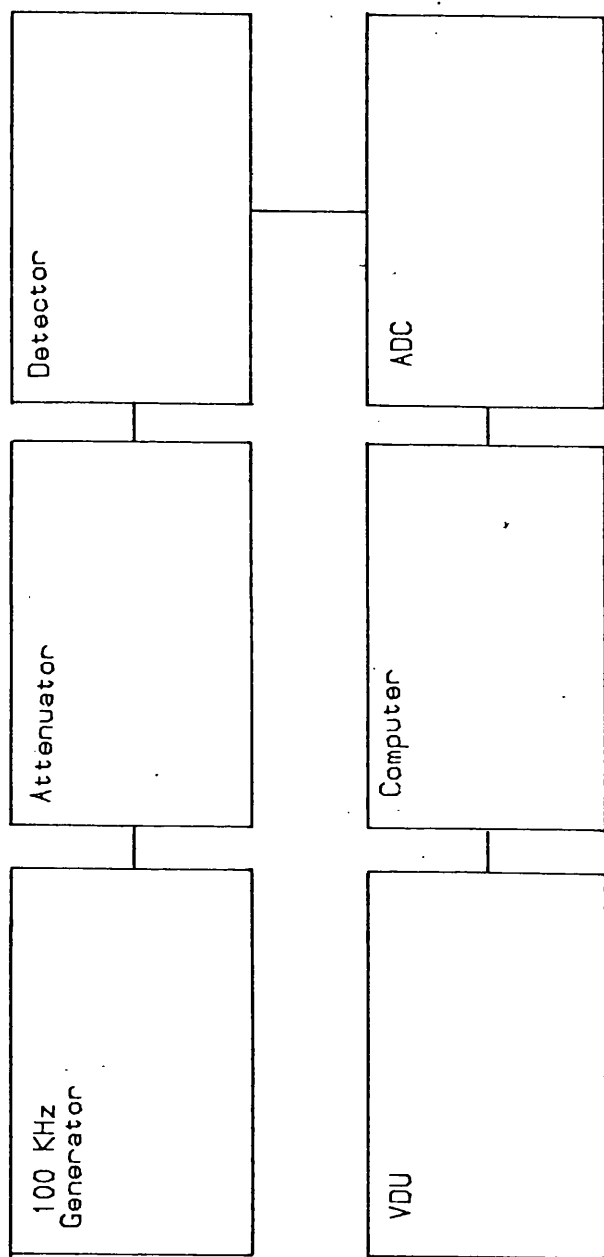


Fig 3.3.1 Detector and ADC Calibration

DbA	V in	ADC	DbA	V in	ADC
0	3.5	253	12	0.9	55
1	3.1	240	13	0.8	48
2	2.7	211	14	0.7	40
3	2.5	186	15	0.6	09
4	2.2	165	16	0.55	06
5	1.9	145	17	0.5	05
8	1.3	99	20	0.35	01
10	1.1	73			

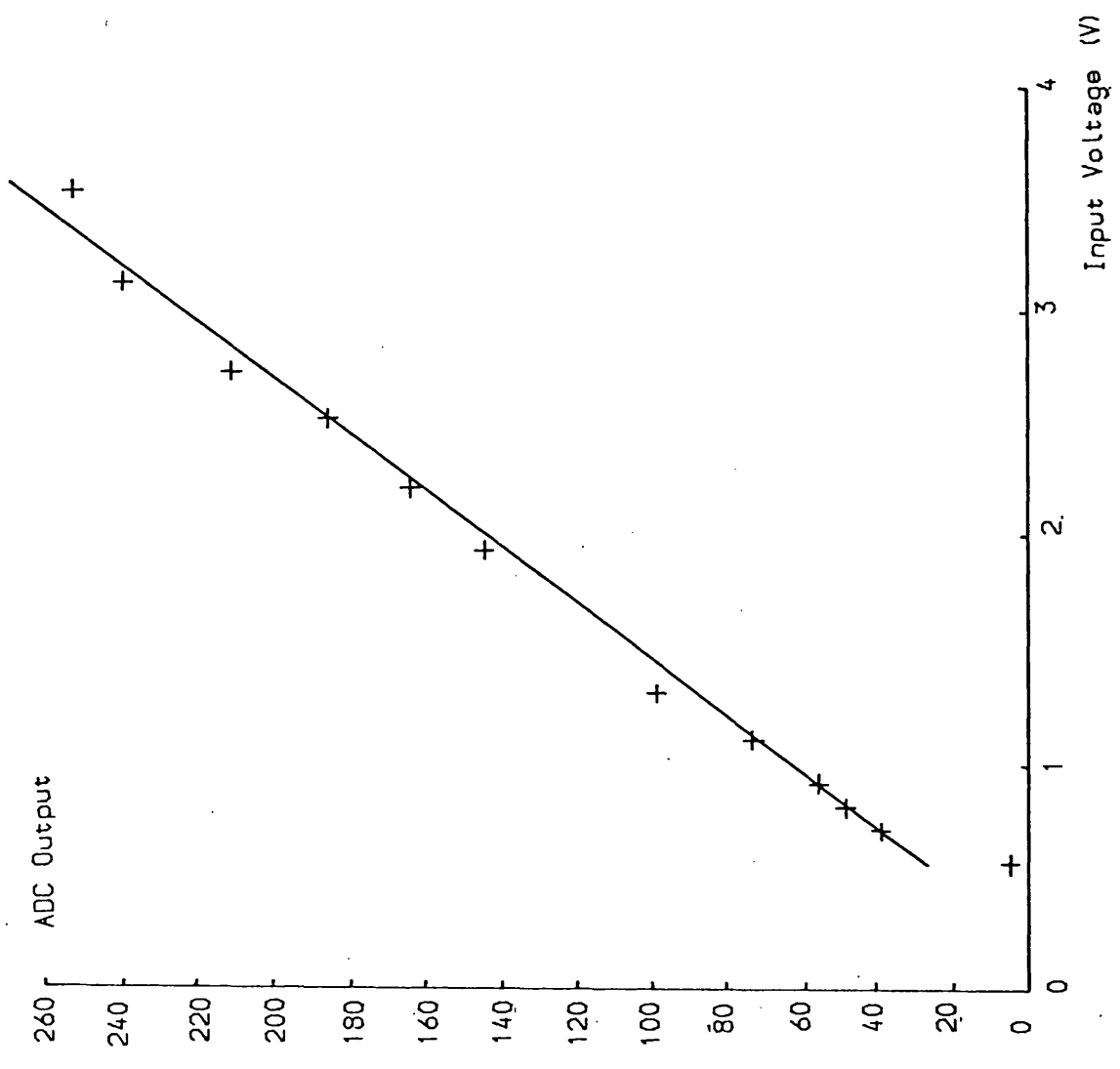


Fig 3.3.2 Detector and ADC Calibration

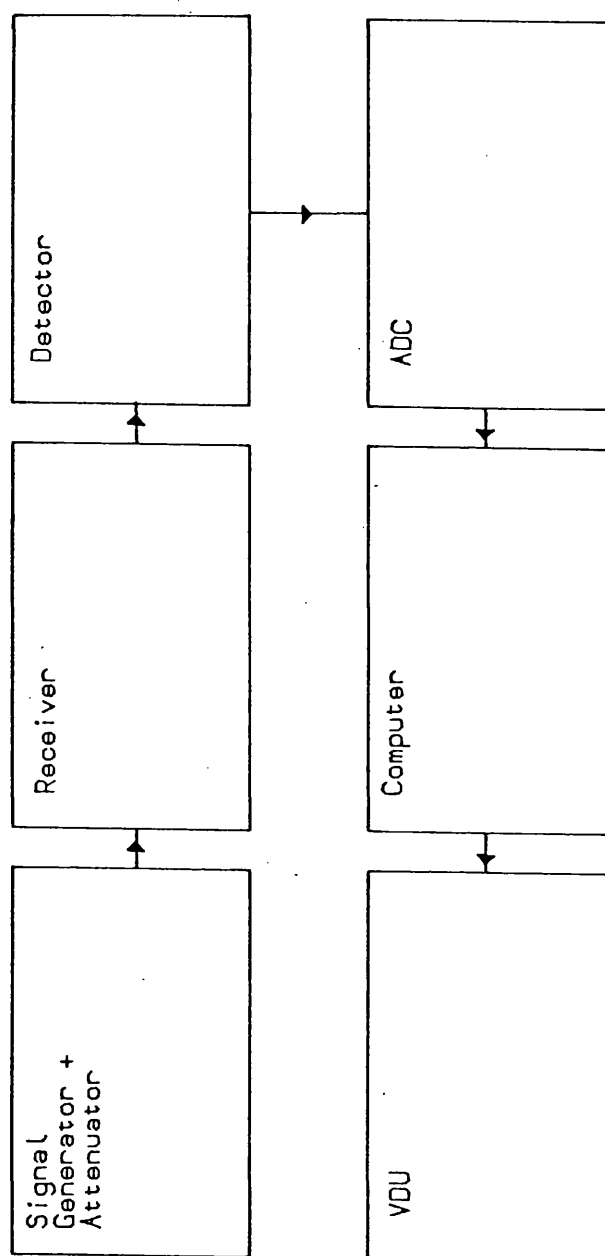


Fig 3.3.3 Calibration Configuration

generator, a Marconi CT 452, was set to 4.7925MHz and its output fed through the stepped attenuator to the antenna input of the RA117 receiver. This was set to mid range manual gain with one stop of attenuation on the input attenuator in order to stop any ringing. The 100KHz output was detected, digitised and fed into the computer for analysis as before.

The input voltage to the receiver was set to 400 microvolts and the attenuator stepped in 5dB increments. The results are presented in fig 3.3.4. This procedure was repeated several times with different settings on the receiver controls and similar results were obtained. Problems of non linearity were only encountered when the receiver gain was set too high where limiting occurred. This setting was never employed during the experiments.

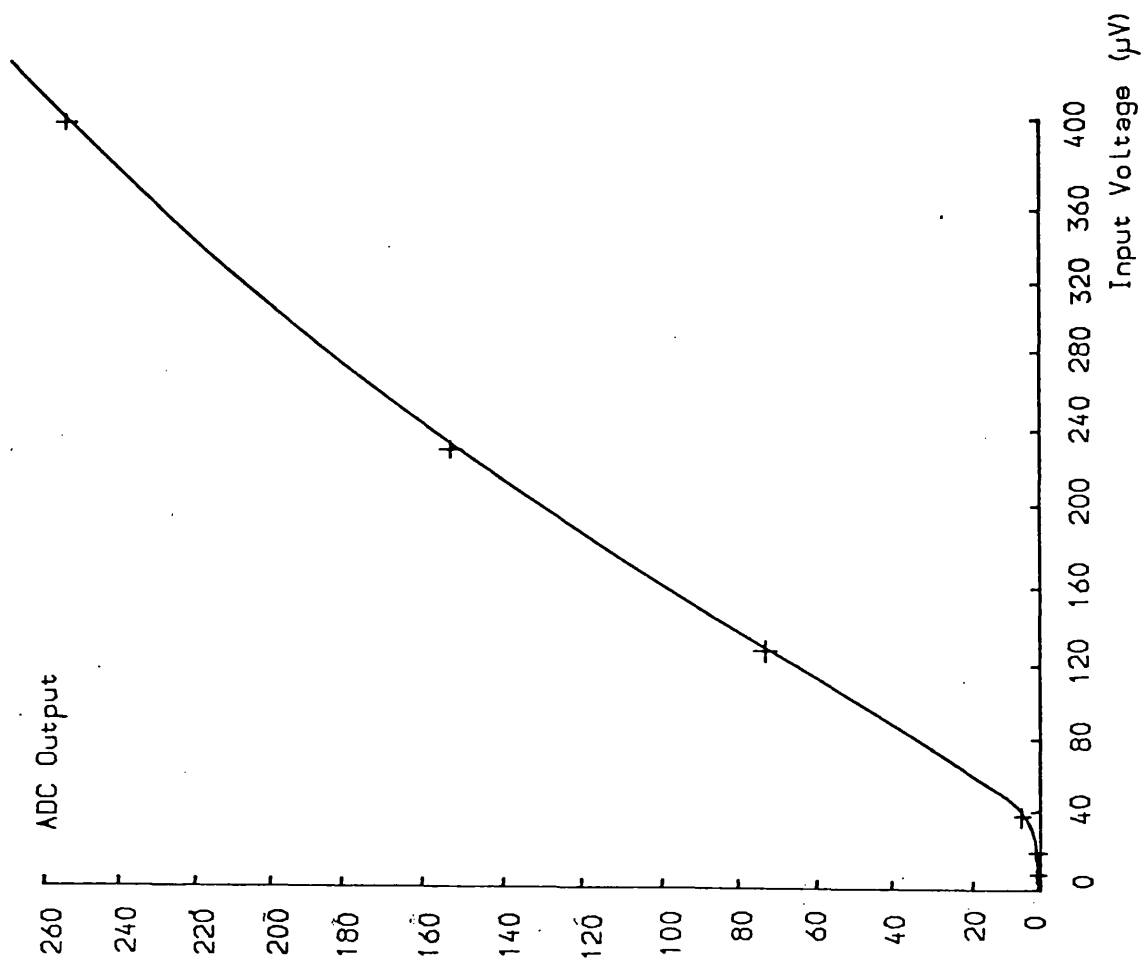
Throughout the experiment the signal amplitude was recorded in ADC units, as only relative sounding pulse amplitude was required. Fig 3.3.2 shows that there is a simple virtually linear relationship between the measured and the actual signal voltages through the complete system.

3.4 DEVELOPMENT OF THE EXPERIMENT

The work described in this thesis originates from Easter 1979 when the project was proposed to Leicester University by the Royal Aircraft Establishment (RAE), Farnborough, Hants. The aim then was to construct an electronic device capable of recognising the pulse sounding signal described in section 3.1, with the proposed elevation steerable antenna and adaptively

Db att	μV	ADC	Decimal
0	400	F0	253
5	225	9A	154
10	126	49	73
15	71	1C	28
20	41	07	7
25	22	02	2
30	13	02	2

Fig 3.3.4 System Calibration



controlling it to reduce multipath interference.

The progress of the work since then is presented in fig

3.4.1. The key to this diagram is given below.

- 1) Build a simulator (section 4.5)
- 2) Design and build the detector and ADC (sections 4.6,4.9)
- 3) Develop the data logging program (sections 5.5,5.6)
- 4) Run test transmissions from Oadby
- 5) Develop the PRS sounder (sections 4.2,5.1)
- 6) Design and construct the project computer (section 4.10)
- 7) Develop the plot programs (section 5.7)
- 8) Carry out experiments from Durham
- 9) Undertake tests with RAE from Bodo Norway
- 10) Receive soundings from Tromso Norway
- 11) Develop Cyber analysis routines (section 5.7)
- 12) Carry out experiments from Elgin Scotland
- 13) Undertake further experiments from Oadby

The implementation of the program will now be described in greater detail. From the start of the project it was thought essential that Leicester should have a unit that could produce the pulsed sounding signal. In order to achieve this a simulator (section 4.5) was constructed from circuit diagrams, some provided by the RAE and some designed at Leicester. Once this was nearing completion, work was started on the design and construction of the analogue to digital converter (ADC) and the detector hardware (sections 4.6 and 4.9). This was designed to a higher specification than was eventually required in terms of speed of operation to allow for future expansion.

An MSI 6800 micro-computer was employed to provide

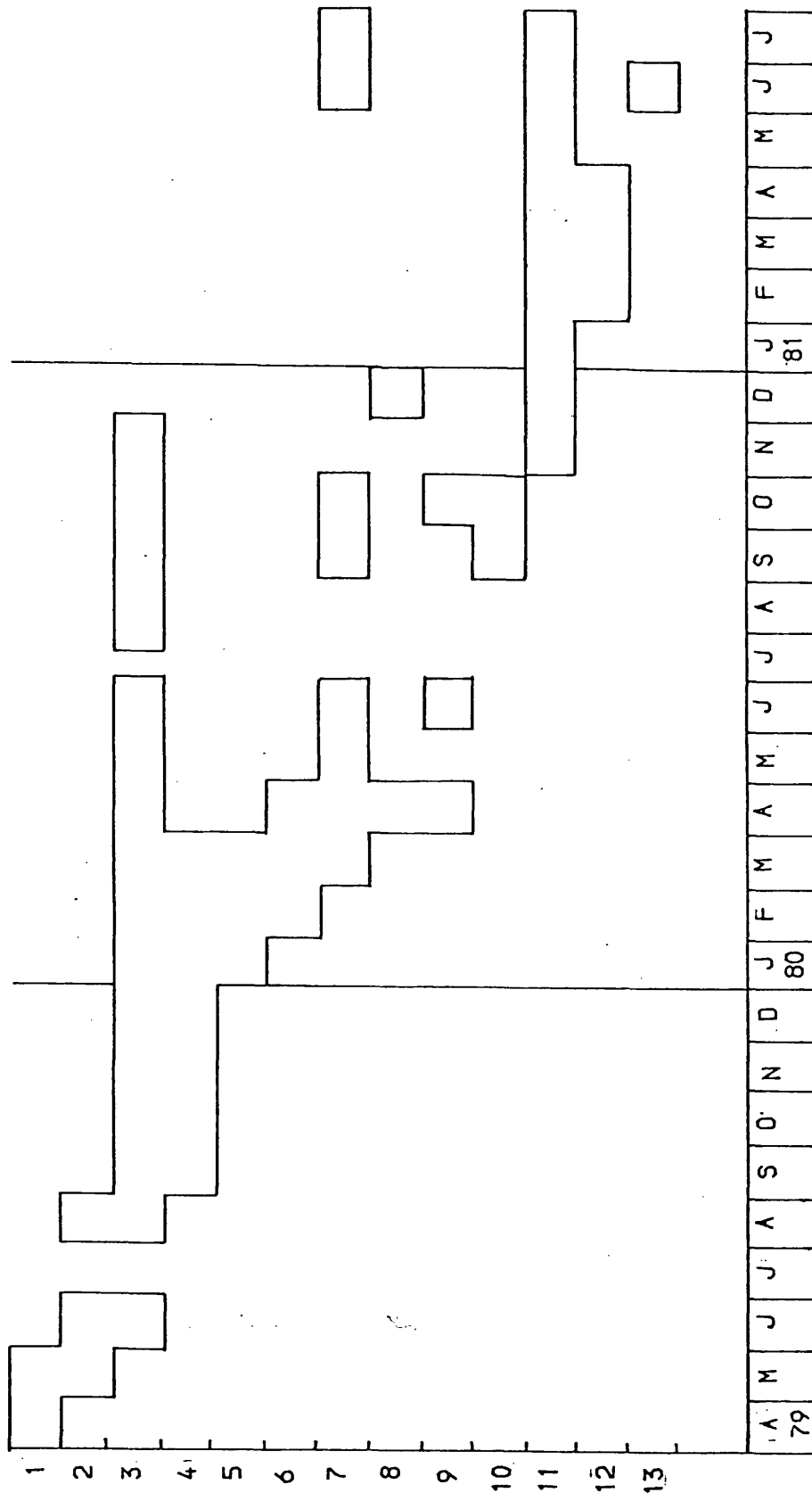


Fig 3.4.1 Experimental Timetable

intelligent control of the equipment. On this computer the first data logging programs were developed (section 5.5). This work continued until about November 1980 with the program gradually being expanded and improved to allow different types of data format to be recorded and to provide greater noise immunity. This software was tested by connecting the simulator to the ADC directly. Subsequently the simulator was used to key a Heathkit DX60B radio transmitter at local field sites at Oadby and Earl Shilton.

At this stage a quantitative assessment of the effectiveness of the project as an aid to data communications was thought necessary. To achieve this a new computer controlled sounder was developed which could produce the PRS data in addition to the pulse sounding signal. Once the new sounder was working and tested it too was deployed at the Oadby field site for tests over the radio link on 4.7925MHz. The data logging software was then written which could recognise and decode the data test transmissions.

Because the MSI 6800 was now required to control a different experiment a replacement had to be found. As the software was already written for a Motorola MC6800 microprocessor it seemed appropriate to buy a second MSI 6800. However, due to purely financial constraints it was necessary to design and build a comparable micro-computer from scratch (section 4.10). This proved to be quite adequate for the task in hand but rather less reliable than a commercial system.

By March 1980 useful results were being gained from tests and so programs were written which could plot out this data on

the University mainframe computer in various formats. The system was now sufficiently well proven to enable information to be gathered over longer paths. The computer controlled sounder and the rack of equipment shown in fig 4.3.3 were transported to Durham University a short series of tests were made on 4.7925MHz.

Also in April 1980 the RAE were running a similar series of tests from Bodo in northern Norway in the 15MHz band. The Durham results were approximately as anticipated (section 6.2) but the Bodo signals contained much broader pulse returns than were expected. It was essential to resolve whether the Bodo pulses were broadened by some ionospheric effect or were the result of the transmitter hardware. To this end a Heathkit DX60B transmitter and the simulator were sent to Tromso in northern Norway for comparative tests on the 14MHz band. The results of these tests are also presented in section 6.2.

At this stage (November 1980) the data analysis programs were developed on the Cyber 73 computer, initially to display the PRS data but later to produce in addition the pulse sounding statistics.

In February 1981 a series of experiments were conducted from the RAF Kinloss site near Elgin in Scotland. These were undertaken using the sounder equipment which had previously been installed at Durham university. These experiments provided most of the data analysed in this thesis. Finally for comparative tests the equipment was returned to the Oadby field site in June 1981 and after one months operation was finally closed down.

The results of the tests described above are presented in detail in chapters 6 and 7.

CHAPTER 4

EQUIPMENT

4.1 HARDWARE OVERVIEW

The hardware consists of a transmitting and a receiving station. The transmitting station radiates the pulse sounding sequences described in section 3.1 and 3.2 from the remote sites. The sounding sequences can be changed without any additional hardware by means of a small dedicated computer (section 4.2) which is programmed to key the transmitter (section 4.3). The transmitter consists of a low power driver and a high power amplifier, the 400W output of which is radiated from a dipole antenna.

The computer controlled receiving station automatically detects the sounding signal and records its parameters in digital form. Data analysis can be carried out on line or alternatively by the campus mainframe computer. The sounding signals transmitted via the ionosphere are detected by a computer controlled receiver (section 4.4). The 100KHz IF output of the receiver drives both an amplitude detector (section 4.6) and a phase detector (section 4.7). The results from both units are converted to digital form (section 4.9) and presented to the computer. All data from the pulsed sounding signal and the amplitude modulated (AM) pseudo random data sequence reach the computer via this route. The data sequence

transmitted from Bodo was sent as frequency shift keying (FSK) for which a separate detector was constructed (section 4.8). To enable re-examination of raw received data an FM tape recorder was connected to the amplitude detector to store the results for later study.

The computer (section 4.10) examines the sounding signal noting the amplitude, phase, and time of arrival of any sounding pulses present. It also measures the error rate in the pseudo random sequence. These results are displayed on the visual display unit (VDU). Finally the digital data is logged onto either floppy disk or nine track magnetic tape for further analysis on the mainframe computer.

Before the system was applied to ionospherically propagated signals, tests were carried out on a more stable source to ensure correct operation. A pulse sounding simulator was therefore built, and a general purpose micro-computer was programmed to simulate the data transmissions (section 4.5). The system configuration is presented in block diagram form in fig 4.1.1.

4.2 PROGRAMMABLE SOUNDER

The programmable pulse form generator was developed around a Motorola 6800 based micro-computer, containing a clock, support chips, two digital to analogue converters and 768 bytes of random access memory (RAM) in MC6810 chips. Programs are stored in up to six MC6834 UV eraseable read only memory (EPROM) chips giving a total maximum program size of 8K bytes.

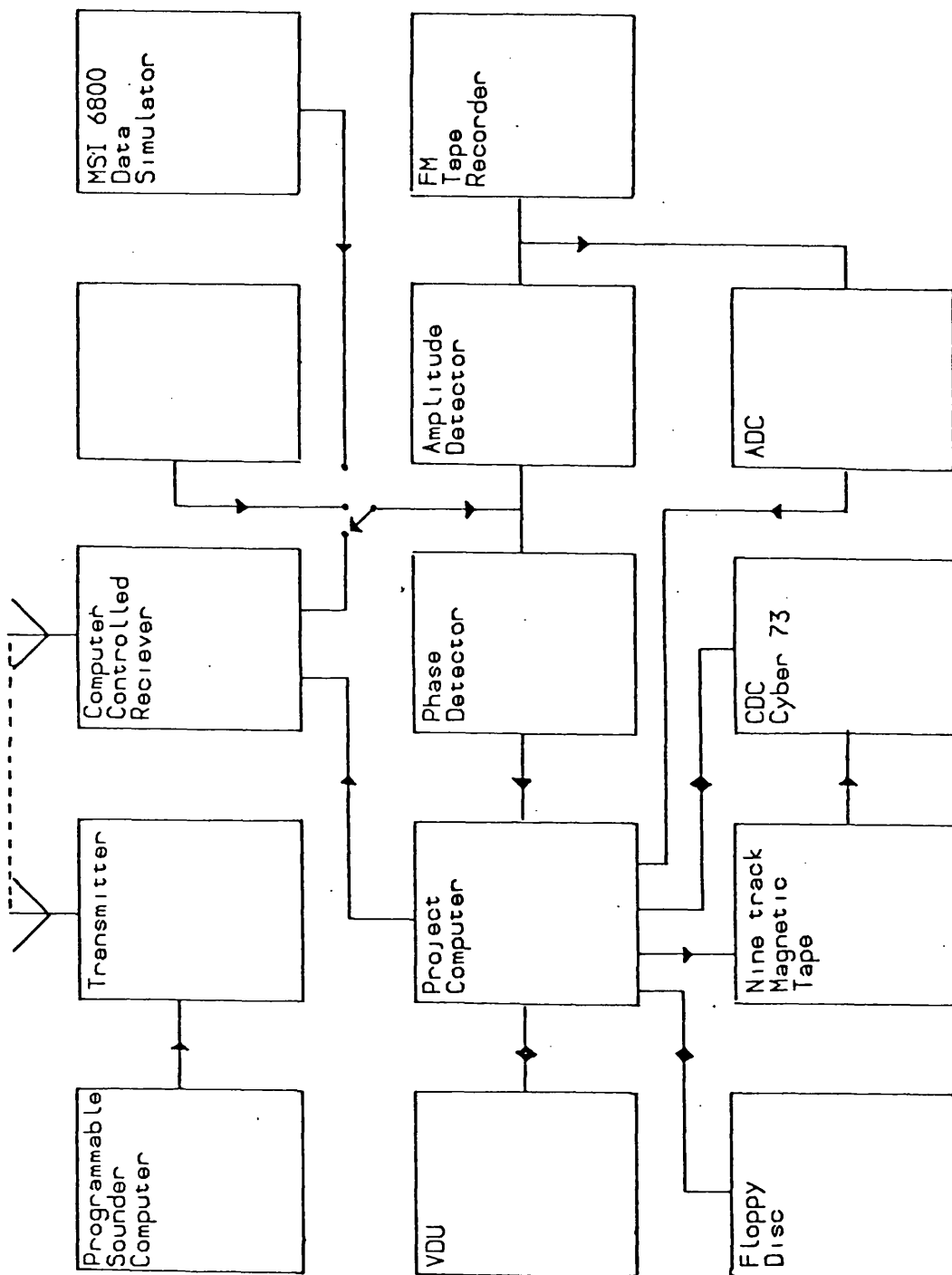


Fig 4.1.1 Block Diagram of System Hardware

To interface with the rest of the receiving station, three MC6820 parallel interface adapters (PIA) were provided giving up to 54 bidirectional control lines.

As the system was operated without supervision at remote field sites where power could possibly fail for short periods, an automatic restart facility was included. The sounding software was written into EPROM and is discussed further in section 5.1.

The design of the interface between the computer and the radio transmitter is given in fig 4.2.1. The correct timing for the sounding signal is generated by applying a non maskable interrupt (NMI) to the microprocessor every 0.703ms. The exact interrupt frequency of 1.4222 KHz results from a convenient subdivision of the crystal frequency reference. These interrupt pulses cause the program to switch the CA2 line from one of the PIAs, low for 97 cycles, high for 15, low for 1, high for 15 and then repeat, thus generating the pulse sounding signal. The CA2 line then keys the transmitter on and off with a transistor switch. One of the nine different sounding patterns can be selected by a thumbwheel switch on the front panel. The frequency of the crystal oscillator was chosen to enable the test transmissions from RAE Farnborough to be monitored.

4.3 RADIO TRANSMITTER

The sounding sequence generated by the micro-computer drives a Heathkit DX60B radio transmitter. The DX60B is an amateur band transmitter modified to produce about 20W on our

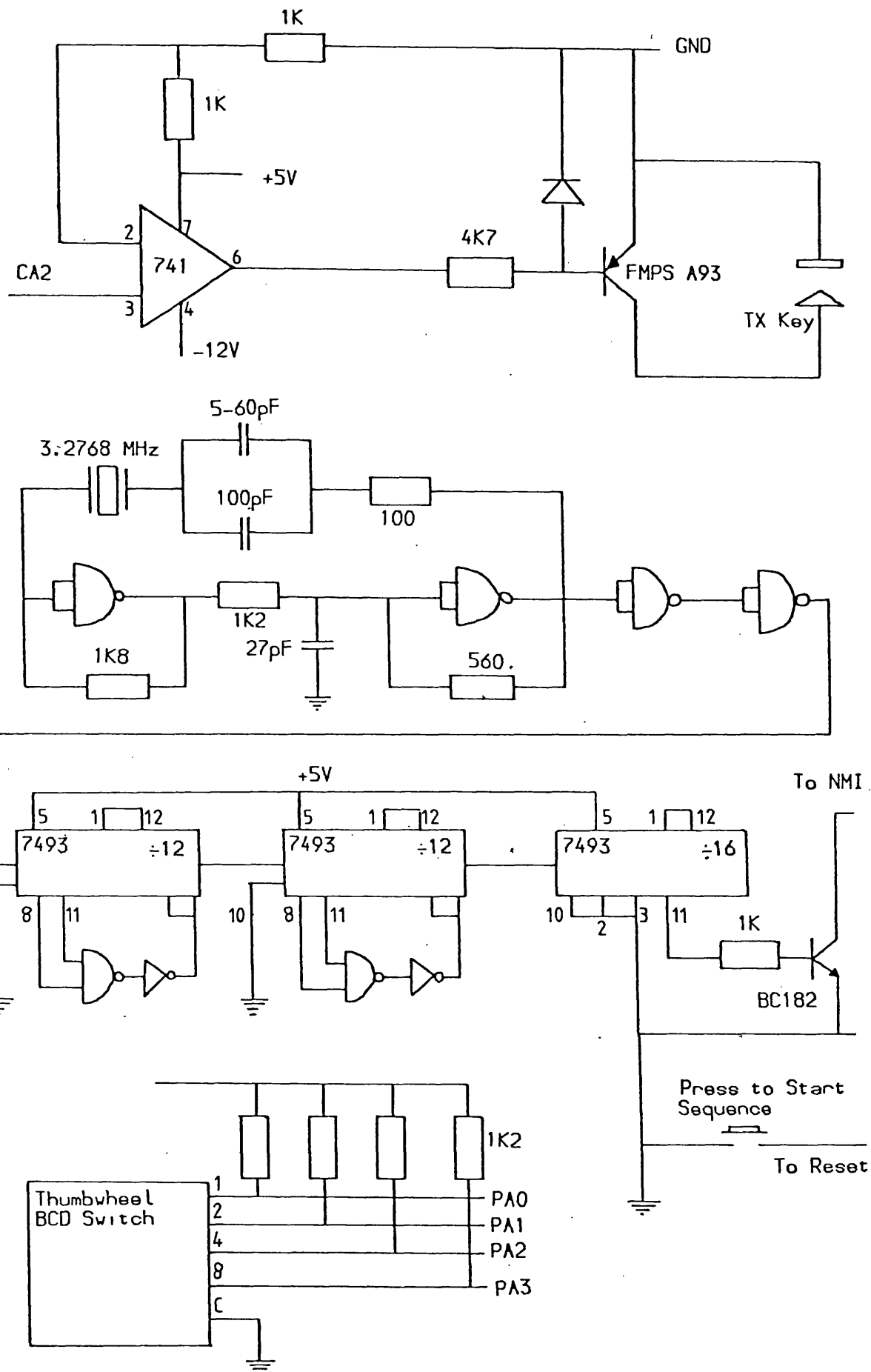


Fig 4.2.1 Sounder Interface Electronics

allocated frequency of 4.7925MHz. The output of the DX60B is fed into a Redifon GA406 linear amplifier producing a CW power output of about 400W. The amplifier output is matched to the antenna by means of a KW E-Zee Match aerial tuning unit (ATU).

A cut out circuit was designed which turns off the transmitter if the SWR exceeds a preset level. The circuit diagram for this unit is given in fig 4.3.1. The unit also automatically breaks the transmission for five minutes after a power failure. The forward and reflected power from the transmitter is measured by a sense wire running inside the coaxial line. The SWR voltage generated is buffered, displayed and then compared with a preset level. If the measured level is above the preset value the 'fault' LED operates and relay RL2 cuts off the key signal to the DX60B. The key is cut off for five minutes after which time the SWR is measured again. If conditions have returned to normal the transmitter will automatically restart. However should the fault persist the transmitter will not be damaged.

The configuration of the transmitting station is summarised in fig4.3.2 and 4.3.3.

4.4 RADIO RECEIVER

A frequency of 4.7925MHz was allocated for the present work. In addition to this frequencies in the 6MHz, 14MHz, 15MHz and 18MHz bands were utilised in cooperation with RAE Farnborough.

The first receiver to be employed was a Racal RA117. This

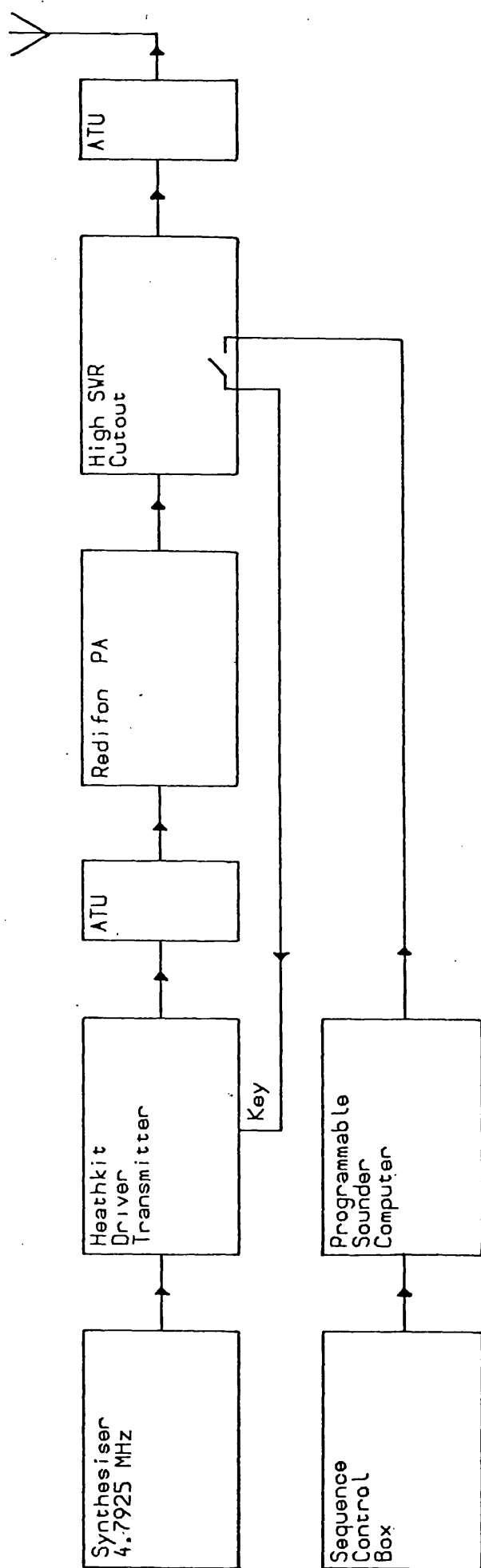


Fig 4.3.2 Programmable Radio Transmitter Block Diagram

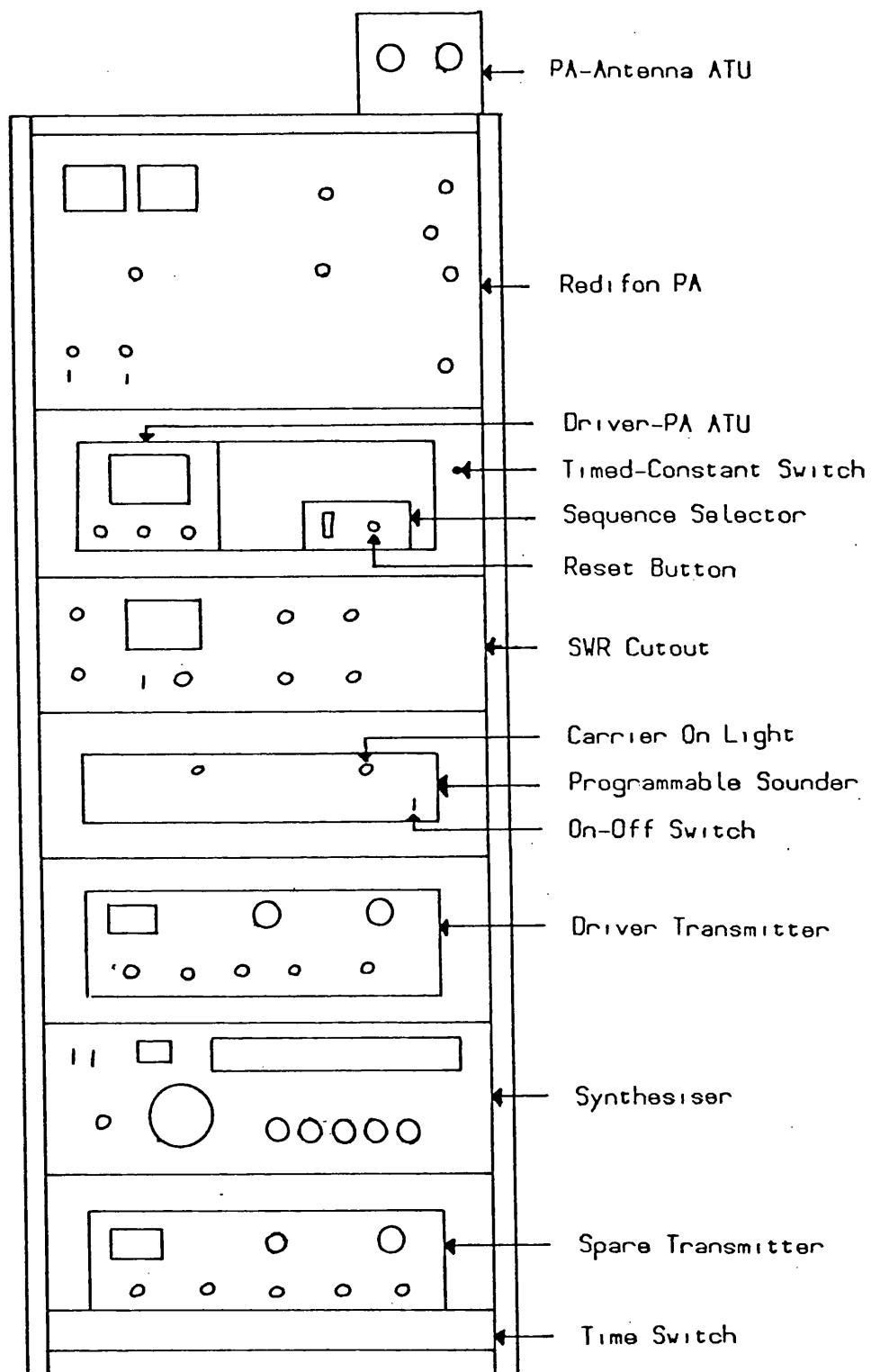


Fig 4.3.3 Programmable Radio Transmitter

was a general purpose HF receiver for which the band pass filter was variable from 100Hz to 12KHz and the gain controlled either manually or by means of the automatic gain control (AGC). The 100KHz IF output was fed to the external detection system described in section 4.6. This receiver is quite adequate for amplitude measurements but is not suitable for phase measurements because of its free running local oscillator. For phase the receiver requires a locked reference 100KHz which can be compared to the 100KHz IF output. An KA117 slave receiver, tuned by generating the first and second VFOs from external synthesisers proved to be suitable. The receiver computer interface configuration is illustrated in fig 4.4.1

The two synthesisers are set up with a remote control facility. The operating frequency is typed into the project computer which determines the frequencies required for the two VFOs. It then outputs these frequencies as binary coded decimal (BCD) to the interface electronics. The BCD information is latched and loaded out to the synthesisers in the correct format. The computer simplifies the receiver tuning considerably since the first and second VFOs are calculated automatically.

4.5 SIMULATOR HARDWARE

The simulator hardware (fig 4.5.1) performs three main functions :-

- 1) Keying the Heathkit DX60B transmitter with the pulse sounding signal.

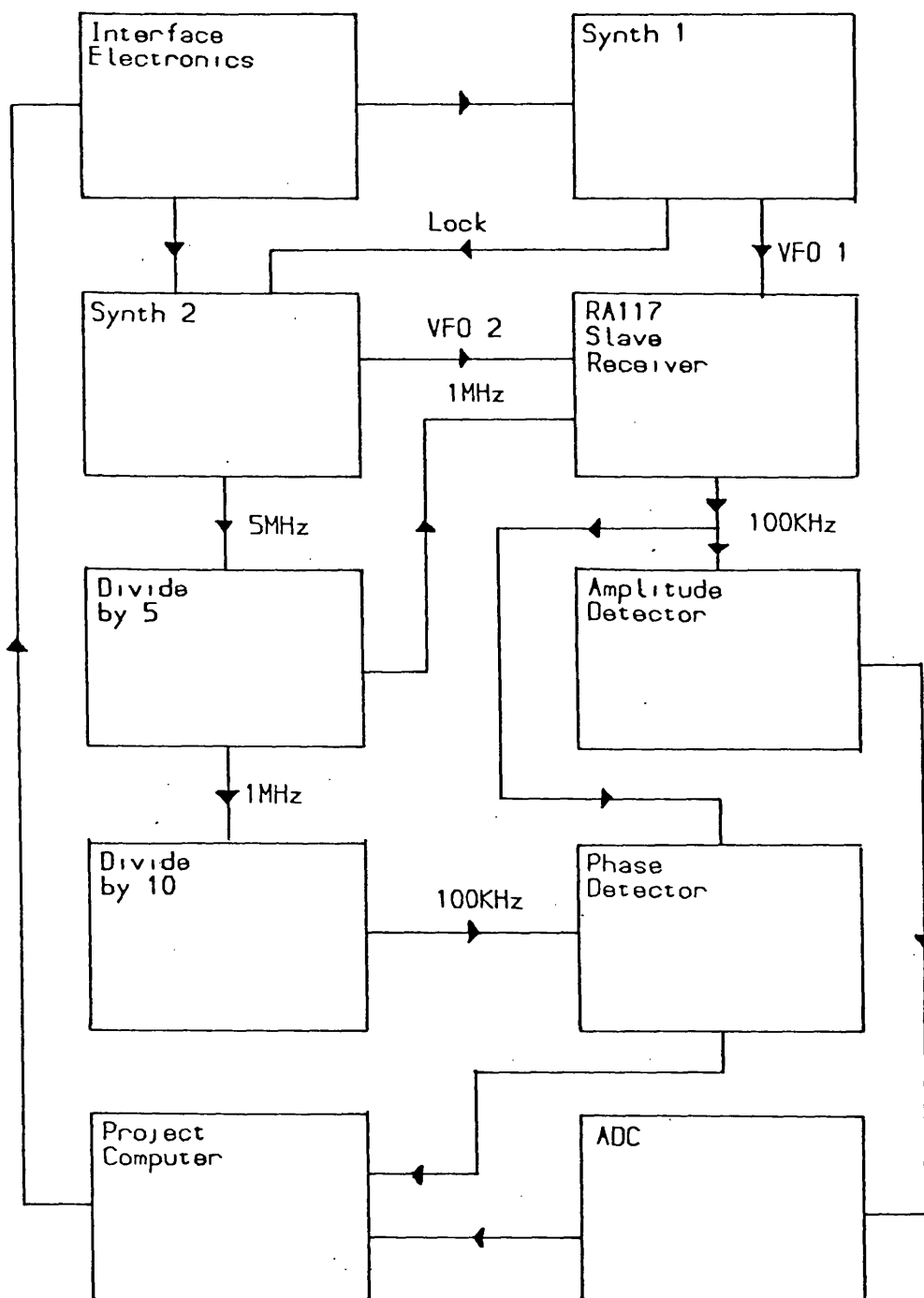


Fig 4.4.1 Computer Controlled Receiver

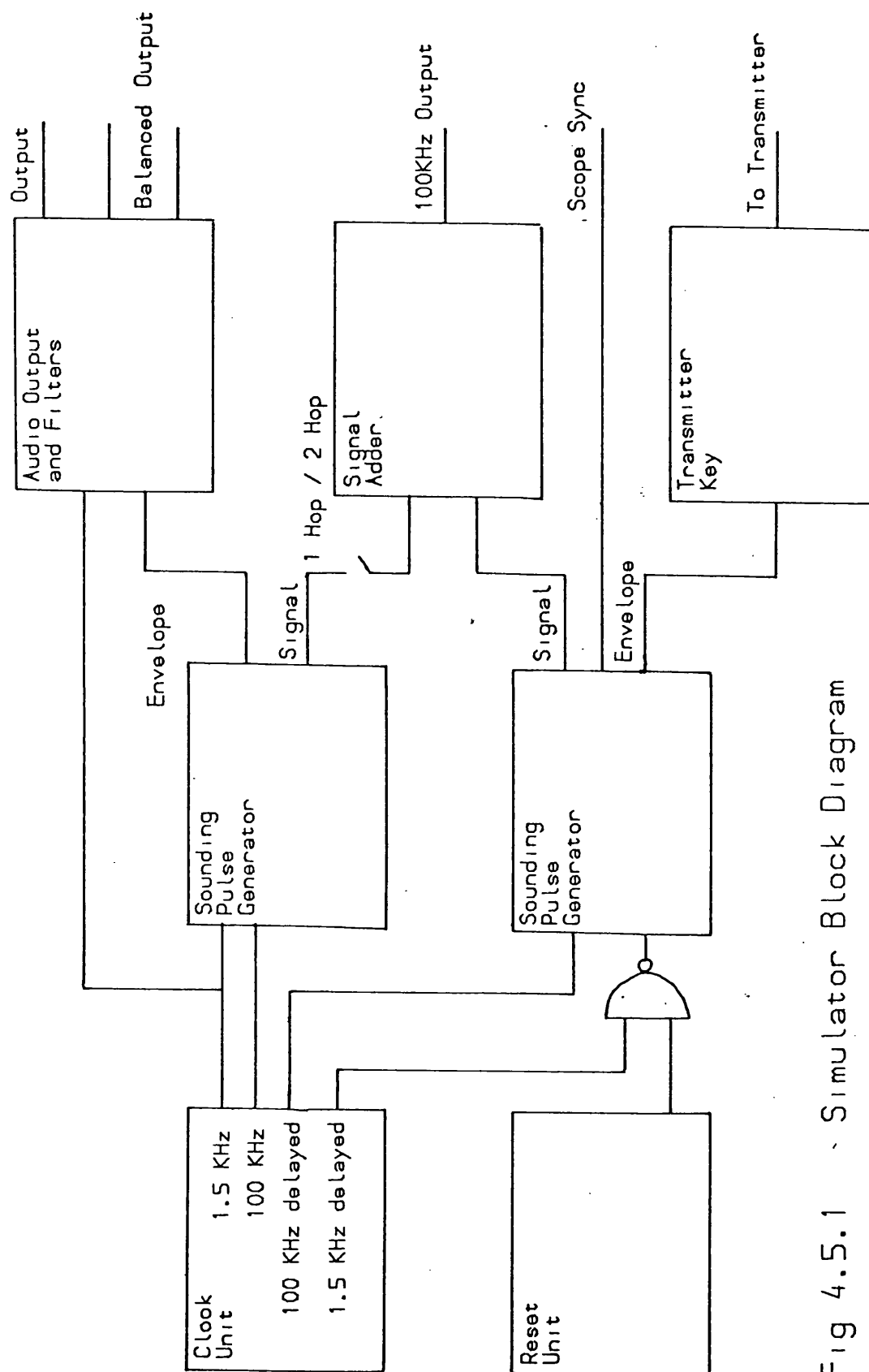


Fig 4.5.1 Simulator Block Diagram

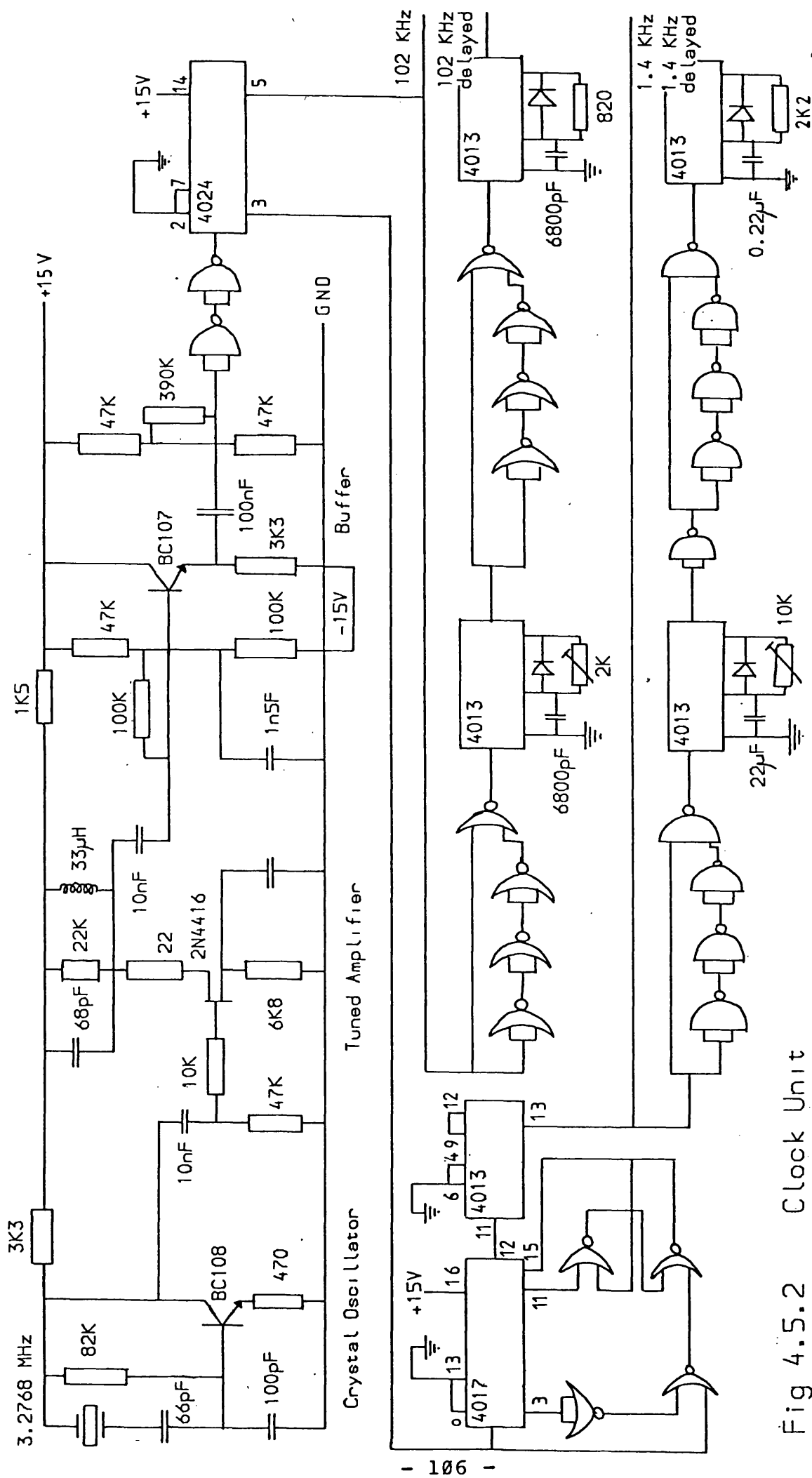
- 2) Generating the audio frequency output suitable for modulating a standard aircraft transmitter.
- 3) Simulating the output of an RA117 under either one or two mode propagation conditions with any relative time or phase delay between modes.

The simulator a master oscillator driving two identical pulse sounding generators. Each generator produces a signal similar to the receiver IF output. These are added in a signal combiner to simulate two mode propagation. In addition to the signal output each generator produces an envelope waveform. One of these gates an audio frequency signal to operate a radio transmitter from the microphone input. The second envelope output controls a transistor switch which keys the DX60B.

The master clock unit (fig 4.5.2) consists of a 3.2768MHz crystal oscillator which is divided down to give 1.4222KHz and 102.4KHz with division ratios of 2304 and 32 respectively. The sounding sequence is generated from the 1.4222KHz waveform and the 102.4KHz simulates the RA117 100KHz output. By applying a logic phase shifter to each of these frequencies, two phase independent versions of each are supplied from the clock unit.

Fig 4.5.3 is the circuit diagram of the pulse generator. The 1.4222KHz clock input triggers a group of counters and dividers. The outputs of these are gated together to produce an envelope signal which is high for 97 cycles, low for 15, high for 1, low for 15 and repeating as required.

The signal then gates the 102.4KHz from the clock unit when the envelope signal is high. The final analogue switch and potential dividers make the output oscillate between 0 and 7.5V



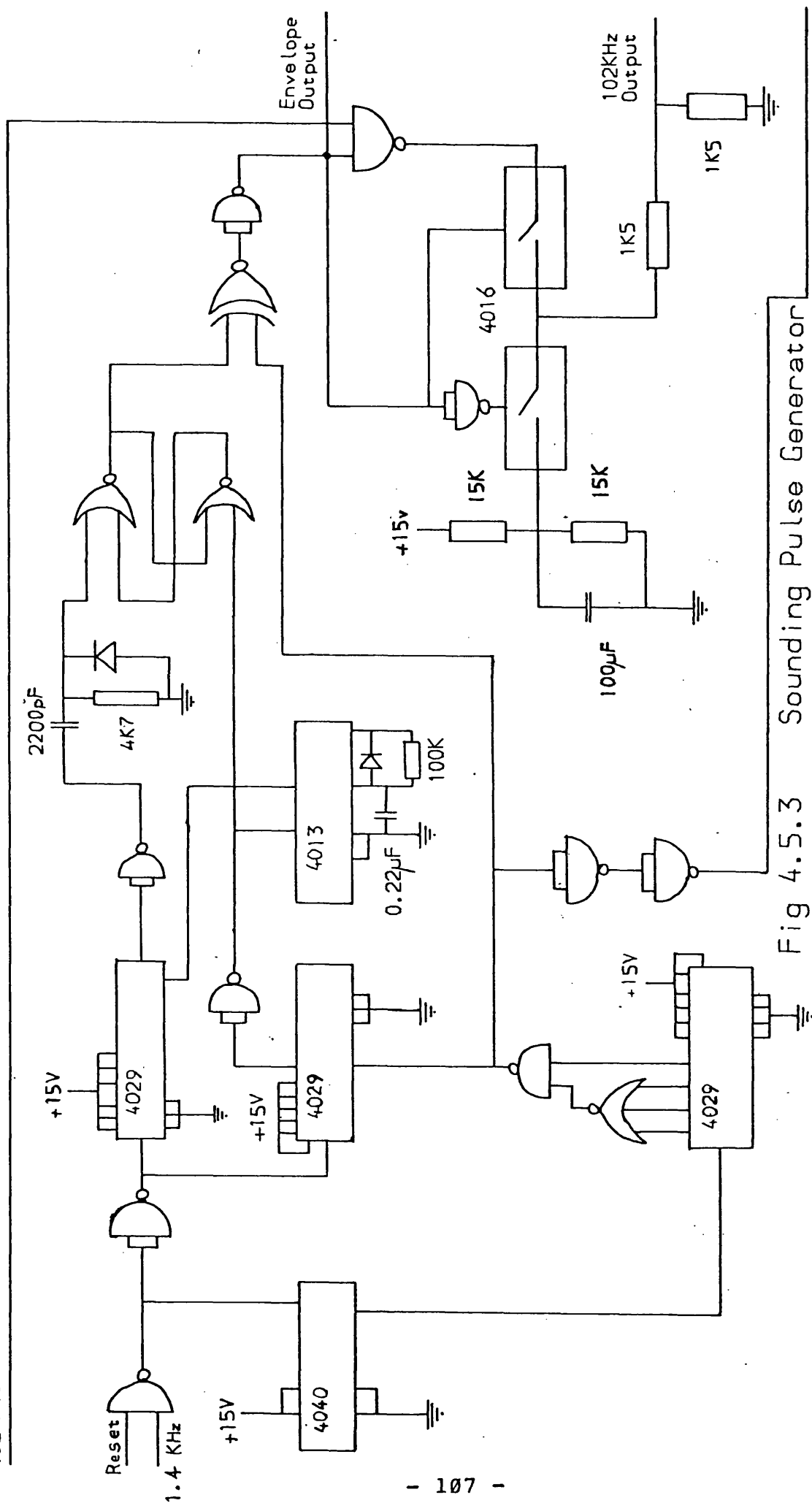


Fig 4.5.3 Sounding Pulse Generator

when the envelope is high and sit at half level when the envelope is low. This is to produce an output compatible with that of the RA117.

The reset unit (fig 4.5.4) consists of a triggerable monostable of variable time constant. This disables the clock input to the second pulse generator for a short period thus shifting its time reference relative to the first. By making the monostable period shorter than the clock period. The direction of shift can be reversed.

The audio output and filters (fig 4.5.5) switch the 1.4222KHz clock in a similar manner to the pulse generator switching of the 100KHz clock. The output is filtered to remove high frequencies and provide a balanced output for modulating a transmitter.

The signal adder (fig 4.5.6) is a simple operational amplifier circuit. The relative gains of the two input channels are determined by the 50K variable resistors. If a single path is to be investigated, the input to the first channel is simply disconnected.

The preferred method of modulation is the transmitter key rather than the audio output since the pulses produced are sharper and give improved time resolution in the sounding mode of operation. This is accomplished with a CMOS controlled solid state switch (fig 4.5.7)

The pseudo random data sequence is simulated by a commercial general purpose micro-computer. This is an MSI 6800 with 8K of RAM, 3 ACIAs, 2 PIAs and 4K of ROM. The computer runs an almost identical program to that in the programmable

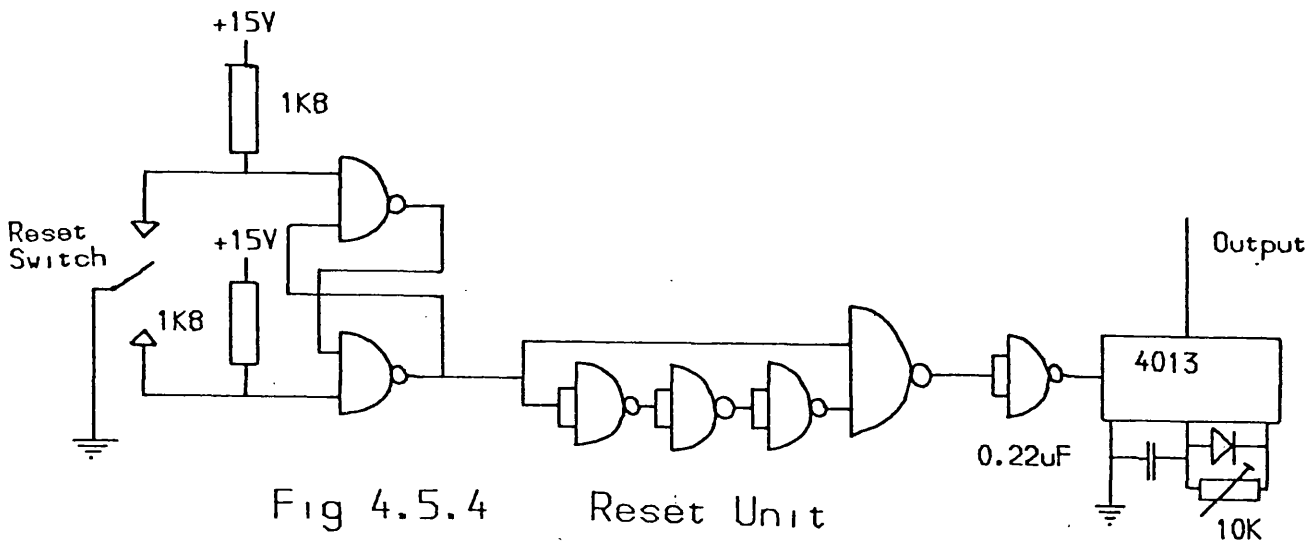


Fig 4.5.4 Reset Unit

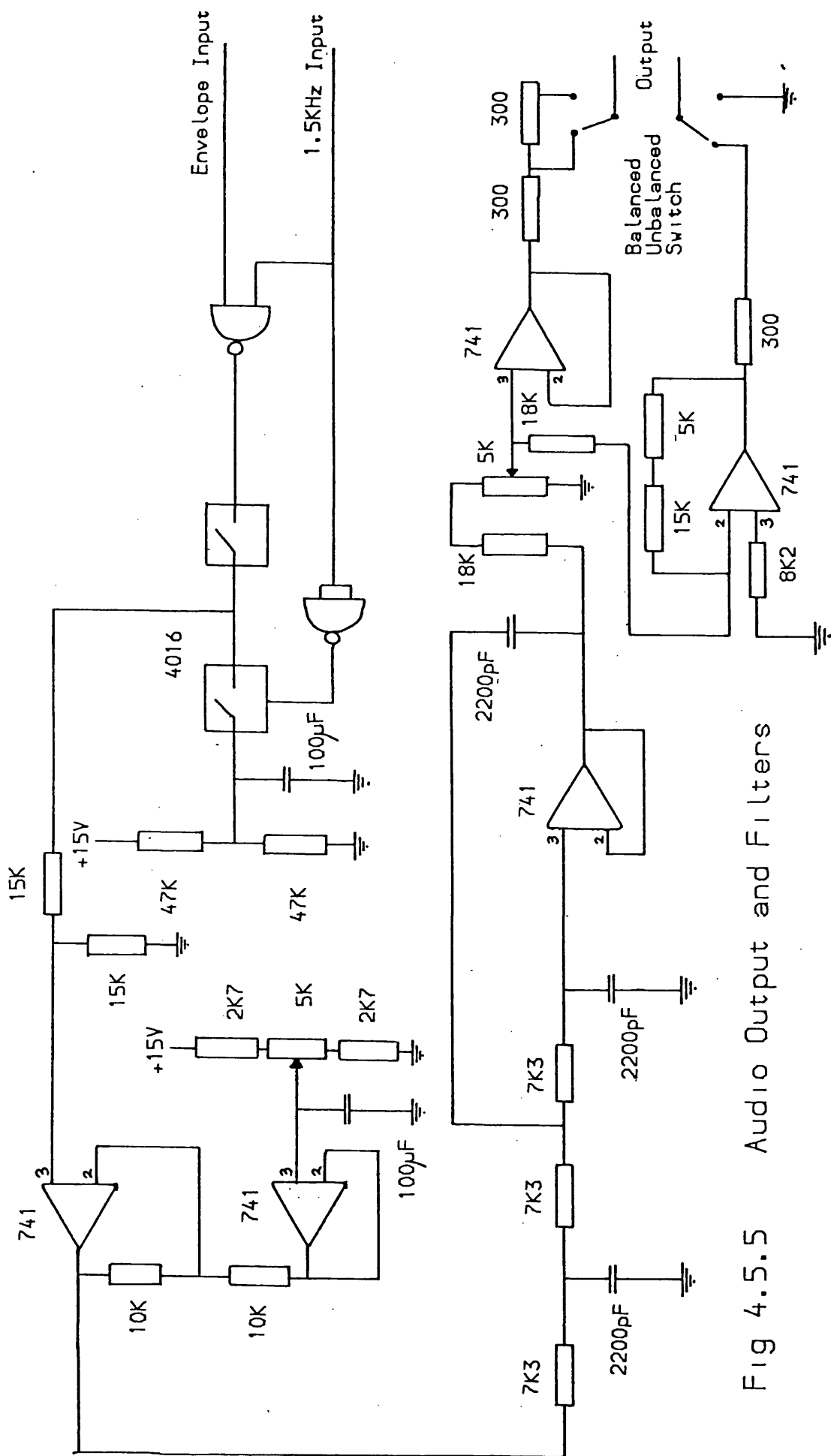


Fig 4.5.5 Audio Output and Filters

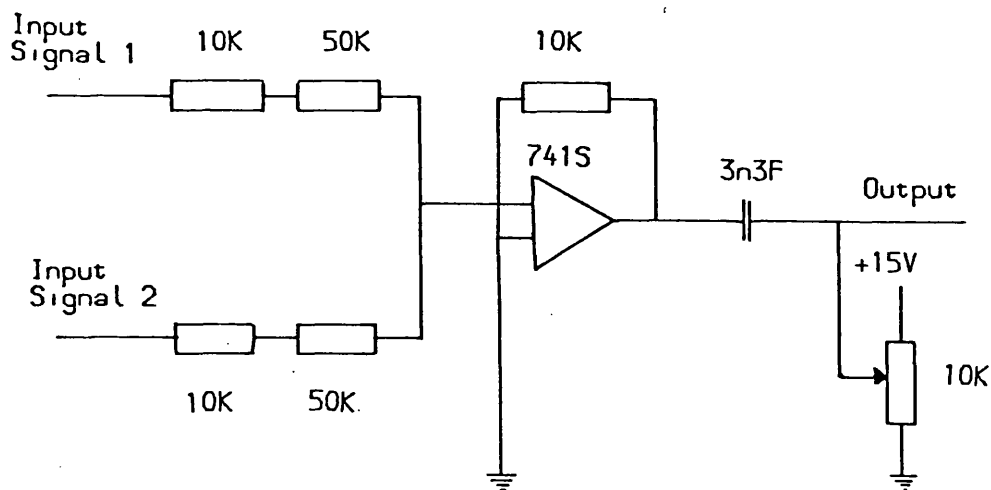


Fig 4.5.6 Signal Adder

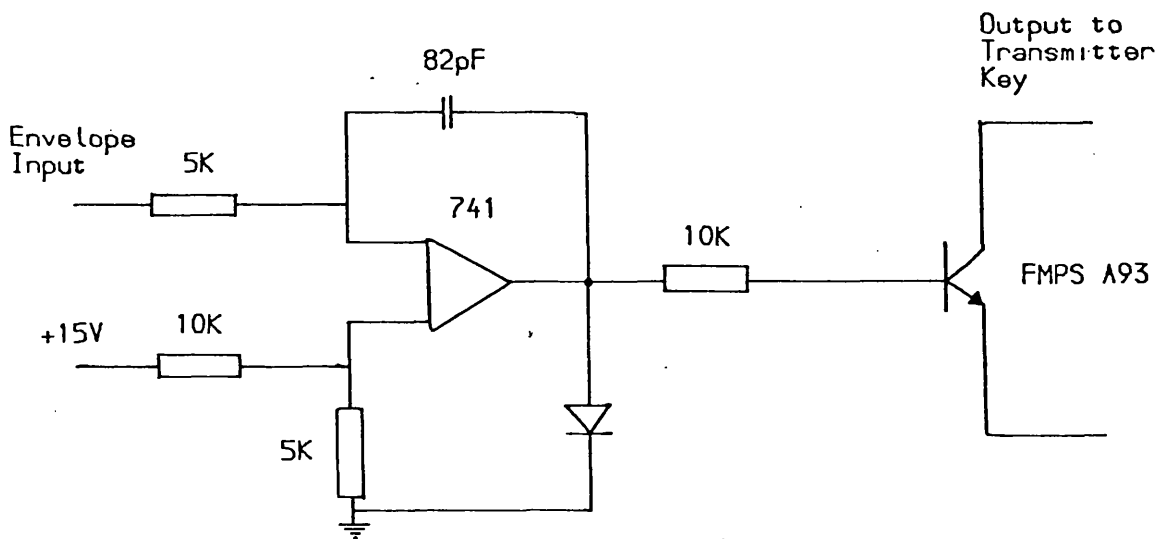


Fig 4.5.7 Transmitter Key

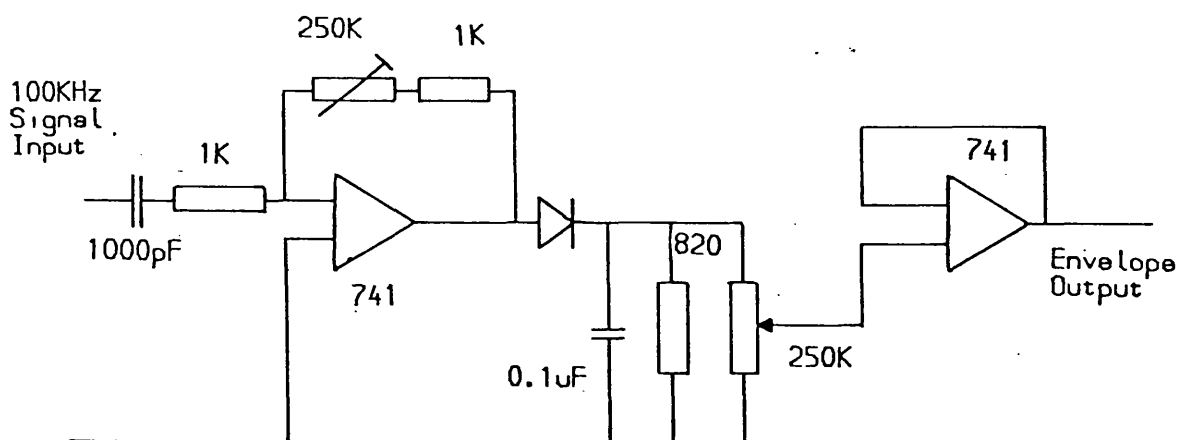


Fig 4.6.1 Amplitude Detector

sounder with several small differences as indicated below :-

- 1) The sequence number is input via a vDU rather than a switch.
- 2) The timing source is taken from the analogue to digital converter rather than an internal oscillator.
- 3) The output comes directly from a PIA as a TTL signal rather than through a modulator and detection process.

The program developed for this unit is described in section 5.1.

4.6 AMPLITUDE DETECTOR

The detector circuit (fig 4.6.1) is basically a diode envelope detector. Both input and output have 741 buffer amplifiers of variable gain in order to provide the optimum signal strength into the ADC.

4.7 PHASE DETECTOR

The phase detector (fig 4.7.1) measures in arbitrary units the phase difference between the incoming signal and a 100KHz reference waveform from the dividing logic. The input signal is first buffered. If it is of sufficient amplitude it is then fed to a second buffer and a discrete network to convert the incoming waveform to a standard TTL level. If the input signal is of poor quality or of rapidly changing amplitude a phase lock loop (PLL) is inserted between the buffers. This produces a 100KHz output locked to the input signal and with higher

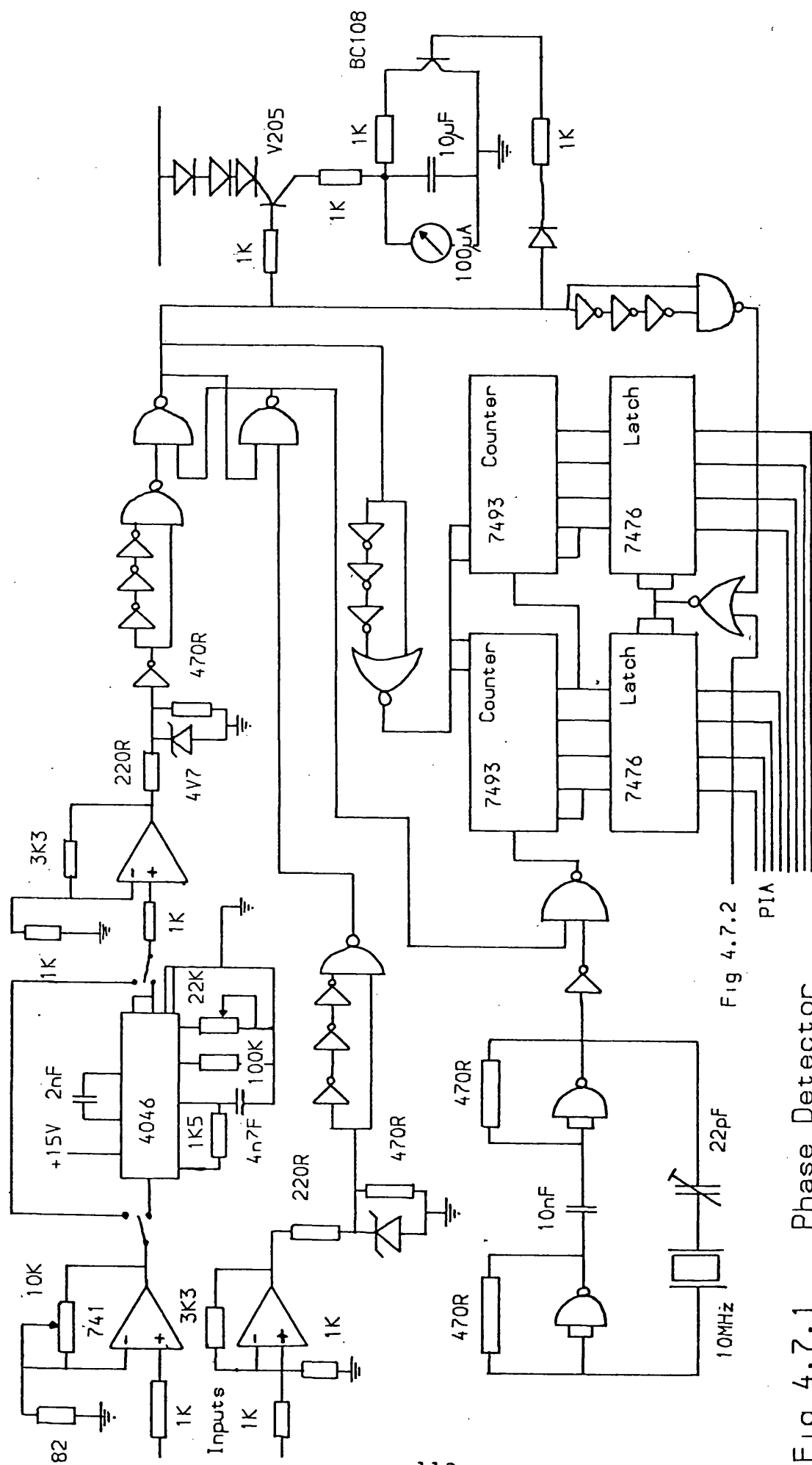


Fig 4.7.1 Phase Detector

Fig 4.7.2

immunity to noise and level changes. The PLL needs 10 cycles to lock onto the input.

The reference 100KHz is also buffered and limited to TTL levels. Both 100KHz signals then feed an edge triggered flip flop constructed to 'set' on a high to low transition from the signal and to 'clear' on a similar transition from the reference. The phase is measured as the number of cycles of a 10MHz waveform, counted while the flip flop is set. When the counting is completed the result is loaded into latches and the counters cleared for the next cycle. The result latches can then be read by the computer. A meter gives the operator a guide to the mark-space ratio of the flip flop output and hence the phase. This is most useful when accurately tuning the receiver by observation of the beat frequency.

The phase of the received sounding signal provides valuable information regarding the stability of the propagation path. The phase is read by triggering the phase detector on the edge of the received pulse. The computer is too slow to measure close to the leading edge of the pulse. This difficulty is overcome by constructing a hardware comparator (fig 4.7.2). The output of the ADC is compared with a preset digital value from a DIL switch. Once the signal exceeds this level a monostable of variable time constant is triggered. This in turn clears a flip flop which locks the phase latches hence taking a 'snap shot' of the phase at a known time from the beginning of a pulse. The PIA control lines CA1 and CA2 determine whether the phase measurement is continuous or single shot as described above.

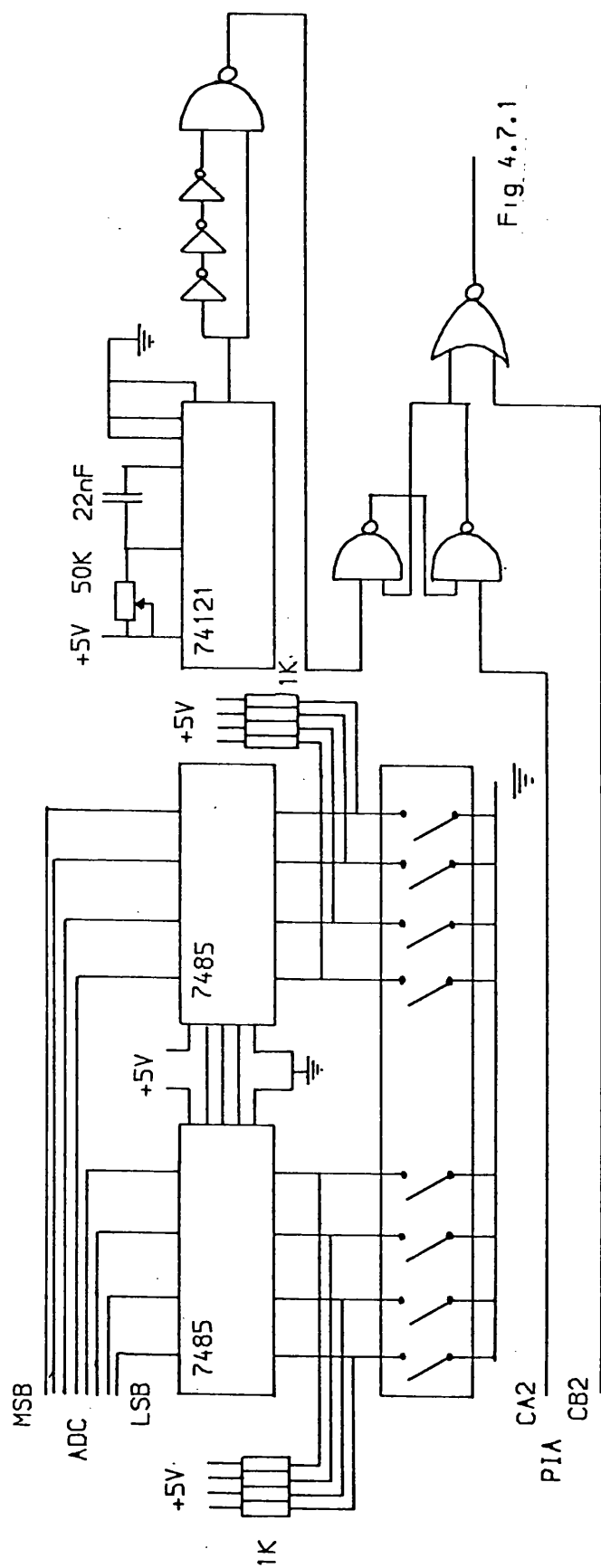


Fig 4.7.2 Comparator Trigger

4.8 FSK DETECTOR

Pseudo random data sequences were transmitted in FSK by RAE Farnborough and a demodulator was built to detect them. This unit (fig 4.8.1) takes the input signal (detected 100KHz), limits it to give a standard amplitude, then buffers it into the two high Q tuned circuits set at standard frequencies of 1275Hz and 2115 Hz. Thus one oscillator resonates on mark and the other on space. This sends the input of the 741 slicing amplifier either high or low. The output of this amplifier is then converted to TTL levels and can be input to either the computer or the ADC for analysis

4.9 ANALOGUE TO DIGITAL CONVERTER

The analogue to digital converter (ADC) board (fig 4.9.1) is built around the Datel ADC-EHB2-6001 chip which can produce an eight bit conversion in 4 microseconds. This digital value is fed to the computer through the A word of the first PIA.

The analogue input to the board is buffered to vary between 0 and 10V (the input range of the ADC chip). To keep the level into the ADC constant during a conversion the analogue signal is fed through a sample and hold chip (SHM-IC-1). The SHM chip contains a small capacitor and a buffer. It effectively samples by charging up the capacitor to the input voltage very quickly, then disconnecting the input. The voltage on the capacitor is then buffered out.

Also contained on the ADC board is the control clock for

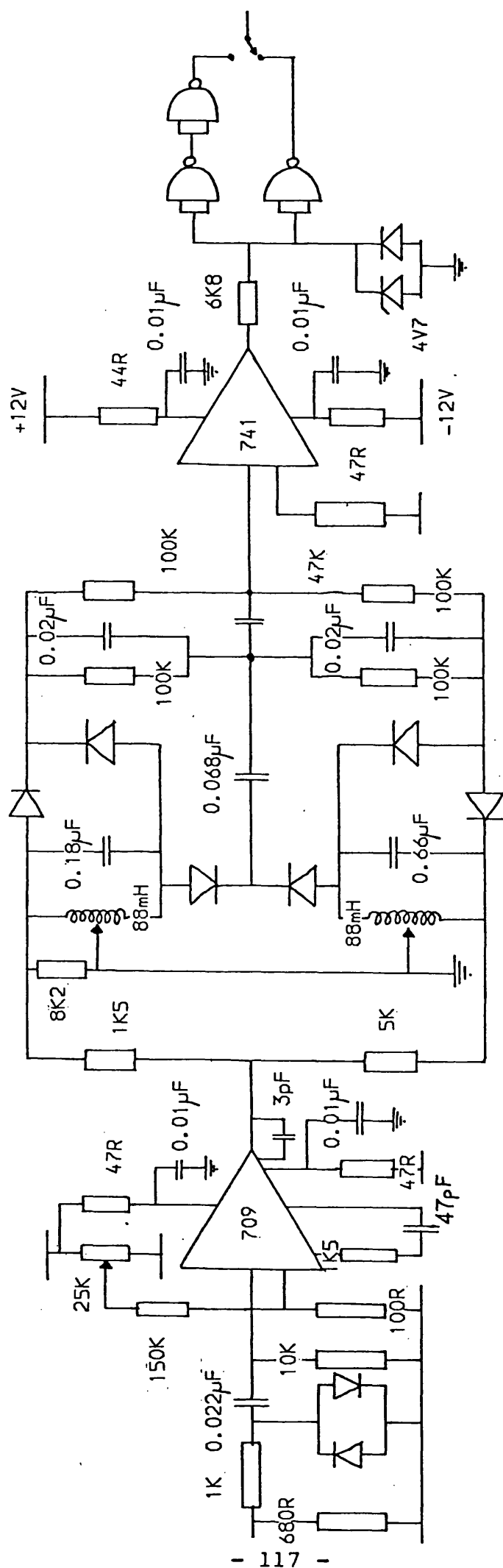
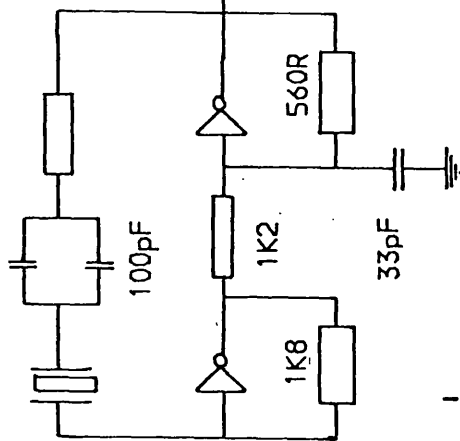


Fig 4.8.1 FSK Detector

3.2768MHz 5-60pF 100R



118

Analogue Input

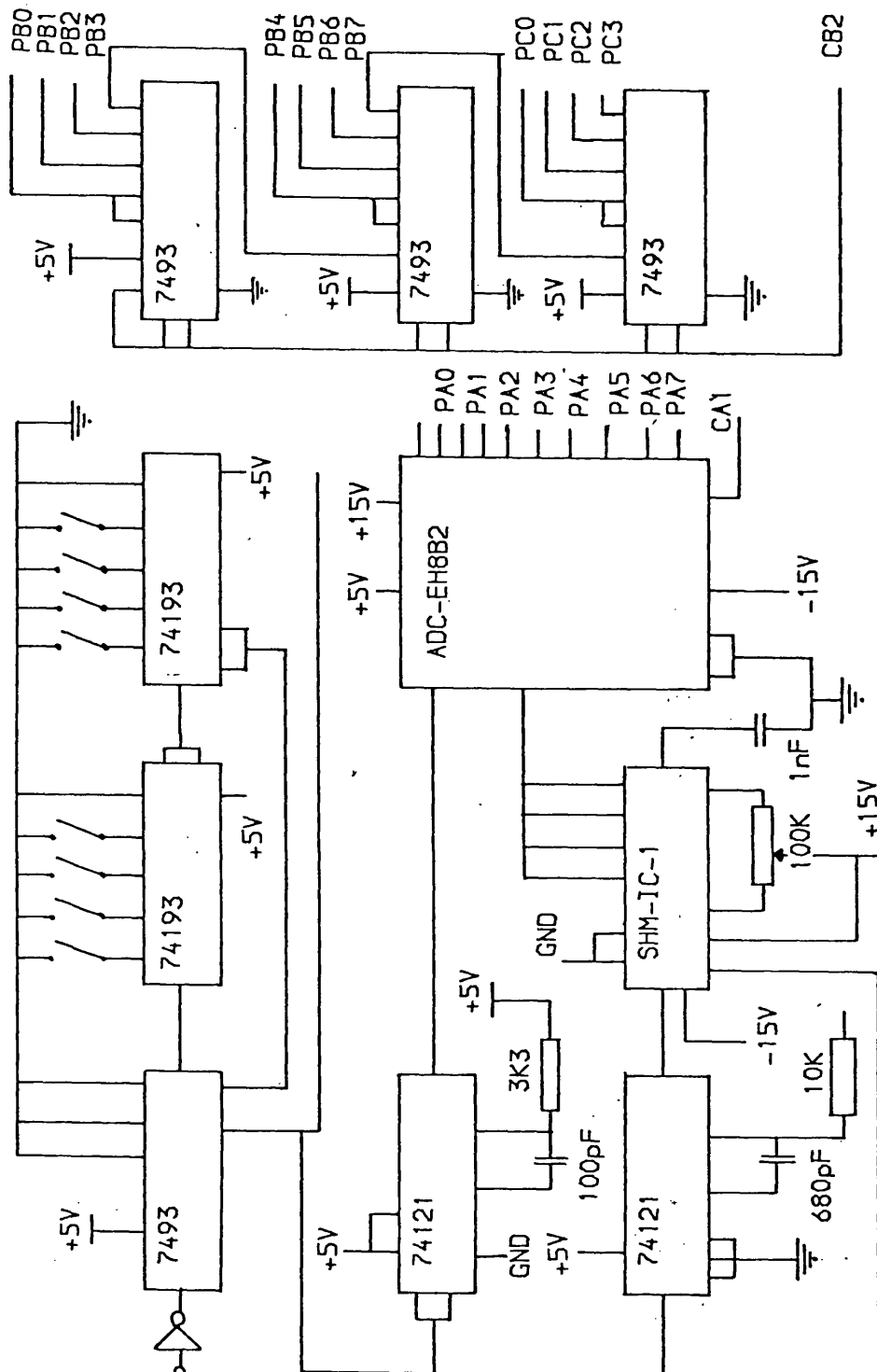
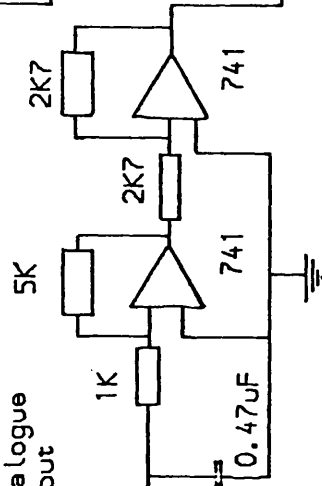


Fig 4.9.1 Analogue to Digital Converter

the ADC and the project computer. The master clock is the same as in the sounder (ie a 3.2768MHz crystal oscillator). This is fed into a divide by 16 chip and a series of programmable dividers. The counters are set by DIL switches to give one sample every 87.9 microseconds. This gives exactly eight samples per sounding pulse. The monostable integrated circuits control the timing of the ADC and the sample and hold. First a 4 microsecond pulse is sent to the SUM-IC-1 then a 100 nanosecond pulse to the ADC. This ensures the ADC only operates when the sample and hold is in the hold mode.

The final three dividers count the ADC trigger pulses to provide an external clock for the project computer. This clock instructs the processor when to read the ADC and when to expect a carrier break. The clock can be reset by the processor through the PIA control line CB2.

4.10 PROJECT COMPUTER

Initially the MSI 6800 described in section 4.5 was the control computer for this project. This machine was needed for other work and so a replacement was constructed. A block diagram of the new control computer is given in fig 4.10.1. The system is built around the S50 bus common to most 6800 based computers. A bus or mother board carries power, address, data and interrupt information between the processor board and any other board in the system.

The CPU board contains the MC6800 microprocessor itself and an ACIA (asynchronous communications interface adapter)

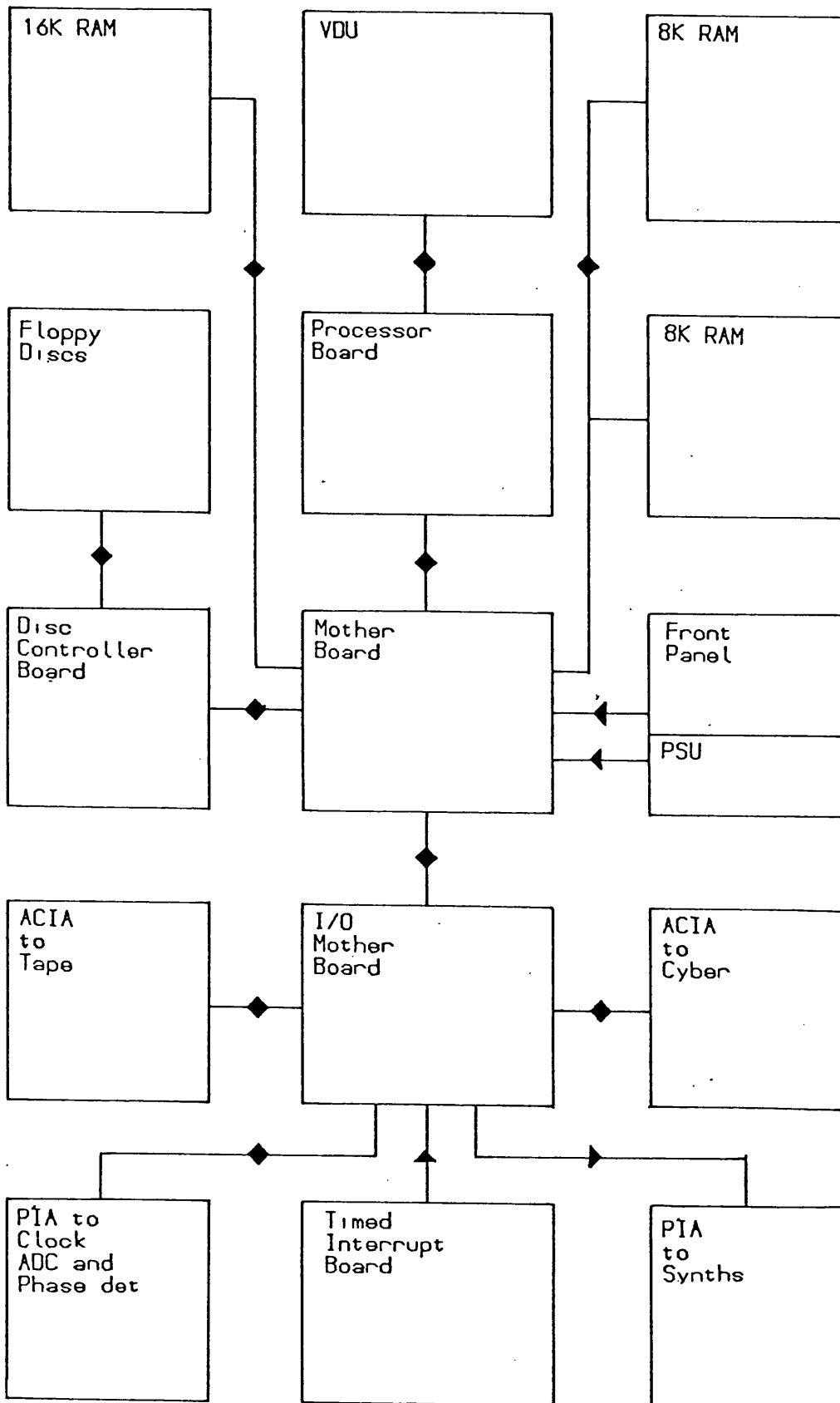


Fig 4.10.1 The Project Computer

which connects the computer to the VDU. Also on the processor board are 1K of RAM and up to 6K of EPROM. Contained within the EPROM space is a small monitor program named Ionbug 1.2. Ionbug enables the operator to examine and change the contents of any location in the computer.

Each board in the computer has its own address, for example to access a memory location on an 8K RAM board, the address of the location is put, by the processor, onto the address bus and the data from that location passes back along the data bus to the processor board. The two 8K RAM and the 16K RAM boards are simply extensions of the 1K memory on the processor board. The 8K boards were constructed for the project at Leicester while the 16K board is a commercial product. They occupy hex addresses from 0000 to 7FFF and are employed for storing both programs and received data before writing it to tape or floppy disk.

The disk controller board is again a commercial unit located at address 8000 hex. It takes data from the bus and places it in file format on the floppy disks. It can also load programs stored on disk into RAM, checking for errors on both the disk and in memory as it does so. The disk unit itself is a 'Smoke Signal Broadcasting BFD-3D' triple drive double sided minifloppy, each drive being able to store up to 256K.

The front panel enables the operator to reset or interrupt the processor manually. To drive the computer a power supply was constructed capable of providing 10A at 8V which is regulated down to 5v TTL. 15V and -15V at 1A supply the RS232 interface and EPROM chips. A memory map is given in fig 4.10.2

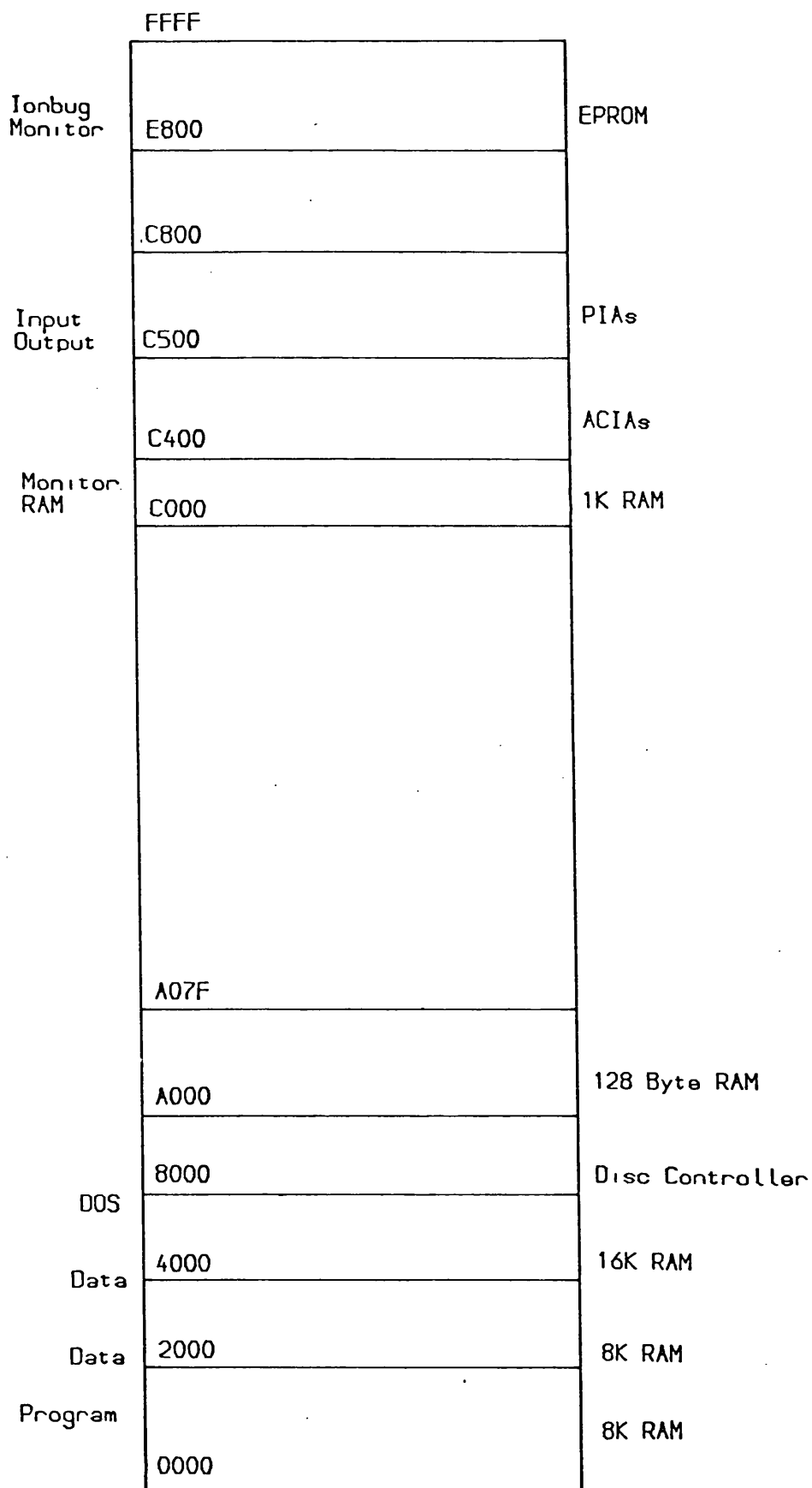


Fig 4.10.2 System Memory Map

which summarises the system configuration.

All input/output other than that to the VDU goes through the input/output mother board. This is similar in function to the main mother board but contains fewer lines. Attached to it are two ACIA boards, the first of which connects the computer to a cassette recorder for backup storage of programs and data. The second ACIA board communicates with the CDC Cyber 73 mainframe for direct program and data transfer.

Two double PIA boards are also connected to the input/output mother board. Each of these contains two PIA chips giving a total of 32 individually programmable input or output lines. The first board reads data from the ADC, clock and phase detector. The second board controls the synthesisers which drive the programmable receiver.

The final element of the hardware is a timed interrupter (fig 4.10.3). This consists of a 1MHz crystal oscillator driving six divide by ten counters. The outputs of the last five dividers give square waves of frequencies from 1Hz to 10KHz. A multiway switch on the back panel selects which of these is fed through a BC108 transistor to drive either the NMI or the IRQ interrupt line.

With the interrupter set to 1Hz it is employed to update a time of day clock. When an interrupt is received the program jumps to a service routine which increments the seconds counter thus enabling data and time of day to be recorded together automatically.

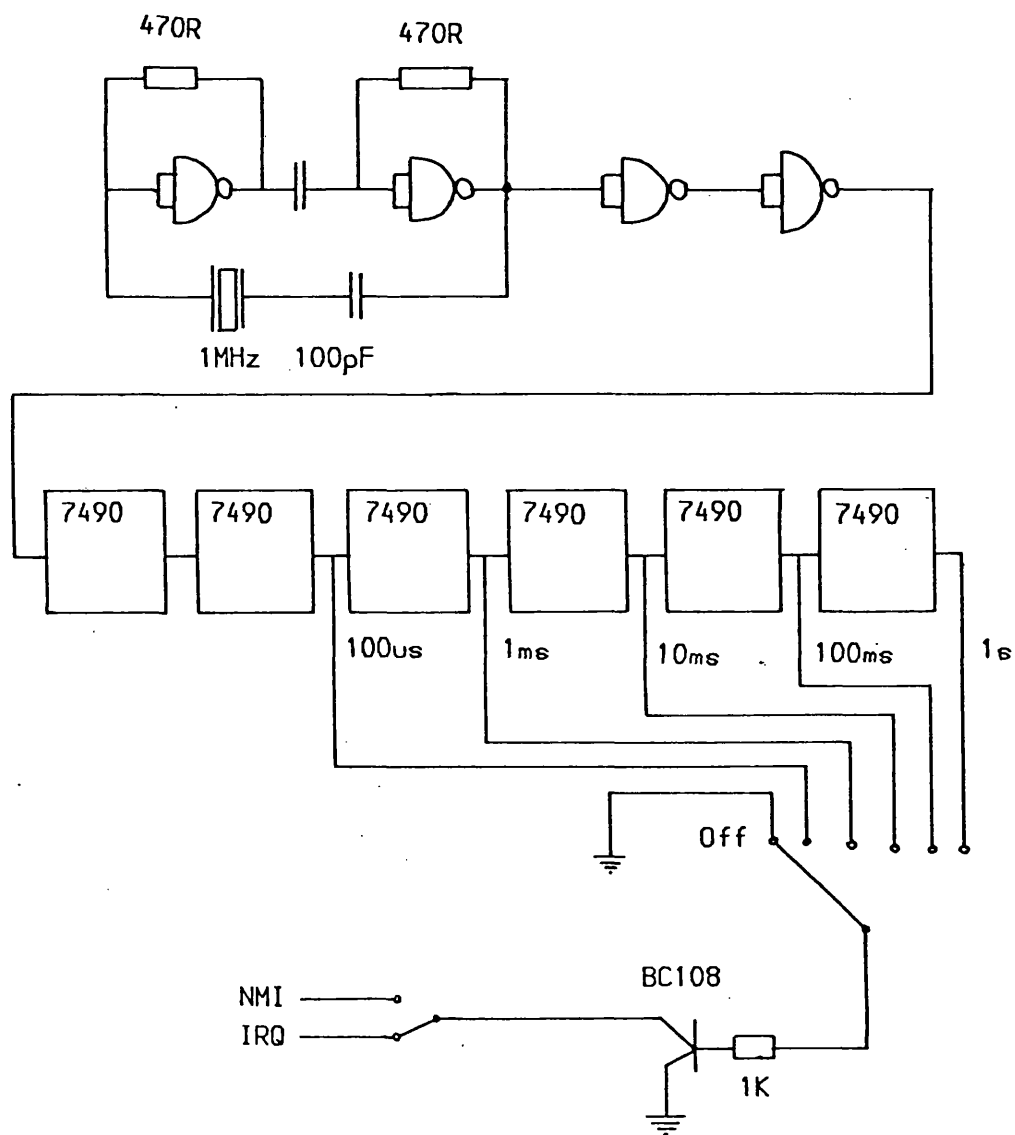


Fig 4.10.3 Interrupt Timer

4.11 SYSTEM RELIABILITY

The transmitting station equipment proved to be extremely reliable and only one major breakdown and three minor faults occurred during the entire period of operation. The first fault was caused by one of the EPROMs suffering a bit error making the pulse sounding speed up fractionally. This led to the drifting phenomenon discussed in section 6.5. Later an intermittent fault was noticed in reading the thumbwheel switch sequence selector. This resulted in an incorrect sequence being keyed. A second attempt to read the switch usually cured the problem.

In the radio transmitter hardware the GEC synthesiser occasionally went out of lock. This was rectified by buffering the output to prevent overloading. The only major fault occurred in the Redifon high power transmitter where the high tension transformer failed. This resulted in the transmitter being out of service for several months while the transformer was replaced.

At the receiving station most of the commercial equipment worked without fault. Slight lock problems were encountered with one of the Adret synthesisers. This was traced to a faulty circuit card and did not cause any loss of data. The analogue to digital converter and simulator hardware, both designed and built at Leicester functioned well throughout.

The phase detector was found to work correctly for strong continuous signals. The results obtained from pulsed work were more difficult to interpret due to a heavy amplitude dependence

and low noise tolerance. The phase lock loop which was inserted to combat this proved inadequate hence the lack of meaningful phase data for low amplitude signals.

The project computer was the least reliable part of the system. One months effort was necessary after construction to get it working and some new fault developed on average once every three weeks after that time. These faults were generally traced to either the processor board or the in house memory boards.

The design of the Leicester built computer was basically correct but it lacked the high quality robust construction of a commercial product. Small scale printed circuit board (PCB) production techniques and inexperience in board design caused many problems as indicated below :-

- 1) Thin tracks on the PCB led to high resistive losses and many breaks.
- 2) The lack of plated through holes on the PCB led to larger board size and an increase in the number of soldered links and hence the possibility of dry joints etc.
- 3) As the circuit boards were large and not securely mounted flexing and vibration led to a general weakening of the soldered joints as well as increasing the problems caused by the thin tracks.
- 4) For economic reasons the 8K memory boards were designed around the 2102 (1024 bit) RAM chip, rather than the more expensive 2114 (4*1024 bit) type. This led to an excessively high chip count, high power consumption and a large board size thus aggravating the other faults. Also

much difficulty was encountered purchasing the high speed version of this chip which virtually went out of production once the project started.

The above faults could be tolerated at standard speed operation. To accomplish the real time processing however it was necessary for the CPU clock frequency to be increased from 1MHz to 2MHz. This is available on a commercial system but it proved impossible to raise the in house computer above 1.5MHz. Even at this speed the memory boards intermittently failed on certain locations thus causing the disk operating system to crash and faulty data to be logged. Examples of this can be most clearly seen in the bottom right hand corner of many of the waterfall graphs in chapter 6 (eg fig 6.2.5)

The trouble with the computing element of the project stemmed from the false economy of building a computer rather than buying an available commercial unit costing only 30% more than the cost of the components used.

CHAPTER 5

PROJECT SOFTWARE

5.0 PROGRAM OVERVIEW

The programs or software employed on this project will be described in the same order as the hardware in the previous chapter. They fall into three groups as indicated below :-

- 1) Control software for the programmable sounder and the MSI 6800. This section also includes the software to drive the synthesisers and hence the slave RA117 at the receiving station.
- 2) Data collection and logging software. This software recognises the pulse sounding signal (section 5.3) and also the pseudo random data sequence (section 5.4). These two routines leave the received data in the main RAM memory of the project computer. There is only limited space in the computer for this data and consequently it has to be placed as quickly as possible onto a larger temporary storage area, such as floppy disk or magnetic tape. The programs to implement the transfer are described in section 5.5.
- 3) Analysis and presentation of data. After collecting the data it is analysed and plotted out as follows. First the data is retrieved from the floppy disk and sent down to the Cyber 73 mainframe computer via a slow speed serial

line or on magnetic tape (section 5.6). The data is then checked for errors caused by the transfer process and then plotted out in graphical form (section 5.7). Also at this time further analysis of the results can be undertaken, for example, examination of burst errors in the pseudo random sequence or the determination of the mode content of the pulse sounding.

5.1 PROGRAMMABLE SOUNDER

The program which controls the sounder is outlined in fig 5.1.1 and is fully reproduced as appendix I. The subroutine flow diagrams are presented in fig 5.1.2.

When the processor is reset or power is restored after a failure, the program goes through the restart procedure. This first involves setting up the interrupt routine. All timing in the program is done by interrupts supplied by the external electronics. To achieve this the program waits until an interrupt is received before continuing execution hence locking the program running speed to an external standard. The startup routine also initialises the PIA to output control signals to operate the transmitter and finally to accept information from the BCD switch within the additional electronics.

The program then reads the number of the sequence from the BCD switch and jumps to the relevant routine (seq 0 to seq 7). The most simple of these is sequence 1. This sends the callsign G9BLD in Morse code followed by about an hour of pulse sounding. This is repeated until the processor is reset or a

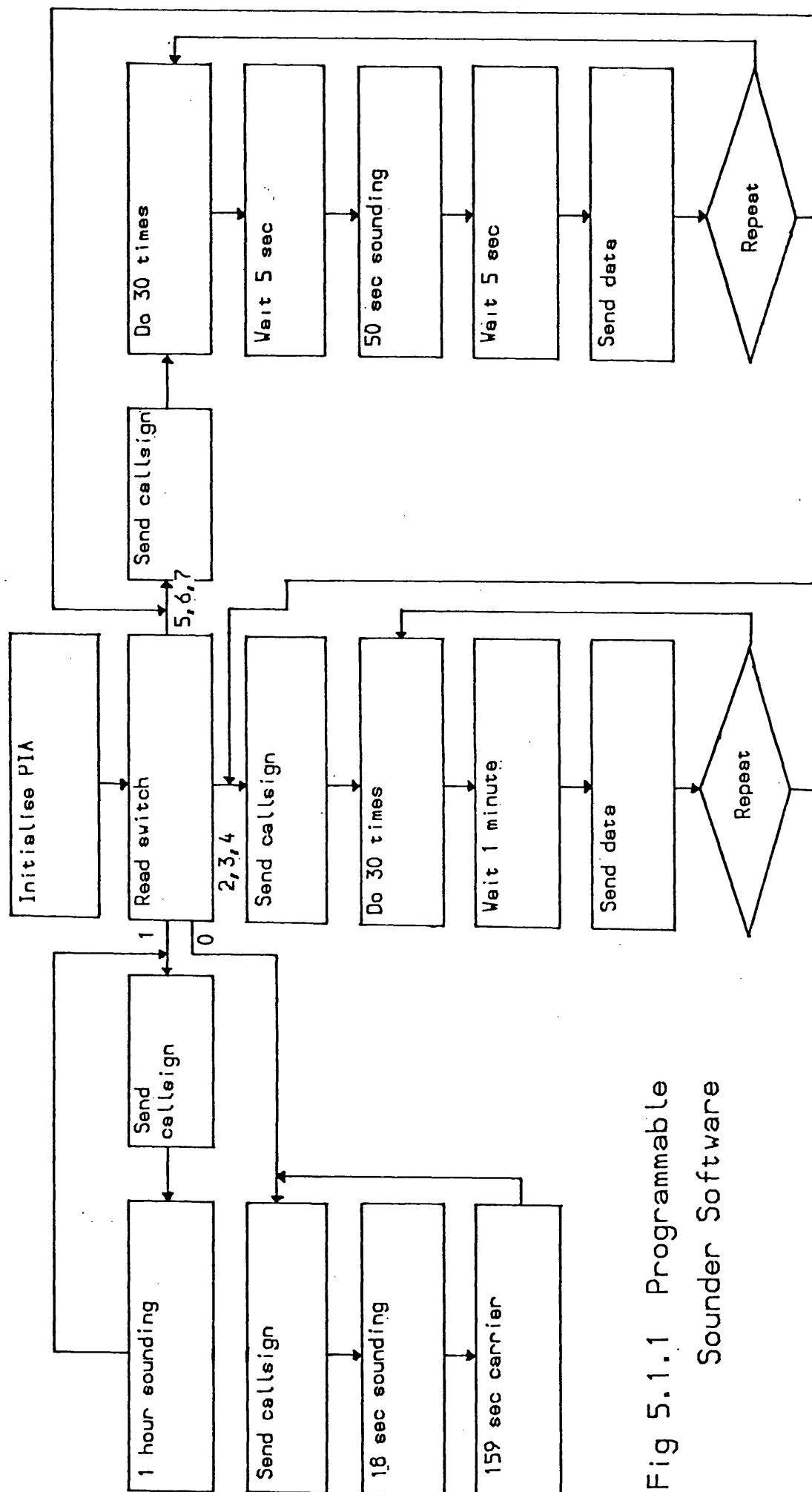


Fig 5.1.1 Programmable
Sonder Software

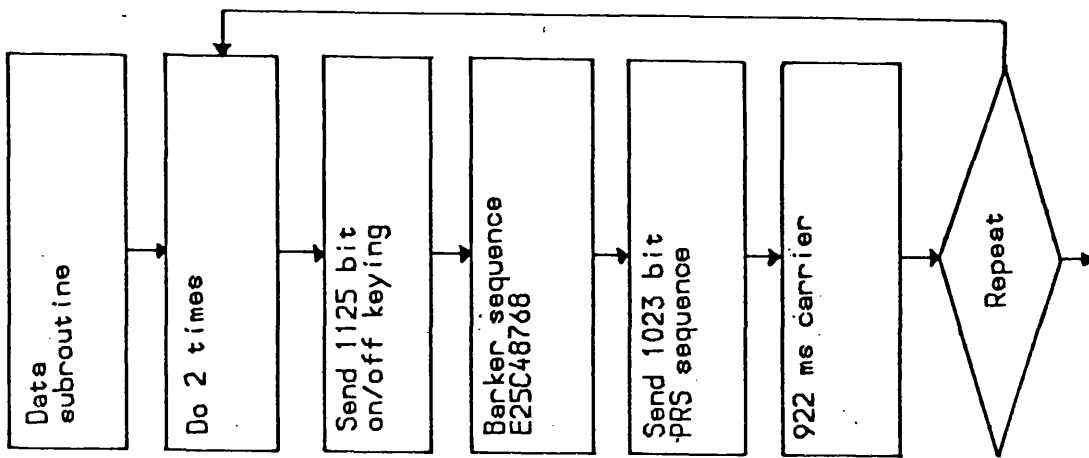
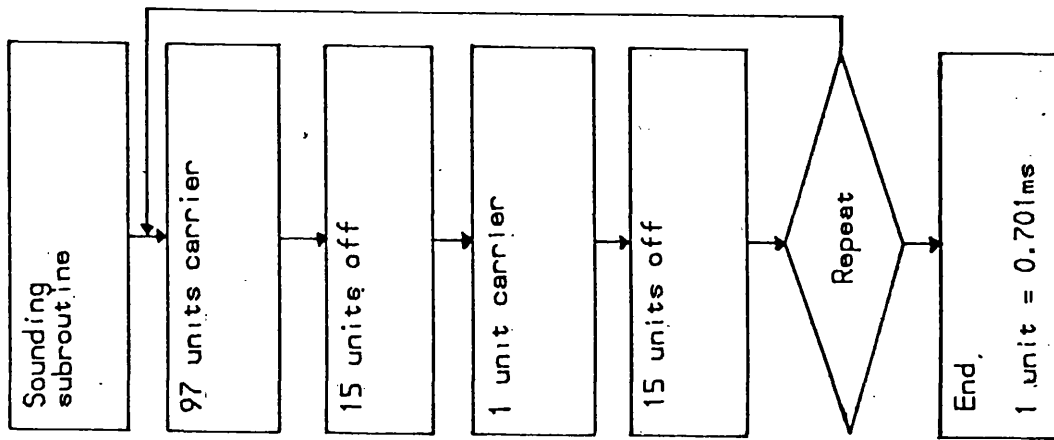
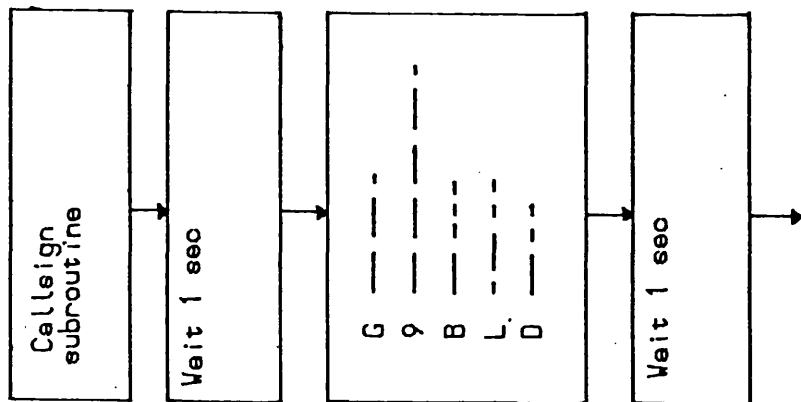


Fig 5.1.2 Programmable
Sounder Subroutines

new sequence. Sequence 0 is useful in setting up the equipment. As with sequence 1 it starts by keying G9BLD in Morse code followed by 18 seconds of pulse sounding and 159 seconds of carrier on. The entire sequence repeats until stopped by reset.

The other sequences are for use with the data and error detection parts of the project. Sequences 2,3 and 4 as before send G9BLD every hour. Throughout the rest of the time they alternate, sending a minute of silence followed by a minute of data. The difference between the three sequences is that 2 sends at 50 baud, 3 at 75 baud and 4 at 600 baud. Sequences 5,6 and 7 are the same as 2,3 and 4 except that in place of the one minute break in transmission are 5 seconds of silence, 50 seconds of pulse sounding and a further 5 seconds of silence. These sequences are summarised in the table below.

Sequence Number	Description
0	G9BLD 18 sec pulse sounding 159 sec carrier repeat
1	G9BLD 1 hour pulse sounding repeat
2,3,4	G9BLD 1 hour 1 min break 1 min data sounding repeat repeat 2=50 baud, 3=75 baud, 4=600 baud

5,6,7

G9BLD

1 hour 5 sec break

50 sec pulse sounding

5 sec break

1 min data sounding

repeat

repeat

5=50 baud, 6=75 baud, 7=600 baud

The data sequence itself is made up of 3 sections :-

- 1) 1125 bits of on/off keying are first sent to synchronise the transmitter and the receiver so the latter knows when a data bit will arrive.
- 2) To enable the receiver to lock onto the start of the message a 33 bit Barker sequence is sent (E25C48768 hex).
- 3) After this synchronisation sequence comes the test data message itself.

This message consists of a 1023 bit pseudo random data sequence (PRS), produced from the output of a shift register. The feedback to the input is provided by an exclusive OR gate fed from bits 5 and 10 of the shift register. In the program the PRS is actually stored in PROM rather than being generated at run time, for ease of checking. An assembly listing of the program is given as appendix I. The data and pulse sounding sequences are described in greater detail in sections 5.4 and 5.3 respectively.

5.2 RECEIVER CONTROL

The computer controlled receiver described in section 4.3 is operated by several control routines located in EPROM on the project computer CPU board. The routines can either be called from a control program or from a small driving program also located in EPROM. The driving program recognises the command characters M,F,S,+,-,., which produce the following action :-

Command	Action
M	Return to the monitor
F	Input new frequency
S	Review the receiver status
+	Scan up in frequency
-	Scan down in frequency
.	Stop scan

A new frequency is entered as MM.HHHHHH where MM are the MHz digits and HHHHHH are the Hz digits. The first receiver VFO is then calculated.

$$VFO1 = ((MM/2) + 20.25) \text{ MHz}$$

Then the second.

$$VFO2 = (4.599902 - 0.HHHHHH) \text{ MHz}$$

The two VFO frequencies are then loaded into the interface electronics and finally both the required frequency and the two VFO frequencies are displayed on the control VDU.

After a '+' or '-' scan command a two digit hex number is input. This number is in Hz and is either added to or

subtracted from the current frequency. The result is then fed back into the program to set up VF01 and VF02 which then control the receiver. The program is given as a block diagram in fig 5.2.1 and in full as appendix II.

5.3 PULSE DETECTION

A block diagram of the pulse data collecting software together with a diagram of a simplified pulse waveform is reproduced in fig 5.3.1. The analogue to digital converter supplies a new sample every 89.9 microseconds. The pulse detecting program must first recognise the break after the large block of carrier in the pulse sounding waveform. This is achieved by setting a trigger level above which the carrier is defined as present.

As each of the samples are read, a counter in the computer is incremented up to a maximum value of 128 if the carrier is above the trigger level and decremented to a minimum value of zero if the carrier is below the trigger level. During the on/off transition which is to be located the counter should go from 128 to 0 in 128 samples. Allowing for noise and interference the program will recognise a transition if it is completed within 150 samples.

Having successfully recognised the transition (A,B) the program then inspects the incoming waveform over a complete cycle (C,E) and checks that the format is that expected for pulse sounding (ie approximately 69ms high followed by 22ms low). This procedure ensures that transition (A,B) belongs to

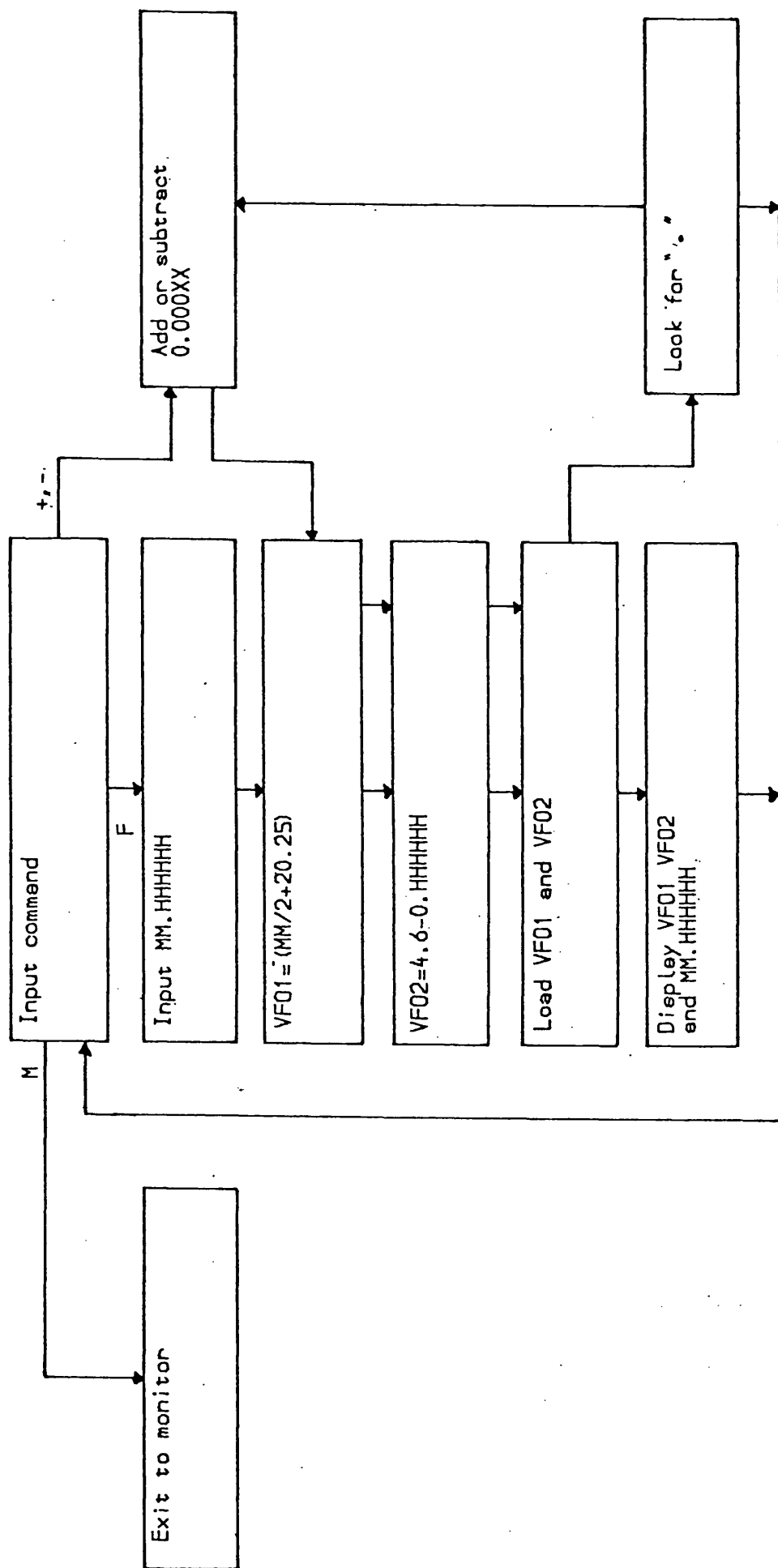


Fig 5.2.1 Receiver Control Software

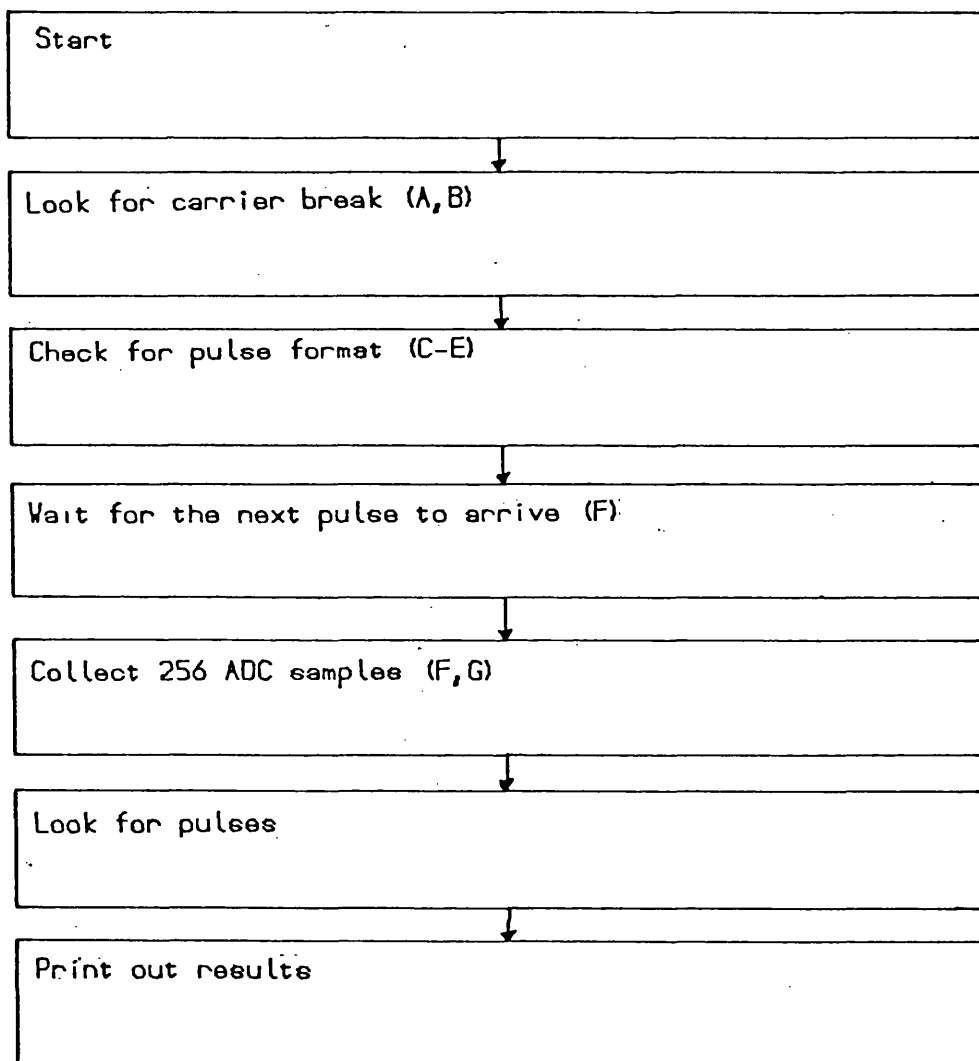
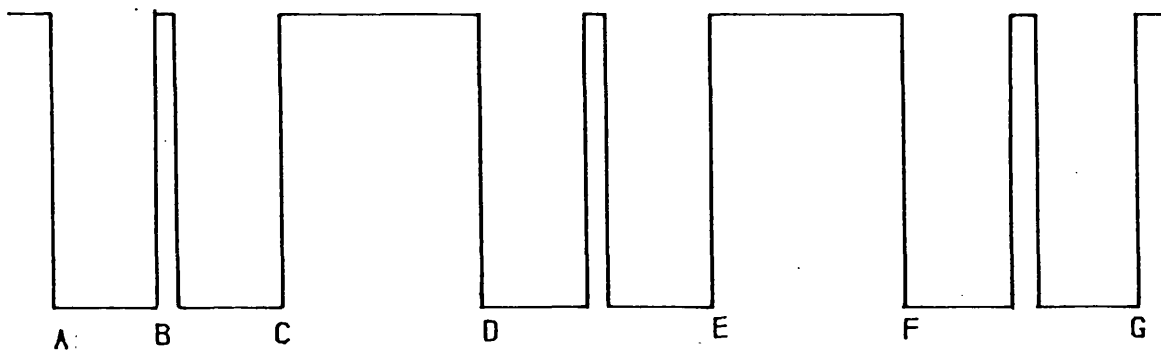


Fig 5.3.1 Pulse Data Collection

the pulse sounding rather than to the data sequence or the callsign.

If this test succeeds the program waits for 67ms (point F) and then reads 256 values from the ADC and stores them in main memory. Depending upon which control program is in use (section 5.5) the data from as many as 64 successive pulses can be stored in memory until this space has been exhausted. Once the first set of pulses has been found using the technique outlined above all further pulses are logged by waiting 69ms and then taking a further 256 ADC samples. Thus all the sets of pulse information are synchronised to the arrival time of the first, so if for example, a fade occurred during the period of logging, continuity would be maintained. Examples of this effect can be seen in chapter 6.

Once the pulse set has been captured, several possible options are available to the program. Usually the ADC points are stored on floppy disk or magnetic tape, then plotted out and analysed by the Cyber 73 mainframe computer. It is also possible for the project computer to analyse the returned pulse and display the relative amplitudes and arrival times of the propagation modes present. To reduce the effect of random noise eight consecutive pulse data sets are averaged and the search for the pulses is conducted on this. A simplified flow diagram of this process is presented in fig 5.3.2. The program searches through the data set first looking for the signal to go low (A) and only then starts to search for pulses. A pulse is defined as a group of more than one data points above the trigger level. When a pulse is found, its peak (C) is taken to define

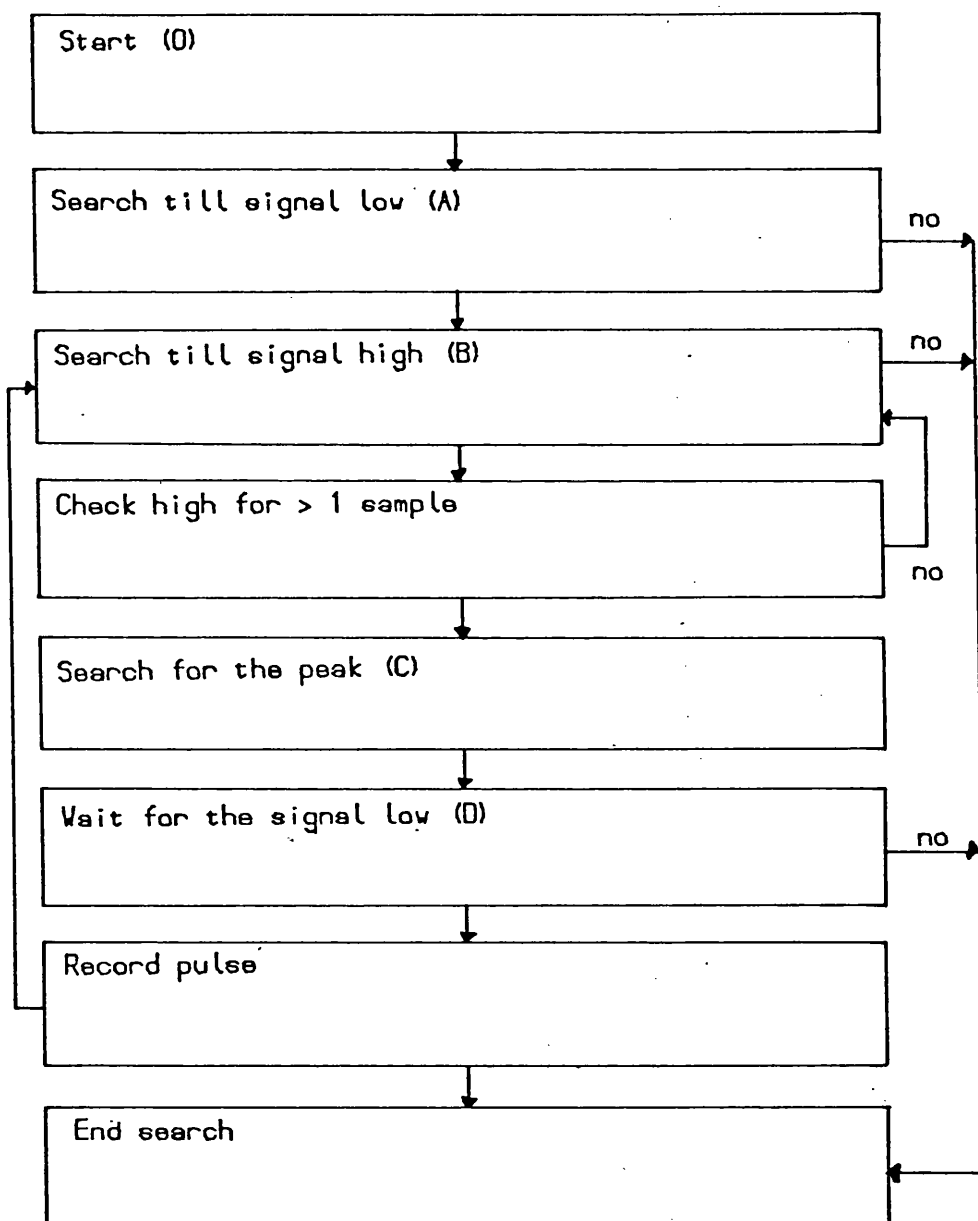
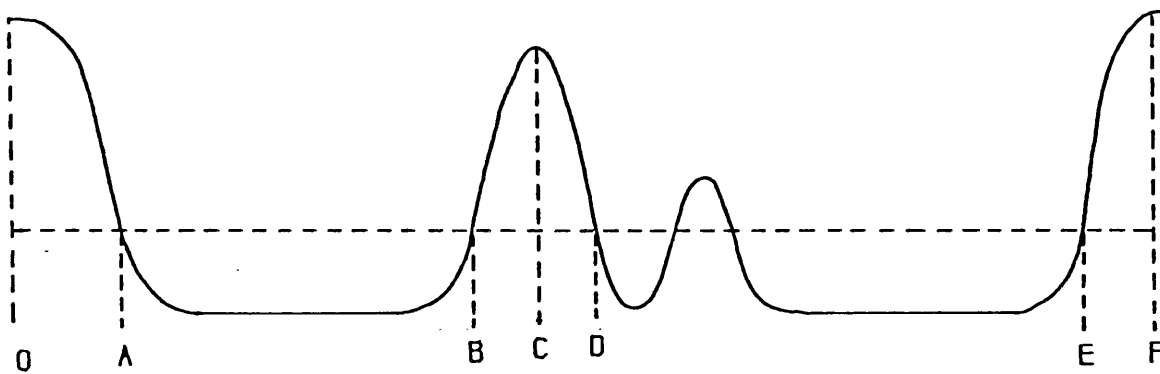


Fig 5.3.2 Pulse Data Analysis

the time of arrival and amplitude. This process is repeated until the program meets either the start of the carrier block (E) or the end of the data set (F). up to eight pulses can be detected using this software.

Two improvements were later added to this detection method. Firstly the time of arrival was redefined as the instant half way between the times where the signal crossed half the maximum level. This ensures that the time of arrival is less susceptible to the noise on the flat peak of the sounding pulse. The second improvement enabled the program to separate two pulses arriving so close together that the signal did not fall below the trigger level in the interval between them. To recognise this effect, the requirement for the signal to fall below the trigger level was replaced by the need for the signal to drop at least 20 points below the adjacent pulses. The measured amplitude and time information is then displayed on the control VDU.

5.4 PSEUDO RANDOM DATA DETECTION

The data format chosen to examine the errors in the received signal is described in section 3.2. The objective is to read the 1023 bit PRS and thus measure the error rate. This requires that the exact starting time is determined. This is achieved in two separate operations :-

- 1) On/off keying. A transition from a '1' (voltage above the trigger level) to a '0' (voltage below the trigger level) is detected and taken to be the start of a bit of

information. The next eight bits of information are then read. If these bits form the word (01010101) then bit synchronisation has been achieved. If however at any point in this sequence an error bit is found the program returns to the beginning (fig 5.4.1).

- 2) Barker sequence. Once bit synchronisation occurs the program starts looking for the Barker sequence which indicates the start of the 1023 bit PRS (fig 5.4.2). The Barker sequence contains 33 bits of information in the pattern (11100010010, 11100010010, 00011101101). This is made up of three 11 bit Barker sequences. For greater clarity only one of these is shown in fig 5.4.2. The reasons for employing a sequence of this type are discussed in section 3.2. The incoming signals from the ADC are converted by the program into '1' or '0' data bits which are fed into the software equivalent of a shift register, (actually a continuous loop of memory). After the latest bit has been added to this loop by clocking the shift register the contents are compared with the known values of the Barker sequence. If the sequence has been received correctly the result will be 33, one for each correct bit. As over an ionospherically propagated path errors are likely, a threshold of 25 is set over which the Barker code is said to have been recognised. If the result of the comparison yields a value of less than 25 the Barker code has not been found and therefore the next bit of data is clocked into the shift register and the test repeats. The implementation

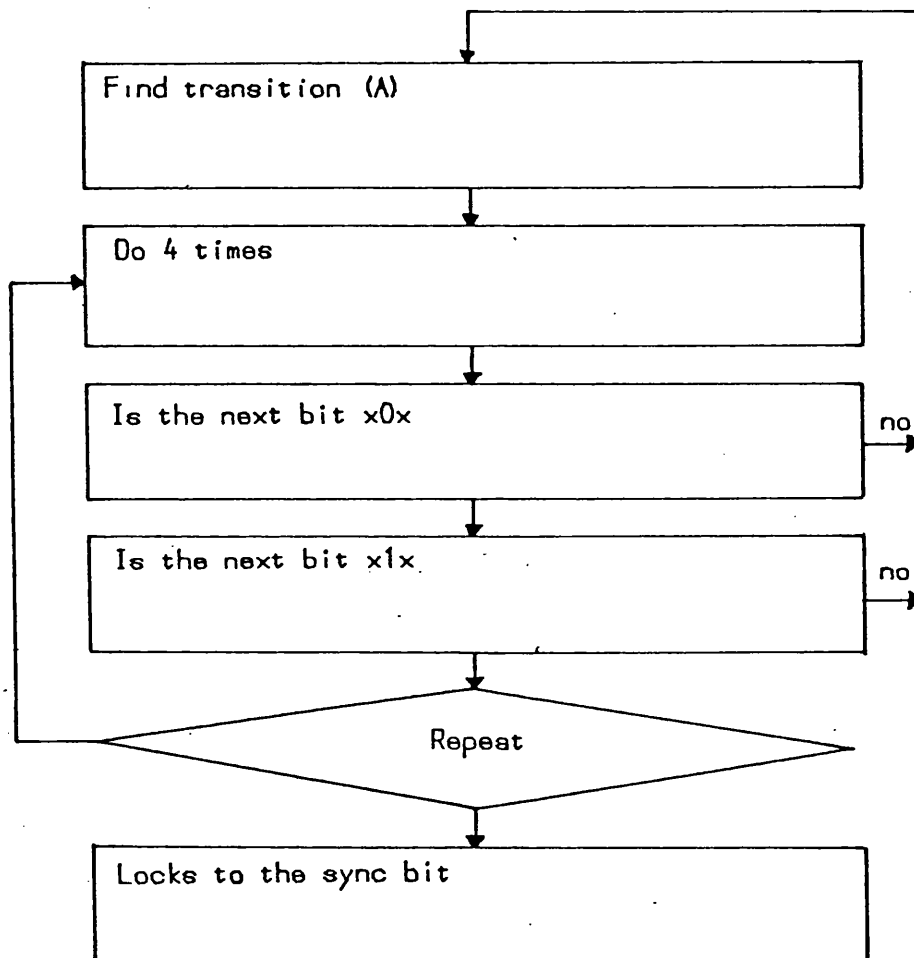
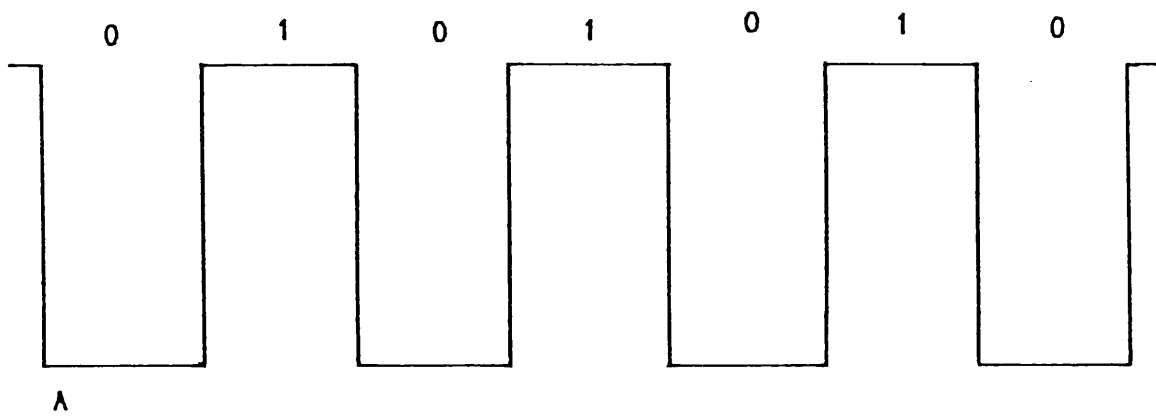


Fig 5.4.1 Bit Synchronization

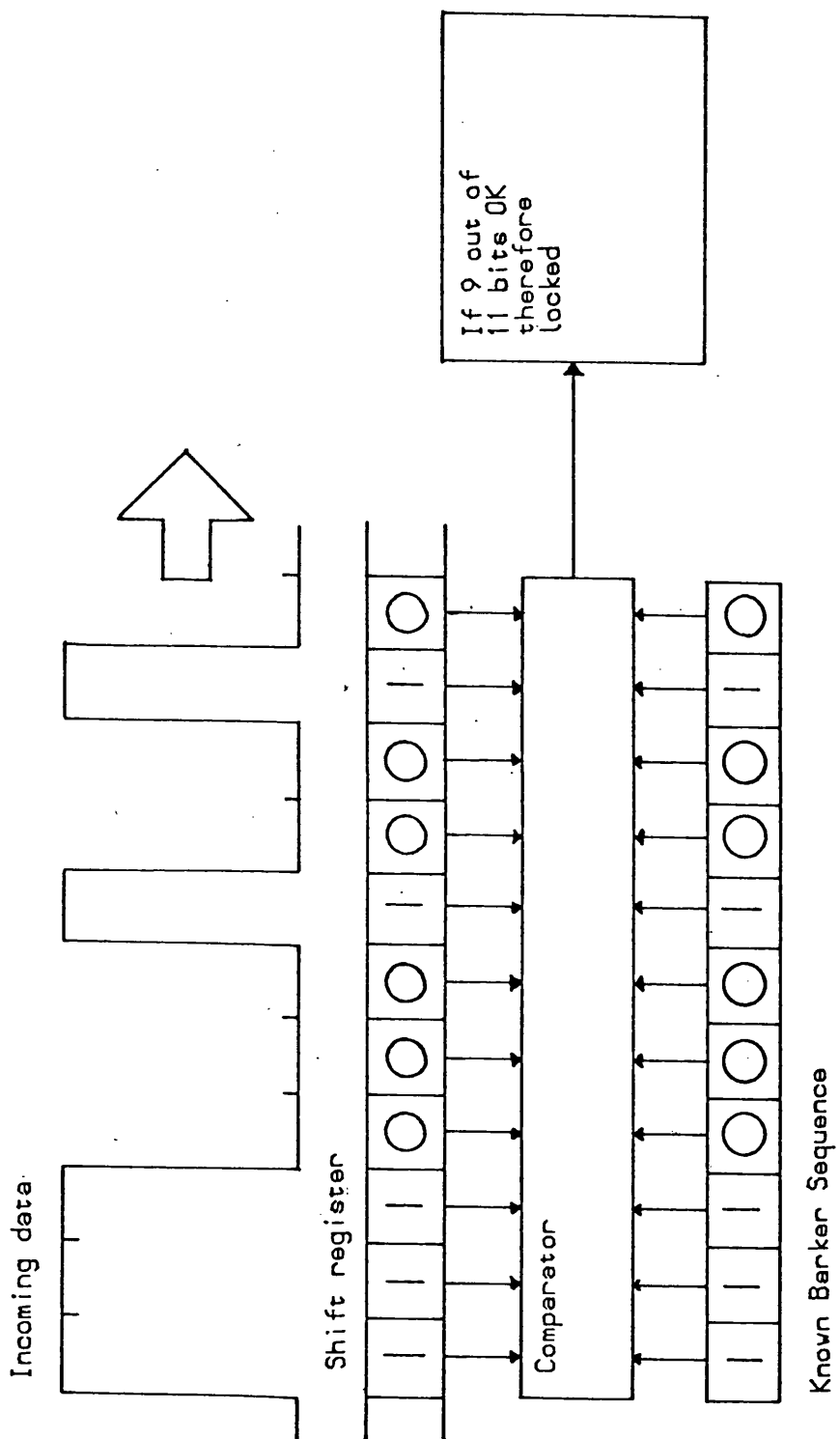


Fig 5.4.2 Barker Sequence Recognition

of this routine is the most difficult part of the entire process involving 33 comparisons plus the associated instructions to set up addresses and collect the data bit taking place within 1.6ms (1 bit at 600 baud). Ideally a faster microprocessor or some hard wired logic would have been useful to accomplish this as the computer system described in section 4.10 becomes rather unreliable at high speed.

Once the Barker code has been recognised the program reads the 1023 bit PRS into main memory. When this has finished the contents of memory are compared bit by bit with the known composition of the data sequence which is stored in EPROM. The number of bit errors is then displayed on the VDU connected to the project computer.

5.5 DATA LOGGING

The data is stored in the project computer RAM memory. Since only a limited amount of space is available here (16K) it has to be transferred onto either floppy disk or tape. To put a character onto the disk the only steps needed are first to transfer the data from memory into the A register of the MC6800 microprocessor and secondly to call the subroutine DFM which was supplied as part of the commercial disk operating system (DOS).

All the routines required to take the data from the receiver and put it onto disk are contained within one program which is reproduced in full in appendix III. The program is

driven by a questionnaire type command structure. The first question is whether to place the data on tape, VDU, or disk and if onto disk under what file name. The second question asks what type of data is required. The possible responses and the actions they produce are outlined below.

A - will accept data from the ADC until memory is full, then dump this information to floppy disk. The data acquisition rate is set as one sample every $(N * 89.9)$ microseconds, where N can be input from the terminal and is an integer between 1 and 256. 16384 samples of amplitude information can be taken which depending on N gives a time window from 1.46 seconds to 6 minutes 13 seconds. This routine is particularly useful for recording data of unknown format or when investigating the amplitude variations over an entire cycle rather than just the period around the sounding pulse.

M - will store 64 of the 256 byte data sets described in section 5.3. The time covered by the 64 data sets is approximately six seconds. Observations have shown that during this time modes of propagation can noticeably fade out or strengthen, thus causing the trigger time to vary with respect to the transmitted signal envelope. As this would make it difficult to compare successive sets of data, all the data sets are synchronised with the arrival time of the first. This type of file allows easy investigation of the variation of propagation conditions under noise or fading. If both amplitude and phase information are required only 32 data sets can be held.

E - has approximately the same function as M but takes only

eight data sets rather than 64 and is mainly used for demonstration purposes.

D - collects two data sets of PRS data (described in section 5.4) and then calculates the number of received errors. The data sets are then stored on floppy disk or magnetic tape for later more detailed analysis. The program then waits for a further set of data to arrive and then repeats the process until it fills the available storage space. This data logging routine corresponds to sequences 2, 3 and 4 in section 5.1.

B - collects both pulse and PRS data so that some comparison can be made between the amplitude stability of the incoming modes and the errors detected in the PRS data. To do this the program reads two sets of PRS data from the ADC, then stores these in main memory. After this it reads eight sequential sets of pulse sounding data as in the E command. Both the pulse and PRS data are then stored on disk or tape as one block of information and the program returns to look for the next burst of data.

Of the remaining commands T tests the interrupt timer and S activates the program described in section 5.3. The following five questions are asked by the computer to set up parameters inside the program. They are :-

- 1) Should the program echo the logged data to the control VDU
- 2) Which of the antenna inputs to the receiver should be used
- 3) Is phase information required ?
- 4) What is N ? (Data type A only)

5) What is the data baud rate ?

Finally the program requests the time, date, transmitter site, callsign, operating frequency and a forty character text buffer for comments. The receiver frequency is then set up, the interrupt clock is initialised and all the above information is put onto the disk or tape in a standard format irrespective of the data that follows. This forms a header which will enable future programs working on the file to decide which type of data it contains.

The data set is then put onto either disk or tape as compressed ASCII code or as HEX digits. It is more efficient to dump hex digits as each data point is stored in only eight bits. However it is harder to decode than ASCII especially for the more complicated formats such as B type data. ASCII dumping occupies more disk space (12 bits per point) but makes decoding easier, moreover with the greater redundancy error checking is much more simple. The program that collects, analyses and logs the data is given as appendix III.

5.6 DATA DUMPING

Data sets collected by the above routines and stored on disk have next to be transferred to the cyber 73 for further analysis and graph plotting. Three methods are available, a) cassette tape, b) down line loading, c) nine track magnetic tape.

a) Initially the data sets were taken from the disk to the Cyber by reading the information character by character through

Texas 733 electronic data terminal at a constant rate of 1200 baud. The cassettes written by the Texas 733 are of a format readable by the mainframe computer.

b) Down line dumping involves the same procedure as described above but with the data being transferred via a serial line into the Cyber. All the early experimental results from Tromso and some of the Elgin work was processed in this way. The very slow dumping rate that could be achieved, only about 350 baud, meant that a disk would take approximately five hours to dump, thus occupying a much needed line for an extended period. After dumping finished the project computer was programmed to send an end of text character to the Cyber followed by a message to save the data set as a permanent file. A further problem found with this method is that should either the micro-computer or the mainframe crash during the period of the dump the entire contents of the file would be lost and the process would have to be restarted.

c) Towards the end of the Elgin experimental work a nine track magnetic tape deck became available as a route to the Cyber. This unit consists of an EMI data 800 deck controlled by a micro-computer (identical to the project computer) which was programmed to accept characters from a serial line. The tape deck is easily able to accept characters at 9600 baud and therefore considerably speeded up the dumping process.

All data sent to the Cyber is coded in ASCII as this makes reading easier and there is no space constraint on the magnetic tape, as in the case of floppy disks. The dumping program reads the header line to discover in what code the disk is written

and then converts it to ASCII if necessary. A final version of the dumping program is given as appendix IV.

5.7 DATA ANALYSIS

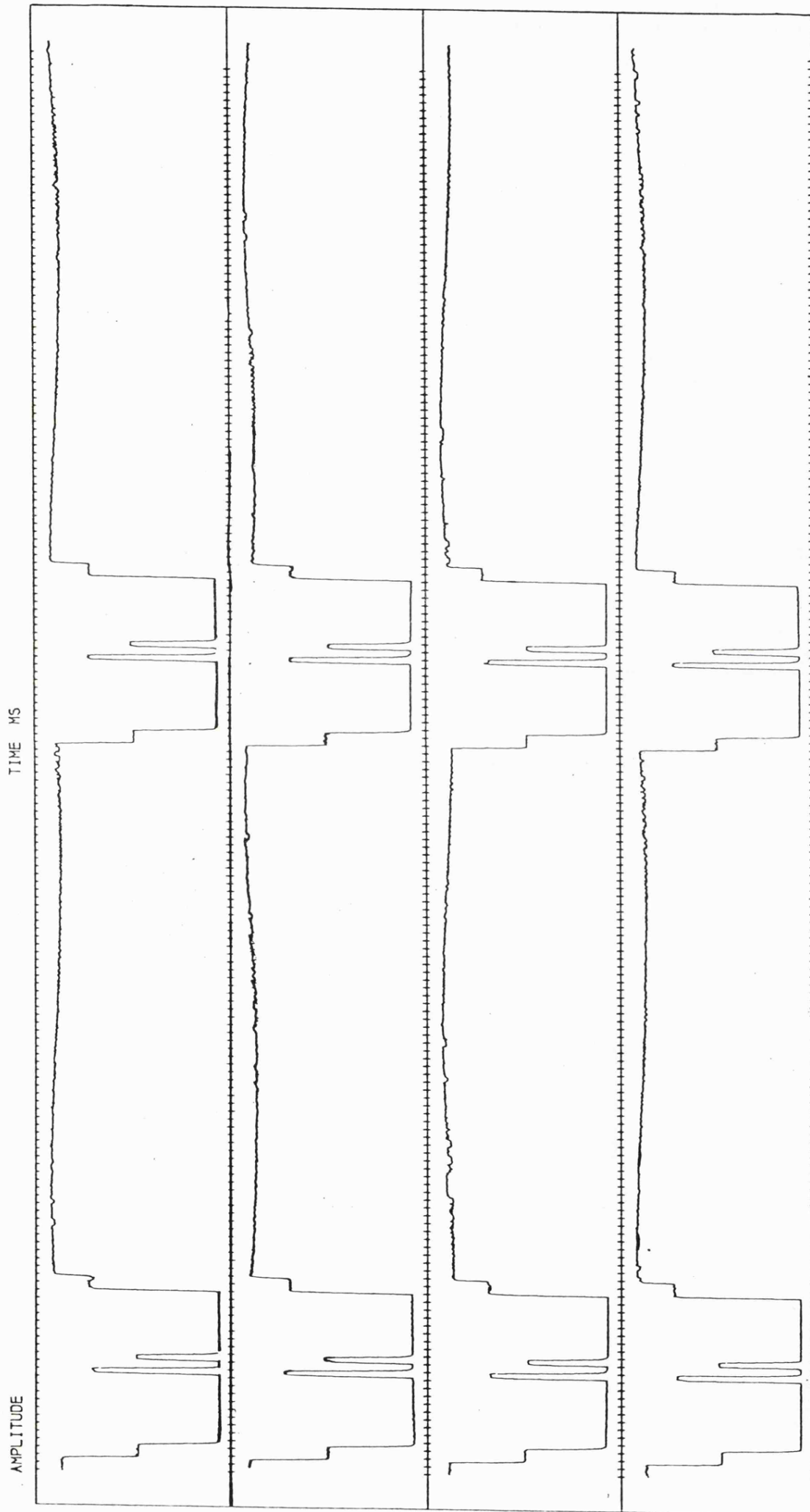
Most of the data analysis performed on the information from the magnetic tape is done by the program PLOT, given in full as appendix V. The four major types of data dealt with by plot are A, M, B and R. A, M, and B have already been described in section 5.5 and R is a simulated data type described in greater detail in section 5.7.4.

5.7.1 A Format

The A format consists of the normal header information followed by the ADC samples in rows of 16. The analysis program takes in the header information and writes out the callsign, transmitter site, time, date, frequency and comment line at the bottom of the graph. It then draws the axes and calculates the time scale from the given sample rate. Finally the ADC samples are plotted out. An example of this type of plot is given as fig 5.7.1. This is a test plot of simulated data produced by the unit described in section 4.4.

5.7.2 M Format

The M format consists of 64 sets of 256 data points which are plotted out in a waterfall style graph, an example of which



MICRO MSI 16.49 GMT 31.03.81 4.792500 MHZ (3)

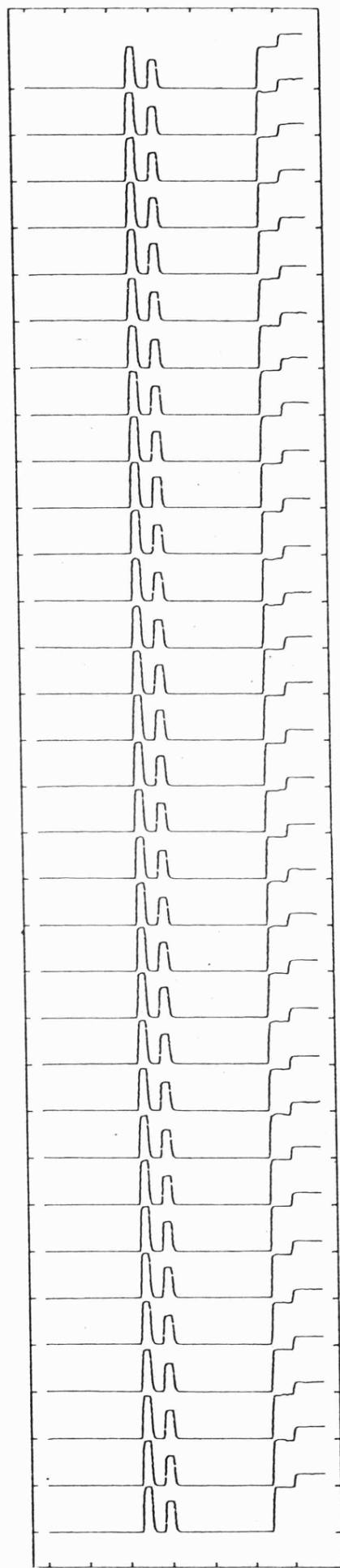
Fig 5.7.1 Amplitude Plot (A Format)

is given in fig 5.7.2. This graph is again of simulated data, hence the good signal to noise ratio. The scales on this plot are as follows. The vertical axis marked (time * 90ms) indicates that each pulse record displayed is separated in time by 90ms. The horizontal axis also presents time but, is scaled in distance traveled in that time by a radio wave in free space. This is useful when investigating the differences in path length between two different modes of propagation. In addition to plotting the graphs the program also analyses the pulse sounding data by repeating the process described in section 5.3 to find the arrival times and amplitudes for all the pulses. Having located the pulses, the computer, using a pre-programmed model of the ionospheric path, predicts which modes of propagation are present. It also provides an estimate of how reliable the prediction is. This process is described in greater detail in section 6.7. The program then goes on to produce the following statistics :-

- 1) Number of modes present.
- 2) Likelihood of multimode fading (see section 6.7).
- 3) Average amplitude level.
- 4) Percentage power of the signal in the secondary modes.
- 5) Expected data error rate (see section 5.7.4).

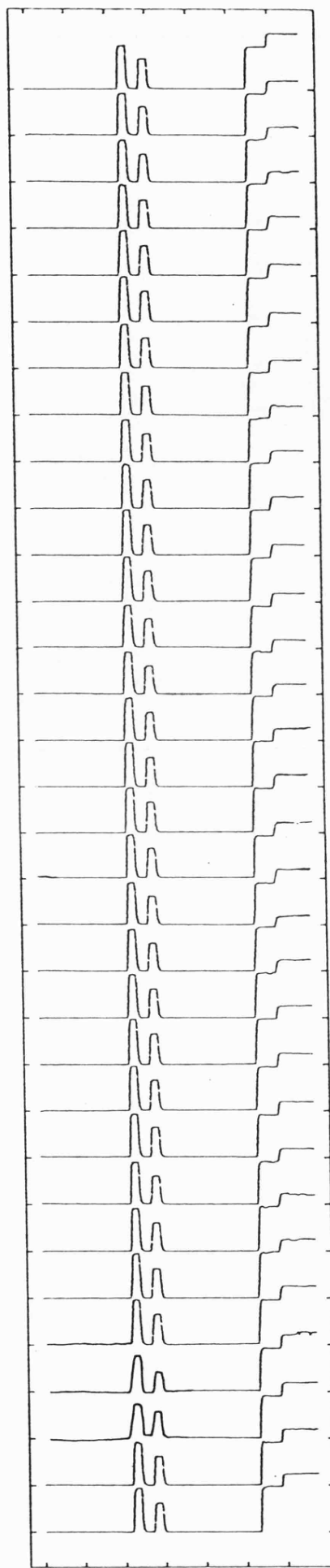
These statistics are useful in quantifying the general impression gained by inspection of the sounding signal. The ratio $S/S+N$ is derived from the sounding signal by measuring the amplitude of the dominant mode of propagation and calling that $S+N$. With reference to fig 5.7.3 the incoming signal (D) is analysed by the computer, which calculates the constituent

TIME
(90MS)



DISTANCE (1000KM)

TIME
(90MS)



DISTANCE (1000KM)

MICRO MSI 16.58 GMT 31.03.81 4.792500 MHZ

Fig 5.7.2 Pulse Plot (M Format)

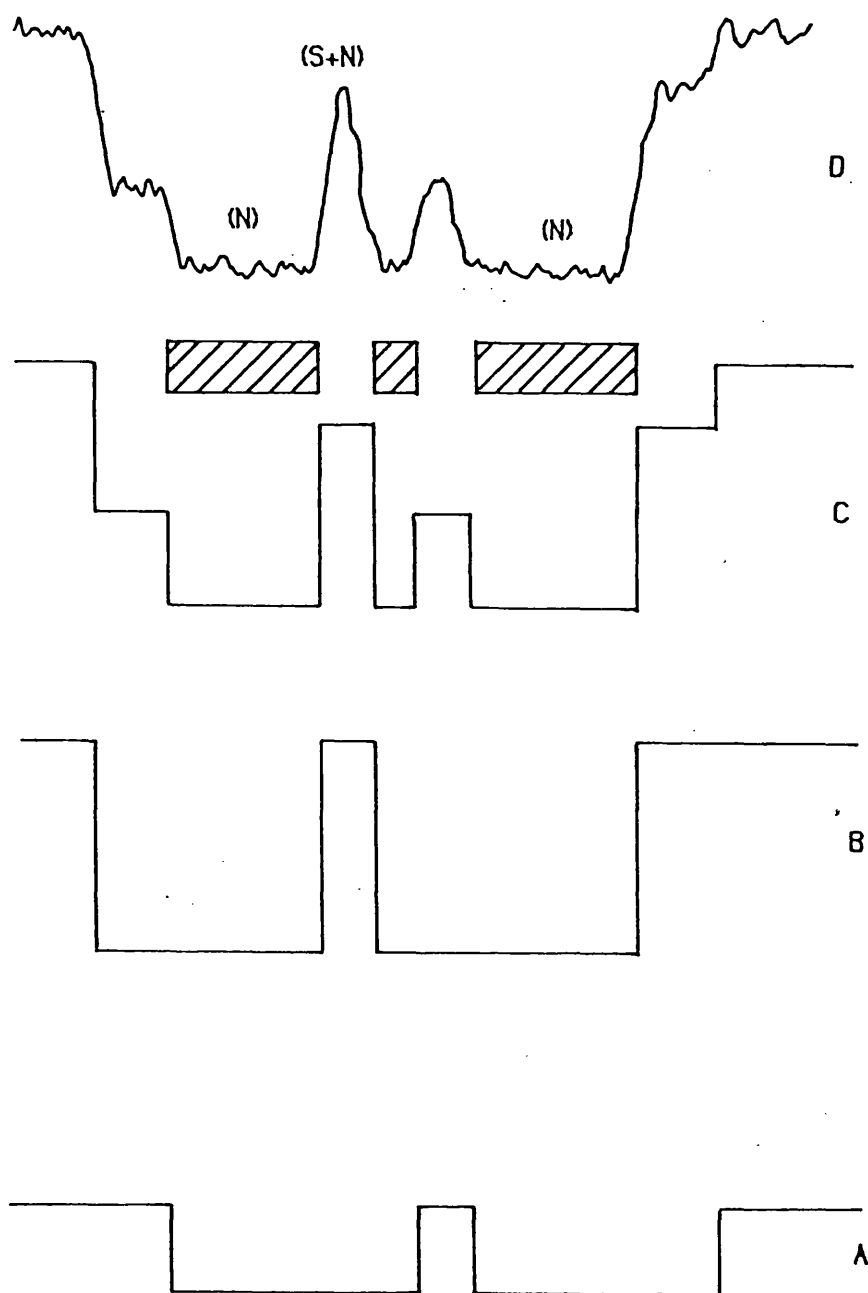


Fig 5.7.3 $(S/S+N)$ Calculation

signals (A) and (B). These are added to give (C) which is the theoretical received signal. The periods for which no signal is present in C (shaded) and a signal is present in D must be due only to noise, therefore $S/S+N$ can easily be calculated. This ratio is useful when attempting to predict the data error rate.

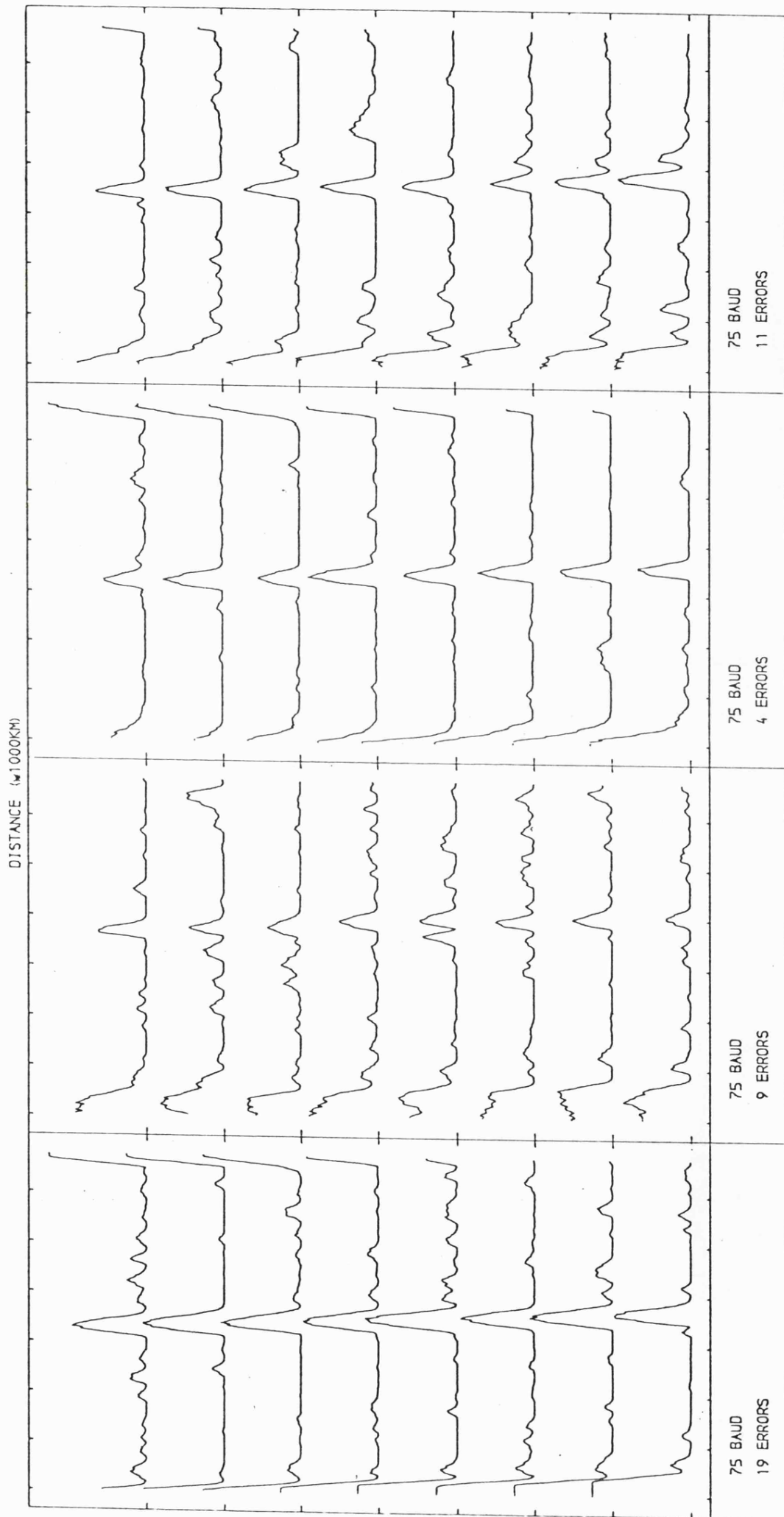
5.7.3 B Format

The B format consists of two sets of PRS data followed by eight sets of 256 sample ADC pulse records. As before the header information is transferred to the foot of the graph. An example of the graphical output is given in fig 5.7.4. Each block of PRS and pulse data occupies a quarter of the graph. The pulse information is displayed as a waterfall and the pulse statistics are calculated and printed out on the line printer. The errors are measured as in section 5.4 by comparing the received data with the known test sequence. The number of errors written on the graph is the sum of the errors from the two blocks of data. A full explanation of the line printer output is given in section 7.1.

5.7.4 R Format

The R format differs from previous formats in that it contains instructions on how to construct a data set. The information fed into the program in the R format consists of :-

- 1) the pulse arrival times and amplitudes.
- 2) the signal to noise ratio



G9BLD ELGIN 15.7 GMT 29.03.81 4.792500 MHZ

Fig 5.7.4 Quiet Data (B Format)

- 3) the receiver bandwidth
- 4) the data baud rate
- 5) the fading rate

From this information, graphs similar to fig 5.7.5 are produced which show the pulse picture and then the entire PRS data set. The horizontal line drawn through the PRS data set is the trigger level between a '1' and a '0' data bit. With this level the data was decoded and the number of errors calculated.

The method of constructing the simulated data set is described in fig 5.7.6. The components A and B representing different propagation modes are added together vectorially to form C. The vector sum allows the simulation to take into account fading effects. Next a normal noise distribution is added centred on the mean level from the S/S+N ratio (D). Part of the noise energy is added in the form of short pulses to simulate local electrical noise at the receiving site. A simple running mean filter is then applied to the data to simulate the bandwidth limits of the radio system (E).

Fig 5.7.6 illustrates this being applied to a sounding pulse, exactly the same operations were applied to each data bit to produce the final result. The accuracy of the simulation is demonstrated by a comparable set of data taken from the Oadby radio transmitter (fig 5.7.7). It is just coincidence that one of the multimode fades in both fig 5.7.5 and Fig 5.7.7 occurs at the same point in the data sequence.

This method is quite successful at reproducing the data sequence however it takes a large amount of processing time on the Cyber 73 computer. As the aim of the project is to do this

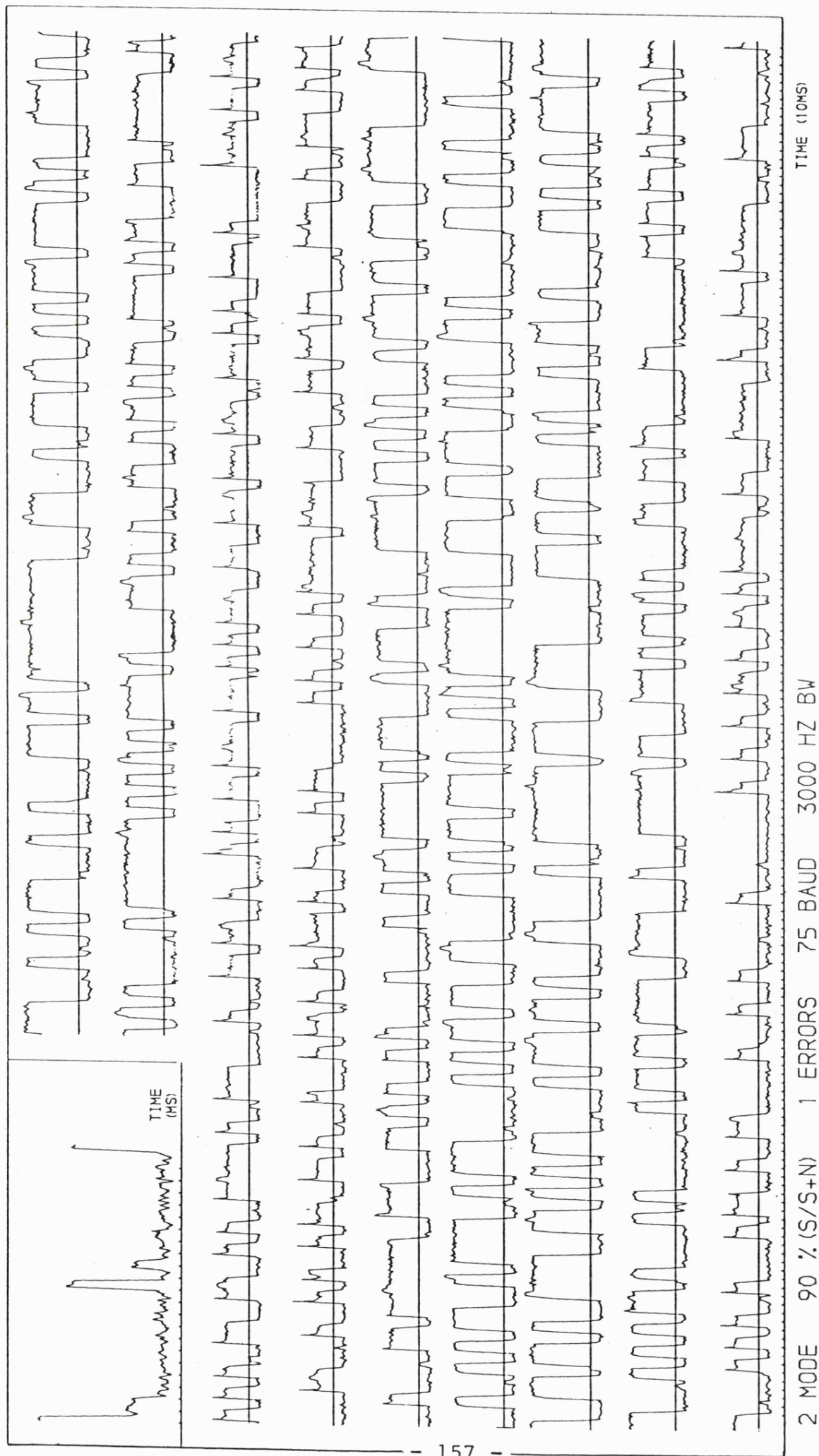


Fig 5.7.5 Simulated Data (R Format)

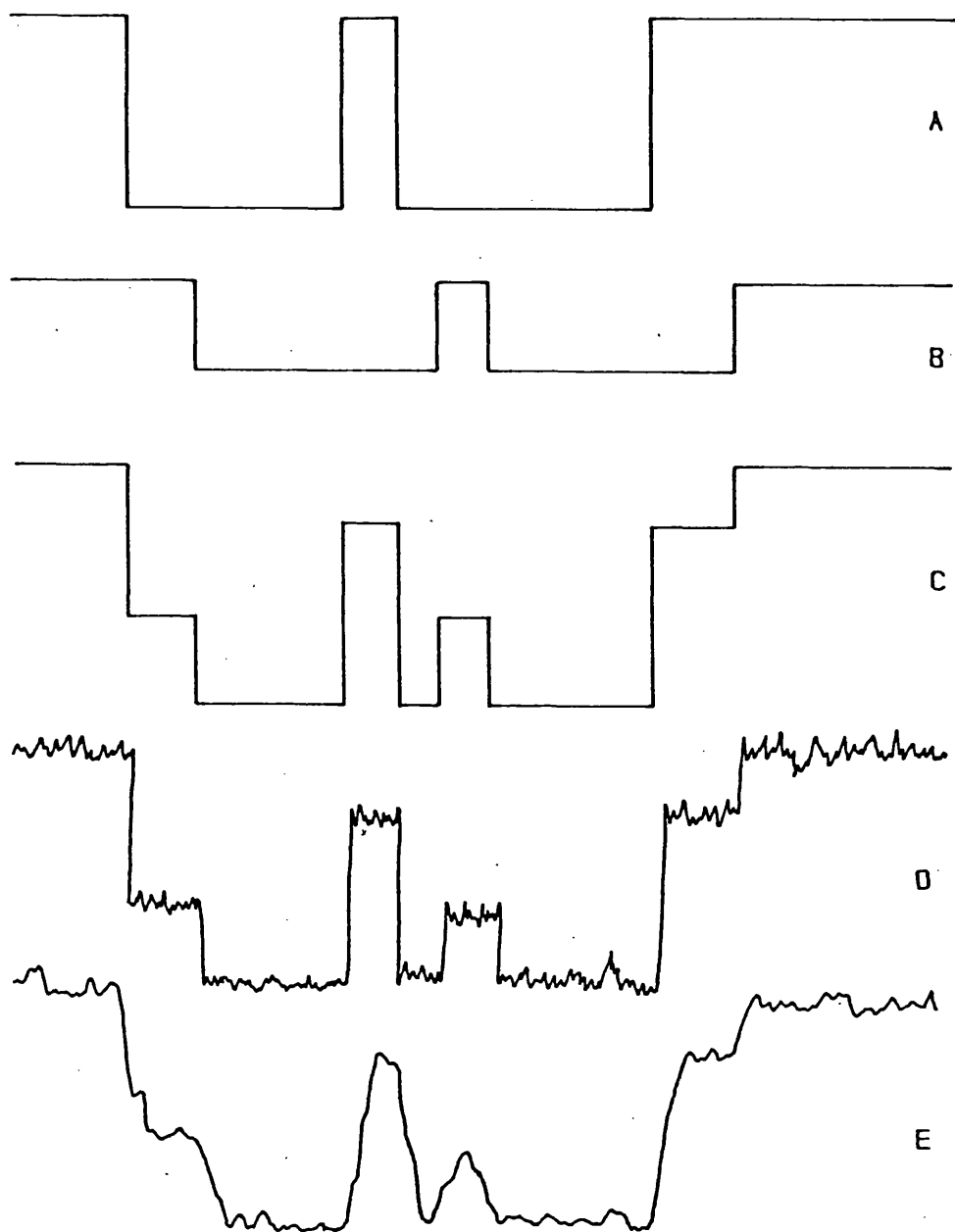


Fig 5.7.6 Signal Reconstruction

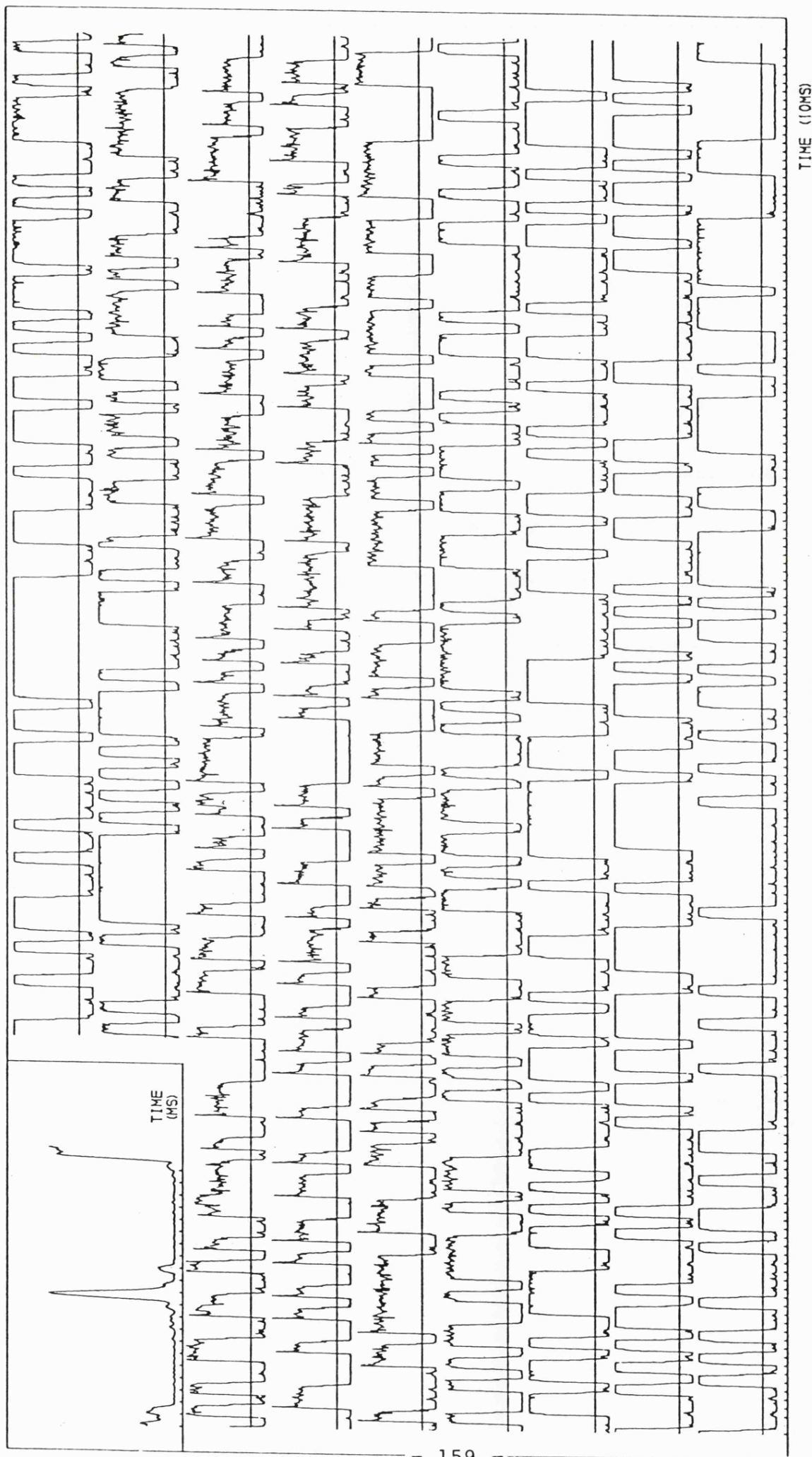


Fig 5.7.7 Received Data (0adby 01.07.1 16.48 GMT)

work on the micro-computer in real time, a simplified version of the above method was developed. This method is shown as subroutine GAUSSIAN in appendix V. Here possible errors are separated into noise induced and multipath induced errors affecting low and high data bits separately. Thus only four error cases have to be considered instead of 1023 in the previous methods. The probability of each type of error is calculated with the same noise distribution as the first method and an overall predicted error figure is produced. The purpose of this figure is described in section 7.1.

5.8 SUMMARY

Software was written to control the experimental hardware, log the data collected and to analyse and plot out this data in graphical form. The control software was written in assembler language for ease of interface with both the transmitter and the receiver. Assembler programs were also written to collect and log the data produced. In this case speed of operation as well as ease of interface were the reasons for employing a low level language. Both of these blocks of software worked satisfactorily throughout the experimental period with two small exceptions. Due to the speed limitations of the project computer both recognition of the Barker code at 600 baud and fast logging of both amplitude and phase information could occasionally fail to keep up with the external clock, thus confusing any results produced.

The analysis and plotting software was written in FORTRAN

4 on the Cyber 73 mainframe computer. Fortran allows access to high level mathematical functions and also the GHOST graphical package which together greatly facilitated the presentation of the data.

CHAPTER 6

PULSE EXPERIMENTS

6.1 IONOSPHERIC MODELS

One of the principal objectives of this investigation is to identify which modes of propagation are active over a given path by means of the sounding signal. This requires a knowledge of the differences in arrival times of predicted propagation modes and this information must be programmed into the control computer.

The most accurate method of determining the time of flight for the various modes is to obtain an ionogram close to the path mid point for the time of interest. From this the electron density, true height distribution can be obtained and the modal structure and flight times for the circuit can then be determined from a ray tracing analysis. This procedure is complicated and impractical if suitably located ionosondes are not available. Also it is difficult to carry out the analysis in real time without a large computing facility.

A simpler solution can be based on an average model of the ionosphere (fig 6.1.1) from which the active modes are determined by geometrical considerations. The relative arrival times of the various modes determined in this way are generally in reasonable agreement with the ray tracing results. The elevation angle is also determined since this provides an aid

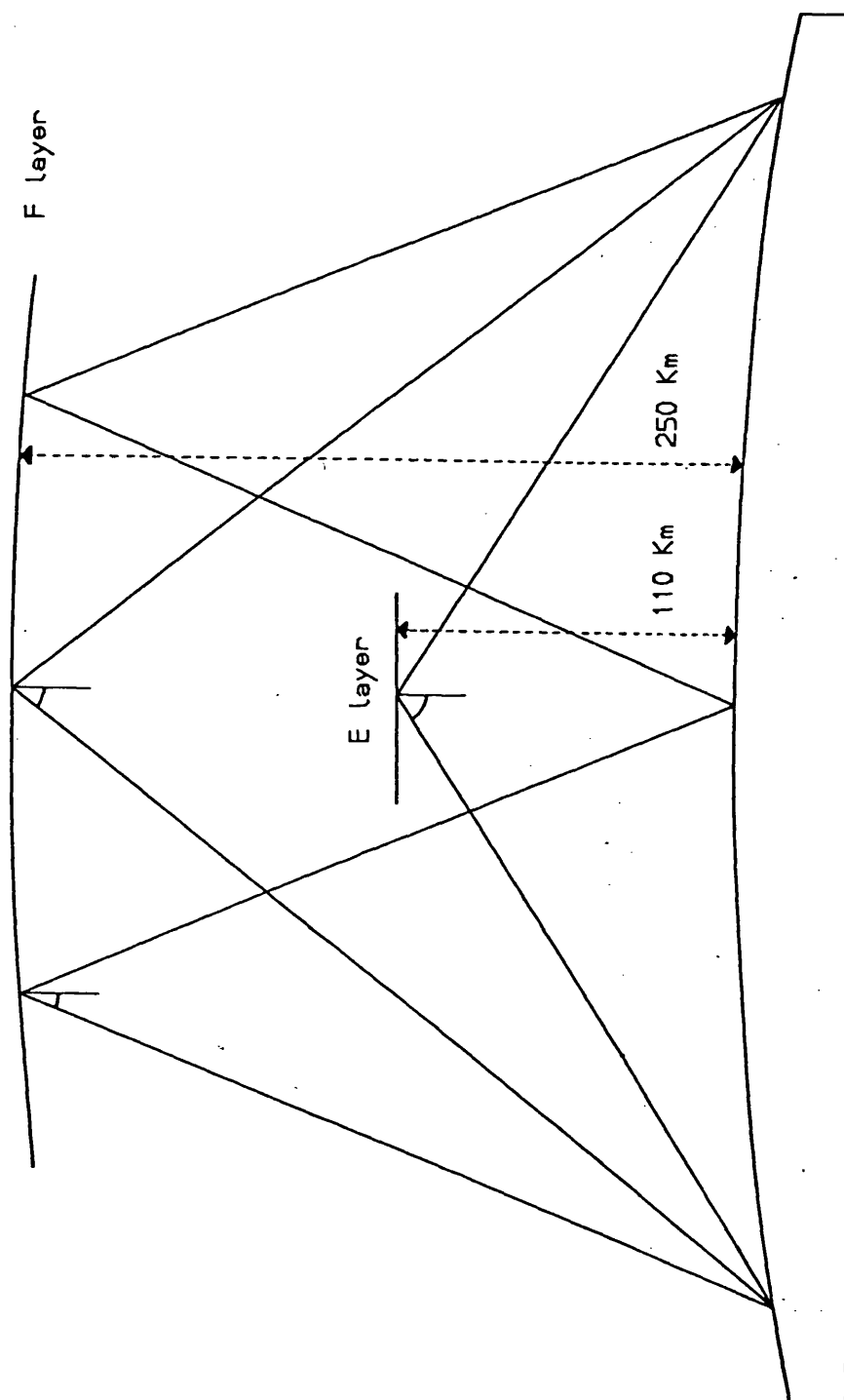


Fig 6.1.1.1 Ionospheric Model

for controlling the elevation steerable antenna. The results of the mode estimation are presented for the four paths that make up the project data set. When the pulse sounding technique is employed operationally this procedure would be performed by the micro-computer when the ground range and frequency are entered.

The simplest path is that from Oadby to Leicester over which a frequency of 4.7925MHz was radiated. The most likely mode of propagation in this case is the ground wave. With a range of 4Km the time of flight is approximately 0.01ms. As 4.7925MHz is above the E region critical frequency, E layer reflection will only occur when a sporadic E layer (Es) is present. Pulses reflected from the F layer travel some 500Km in this model and hence take 1.67ms to arrive at the receiver. Times of flight for the various modes are tabulated below.

Mode	Path length (Km)	Flight time (ms)
GND	4	0.01
Es	220	0.73
F	500	1.67
2F	1000	3.33
3F	1500	5.00

Absorption of the radio wave occurs each time the ray travels through the lower ionosphere. For this reason we would expect the absorption to increase as the number of hops increases.

The next path in increasing range is the steep incidence path from Durham to Leicester. The ground range is 241Km and

experiments were again conducted at 4.7925MHz. The elevation angle of arrival (θ) was determined from the simple model by trigonometry. The angle (θ) is 90 degrees minus the angle of incidence (i) where :-

$$i = \arctan(r/(2*h*n))$$

r = ground range

h = height of ionospheric layer

n = number of hops

Similarly the distance traveled can be calculated from the following equation.

$$d = 2*n*((h^2)+(r/2*n)^2)^{0.5}$$

From these equations the characteristics of the Durham path tabulated below were calculated.

Mode	Elevation angle (degrees)	Path length (km)	Flight time (ms)
GND	-	241	-
E	43	325	1.08
F	65	555	1.85
2F	77	1028	3.43
3F	81	1519	5.06

E layer propagation is now possible as the equivalent oblique frequency of 4.7925MHz, is 3.27MHz which is below the average E layer critical frequency (3.4MHz) during the middle of the day. The expected amplitude ranking of the different modes is, first the one hop F as that spends least time in the area of high ionospheric absorption, the 2 hop F and E layer

reflections should be next followed by the 2 and 3 hop F propagation respectively.

The third path, for which most of the data was obtained, is from Elgin in Scotland to Leicester. The path has a ground range of 578km and the usual frequency of 4.7925MHz. The values for the elevation angle and time of flight are given below.

Mode	Elevation angle (degrees)	Path length (km)	Flight time (ms)
GND	-	578	-
E	21	618	2.06
F	41	764	2.55
2F	61	1154	3.85
3F	69	1606	5.35

The calculations are complicated by the problem arising from E layer screening. In this situation signals normally reflected from the F region are prevented from going so when they are radiated below a certain elevation angle. The E region angle of incidence this produces causes the wave to be reflected and prevents it from reaching the receiver by the normal F layer path. For most of the daylight hours over which the experiment was conducted (10.00 to 1500 GMT) the E layer critical frequency (FOE) was about 3.4MHz (Slough ionospheric data 1980). This means that the 4.7925MHz transmissions will be reflected by the E layer if they arrive at an angle of incidence greater than (i).

$$i = \arccos(3.4/4.8)$$

$$= 45 \text{ degrees}$$

In this case the one hop F mode has an angle of incidence of 49 degrees and is therefore unlikely to be propagated until later in the day when the F_oE falls below 3.15MHz. It appears that for most of the time during an average day the dominant mode on this path should be the 1 hop E or the 2 hop F with the possibility of a small 3 hop F mode. Propagation via the 1 hop F mode is possible later in the day or in cases of below average ionisation, when this mode occurs it is likely to be dominant.

The final paths to consider are those from Tromso and Bodo in northern Norway in the 14MHz and 15MHz bands. Both paths are very similar and their mode structure is assumed to be the same. For the Tromso Leicester path the mode structure is tabulated below.

Mode	Elevation angle (degrees)	Path length (km)	Flight time (ms)
GND	-	2156	-
E	6	2167	7.22
F	13	2213	7.38
2F	25	2377	7.92
3F	35	2625	8.75
4F	43	2940	9.80

As before the E layer screening effect occurs since the elevation angle below which the E layer reflects radio waves

is calculated as.

$$\begin{aligned}\theta &= 90 - \arccos(3.4/14.1) \\ &= 14 \text{ degrees}\end{aligned}$$

For average conditions the F layer reflection will be screened by the E layer, but only a small deviation from the average conditions is required for this not to occur. This is of little consequence however, since the times of flight for these modes differ by only 0.16ms which cannot be resolved by the equipment. Even the 1F and 2F modes with a separation of 0.54ms could not always be detectable under noisy conditions. The relative amplitude estimates are therefore 1E and 1F largest and the 2 hop F and 3 hop F in decreasing order.

The results of the geometric modelling are summarised in fig 6.1.2. These results have been checked against a ray tracing calculation. Close agreement was obtained between the relative times of arrival, ie the differences are always within half the sounding pulse width and usually smaller (fig 6.1.3). As a further check a prediction (section 2.1.1) was employed to determine the mode structure for the various paths. This analysis indicated that E, F or multiple F layer reflections could occur for any of the paths (Durham, Elgin and Tromsø) during the times when the experiment was undertaken.

Finally the possibility of receiving sounding pulses on both high and low angle ray paths was investigated. The transmission curves for the four paths were calculated and superimposed on typical ionograms for the periods of interest. The high angle path was not active for any of the locations during the periods monitored by the experiment.

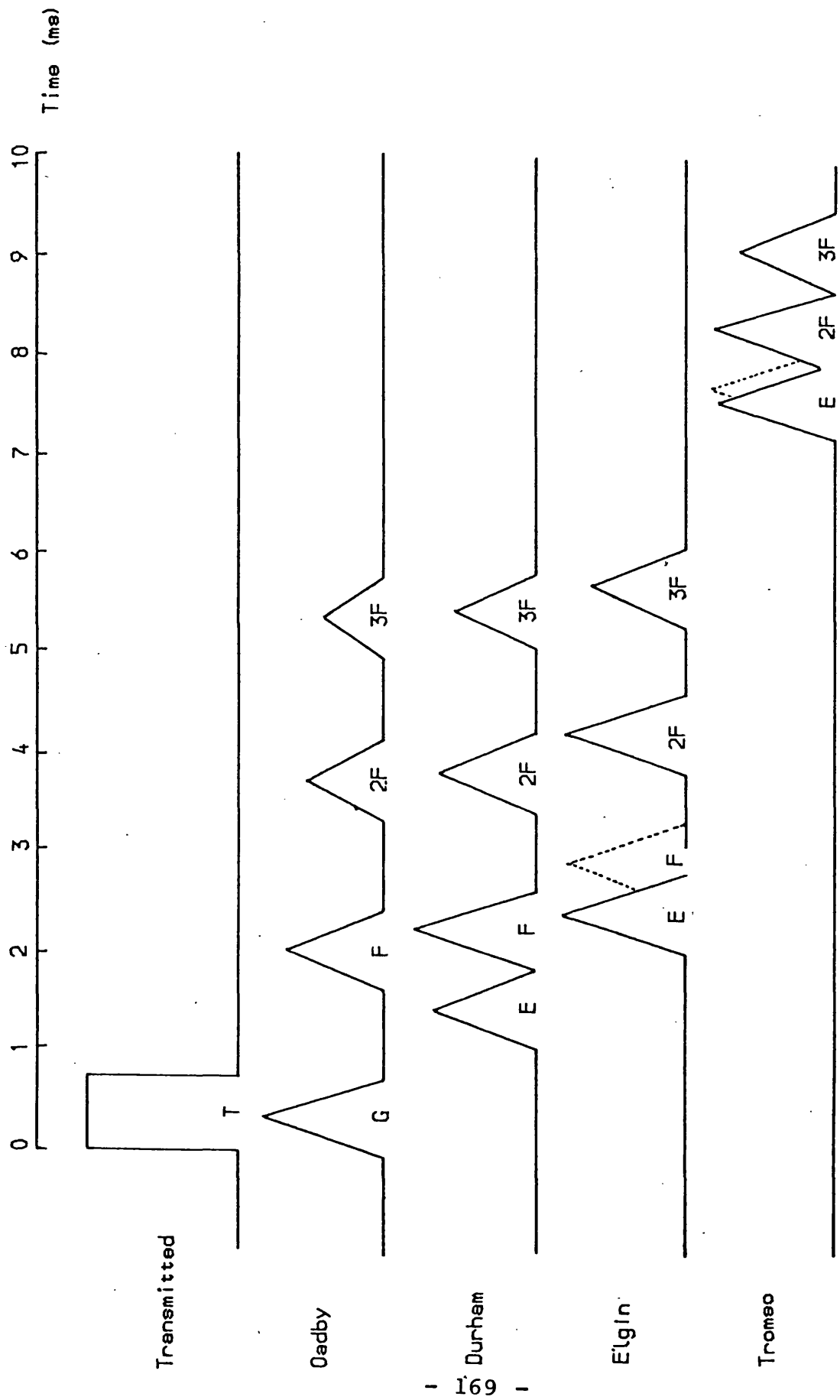


Fig 6.1.2 Geometric Modeling Results

Place	Prediction method	Relative arrival times (ms)			
		E	F	2F	3F
Oadby	G		1.67	3.33	5.00
	RT		1.56	3.12	4.68
Durham	G	0	0.77	2.35	3.98
	RT	0	0.69	2.17	3.71
Elgin	G	0	0.49	1.79	3.29
	RT	0	0.36	1.56	2.97
Tromsø	G	0	0.16	0.70	1.53
	RT	0	0.18	0.33	1.42

Fig 6.1.3 Geometric and Ray Tracing Predictions of Relative Pulse Arrival Time

6.2 EXPERIMENTAL RESULTS

In total 280 sets of M format data each containing 64 consecutive pulse records (section 5.7.2) were collected during the course of the experiment on the four paths. It is not possible to present all these data sets in this thesis so examples have been selected which illustrate their typical features. Of the 280 waterfall graphs of pulse sounding waveforms 4 were from the simulator, 12 from Oadby, 22 from Durham, 144 from Elgin, 75 from Tromso and 23 from Bodo. The reasons for the uneven distribution are as follows.

The simulator and Oadby data are both predictable and repetitious, therefore there was little point in collecting large quantities. The Durham site proved difficult, firstly because the radio transmitter was interfering with other experiments and secondly because the linear amplifier failed, requiring lengthy repairs. Both of these factors lead to the collection of a relatively small amount of data. At the Elgin site the transmitter was operated each day for almost three months under perfect conditions and a large quantity of data was therefore available. Similarly at Tromso the transmitter ran every day for a week under good conditions and the amount of information recorded was limited only by the disk storage capacity. Finally only 23 sets of Bodo data were collected due to the more sporadic nature of the RAE tests.

A typical set of data from the Oadby transmitter is reproduced in fig 6.2.1. The first feature to note is the very

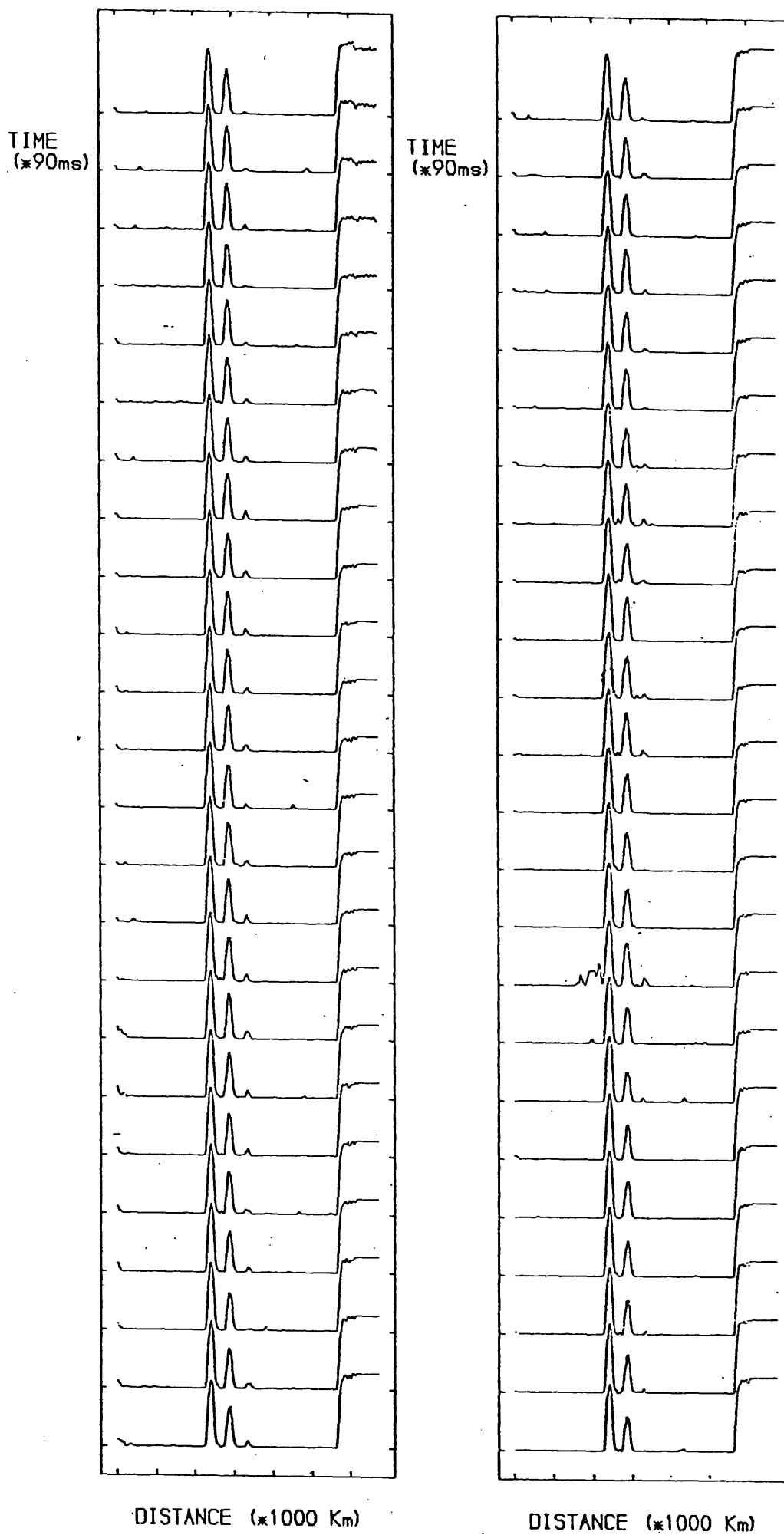


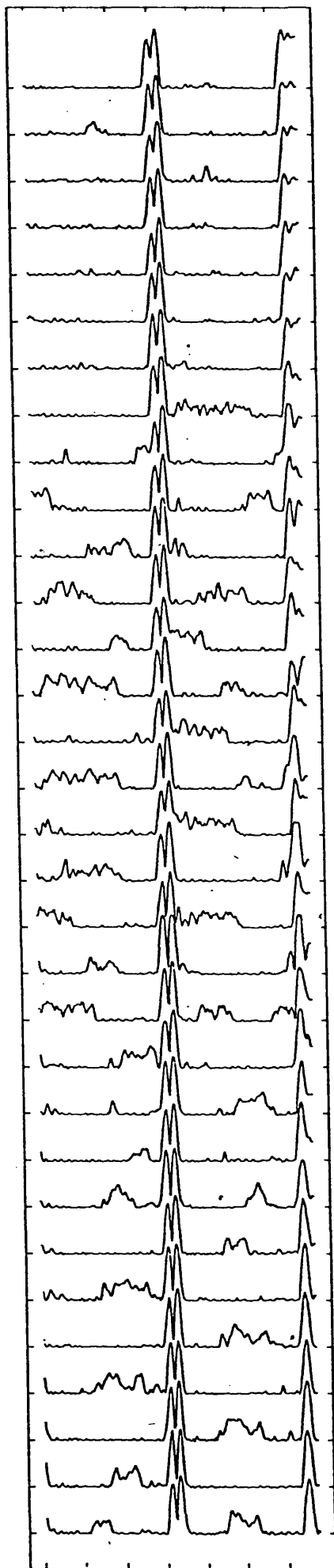
Fig 6.2.1 G9BLD OADBY 08.03.80 16.40 GMT
- 172 -

low noise level even though on several occasions the signal is limiting. In the sounding records, three pulses can clearly be seen with relative arrival times (ie the arrival times relative to the first pulse received) of 0ms, 1.6ms and 3.2ms respectively. Comparison with the results of the previous section (fig 6.2.1) indicates that the three propagation modes present are ground wave, 1 hop F and 2 hop F. Only 48, 256 byte data sets are shown in place of the normal 64 as the early version of the logging program had a smaller available memory than the later version.

A second feature of the Oadby data is the ease with which sporadic E or Es modes can be recognised (section 1.1). Fig 6.2.2 presents data over 5.7 seconds from Oadby containing two obvious propagation modes separated by 0.7ms. The first of the two pulses must be the ground wave, consequently the second must be reflected from the ionosphere at a height of about 105km, which is consistent with an E layer path. This Es blankets out all the longer F layer propagation paths.

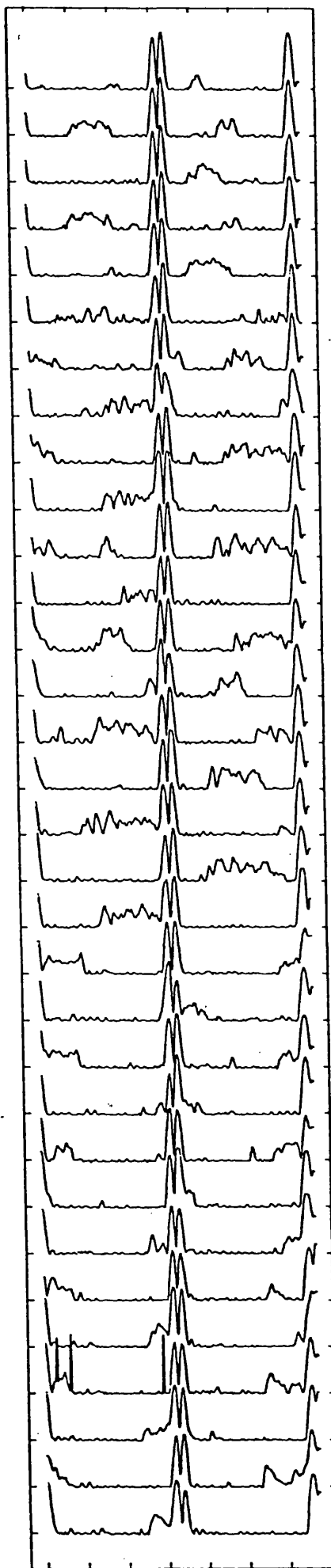
An example of the data collected over the Durham path is presented as Fig 6.2.3. The slow drifting of the pulses across the page results from the temporary replacement of the crystal oscillator by a free running oscillator due to equipment problems. In fig 6.2.3 usually two and occasionally three modes are present, which have relative arrival times 0ms, 1.5ms and 3ms. When these are compared with the predictions in fig 6.1.2 the active modes probably correspond to 1F, 2F and 3F. In this example E layer screening does not take place as the observations were made late in the afternoon when the E layer

TIME
(90MS)



DISTANCE (1000KM)

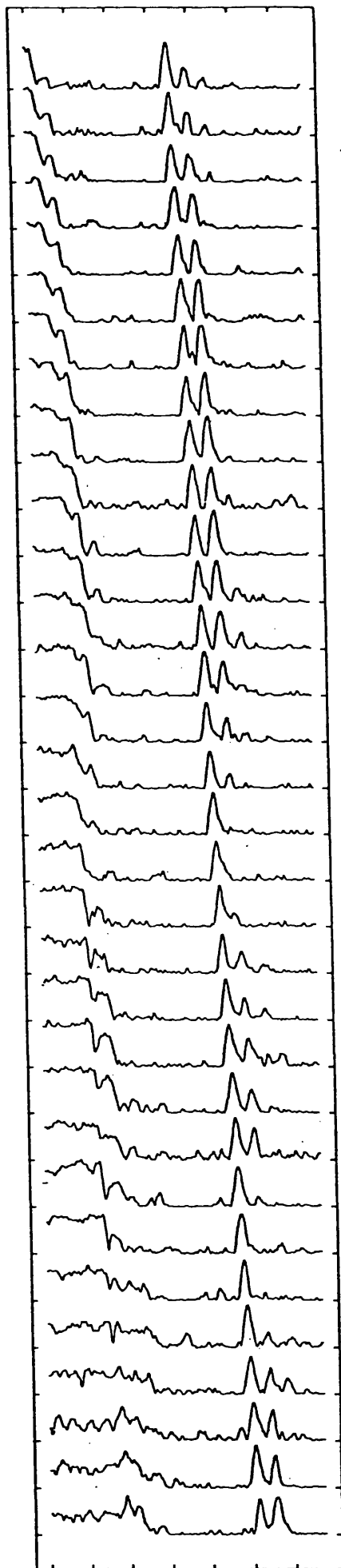
TIME
(90MS)



DISTANCE (1000KM)

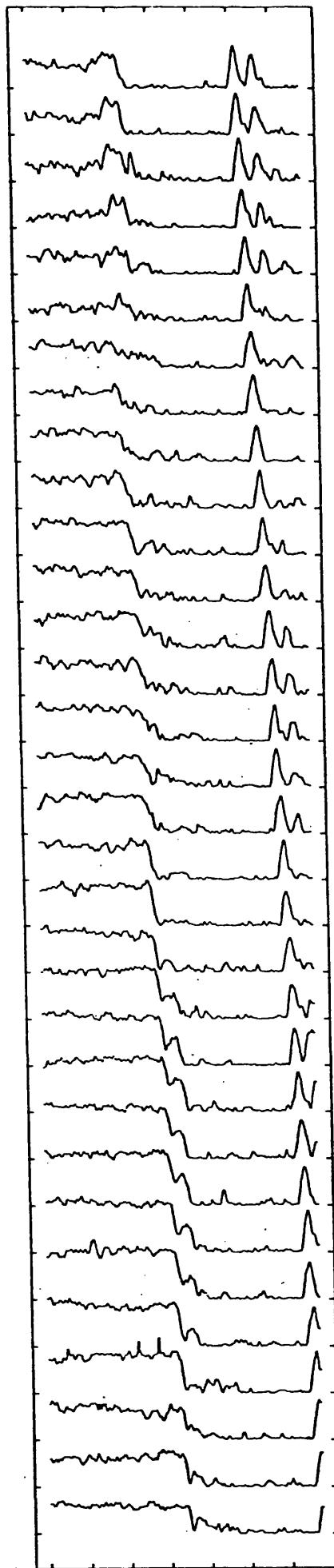
Fig 6.2.2 OADBY 13.35 GMT 10.06.81 4.792500 MHZ
- 174 -

TIME
($\times 90$ MS)



DISTANCE ($\times 1000$ KM)

TIME
($\times 90$ MS)



DISTANCE ($\times 1000$ KM)

Fig 6.2.3 DURHAM 17.3 GMT 16.12.80 4.792500 MHZ
- 175 -

critical frequency had fallen below 3.27MHz (see section 6.1).

Fig 6.2.4 indicates that E layer propagation can and does occur on this path. This plot contains two modes separated by about 0.7ms, and reference to fig 6.1.2 suggests that they correspond to E and F layer propagation. The E layer reflection is much stronger than the F at times which could be the result of Es reflection. The presence of Es could also account for the lack of higher order F layer reflections.

The majority of the data was collected over the Elgin Leicester path. The pulse sounding data from this path was however rather dissapointing for several reasons. Firstly the presence of interfering stations and noise made the signal difficult to interpret (see section 6.4) and secondly our allocated frequency was rather low for this path and suffered quite high absorption. Fig 6.2.5 is one of the clearer examples giving two pulses separated by about 1.6ms. Comparison with the predictions suggests E and 2 hop F propagation but not 1F due to the E layer screening. A more typically, noisy specimen, of Elgin data is given in fig 6.2.6. Here the pulse structure can be seen at times but usually recognition is hampered by the random noise on the record.

The longest paths considered are those from Norway to Leicester. A good clear set of data is reproduced as fig 6.2.7. On this plot two pulses separated by about 0.5ms are present. From the predictions we see that this could either be 1 hop E or 1 hop F together with 2 hop F. 1 hop F appears to be more likely than 1 hop E for the day when the measurement was made. The E layer signal would be quite heavily attenuated and it is

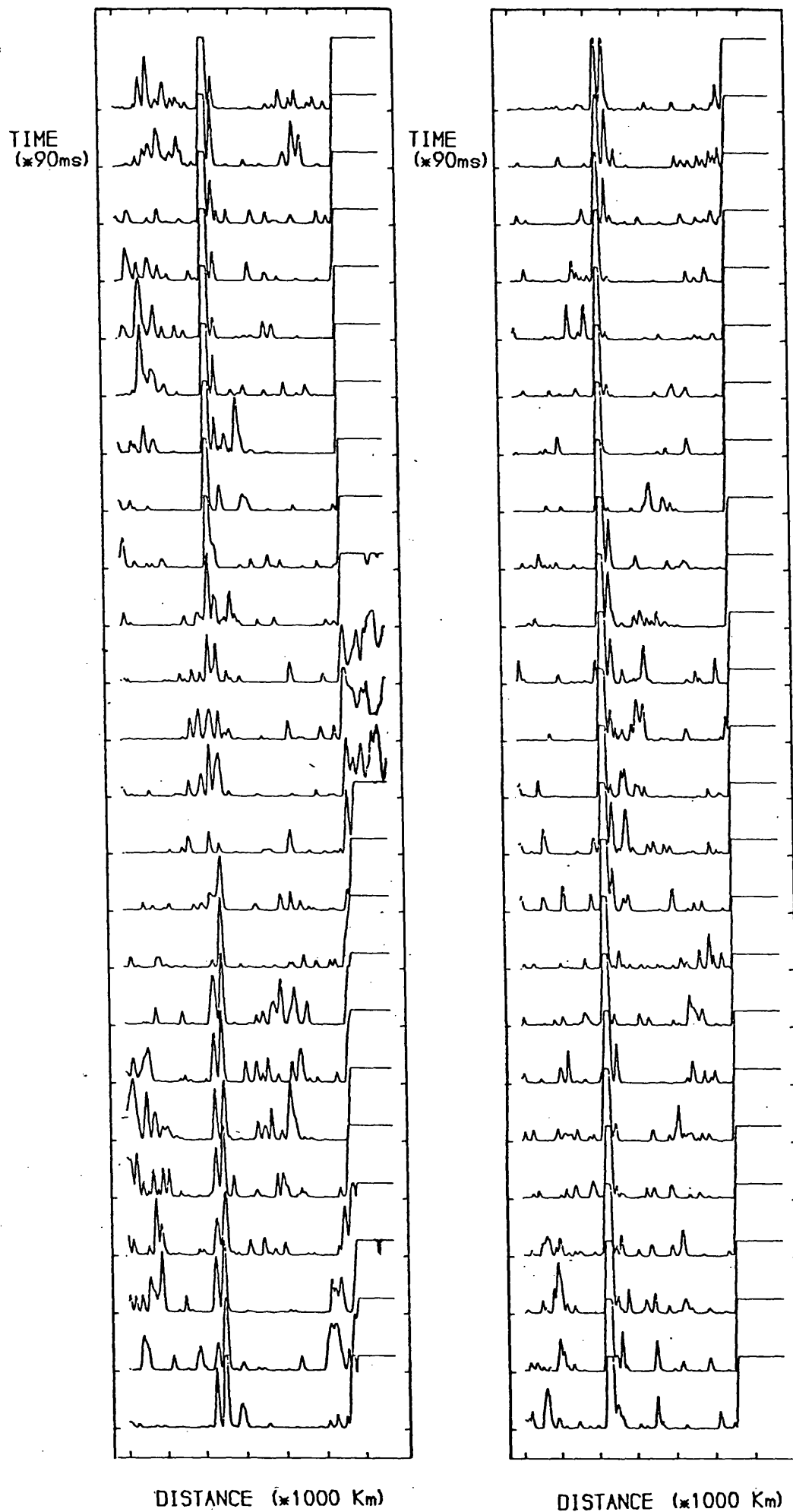


Fig 6.2.4 DURHAM 08.04.80 12.30 GMT
- 177 -

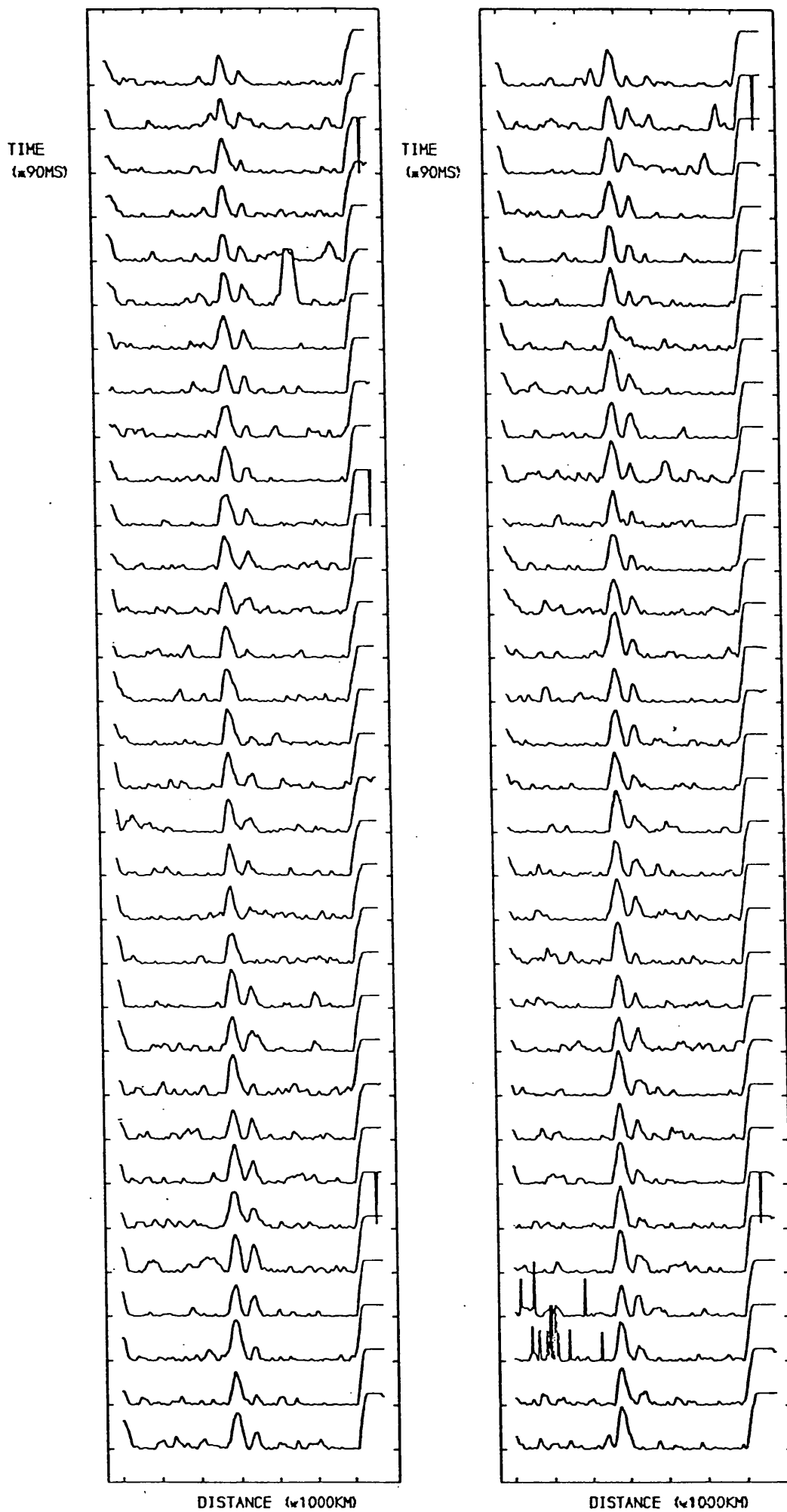
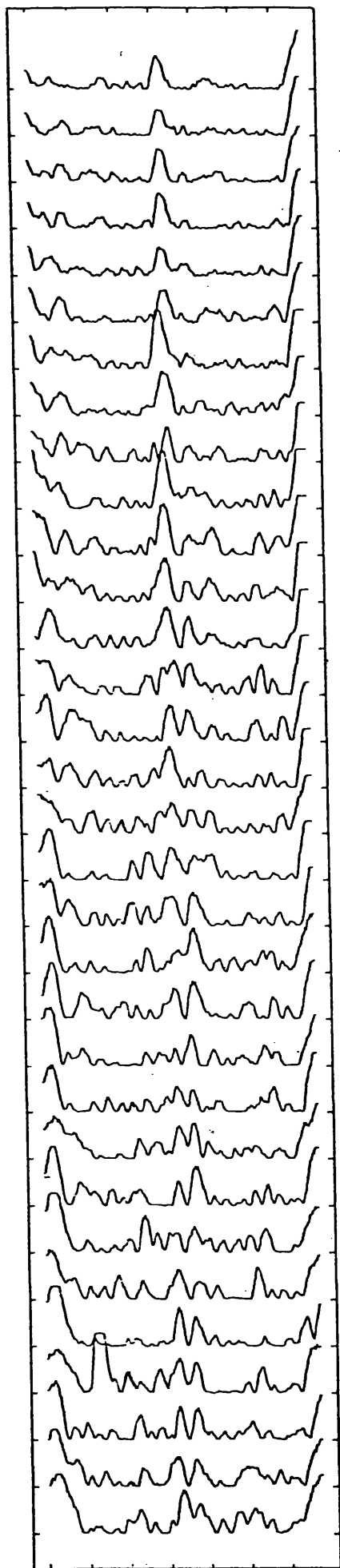


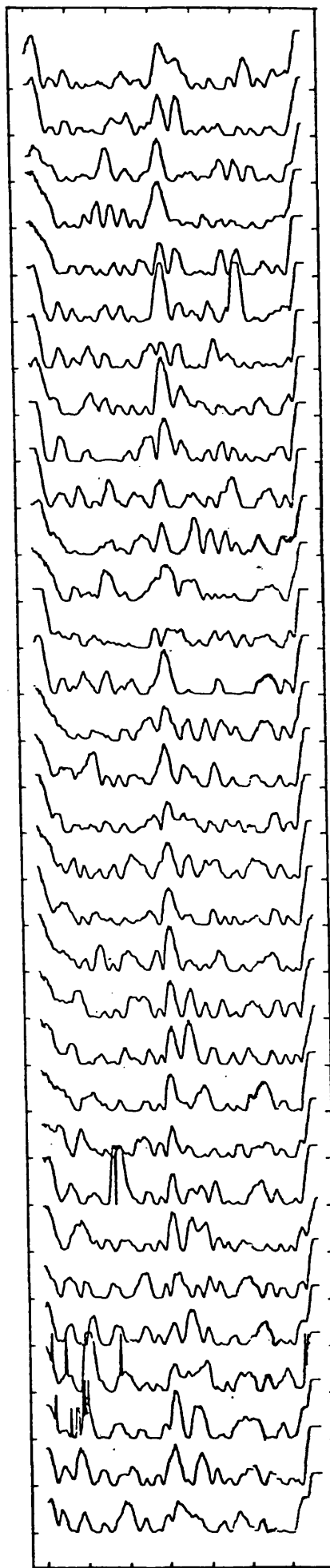
Fig 6.2.5 ELGIN 11.45 GMT 25.02.81 4.792500 MHZ
- 178 -

TIME
(≈ 90 MS)



DISTANCE (≈ 1000 KM)

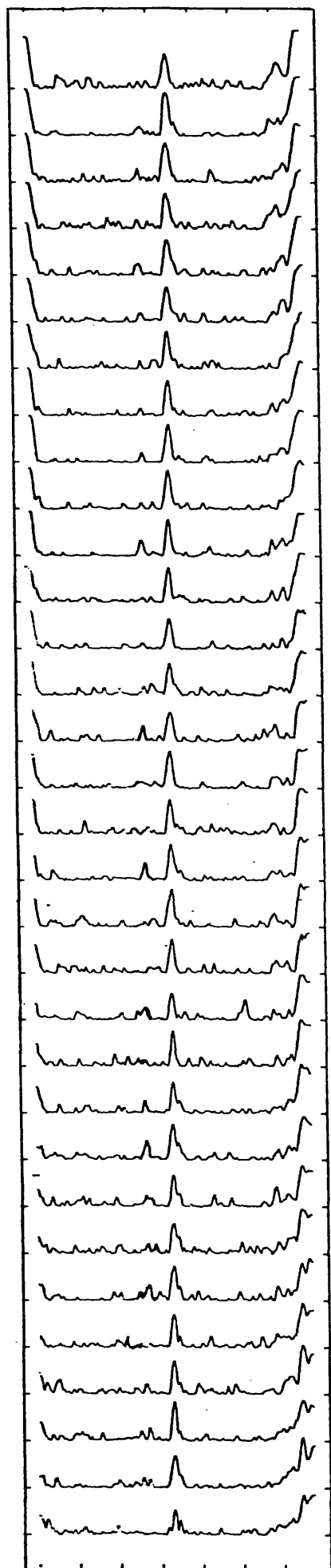
TIME
(≈ 90 MS)



DISTANCE (≈ 1000 KM)

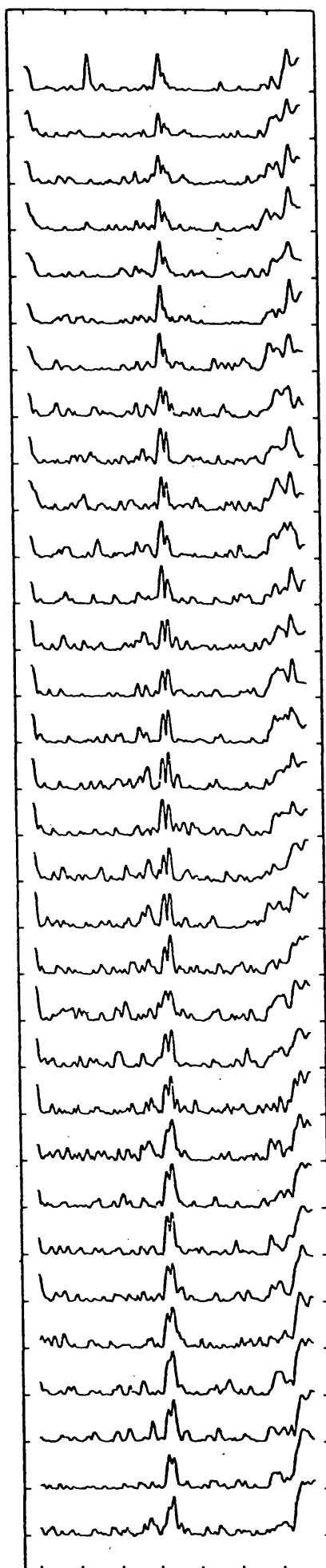
Fig 6.2.6. ELGIN 9.36 GMT 25.02.81 4.792500 MHZ

TIME
(μ 90MS)



DISTANCE (\times 1000KM)

TIME
(μ 90MS)



DISTANCE (\times 1000KM)

Fig 6.2.7 TROMSO 15.44 GMT 01.10.80 14 MHZ BAND
- 180 -

also possible that for non average conditions (ie lower E layer reflection height) the Tromso Leicester path would be longer than the maximum range of an E layer reflection (2365km for a reflection height of 110km).

One of the data sets from the RAE tests from Bodo in the 15MHz band is presented as fig 6.2.8. This data is fairly typical showing quite significant amounts of random noise and wide pulse returns. These wide pulse returns, probably caused by a narrow bandwidth transmitter filter, merge into one at times and make detection more difficult. At times however certainly two and possibly three modes are present, although with the variations in arrival time caused by noise etc identification is rather speculative. A clearer view of the same problem was achieved when the test frequency moved up to the 18MHz band (fig 6.2.9). Here two pulse returns are visible separated by about 0.7ms, probably making them again 1E or 1F and 2 hop F mode propagation. The effect of transmitting a wider sounding pulse is clear when the Bodo data in fig 6.2.8 and 6.2.9 is contrasted with results obtained from the Tromso tests in fig 6.2.7.

6.3 RAPID MODE CHANGES

One of the more interesting observations of this experiment has been the rapid changes which can occur in the mode composition of the received signal as decoded from the pulse sounding. Examples of this are given in fig 6.2.4, 6.2.7 and 6.3.1. In each of the diagrams the dominant mode at the

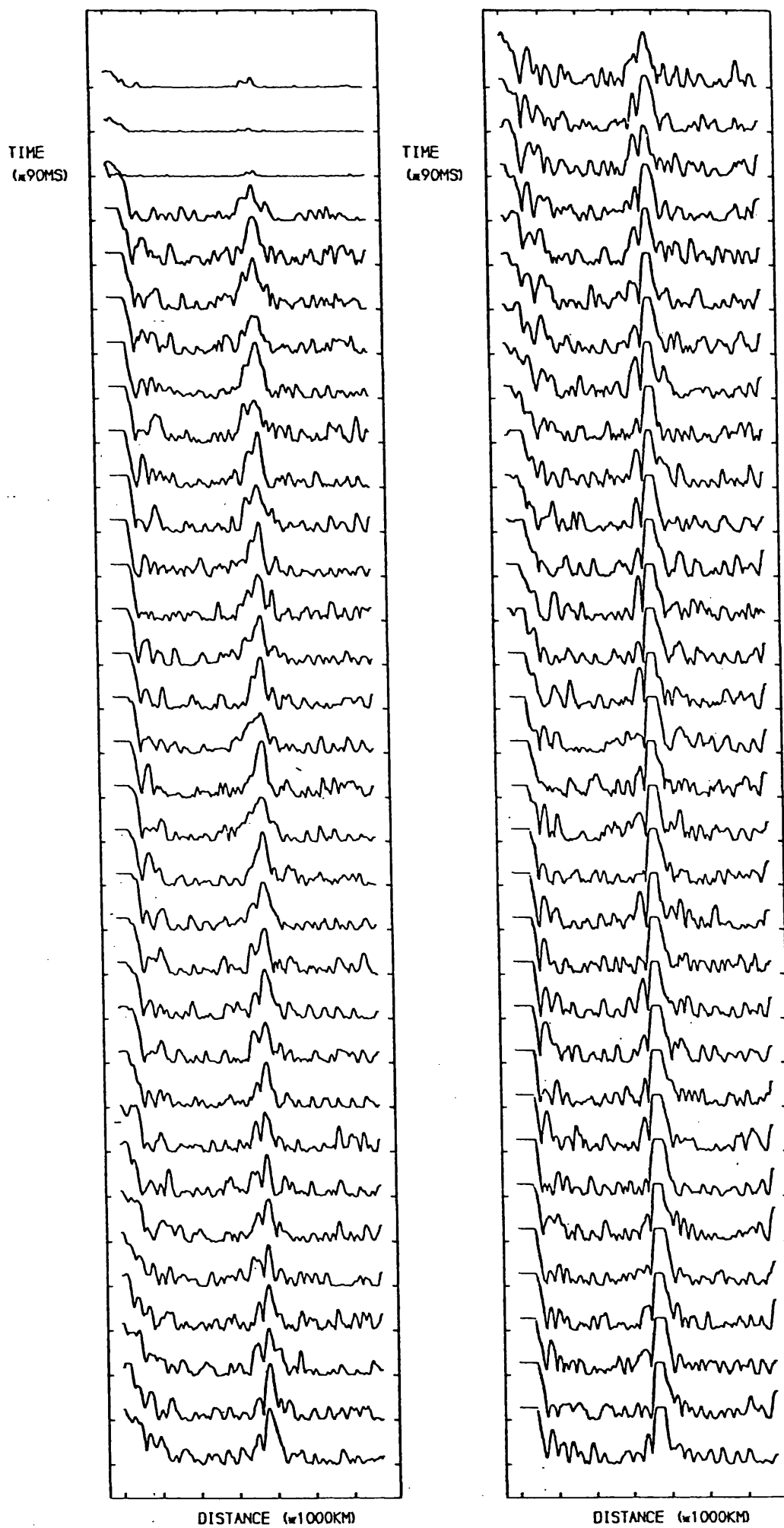


Fig 6.2.8 B000 10.3 GMT 21.10.80 15 MHZ BAND

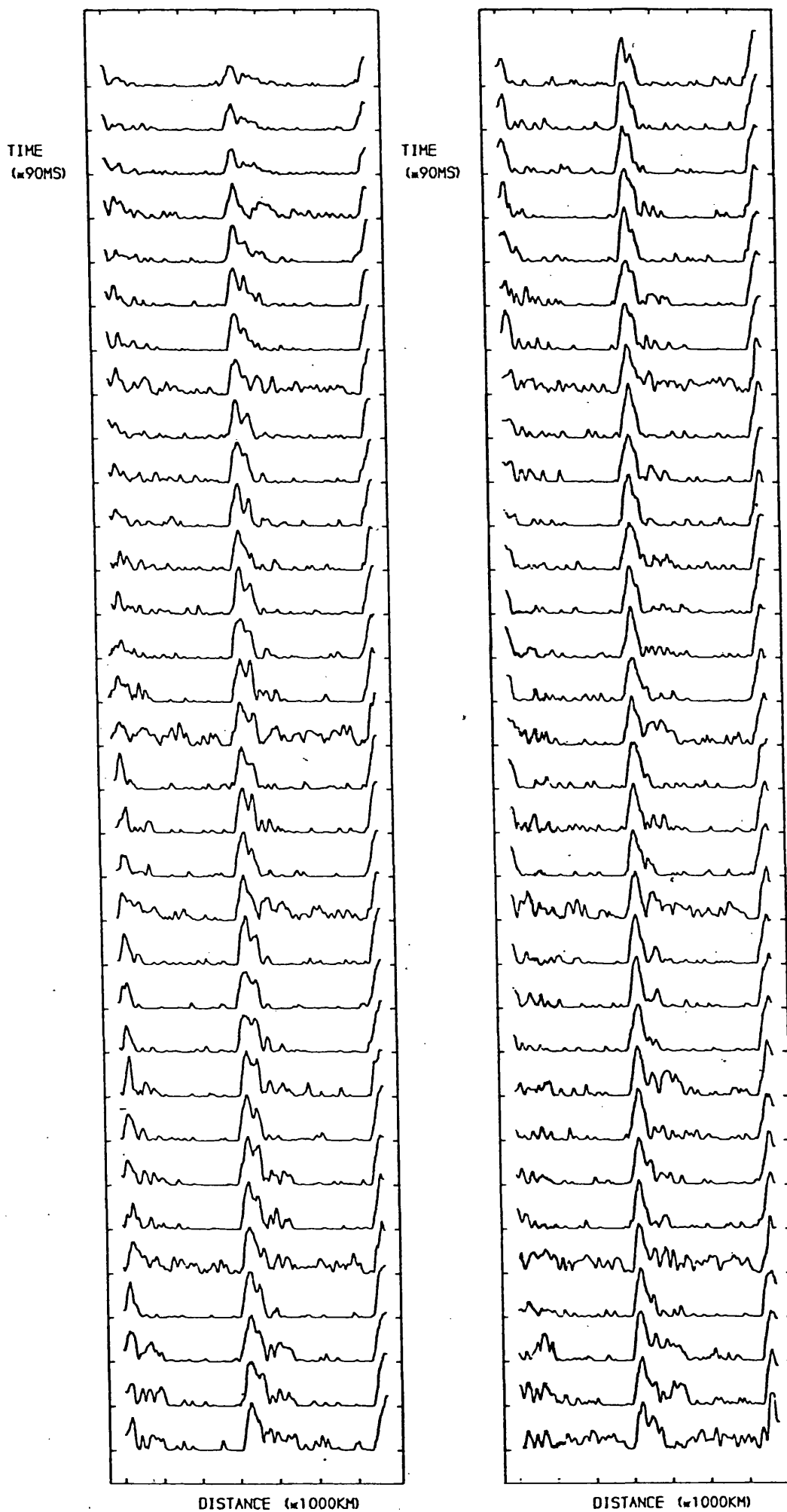


Fig 6.2.9 B000 14.34 GMT 21.10.80 18 MHZ BAND
- 183 -

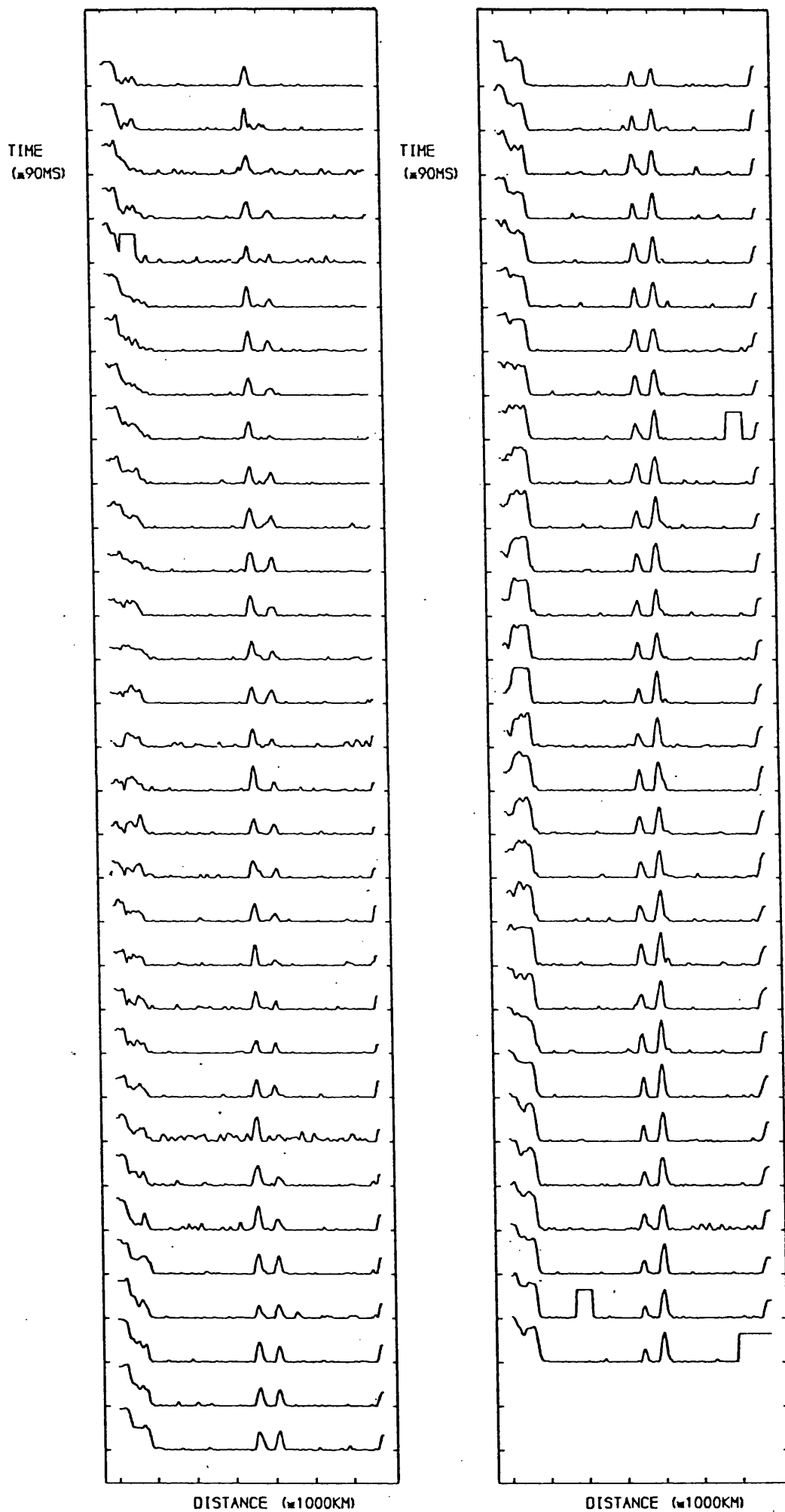


Fig 6.3.1 TROMSO 15.16 GMT 01.10.80 14 MHZ BAND
- 184 -

start of the time sequence has been replaced by another mode which becomes dominant by the end of the time span of the plot (5.7 seconds). This has serious consequences for the operation of the steerable antenna for mode selection as it would be extremely difficult to predict these short term changes. For example in fig 6.3.1, at the start of the period, the steerable antenna would be pointing in the direction of the first mode of propagation. Over the period of the plot this mode decreases in strength and a second one almost completely replaces it. Choosing the first mode for passing data would lead to data errors worse than could be expected with a conventional omnidirectional antenna which would of course receive both modes. Changing the direction of the antenna to follow the mode changes would be difficult on such short time scales and would inevitably lead to loss of data.

A possible solution would be to have a two beam antenna tracking the two strongest modes at any given time and employ a small computer to monitor the pulse sounding signal and decide for any given condition which mode would give the least errors. A less expensive compromise would be to go back to the single beam and instead of switching from the first to the second mode, open up the antenna polar diagram during the changeover period to try to maintain continuity. This would only work if the block of carrier and hence the data bits were not undergoing destructive interference during the changeover period (eg middle right hand column fig 6.3.1).

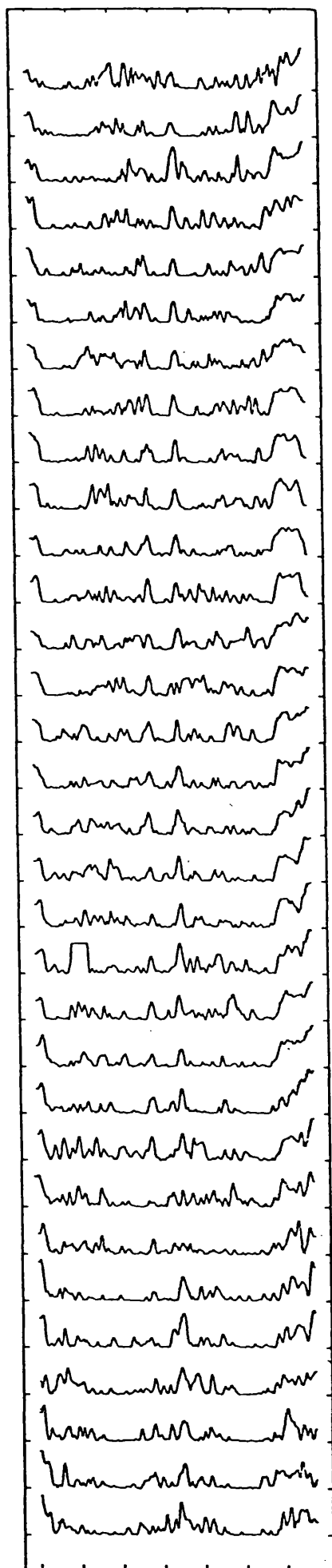
6.4 NOISE AND INTERFERENCE

Noise or unwanted signal come from three distinct sources. These are atmospheric radio noise, local electrical noise and co-channel interference or jamming. It is often difficult to distinguish between the local electrical and the atmospheric noise, as both have a random very short pulse-like signature. The university campus has a high level of electrical noise caused by lights, machine tools, and several computers operating in the vicinity of the receiving equipment and its antenna. Examples of low level random noise are present in fig 6.2.7 and 6.2.4. Inspection of one of the 256 byte data sets suggests that it is possible to resolve the sounding pulses from the noise. At intermediate noise levels, eg fig 6.4.1, this is not the case, but by comparing several consecutive 256 byte data sets the sounding pulses can be distinguished from the noise as the spikes that reoccur at the same relative position in the record.

In extreme cases (eg fig 6.4.2) it is only possible to recognise the pulse sounding signal after careful scrutiny of the quieter periods. See for example the top of the right hand column of fig 6.4.2. Under these conditions it is virtually impossible for the computer to evaluate the incoming signal. If this situation occurred operationally a change of frequency would be recommended.

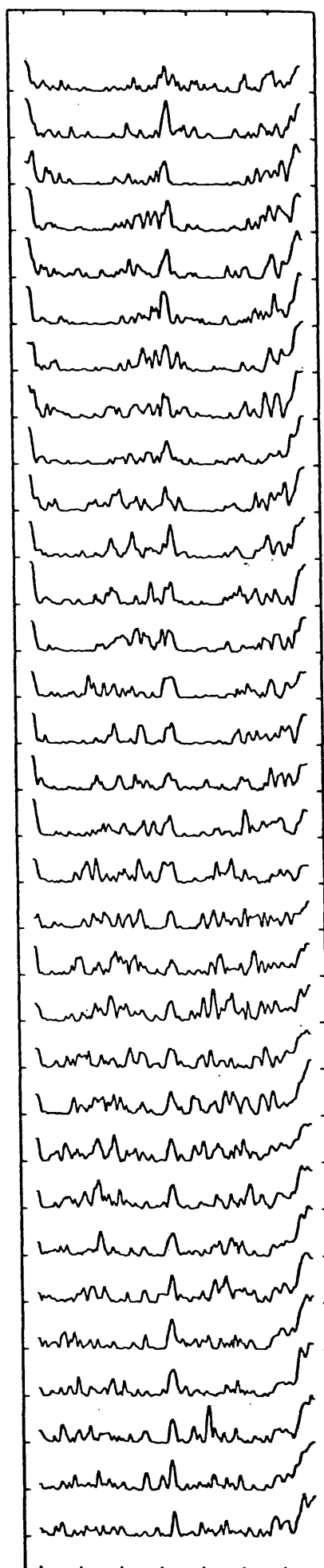
Two examples of co-channel interference are given in fig 6.4.3 and 6.4.4. Fig 6.4.3 demonstrates the effect on the sounding pulses of a signal modulated with Morse code. The

TIME
(≈ 90 MS)



DISTANCE (≈ 1000 KM)

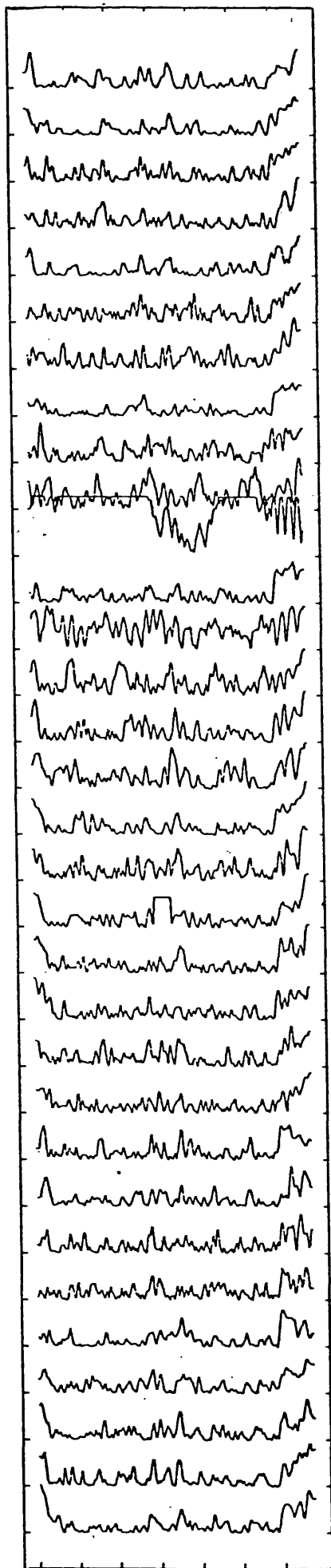
TIME
(≈ 90 MS)



DISTANCE (≈ 1000 KM)

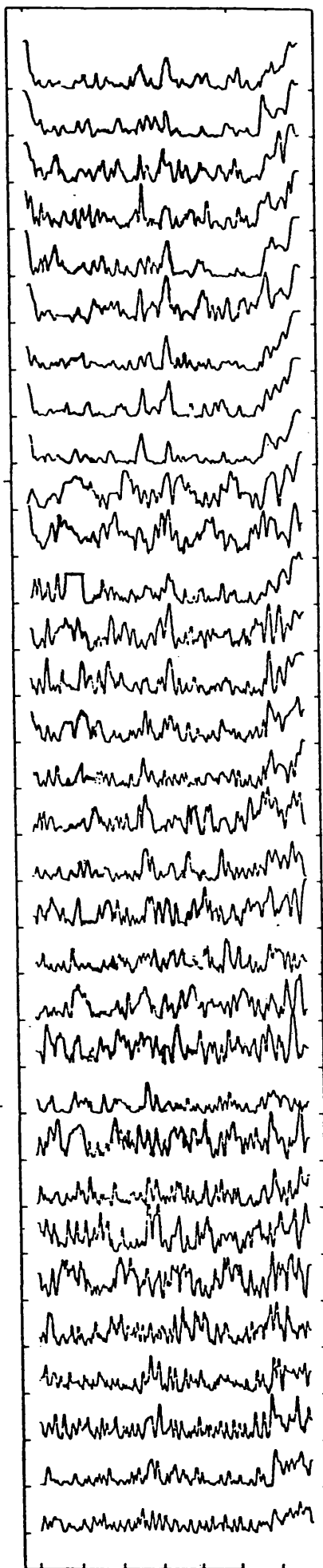
Fig 6.4.1 TROMSO 14.57 GMT 02.10.80 14 MHZ BAND
- 187 -

TIME
(x90MS)



DISTANCE (x1000KM)

TIME
(x90MS)



DISTANCE (x1000KM)

Fig 6.4.2 TROMSØ 16.1 GMT 01.10.80 14. MHZ BAND

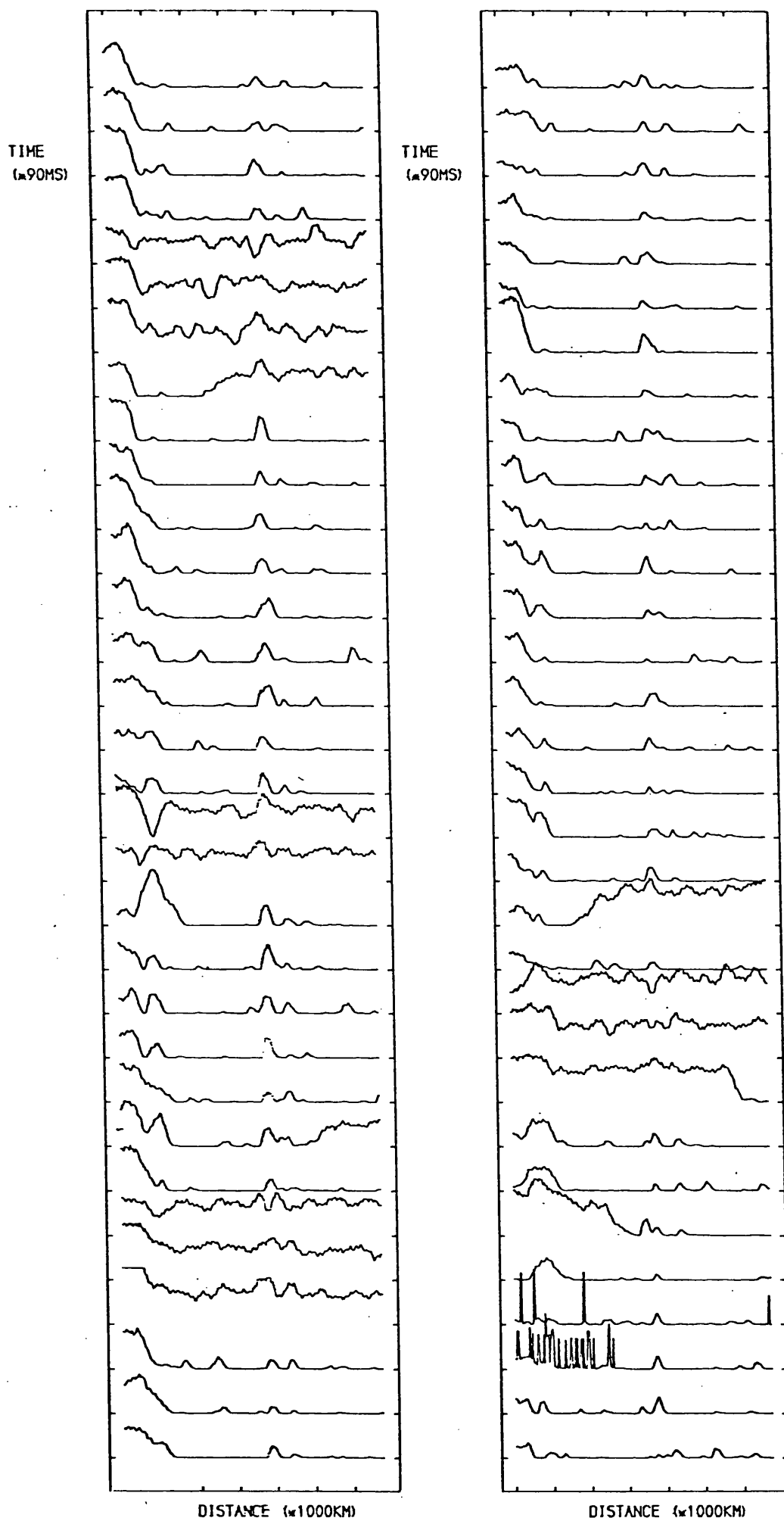
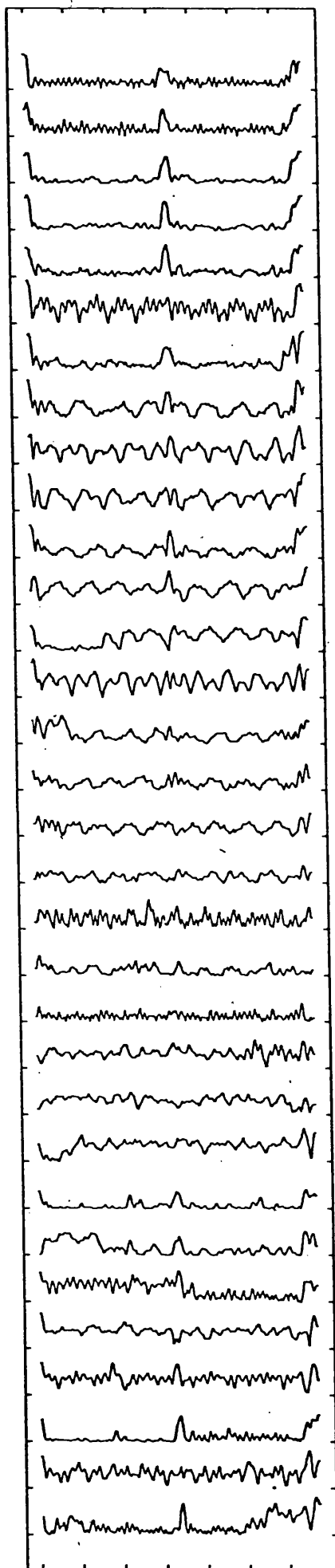


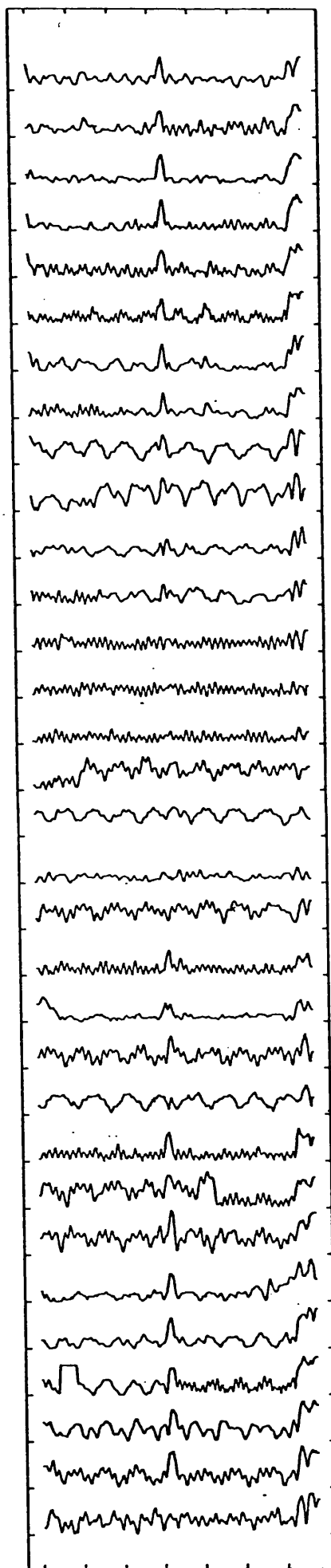
Fig 6.4.3 ELGIN 14.39 GMT 05.03.81 4.792500 MHZ
- 189 -

TIME
($\times 90$ MS)



DISTANCE ($\times 1000$ KM)

TIME
($\times 90$ MS)



DISTANCE ($\times 1000$ KM)

Fig 6.4.4 TROMSO 14.11 GMT 01.10.80 14 MHZ BAND

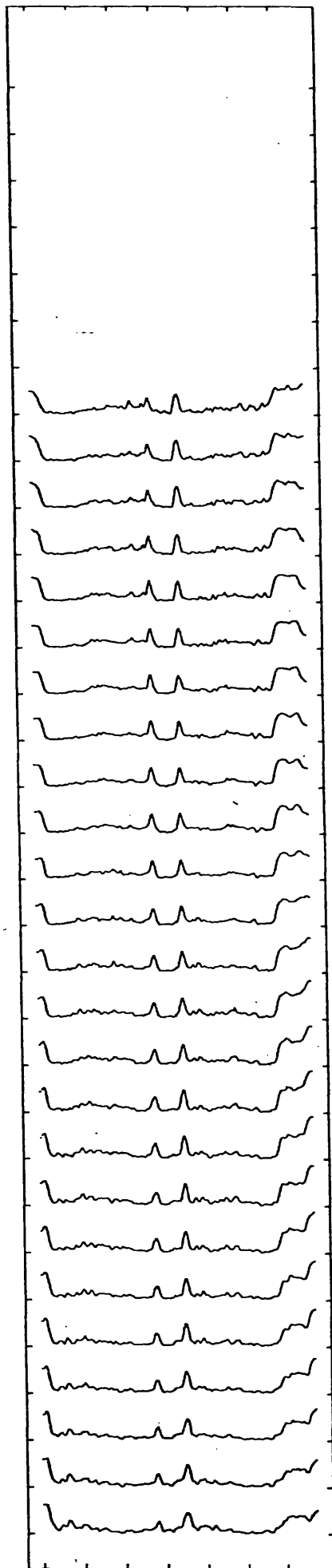
results in fig 6.4.4 contain noise resulting from a carrier wave beating with a local free running oscillator. The only possible way to avoid some of the harmful effects of the interference is to reduce the bandwidth of the receiver, but this is effective only if the interference is off set in frequency from the sounding signal. Reducing the bandwidth will broaden the pulses, which in turn reduces the time resolution and also reduces the random background noise (fig 6.4.3). The available receiver bandwidths are 100Hz, 300Hz, 1.2KHz, 3KHz, 6.5KHz and 13KHz. Only 1.2, 3 and 6.5KHz were employed, examples of the results obtained with the three bandwidths are given in fig 6.2.5, 6.2.1 and 6.2.4 respectively.

6.5 AVERAGING EFFECTS

As a means of reducing the impact of random noise, averaging has proved useful. The noisy plot in fig 6.4.1 when averaged gives fig 6.5.1. The averaging process in this case was applied over eight consecutive 256 byte data sets to produce the final result. The regular pulses stand out clearly above the noise pulses which simply smooth down to an average noise level. For this reason the software decision on which modes are present is always based on the average data rather than the original data block.

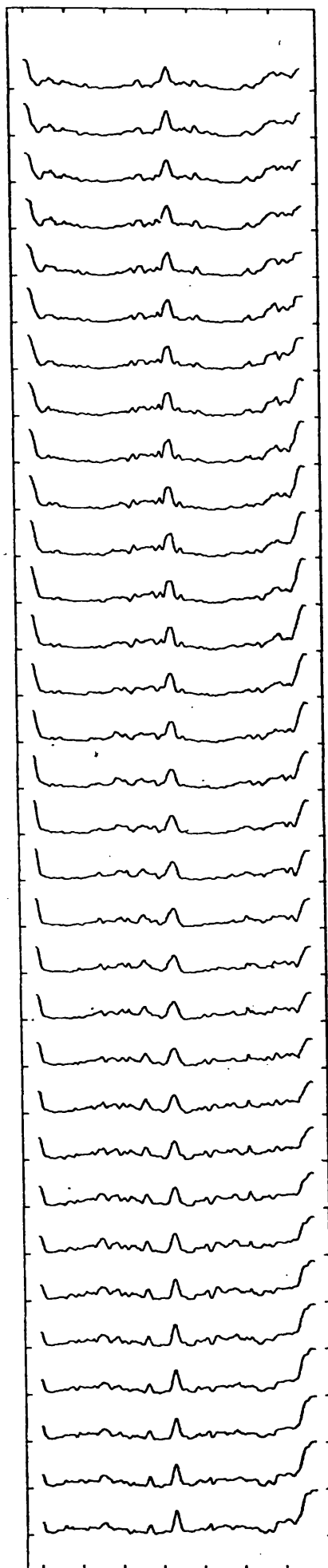
A second set of examples are plotted out in fig 6.5.2, 6.5.3 and 6.5.4, where 6.5.2 presents the original and the other two figures are averaged over three and eight data sets respectively. For noisy data, averaging over three data sets

TIME
(μ 90MS)



DISTANCE (μ 1000KM)

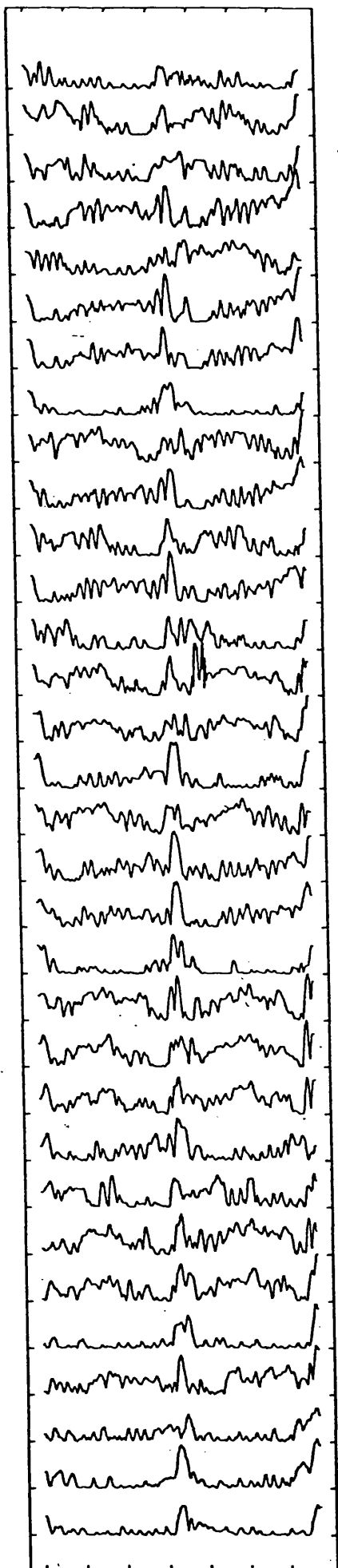
TIME
(μ 90MS)



DISTANCE (μ 1000KM)

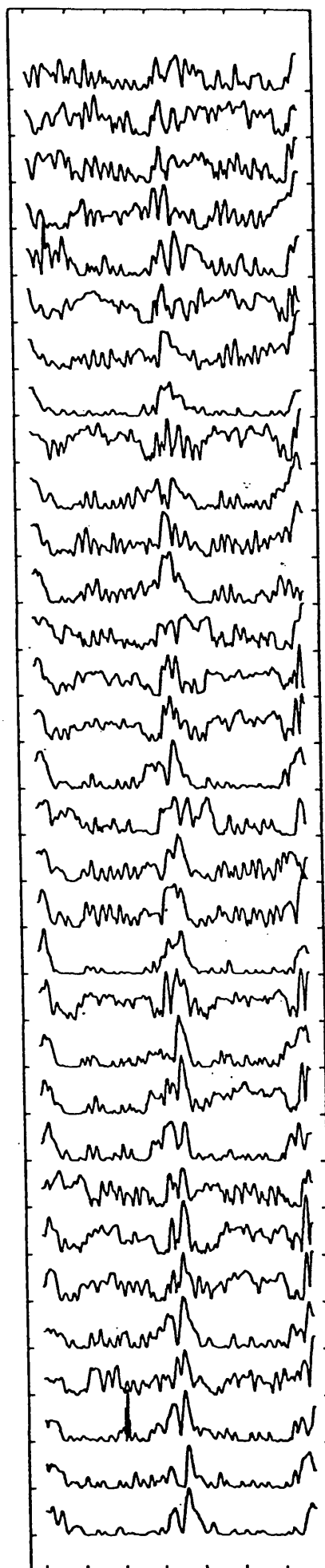
Fig 6.5.1 TROMSO 14.57 GMT 02.10.80 14 MHZ BAND
- 192 -

TIME
($\times 90$ MS)



DISTANCE ($\times 1000$ KM)

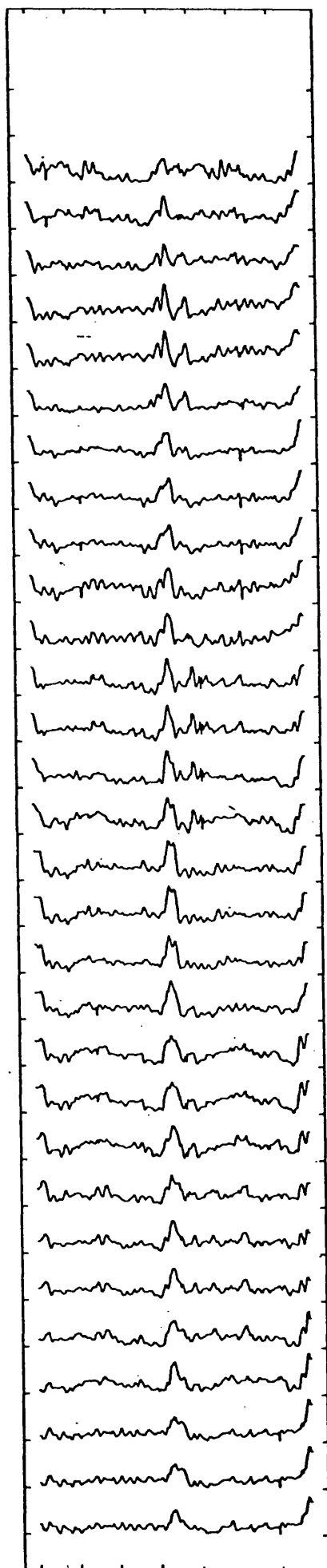
TIME
($\times 90$ MS)



DISTANCE ($\times 1000$ KM)

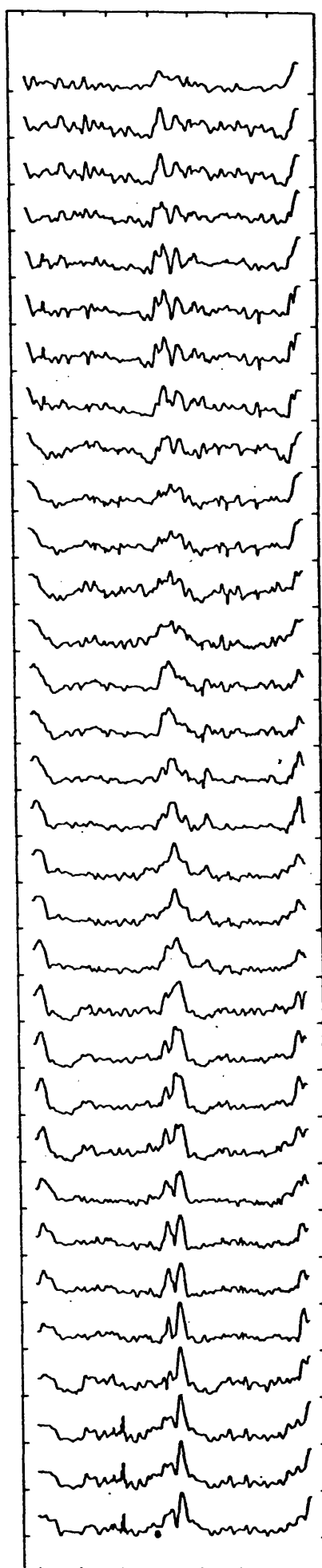
Fig 6.5.2 B000 14.5 GMT 21.10.80 18 MHZ BAND

TIME
($\times 90$ MS)



DISTANCE ($\times 1000$ KM)

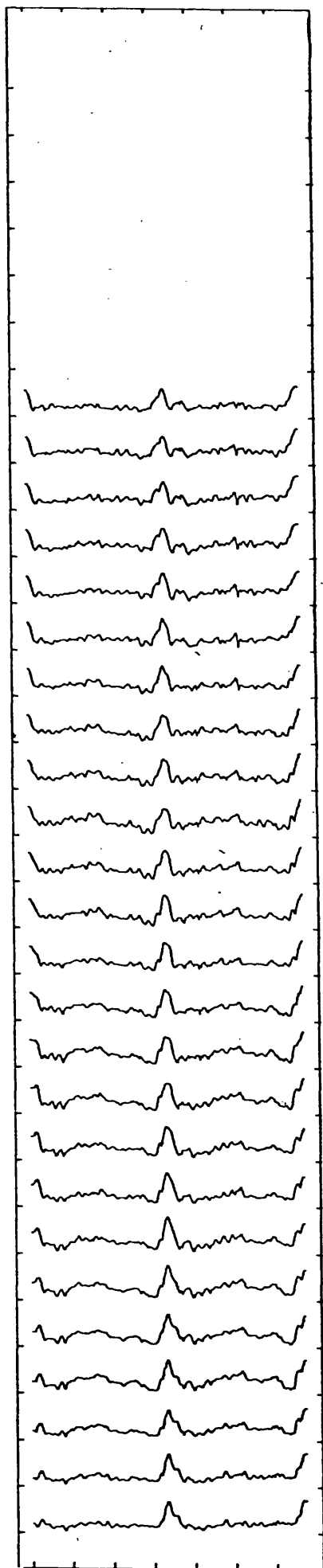
TIME
($\times 90$ MS)



DISTANCE ($\times 1000$ KM)

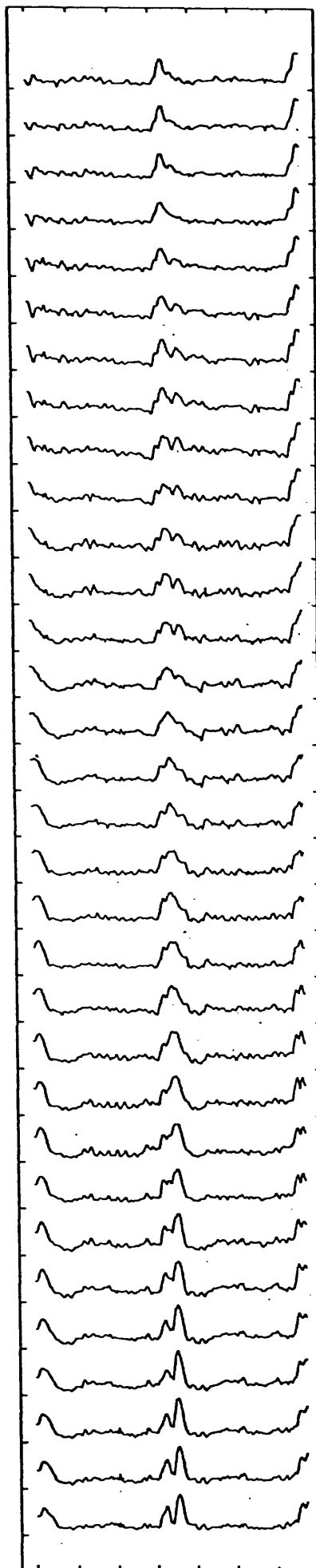
Fig 6.5.3 B000 14.5 GMT 21.10.80 18 MHZ BAND
- 194 -

TIME
(≈ 90 MS)



DISTANCE (≈ 1000 KM)

TIME
(≈ 90 MS)



DISTANCE (≈ 1000 KM)

Fig 6.5.4 BODO 14.5 GMT 21.10.80 18 MHZ BAND
- 195 -

produces a great improvement in readability as judged by the human eye. The computer however could still wrongly identify several of the noise spikes as sounding pulses. To gain greater, though still not complete immunity averages are usually taken over eight data sets (eg fig 6.5.4). Eight is also a convenient number for arithmetic in the micro-computer.

The only unwanted effect of this averaging process occurs if, as in fig 6.2.3, the synchronisation of the transmitter and receiver pulse generators fail. In this case averaging over eight cycles would lead to the two individual sounding pulses being smoothed out to a single echo 4ms long and hence the loss of any ability to recognise the distinct modes.

6.6 AURORAL PROPAGATION

On about 10% of the plots of data received from Tromsø and Bodo in Norway large differences in arrival times of the sounding pulses were noticed. Fig 6.3.1 presents a very clear example of this phenomenon, where there are two pulse returns present separated by about 1.8ms. Comparison with the predictions in fig 6.1.2 reveals that none of the normal propagation modes can have such large differences in propagation times. The only possibilities are 1E, 3F (1.53ms), 2F,4F (1.9ms) and 1F,4F (2.4ms). It is however inconceivable that in the first case the 2F mode would not be observed if the 3F was active and similarly with a 3F and 4F modes in the second and third cases. E layer screening, discussed previously in this chapter if it occurred would only block out the 1F

reflection.

A second example, fig 6.6.1, clearly shows three pulse returns with relative arrival times of 0ms, 0.8ms and 3.2ms. The first two pulses can easily be interpreted as 1E and 2F with E layer screening blocking the 1F reflection. However a conventional interpretation of the third pulse would produce a 4F or even a 5F reflection which is most unlikely, particularly as there is no evidence of a 3F reflection.

From these and other examples it became clear that a none great circle path (NGC) explanation of these results was required. The subject of NGC propagation has been studied for many years (Feldman 1939). More recent work (Bates et al 1966), (Hunsucker & Bates 1969) and (Wagner & Pike 1971) suggests the phenomenon is often connected with the auroral zone. Bates et al (1966) summarises the average time delay caused by the NGC propagation on the College Palo Alto link as "A decrease throughout the afternoon towards midnight followed by an increase", (fig 6.6.2). This behaviour correlates well with the daily movement of the southern edge of the auroral zone (fig 6.6.3) and also the ranges of the auroral scattering belt as detected by the College auroral backscatter radar (Bates et al 1966). It was concluded that the cause of the NGC path signals was an auroral associated phenomenon.

The position of the southern edge of the auroral oval to the north of the UK has been estimated for various times of day. From this it is possible to determine approximate values of time delays of signals received by this route. Fig 6.6.4 is a map of the Tromso Leicester path showing the possible auroral

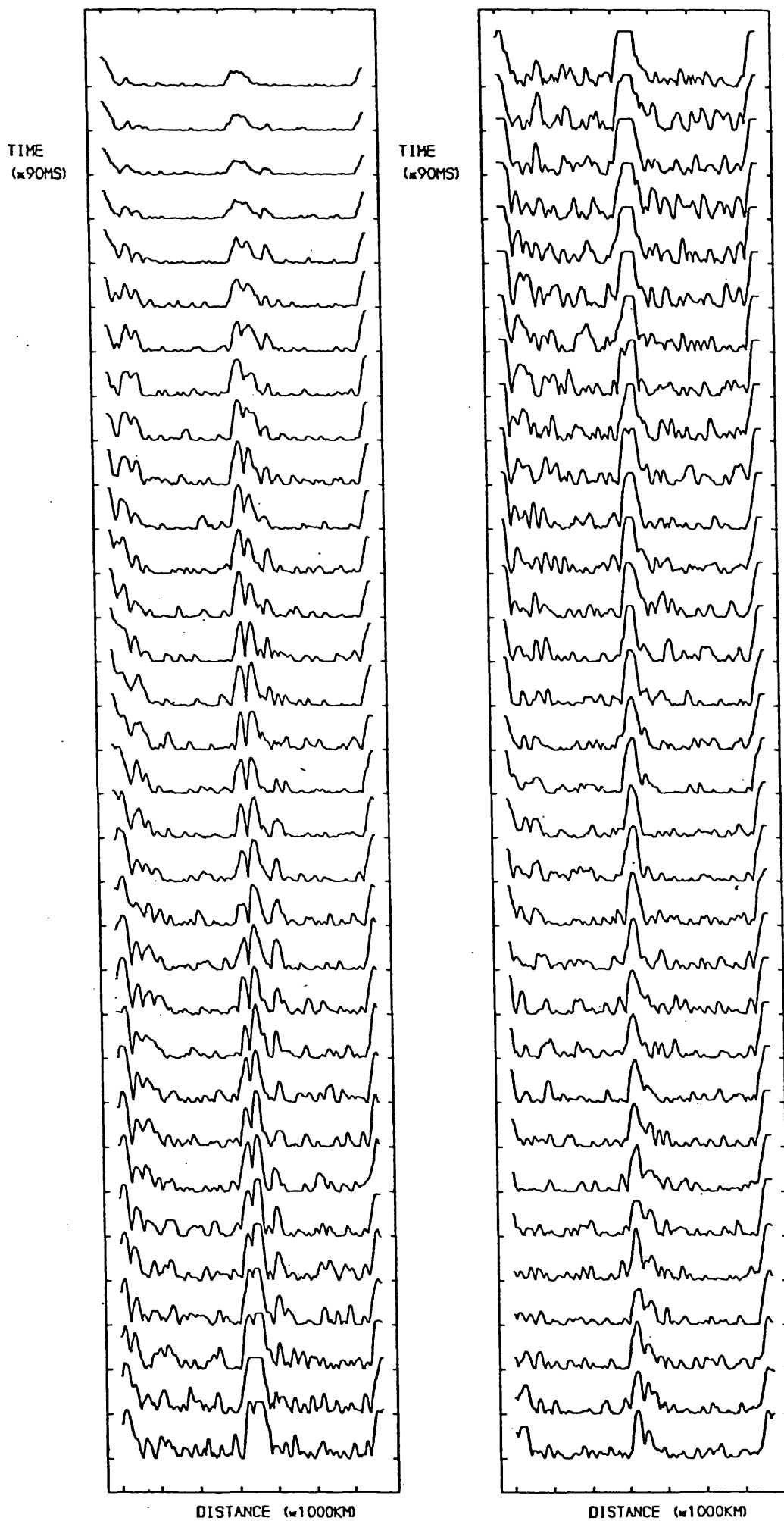


Fig 6.6.1 B000 10.3 GMT 21.10.80, 15 MHZ BAND
- 198 -

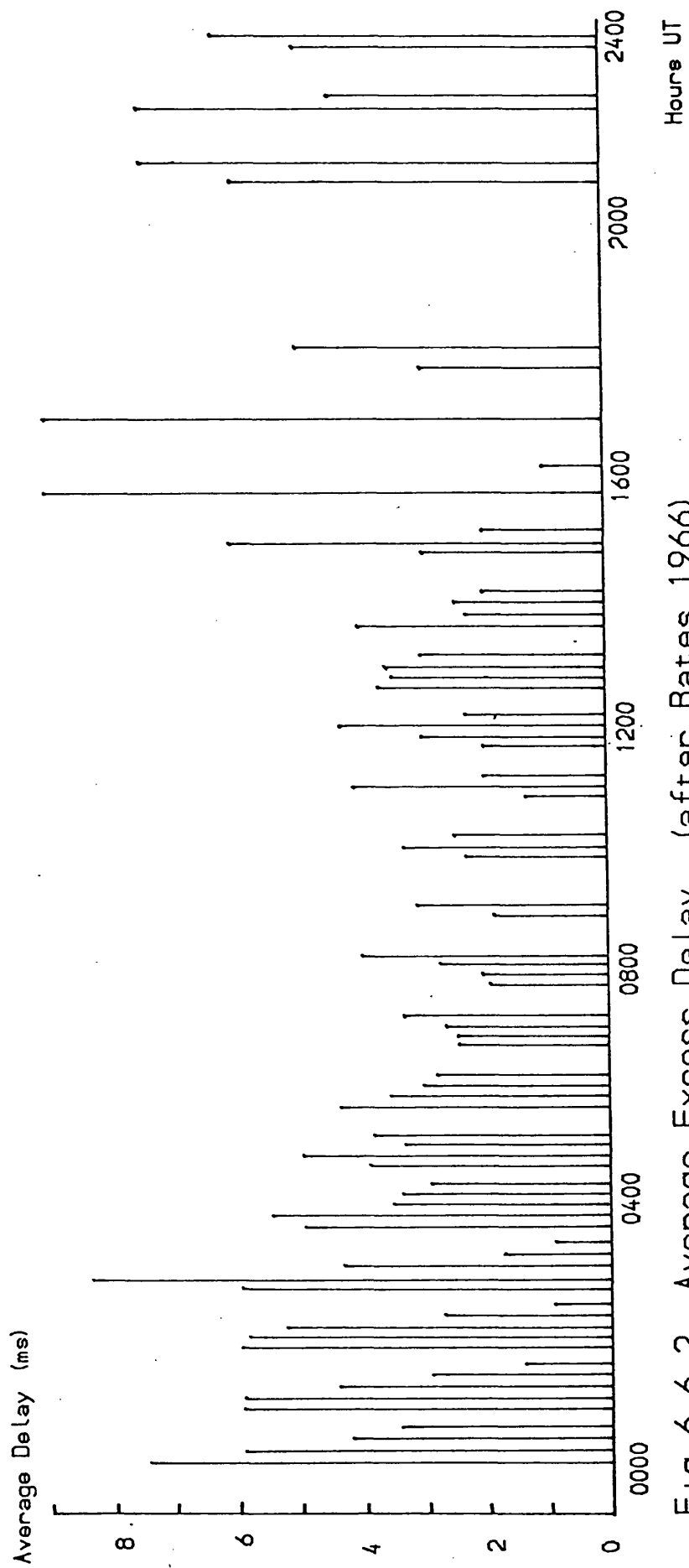


Fig 6.6.2 Average Excess Delay (after Bates 1966)

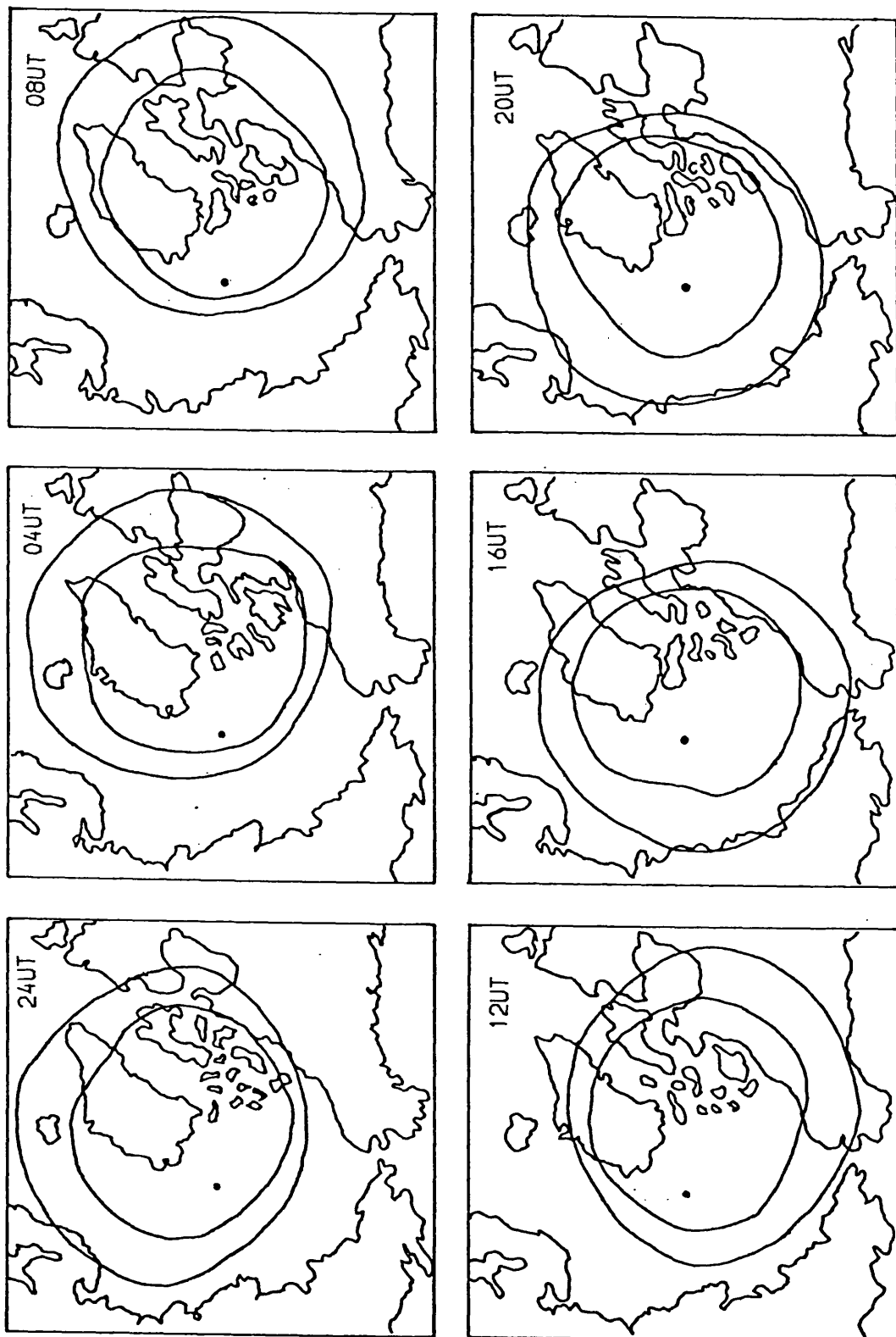


Fig 6.6.3 Approximate Location of the Auroral Oval in the Northern Hemisphere at Different Times UT (after Akasofu 1968)

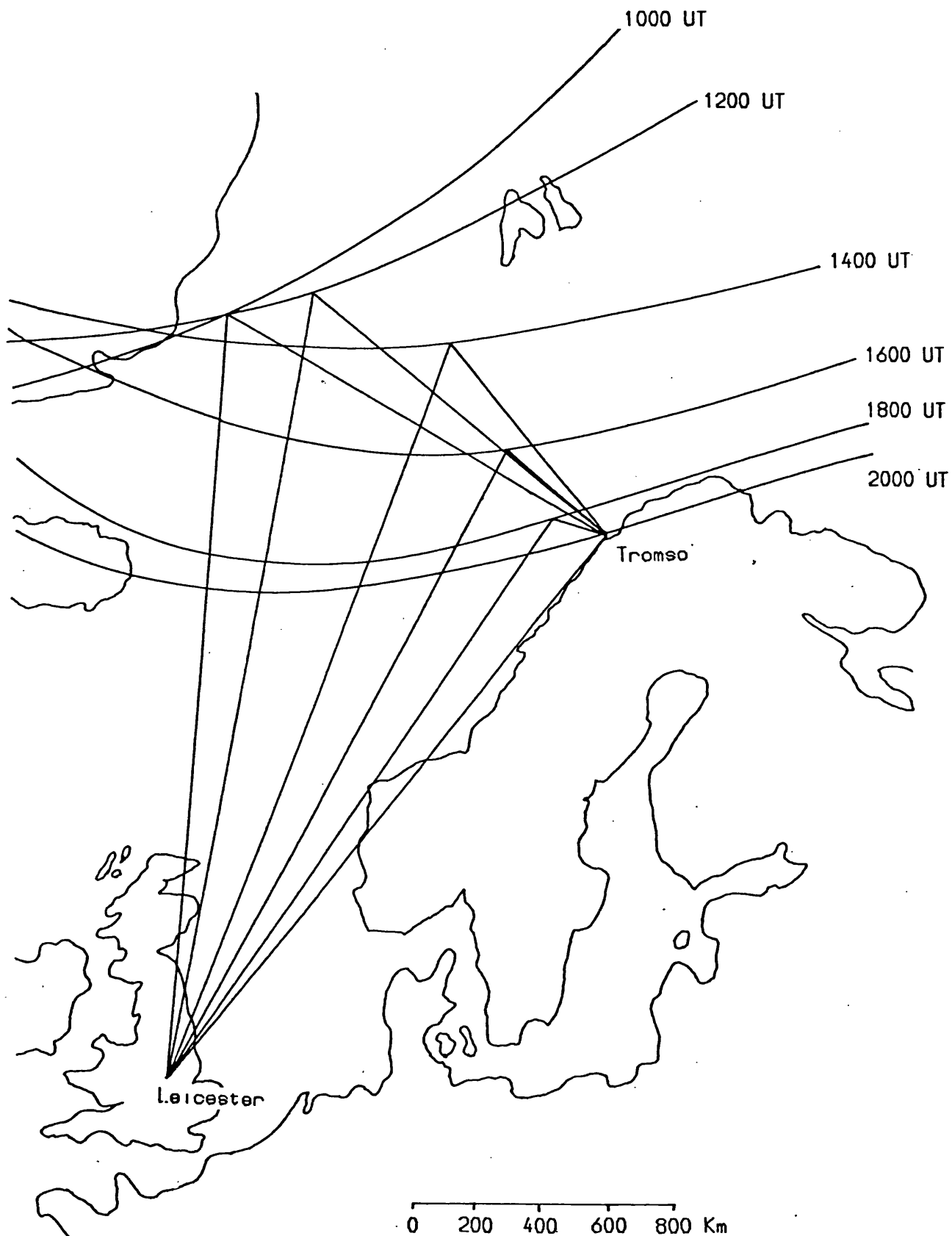


Fig 6.6.4 Possible Auroral Propagation Paths

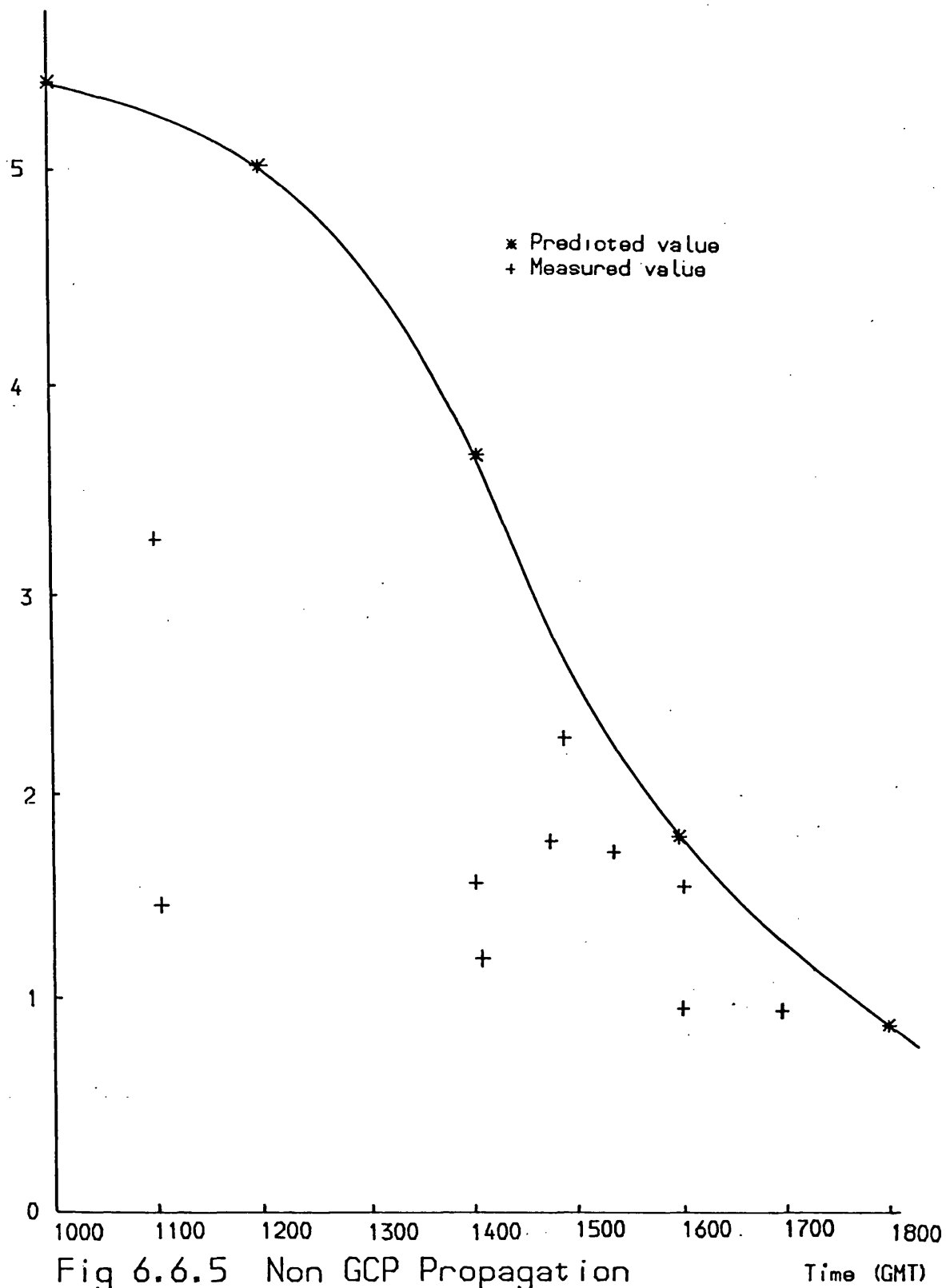
propagation paths. From this map and assuming an auroral reflection height of 250km (Wagner & Pike 1971), the following propagation times were calculated.

Time	Path length	Flight time	Relative arrival
(GMT)	(km)	(ms)	time to 1E (ms)
1000	3798	12.66	5.44
1200	3687	12.28	5.06
1400	3272	10.90	3.68
1600	2723	9.07	1.85
1800	2442	8.14	0.92

These delays are in the same range as the measured values. Both predicted and measured NGC points are plotted in fig 6.6.5. The data set is too small to draw any firm conclusions but the majority of the points seem to be consistent with an auroral NGC explanation. One reason for the delays being somewhat shorter than expected could be that the southern limit of the auroral oval is highly variable and the predictions are only based on average data.

A different and perhaps more compatible explanation for the measured NGC paths appearing to be reflected from below the southern edge of the auroral oval is presented by Stanley (1966). This assumes that the NGC propagation modes are reflected from the poleward wall of the mid latitude trough (MLT). Examples of this phenomenon were seen by Wagner & Pike (1971) in the early evening. The MLT usually lies several hundred kilometers south of the edge of the auroral oval thus

Relative arrival time due
to non GCP propagation



explaining the differences between the measured and expected propagation times. The MLT is generally considered to be a night time phenomenon but there is evidence (Muldrew 1965, Bowman 1969) that it can be observed from 1400 to 0700 local time (fig 6.6.6) which would support this explanation of the present observations. The final evidence for this explanation is that the NGC echos are well defined indicating a specular reflector such as the trough wall, rather than spread as would be expected from a diffuse scattering process. It therefore appears that the long time delays recorded in the present investigation are due to reflections from the wall of the mid latitude trough. A good review of this subject is presented by Pinnock (1981).

6.7 COMPUTER ANALYSIS

The analysis software has already been described in section 5.7.2. In this section examples are presented of its application to real data and an assessment is made of the results produced.

As already stated (section 6.2) the pulses in fig 6.2.2 have been identified as a ground wave and a Es reflection. The analysis undertaken automatically by the Cyber 73 mainframe computer produces the output presented in fig 6.7.1 for this data. Along the top of the sheet is printed the time of the observation in GMT, the date and transmitter site (unless otherwise stated the receiver is always at the Leicester. Following this is the transmitter frequency, and the number of

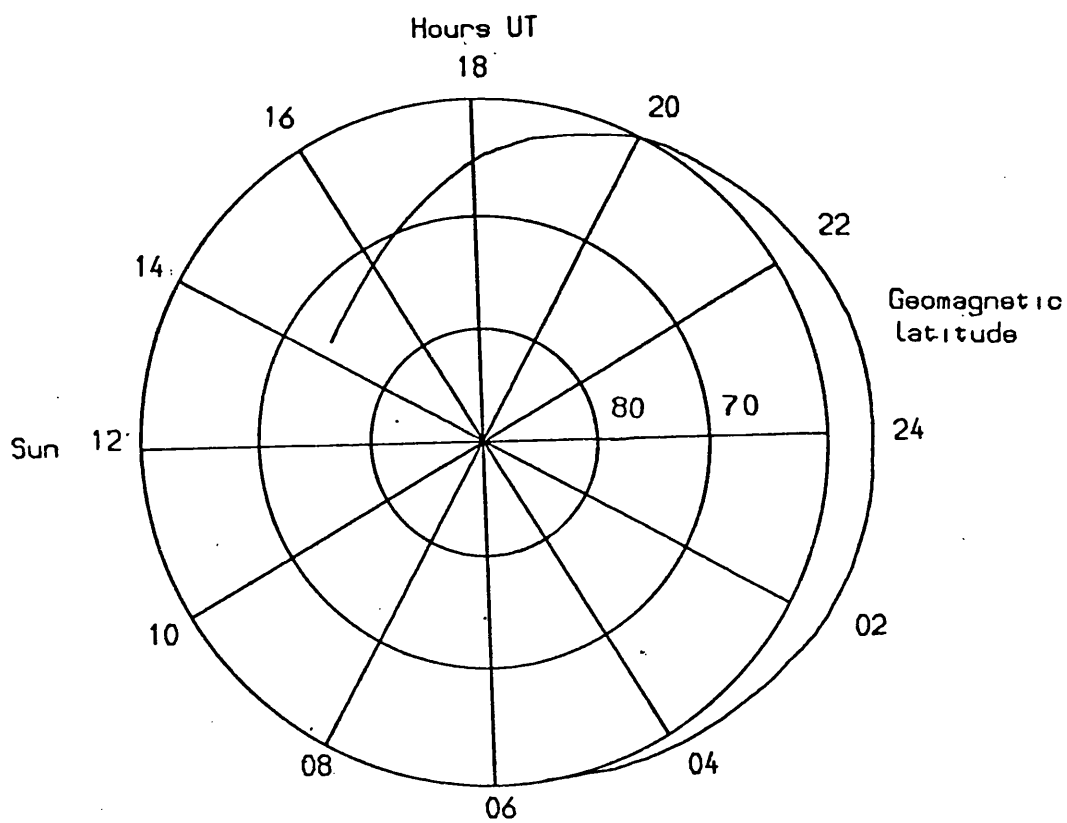


Fig 6.6.6 The Mid Latitude Trough
(after Muldrew 1965)

13.35 GMT 10.06.81 OADBY 4.792500 MHZ ANTENNA 1 AVERAGE OVER 8 DATA SETS
 FIRST OADBY SERIES 2 DATA

PUL NUM	MOD FAD	PUL LEN	TRG LEV	MUL MOD	S S+N	HIG ERR	LOW ERR	ALL ERR	MODES G E F F F A	A1 REL	T1 (MS)	A2 REL	T2 (MS)	A3 REL	T3 (MS)	A4 REL	T4 (MS)	A5 REL	T5 (MS)	A6 REL	T6 (MS)
1	2U	1.4	45	82	95	0	89	89	LP....	206	0.00	251	.62								
2	2U	1.4	45	81	95	0	82	82	LP....	206	0.00	252	.62								
3	2U	1.4	46	81	95	0	74	74	LL....	203	0.00	250	.71								
4	2U	1.4	47	82	94	0	91	91	LL....	206	0.00	250	.71								
5	2U	1.4	48	82	93	0	83	83	LL....	206	0.00	251	.71								
6	2U	1.5	49	83	93	0	98	98	LL....	206	0.00	248	.71								
7	2U	1.4	51	82	92	1	90	91	LL....	205	0.00	248	.71								
8	2U	1.4	52	81	91	4	75	79	LL....	198	0.00	244	.71								
9	2U	1.4	52	80	90	15	70	85	LL....	195	0.00	242	.71								
10	2U	1.4	53	81	90	15	78	93	LL....	195	0.00	240	.71								
11	2U	1.4	53	81	90	15	78	93	LL....	196	0.00	241	.71								
12	2U	1.4	54	80	89	28	73	101	LP....	194	0.00	240	.62								
13	2U	1.5	53	82	90	15	93	108	LP....	199	0.00	240	.62								
14	2P	1.5	54	84	89	28	97	125	LP....	205	0.00	244	.62								
15	2P	1.5	53	85	90	15	108	123	LP....	206	0.00	242	.62								
16	2P	1.5	53	85	90	15	110	125	LL....	211	0.00	246	.71								
17	2P	1.5	51	86	91	7	117	124	LL....	214	0.00	247	.71								
18	2P	1.5	50	88	92	2	125	127	LL....	221	0.00	250	.71								
19	2P	1.5	49	89	92	1	128	129	LL....	222	0.00	249	.71								
20	2P	1.5	47	90	92	2	128	130	LL....	226	0.00	250	.71								
21	2P	1.5	47	88	92	2	125	127	LL....	221	0.00	250	.71								
22	2P	1.5	45	89	93	0	129	129	LL....	220	0.00	246	.71								
23	2P	1.5	45	89	92	1	129	130	LP....	222	0.00	247	.62								
24	2P	1.5	45	91	93	0	130	130	LP....	225	0.00	247	.62								
25	2P	1.4	45	91	92	1	129	130	LP....	225	0.00	247	.62								
26	2P	1.4	44	91	93	0	130	130	LP....	223	0.00	245	.62								
27	2P	1.4	45	90	92	1	129	130	LP....	222	0.00	244	.62								
28	2P	1.5	44	90	93	0	130	130	LL....	222	0.00	245	.71								
29	2P	.7	45	90	93	0	130	130	LL....	222	0.00	245	.71								
30	2P	.7	45	89	93	0	129	129	LL....	223	0.00	249	.71								
31	2P	.7	44	87	93	0	127	127	LL....	219	0.00	249	.71								
32	2P	.6	45	86	93	0	122	122	LL....	214	0.00	248	.71								
33	2P	1.4	45	90	92	1	129	130	LP....	216	0.00	240	.62								
34	2P	1.4	47	90	91	4	128	132	LP....	216	0.00	239	.62								
35	2L	1.5	47	92	91	4	130	134	LP....	222	0.00	239	.62								
36	2L	1.5	49	94	90	10	130	140	LP....	224	0.00	237	.62								
37	2L	1.5	48	95	90	10	130	140	LP....	221	0.00	232	.62								
38	2L	.7	50	96	89	21	130	151	LL....	220	0.00	229	.71								
39	2L	.7	50	97	89	15	130	145	LL....	226	0.00	220	.71								
40	2L	.7	51	99	89	15	130	145	LL....	224	0.00	222	.71								
41	2L	.7	52	96	89	21	130	151	LL....	222	0.00	231	.71								
42	2L	.7	52	97	89	21	130	151	LL....	223	0.00	229	.71								
43	2L	.6	52	95	88	37	129	166	LL....	215	0.00	226	.71								
44	2L	.6	52	94	89	15	130	145	LL....	211	0.00	223	.71								
45	2L	.6	53	95	88	37	129	166	LL....	215	0.00	226	.71								
46	2L	1.5	51	99	88	28	130	158	LP....	217	0.00	218	.62								
47	2L	1.4	51	95	89	15	130	145	LP....	213	0.00	223	.62								
48	2L	1.4	49	93	90	7	130	137	LP....	210	0.00	225	.62								
49	2L	.6	49	95	90	7	130	137	LP....	212	0.00	221	.62								
50	2L	.7	48	95	91	2	130	132	LL....	214	0.00	224	.71								
51	2L	.7	46	97	91	1	130	131	LL....	215	0.00	220	.71								
52	2L	.7	46	98	92	0	130	130	LL....	215	0.00	218	.71								
53	2L	.7	46	99	92	0	130	130	LL....	220	0.00	221	.71								
54	2L	.6	47	94	92	0	130	130	LL....	214	0.00	226	.71								
55	2L	1.4	46	96	92	0	130	130	LL....	217	0.00	226	.71								
56	2L	1.4	47	99	92	0	130	130	LL....	221	0.00	223	.71								
57	2L	1.5	47	98	92	0	130	130	LL....	222	0.00	219	.71								

Fig 6.7.1 Sample Output

data sets the program has averaged over to reduce the effect of the noise. The next line contains the comment buffer "first 0adby series 2 data" typed in at the time of data logging.

Following this buffer are the lines of results. There are 57 lines of output in all compared with 64 input pulse records (fig 6.2.2). This is because each output line requires eight consecutive input data sets and there are only 57 of these distinct sets. The first column labeled PUL NUM is a simple numbering scheme which helps the operator recognise pulses on the graphs from the line printer output. The second column, labeled MOD FAD contains a number followed by a character which represent the number of sounding pulses detected and the programs estimate of the likelihood of data errors due to fading respectively. To produce a data error due to fading the high signal level has to fall below the value 48. If only one mode is detected or the difference between the relative amplitudes is greater than 60, a full stop is typed in this column which means fading is either most unlikely or impossible. If the intermode amplitude difference is between 40 and 60 the character is a 'U' meaning unlikely. Between 20 and 40 a 'P' for possible and from 0 to 20 a 'L' for likely. This '.UPL' key is also employed elsewhere in the output. In fig 6.7.1 when the sounding pulses become closer in amplitude the fading error likelihood changes from U to P to L as expected.

The next column labeled PUL LEN gives the average time duration in milliseconds above the trigger level for received pulses. In the example presented in fig 6.7.1 this column contains values close to 1.4ms or to 0.7ms. The actual result

should be 0.7ms but in some cases where two pulses arrive very close together, the signal level does not fall below the trigger level between them causing the width to be recorded as double the correct value. The pulse length information is useful in detecting any transmitter receiver synchronisation problems leading to the overlapping of the sounding pulses as described in section 6.5.

The next column labeled TRG LEV prints out the trigger level. The trigger level is obtained by averaging the signal level throughout the data set and then adding 16 to this value as a safety margin against triggering on noise. As already stated a sounding pulse is recognised if a signal peak is found above the trigger level. This variable trigger level is an improvement on the constant level utilised in section 5.3 as it automatically adjusts to differing noise levels. For a higher random noise level the trigger level rises thus reducing the probability of mistaking noise for signal information.

The column entitled MUL MOD prints the amplitude of any secondary modes as a percentage of the main (ie largest) mode. Fig 6.7.1 contains percentages varying from 80 to 99 as the two modes are of quite similar amplitude and the received energy is split almost equally between them. The derivation of $S/S+N$ is fully explained in section 5.7.2. The levels printed in fig 6.7.1 are of the order of 89 to 95% proving that, as expected for such a short path the noise level is extremely small compared with the signal.

The next three columns produce an estimate of the errors an operator could expect due to both noise and multimode

fading. These results are derived as outlined in section 5.7.4. In this example (fig 6.7.1) the low errors (ie the bits which should be high and are low) climb as the two pulse returns achieve equal amplitude and are thus associated with the multimode fading. The high errors (ie bits which should be low and are high) increase with falling S/S+N suggesting that noise is probably the cause of this type of error.

Probably the most interesting and useful part of this output is the mode content estimates under the title MODES GEFFFA. Here G represents ground, E, E layer reflection, FFF, 1, 2 and 3 hop F and finally A, an auroral echo. The '.UPL' key is again used to provide an indication of the reliability of the programs evaluation. In the example the program has correctly identified ground and E layer propagation paths with a fairly high degree of confidence. This information would tell the operator which modes are present and therefore in which direction a steerable antenna could be pointed to minimise multipath interference.

The mode content is evaluated as follows. From the simple model considerations in section 6.1 the mode likely to have the greatest amplitude is identified, in this case the ground wave. Next the first two received pulses are examined and the larger of the two is ascribed to the largest expected mode. The other pulses in the received signal are then compared with the predicted time delays and the '.UPL' scale indicates the degree of agreement achieved. In this case '.UPL' are defined as follows :-

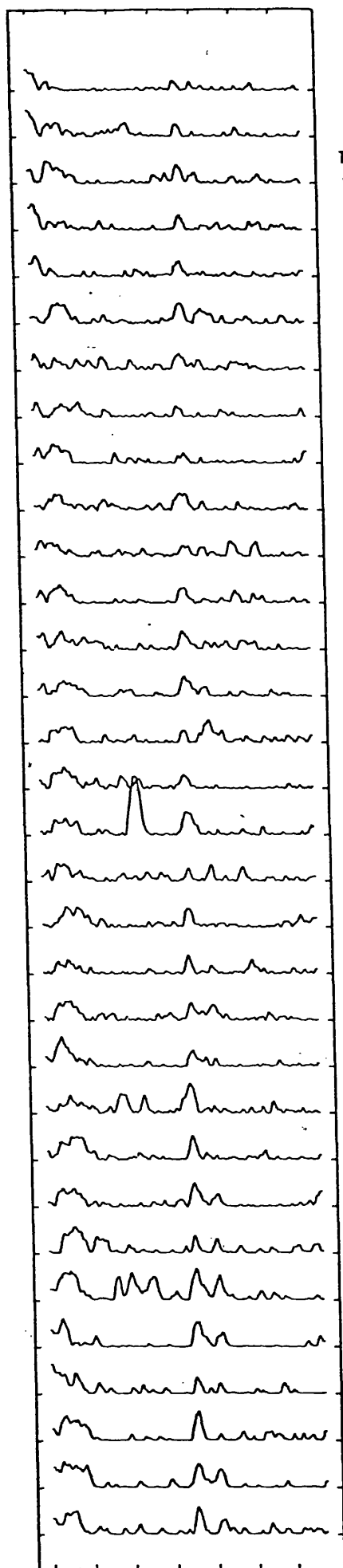
L within 0.1ms
P within 0.5ms
U within 1.0ms
. outside 1.0ms

Other considerations are also included in the evaluation algorithm. For example in fig 6.7.1 the second pulse is actually larger than the first and so following the above procedure would be ascribed to the most dominant predicted mode which is the ground wave. This would make the first pulse physically impossible to explain, and hence this is replaced by the correct interpretation of 1 hop E.

Finally the columns labeled A1 T1 A2 T2 etc contain the relative amplitudes and times of arrival (in ms) of the detected sounding pulses. The software is capable of detecting up to eight individual pulses. It should be noted that in fig 6.7.1 the arrival times of the sporadic E layer reflection jumps between 0.62 and 0.71ms because the time difference is measured in discrete steps of one ADC sample or 0.089ms.

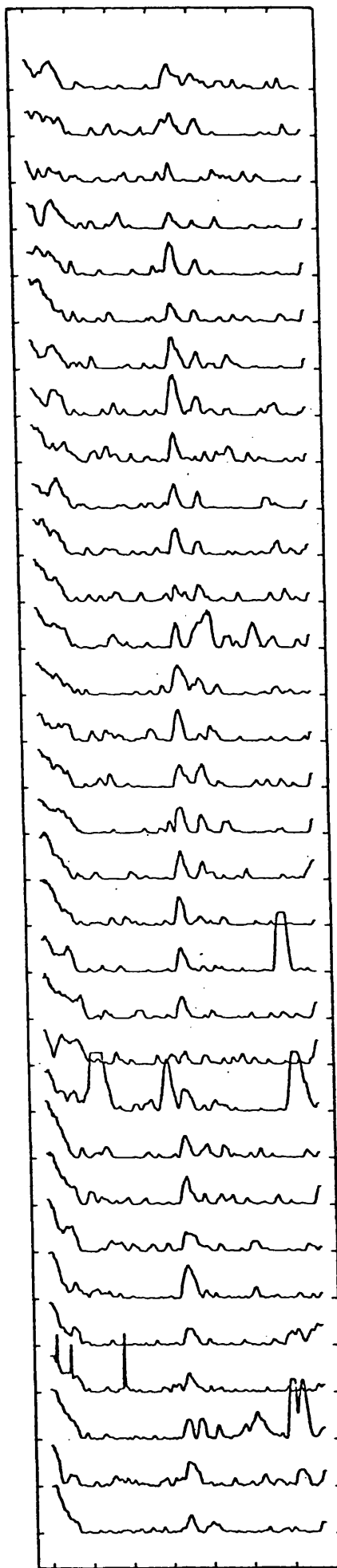
A second example of this type of output is of some Elgin data from 25/02/81. The plot is presented as fig 6.7.2 and the line printer output as fig 6.7.3. Even though the mode structure is far less distinct than the previous example and in addition more noise is present, a correct evaluation of the mode content has been achieved giving 1E and 2F, the 1F being screened by the E layer. In contrast with the previous printout (fig 6.7.1) mode interference fading is less likely. Moreover since the pulses are not as close together as in the previous case, the pulse length is recorded accurately. Both signal

TIME
(≈ 90 MS)



DISTANCE (≈ 1000 KM)

TIME
(≈ 90 MS)



DISTANCE (≈ 1000 KM)

Fig 6.7.2 ELGIN 11.45 GMT 25.02.81 4.792500 MHZ
- 211 -

11.45 GMT 25.02.81 ELGIN 4.792500 MHZ ANTENNA 1 AVERAGE OVER 8 DATA SETS
1.2 KHZ BANDWIDTH

PUL NUM	MOD FAD	PUL LEN	TRG LEV	MUL MOD	S STN	HIG ERR	LOW ERR	ALL ERR	MODES GFFFA	A1 REL	T1 (MS)	A2 REL	T2 (MS)	A3 REL	T3 (MS)	A4 REL	T4 (MS)	A5 REL	T5 (MS)	A6 REL	T6 (MS)
1	1.	.7	30	0	79	0	17	17	.L....	58	0.00										
2	1.	.7	31	0	79	0	17	17	.L....	58	0.00										
3	1.	.8	31	0	78	0	13	13	.L....	60	0.00										
4	1.	.8	31	0	76	0	34	34	.L....	56	0.00										
5	1.	.9	31	0	77	0	27	27	.L....	57	0.00										
6	1.	.9	32	0	75	0	25	25	.L....	58	0.00										
7	1.	1.0	32	0	75	0	25	25	.L....	58	0.00										
8	2P	.5	32	61	80	0	130	130	.L.L..	57	0.00	35	1.87								
9	2P	.5	32	59	81	0	130	130	.L.L..	59	0.00	35	1.87								
10	1.	1.0	34	0	76	0	5	5	.L....	68	0.00										
11	2P	.5	34	58	80	0	130	130	.L.L..	65	0.00	38	1.87								
12	1.	.7	34	0	75	0	4	4	.L....	70	0.00										
13	1.	.7	34	0	77	0	3	3	.L....	71	0.00										
14	2P	.5	34	54	81	0	129	129	.L.P..	71	0.00	39	1.96								
15	2P	.5	34	55	82	0	130	130	.L.P..	68	0.00	38	2.05								
16	1.	.8	34	0	77	0	2	2	.L....	76	0.00										
17	1.	.8	34	0	79	0	2	2	.L....	82	0.00										
18	2U	.4	33	43	86	0	75	75	.L.P..	83	0.00	36	2.05								
19	1.	.7	34	0	81	0	2	2	.L....	86	0.00										
20	2U	.5	36	48	86	0	66	66	.L.L..	93	0.00	45	1.87								
21	2U	.6	36	48	86	0	52	52	.L.P..	97	0.00	47	2.05								
22	2U	.5	36	45	86	0	32	32	.L.P..	97	0.00	44	1.96								
23	2U	.5	37	43	87	0	9	9	.L.L..	104	0.00	45	1.87								
24	2U	.6	37	50	88	0	43	43	.L.L..	102	0.00	51	1.87								
25	2U	.6	37	55	88	0	89	89	.L.L..	102	0.00	57	1.87								
26	2U	.6	38	58	87	0	100	100	.L.L..	103	0.00	60	1.87								
27	2U	.7	39	56	87	0	81	81	.L.L..	105	0.00	59	1.87								
28	2U	.6	36	49	88	0	57	57	.L.P..	97	0.00	48	1.96								
29	2U	.6	37	49	87	0	74	74	.L.P..	93	0.00	46	1.96								
30	2U	.6	37	47	88	0	30	30	.L.P..	101	0.00	48	2.05								
31	2U	.6	38	51	87	0	74	74	.L.P..	97	0.00	50	2.05								
32	2U	.6	38	49	88	0	43	43	.L.P..	100	0.00	49	2.05								
33	2U	.7	39	47	88	0	16	16	.L.P..	107	0.00	51	1.96								
34	2.	.6	39	40	87	0	4	4	.L.P..	108	0.00	44	1.96								
35	2.	.5	39	41	88	0	3	3	.L.P..	113	0.00	47	1.96								
36	2.	.6	40	45	88	0	4	4	.L.P..	116	0.00	53	1.96								
37	2U	.6	41	50	88	0	12	12	.L.P..	116	0.00	58	1.96								
38	2U	.6	43	58	86	0	79	79	.L.P..	111	0.00	65	1.96								
39	2U	.7	43	57	86	0	60	60	.L.P..	115	0.00	66	1.96								
40	2U	.7	43	52	87	0	26	26	.L.L..	116	0.00	61	1.87								
41	2U	.6	43	60	85	0	99	99	.L.L..	107	0.00	65	1.87								
42	2P	.7	42	67	86	0	126	126	.L.L..	105	0.00	71	1.87								
43	2P	.7	43	67	86	0	125	125	.L.L..	107	0.00	72	1.87								
44	2U	.7	42	62	87	0	108	108	.L.L..	108	0.00	67	1.87								
45	2U	.6	43	55	86	0	60	60	.L.L..	111	0.00	62	1.87								
46	2U	.5	41	46	87	0	14	14	.L.L..	108	0.00	50	1.87								
47	2U	.5	42	46	85	0	31	31	.L.L..	100	0.00	46	1.87								
48	1.	.7	47	0	68	66	3	69	.L....	95	0.00										
49	1.	.7	47	0	68	66	2	68	.L....	96	0.00										
50	1.	.7	48	0	69	66	2	68	.L....	98	0.00										
51	1.	.7	48	0	67	66	3	69	.L....	92	0.00										
52	1.	.9	48	0	68	66	3	69	.L....	94	0.00										
53	1.	.9	47	0	68	56	3	59	.L....	91	0.00										
54	1.	.9	46	0	67	56	3	59	.L....	90	0.00										
55	1.	.8	48	0	67	77	3	80	.L....	94	0.00										
56	1.	1.0	43	0	73	21	2	23	.L....	94	0.00										
57	1.	.9	42	0	73	15	2	17	.L....	91	0.00										

Fig 6.7.3 Sample Output

levels and the likelihood of multimode interference are reduced. As a result of this the noise induced predicted errors are increased and the fading induced predicted errors are reduced. Again the modes are recognised with a fairly high level of confidence.

The final examples are given in fig 6.7.4 and 6.7.5. These are for 15MHz signals from Bodo Norway. The first point of interest is that the pulses are wider resulting from the decreased transmitter bandwidth. The analysis is again correct giving the 1F mode as the main mode all the time with some 1E and auroral reflections. It is worth noting that, although when the 1E mode arrives it takes over the A1, T1 designation from the 1F mode, the program recognises that the 1F mode is now the second to arrive and does not mistakenly identify the situation as the equally possible 1F, 2F, auroral solution.

6.8 SUMMARY

A simple geometric model of the ionosphere was developed for calculating the approximate times of flight for the various modes of propagation.

Pulse sounding experiments were carried out over four paths of different length and the results obtained presented. In particular the effects of rapid mode changes, noise, interference, averaging and auroral propagation were investigated. Computer programs were written to identify the active modes of propagation. An assessment of the effectiveness of this technique for mode recognition is given.

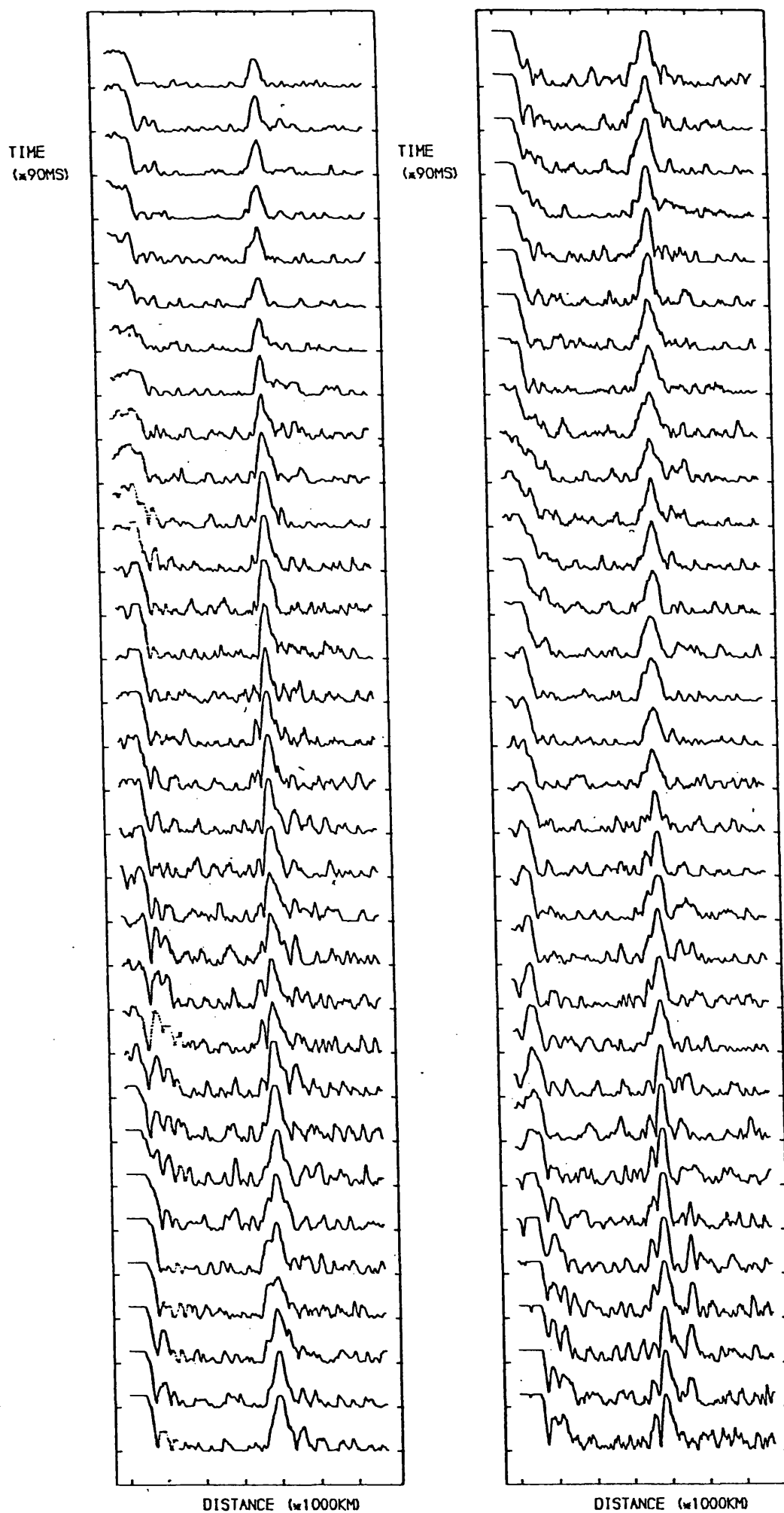


Fig 6.7.4 B000 10.3 GMT 21.10.80 15 MHZ BAND
- 214 -

10. 3 GMT 21.10.80 BODO 15 MHZ BAND ANTENNA 1 AVERAGE OVER 8 DATA SETS
FIRST BODO TO DUMP

PUL NUM	MOD FAD	PUL LEN	TRG LEV	MUL MOD	S S+N	HIG ERR	LOW ERR	ALL ERR	MODES GEFFFA	A1 REL	T1 (MS)	A2 REL	T2 (MS)	A3 REL	T3 (MS)	A4 REL	T4 (MS)	A5 REL	T5 (MS)	A6 REL	T6 (MS)
------------	------------	------------	------------	------------	----------	------------	------------	------------	-----------------	-----------	------------	-----------	------------	-----------	------------	-----------	------------	-----------	------------	-----------	------------

1	1.	1.3	47	0	88	0	2	2	..L...	154	0.00										
2	1.	1.3	48	0	88	1	2	3	..L...	163	0.00										
3	1.	1.3	49	0	88	2	2	4	..L...	172	0.00										
4	1.	1.6	51	0	88	7	2	9	..L...	185	0.00										
5	1.	1.6	54	0	87	21	2	23	..L...	197	0.00										
6	1.	1.6	57	0	87	37	2	39	..L...	209	0.00										
7	1.	1.6	61	0	86	77	2	79	..L...	223	0.00										
8	1.	1.6	65	0	86	100	2	102	..L...	236	0.00										
9	1.	1.6	68	0	86	112	2	114	..L...	245	0.00										
10	1.	1.6	70	0	86	124	2	126	..L...	251	0.00										
11	1.	1.5	72	0	86	124	2	126	..L...	254	0.00										
12	1.	1.5	73	0	85	147	2	149	..L...	251	0.00										
13	1.	1.6	73	0	85	147	2	149	..L...	248	0.00										
14	1.	1.5	74	0	84	170	2	172	..L...	246	0.00										
15	2.	.9	75	36	83	191	2	193	..L...	88	0.00	243	.89								
16	3.	.7	76	78	87	77	2	79	..L..L	101	0.00	240	.89	88	3.03						
17	3.	.8	77	82	86	100	2	102	..L..L	95	0.00	240	.89	103	3.03						
18	3.	.7	79	81	85	136	2	138	..L..L	95	0.00	240	.89	101	3.03						
19	3.	.7	81	80	84	159	2	161	..L..L	98	0.00	238	.89	94	3.03						
20	2.	1.1	82	42	80	255	2	257	..L...	102	0.00	241	.80								
21	2.	2.2	83	46	81	239	2	241	..L...	112	0.00	243	.89								
22	1.	2.1	82	0	80	247	2	249	..L...	237	0.00										
23	1.	2.2	82	0	80	247	2	249	..L...	238	0.00										
24	1.	2.2	81	0	82	211	2	213	..L...	241	0.00										
25	1.	2.2	80	0	82	211	2	213	..L...	241	0.00										
26	1.	2.2	79	0	83	181	2	183	..L...	241	0.00										
27	1.	2.2	77	0	83	191	2	193	..L...	242	0.00										
28	1.	2.1	76	0	84	159	2	161	..L...	242	0.00										
29	1.	2.1	75	0	85	136	2	138	..L...	242	0.00										
30	1.	2.1	73	0	85	147	2	149	..L...	248	0.00										
31	1.	2.0	72	0	86	112	2	114	..L...	247	0.00										
32	1.	2.0	71	0	86	112	2	114	..L...	244	0.00										
33	1.	2.0	70	0	86	100	2	102	..L...	239	0.00										
34	1.	2.0	69	0	86	89	2	91	..L...	233	0.00										
35	1.	2.0	68	0	85	112	2	114	..L...	227	0.00										
36	1.	2.0	68	0	85	100	2	102	..L...	224	0.00										
37	1.	1.9	68	0	85	100	2	102	..L...	222	0.00										
38	1.	1.8	68	0	85	89	2	91	..L...	217	0.00										
39	1.	1.9	68	0	84	100	2	102	..L...	210	0.00										
40	1.	1.9	67	0	83	112	2	114	..L...	203	0.00										
41	1.	1.9	66	0	83	100	2	102	..L...	195	0.00										
42	1.	1.8	65	0	82	100	2	102	..L...	188	0.00										
43	1.	1.8	64	0	83	77	2	79	..L...	186	0.00										
44	1.	1.9	63	0	83	77	2	79	..L...	184	0.00										
45	1.	1.8	63	0	83	77	2	79	..L...	185	0.00										
46	1.	1.9	62	0	84	77	2	79	..L...	195	0.00										
47	1.	1.9	62	0	84	89	2	91	..L...	202	0.00										
48	1.	2.0	62	0	84	89	2	91	..L...	206	0.00										
49	1.	2.0	63	0	84	112	2	114	..L...	214	0.00										
50	2.	2.0	64	42	85	100	2	102	..L...	95	0.00	225	.98								
51	2.	2.0	66	47	85	124	2	126	..L...	111	0.00	234	.98								
52	2.	2.0	69	46	84	159	2	161	..L...	111	0.00	240	.89								
53	2.	2.0	72	46	83	191	2	193	..L...	114	0.00	246	.98								
54	3.	.7	75	83	87	89	2	91	..L..L	120	0.00	247	1.07	87	3.38						
55	3.	.7	79	88	86	112	2	114	..L..L	114	0.00	249	.98	107	3.38						
56	3.	.7	82	91	86	124	2	126	..L..L	116	0.00	252	.89	114	3.38						
57	3.	.7	86	92	85	159	2	161	..L..L	128	0.00	254	.98	108	3.38						

Fig 6.7.5 Sample Output

CHAPTER 7

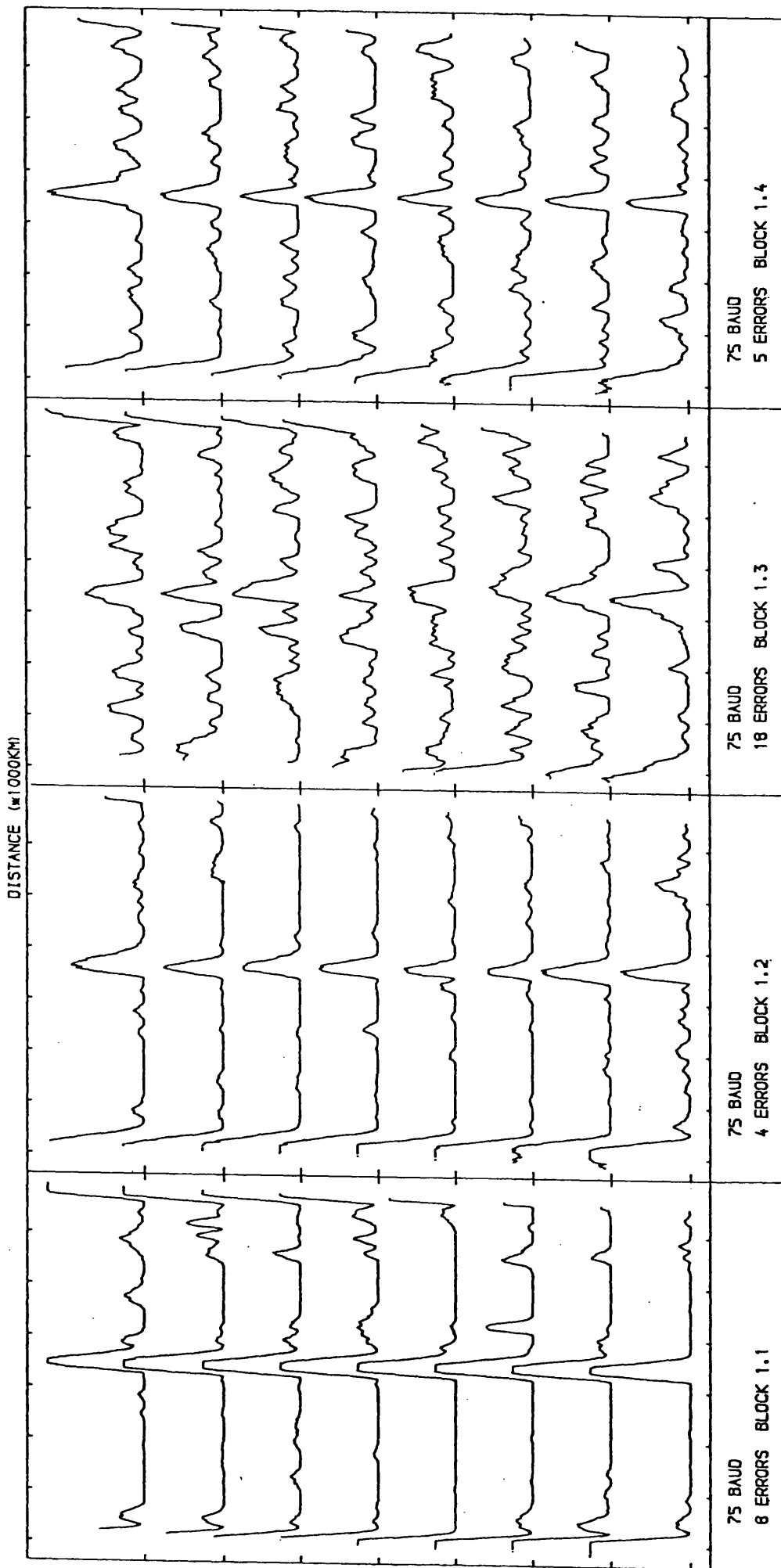
EVALUATION OF ERROR RATES

7.0 INTRODUCTION

It is of considerable practical importance to investigate the relationship between the pulse sounding results and the error rate measured in a sequence of random data. The format of the transmitted sequence is discussed in detail in section 3.2 and the detecting software in section 5.7.3. In this chapter details of the computer analysis procedures together with examples of results obtained are presented. The effects of various ionospheric parameters on the data sequence are examined in a simulation study and finally an attempt is made to establish a correlation between the recorded data errors and the sounding signal records.

7.1 DATA PRESENTATION

As noted in section 5.7.3 each graph produced contains four blocks of the pulse sounding together with the corresponding pseudo random sequence (PRS) observations. An example of this type of plot is presented in fig 7.1.1. Each section of the diagram shows eight consecutive pulse records, the baud rate and number of errors received from 2048 data



G9BLD ELGIN 14.51 GMT 29.03.81 4.792500 MHZ . SUNDAY

Fig 7.1.1 Sample Pulse Experiment Plot

bits. The very slow drift across the page of the pulse record plots (as indicated by the extreme left hand edge of the traces) results from an attempt to compensate for the drift of the crystal oscillator in the pulse sounding generator. As a result of this drift the transmitter and receiver are slightly out of synchronisation, which would otherwise cause pulse broadening to occur when the pulses were averaged (section 6.5). The compensation process reverses the drift and the pulses once more fall above each other and hence produce a sharp average for analysis.

A detailed analysis of the data plotted in the first column of fig 7.1.1 is presented in fig 7.1.2. Along the top of the page is printed the date, time (GMT), transmitter site, callsign, antenna number, baudrate and block number (X,Y). The antenna number refers to the antenna input of the receiver. This feature was incorporated for evaluating different types of antenna but is not used in the present study. In the block number X refers to the plot number and Y to the data block within that plot. Following the header line is the comment line typed in at the time of logging.

Next is the evaluation of the two 1023 bit blocks of PRS data. First error content of the PRS is plotted out as 1024 characters. The character is a '.' if the bit is correct, a '1' if the bit is a '1' and should be a '0' and a '0' if the bit is a '0' and should be a '1'. These errors referred to as high and low errors respectively. The extra bit to make up the 1024 is a '1' from the period of carrier that follows the PRS and is simply included to make the data handling easier in the

microprocessor. The example indicates that five errors have been received, all of them high. These probably result from the light random noise that can be seen in fig 7.1.1.

Following the error printout the distribution of the received errors is evaluated. The errors are divided into three rows, all errors, high errors and low errors. The error 'burst' length is then examined. A 'burst' of errors is defined as a group of incorrect data bits arriving consecutively, the number of bits being the burst length. This statistic is valuable since it provides the computer with a clue to the cause of the errors. For example, in CW interference the proportion of errors contained within long bursts will be higher than for more random types of noise. The number below the burst length is the number of bursts of that length. The total number of errors is displayed at the end of each row.

The next line of analysis contains the computer's assessment of a) the quality of the received data and b) the likely cause of the errors. Under operational conditions this would obviously be arrived at by means of error detecting codes rather than by comparison with a known PRS. Such an evaluation would be a valuable addition to the information gleaned from the sounding signal. In the current manual system the evaluation is printed out, however in an automatic receiver the gain or bandwidth could be altered by the microprocessor to optimise the signal, according to the results of the evaluation program. The criterion upon which the evaluation is based are as follows :-

Good data - Less than 20 errors
Fair data - Between 20 and 50 errors
Poor data - Between 50 and 250 errors
Lost data - Above 250 errors

The sources of the errors are believed to be as follows. If the ratio (high errors/ low errors) is greater than 1.5, noise or interference is mainly responsible. If the ratio (low errors/high errors) is greater than 1.5 fading is the major cause. The relative importance of these sources is evaluated from the difference between the number of high and low errors in a given sample and is described as follows :-

Error designation ABS(High errors-Low errors)

Light	Less than 30
Moderate	Between 30 and 60
Severe	Greater than 60

The distinction between noise and interference is made on the ratio of the 3 bit error bursts to the 2 bit error bursts. Interference is identified as the major source if the ratio (3 bit bursts / 2 bit bursts) is greater than 0.2, ie a larger than normal number of longer bursts have been recorded. A final cause of poor or lost data can be synchronisation problems between the transmitter and receiver clocks. This produces a low number of errors at the start of the PRS after initial synchronisation that gradually increases as time progresses. This condition is easily recognised and is displayed as part of the evaluation.

These test criteria are somewhat arbitrary however, any qualitative assessment whether done by man or machine must be based upon divisions of this kind. The results obtained are in close agreement with manual monitoring of the interference sources.

After the evaluation of the two blocks of PRS data the eight consecutive pulse records are analysed in a similar manner to that described in the previous chapter. The number of modes, trigger level, predicted errors, pulse amplitudes and arrival times are displayed. The only new statistic is the (S/N) ratio in dB ($20 * \text{LOG}_{10}(S/N)$). This is a more conventional way of measuring the signal to noise ratio than (S/S+N) which, being bounded, is easier to plot. The next example (fig 7.1.1 and 7.1.2) is of quiet conditions and since only one mode is present a low trigger level, high signal level, high (S/N) and low predicted errors are recognised. A good correlation is obtained with the PRS data. The relatively small pulse length indicates that the compensation for the faulty synchronisation has been successful.

7.2 RESULTS

Throughout the course of the experiment a total of 448 sets of data were recorded. Of these, 28 came from Oadby, 24 from Durham and the vast majority (396) from Elgin. Equal numbers of observations were not made on each path for the reasons outlined below.

As expected the Oadby path data contained so few errors

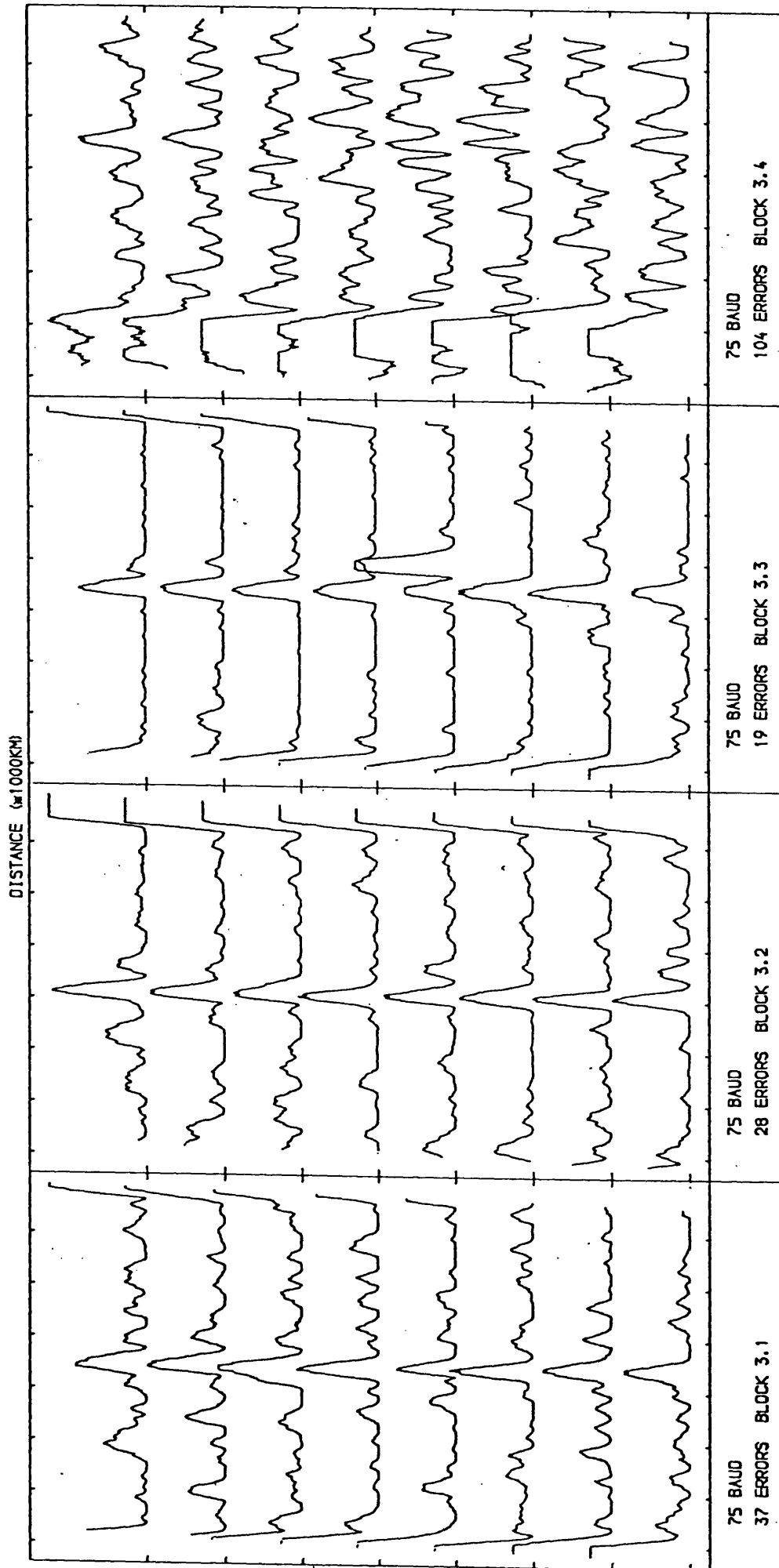
and such clean sounding pulses that there was excellent correlation at all times and therefore nothing to analyse. For this reason, once initial experiments had been conducted to test the software, longer more realistic paths were investigated.

The results from Durham, were hampered by practical difficulties. Even the records which were received were spoilt by bad co-channel interference and so are of limited use.

The Elgin site was operated for almost three months on sounder sequence 6 (section 5.1) allowing both PRS data and pulse sounding. It was sadly not possible to take PRS data from Norway due to difficulties in transporting equipment. Examples of the typical types of data sets are now presented.

7.2.1 Low Noise Conditions

Low noise conditions make up approximately half the measured samples on all paths. These conditions are defined as times when an operator can distinguish between the sounding pulses and the noise from a single sounding record. Examples of the graphs are given as fig 7.1.1 (blocks 1.1, 1.2, 1.4) and fig 7.2.1 (blocks 3.1, 3.2, 3.3) and of the line printer output in fig 7.1.2 and 7.2.2. Fig 7.1.2 has already been discussed in section 7.1, and very similar results are evident in fig 7.2.2 apart from a few random errors evenly distributed over the data set. In these examples quiet single moded conditions prevail.



G9BLD ELGIN 14.27 GMT 29.03.81 4.792500 MHZ SUNDAY

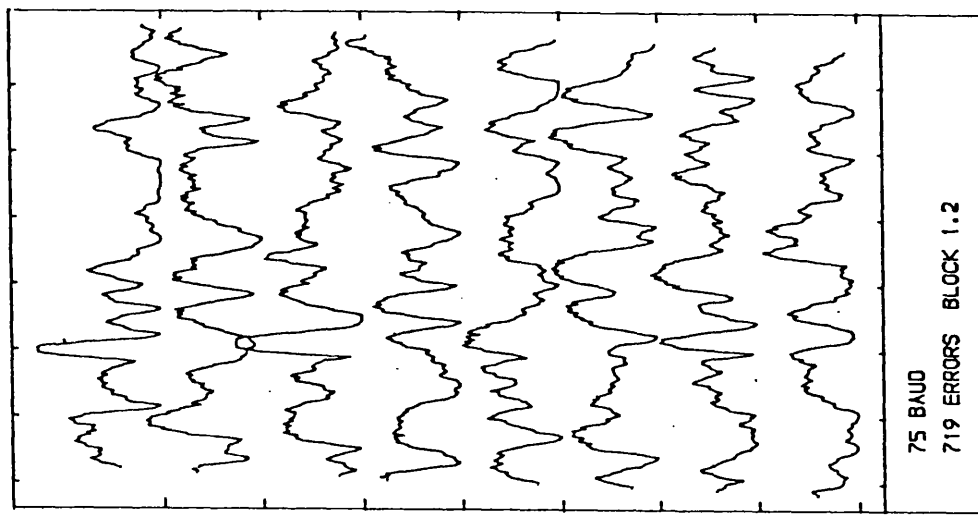
Fig 7.2.1

7.2.2 Noisy Conditions

Fig 7.2.1 demonstrates how rapidly the noise environment of the system can change, eg from block 3.3 to block 3.4. Block 3.4 indicates a sudden large increase in the general noise level and a corresponding increase in the error rate. The line printer analysis for block 3.4 is presented in fig 7.2.3 and the random nature of the noise is clearly evident. It is interesting that the noise is quite short lived, being hardly noticeable in the second 1023 bit PRS. This again demonstrates the great variability of the conditions which suggests the presence of man-made local electrical interference such as that caused by an electric motor.

Further examples of noise are presented as fig 7.2.4 and 7.2.5 demonstrating the effects of medium and heavy noise on the sounding signal. The corresponding line printer outputs are given in fig 7.2.6 and 7.2.7 respectively. In fig 7.2.6 both PRS data sets contain high levels of random noise leading to many errors, which are correctly diagnosed by the data evaluation program. A relatively low (S/N) ratio and high predicted error rate are present as expected. Fig 7.2.7 represents the extreme case where the second PRS data set has been diagnosed as "lost data due to extreme noise". This is typified by the large number of both high and low errors and correlates well with the low (S/N) ratio and the uncertain pulse recognition. Because of the nature of a PRS, with a completely random received data set approximately 512 errors would be expected, split about 256 high and 256 low. Because

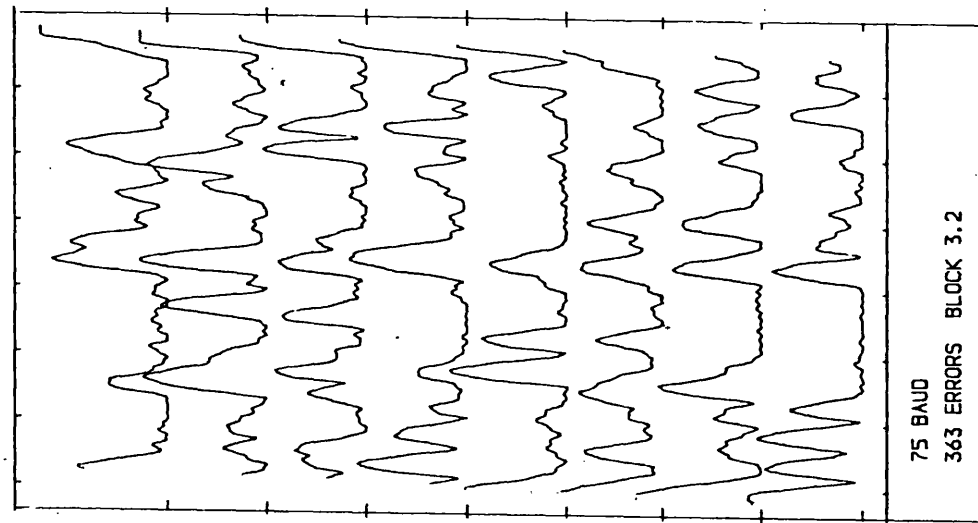
G9BLD Elgin
 13.27 GMT 05.02.81
 4.7925 MHz
 Strong fading



75 BAUD
 719 ERRORS BLOCK 1.2

Fig 7.2.5

G9BLD Elgin
 13.09 GMT 07.04.81
 4.7925 MHz
 1.2 KHz Bandwidth



75 BAUD
 363 ERRORS BLOCK 3.2

Fig 7.2.4

510 errors were measured we must conclude that there is no correlation between the received and expected data and therefore the program must have misidentified the Barker synchronising code. As the errors are split 315 high and 195 low instead of 256,256 the lost data is likely to be caused by radio noise being read as '1' data bits rather than fading giving rise to spurious '0' bits.

7.2.3 Timing faults

An example of the type of data error pattern caused by timing faults previously mentioned in section 7.1 is given as fig 7.2.8 and 7.2.9. This fault in the transmitter oscillator causes the detector to be slightly out of step with the generator. It is apparent in the pulse sounding from a small drift of the sounding pulse across the page. It is however far more obvious in the line printer output (fig 7.2.9) where in both the PRS data sets, the first line is virtually error free, leading on to very high errors in the later lines as the two clocks get further out of step. In both cases the cause is correctly evaluated by the program, so the results produced would not be included in future attempts to correlate data errors with the pulse sounding information.

7.2.4 Bandwidth effects

The bandwidth requirements of the data sounding at 75 baud are far less than those required for acceptable time resolution

G9BLD ELGIN
12.5 GMT 27.03.81
4.792500 MHZ

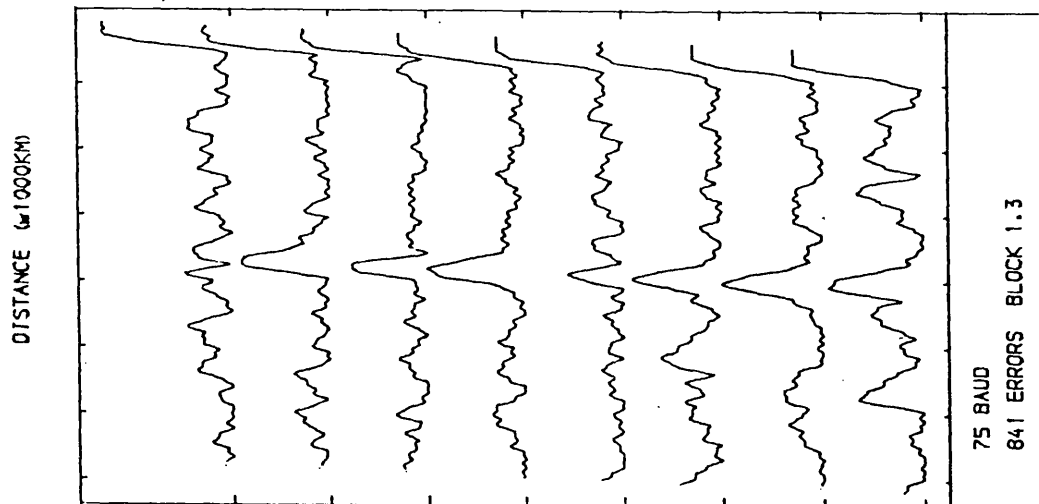


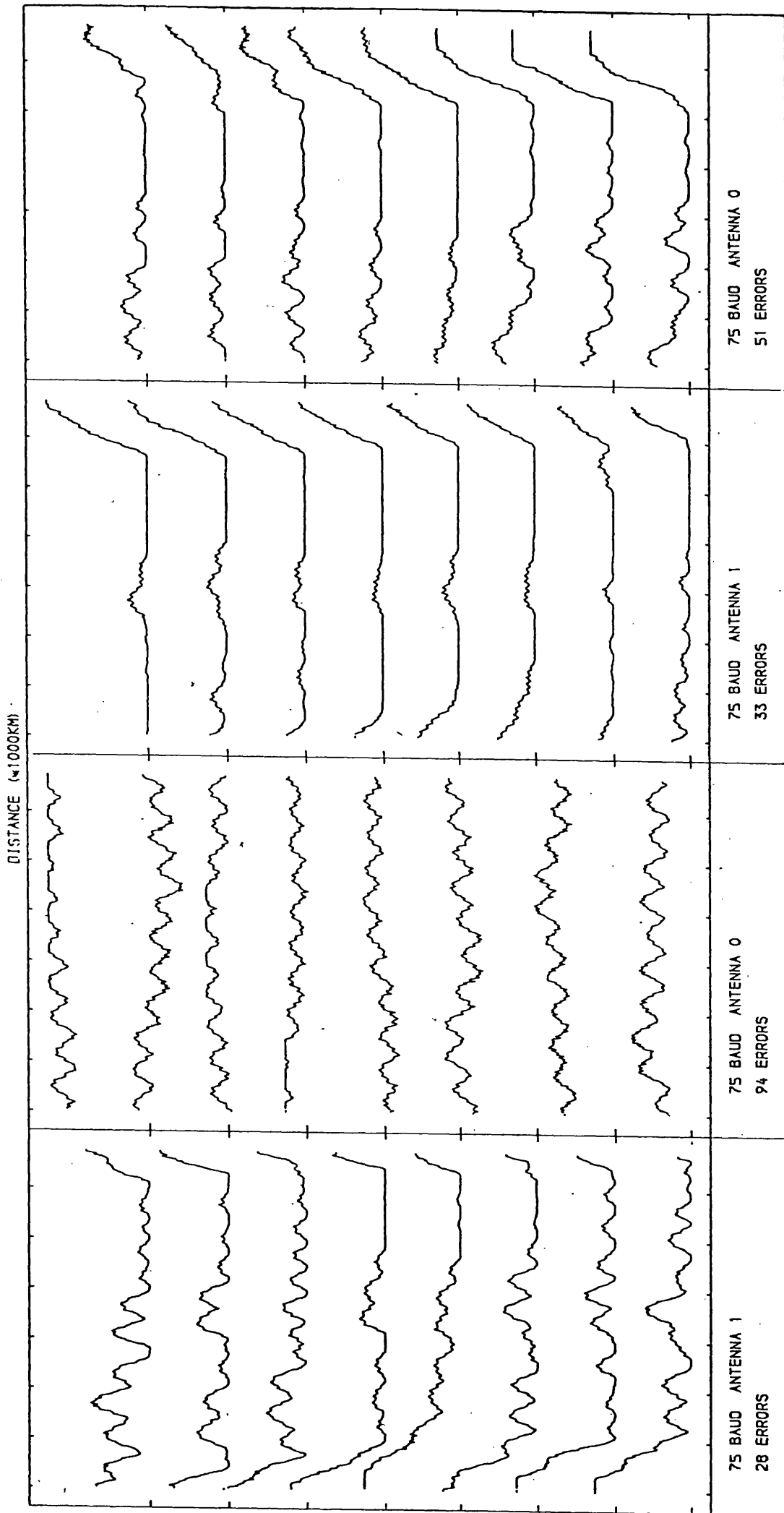
Fig 7.2.8

from the pulse sounding signal (section 6.4). The reason for this is the 75 baud data needs a bandwidth of no more than 250Hz to be detected with no degradation. Therefore reducing the receiver bandwidth to 300Hz would harm none of the signal information and actually aid recognition by removing much unwanted noise and co-channel signals(eg fig 7.2.10).

In this example an interfering station was transmitting within about 1KHz of the centre frequency of the pulse sounding. To remove the effect of this a 300Hz bandwidth filter was inserted. As can be seen the PRS data suffered only light errors but the pulse sounding was rendered virtually useless since it requires at least 1.2KHz bandwidth for moderate mode resolution. From this test it was concluded that the pulse sounding system could not function to its full capability in a high co-channel interference environment.

7.2.5 Fading

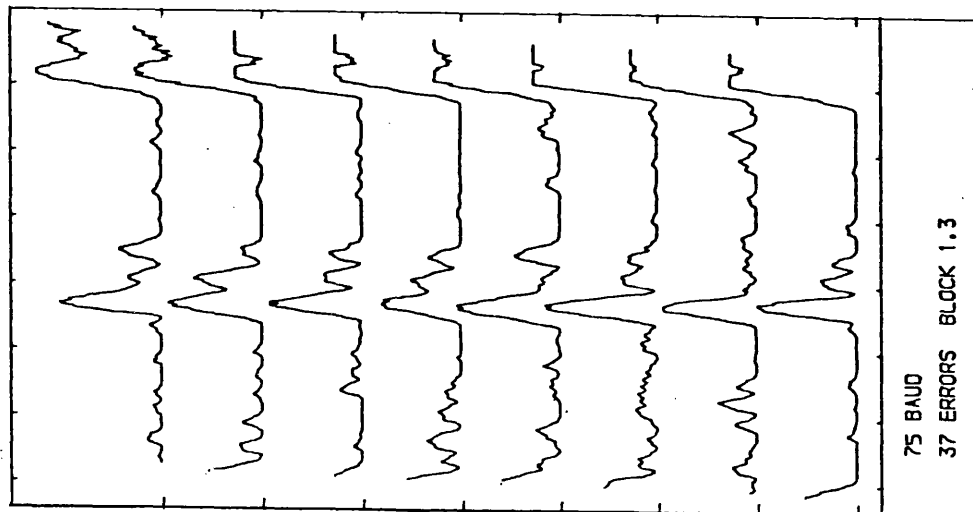
Multipath fading was noticable on about 20% of the data sets recorded. Fig 7.2.11 presents an untypically obvious case. For this record the receiver bandwidth was 3KHz and the transmitter located at Oadby. This accounts for the clean sharp nature of the pulses. The two modes, as discussed before are ground wave and 1 hop E of almost identical amplitude. The computer analysis of these data records is produced in fig 7.2.13. The PRS records contain very characteristic long bursts of low errors where the carrier has faded below the trigger level due to destructive interference between the two modes.



G9BLD DURHAM 18.37 GMT 18.12.80 4.792500 MHZ

Fig 7.2.10 USE NARROW FILTER TO REMOVE INTERFERENCE

DISTANCE (x1000KM)



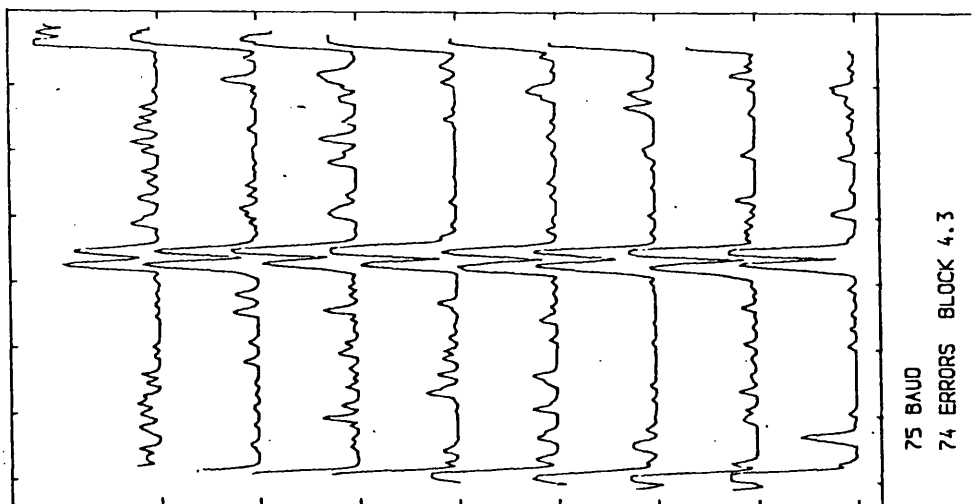
G9BLD ELGIN

16.25 GMT 05.02.81

4.792500 MHZ

Fig 7.2.12

DISTANCE (x1000KM)



G9BLD OADBY

15.3 GMT 10.06.81

4.792500 MHZ

Fig 7.2.11

Each fadeout lasts approximately 50 bits or 0.6 seconds. The program has correctly recognised that fading is present, and has also predicted this from the pulse sounding, hence reasonable correlation has been achieved.

A second example (fig 7.2.12) contains three modes, probably consisting of a dominant 1F and smaller 2F and 3F components (see fig 6.1.2). Because there are more modes, all of differing amplitudes, fewer data errors would be expected compared with the situation in fig 7.2.11. Fig 7.2.14 supports this expectation.

A final example of fading induced errors presents the extreme case of severe fading (fig 7.2.15 and fig 7.2.16). Fig 7.2.15 shows two modes of approximately equal and low amplitude levels. These two conditions cause many low errors. This is correctly recognised as moderate and severe fading induced errors both detected in the analysis and predicted from the pulse measurements.

7.2.6 Interference

Interference from other radio stations on adjacent frequencies can degrade both the PRS and pulse signals. In fig 7.2.17 the pulse sounding can be seen hidden beneath another signal (probably a radio teletype). The data analysis (fig 7.2.19) identifies this as interference on one of the PRS sets and noise on the second because both the wanted data and the interference have approximately the same bit length. In the second example (fig 7.2.18 and 7.2.20) severe interference is

DISTANCE (x1000KM)

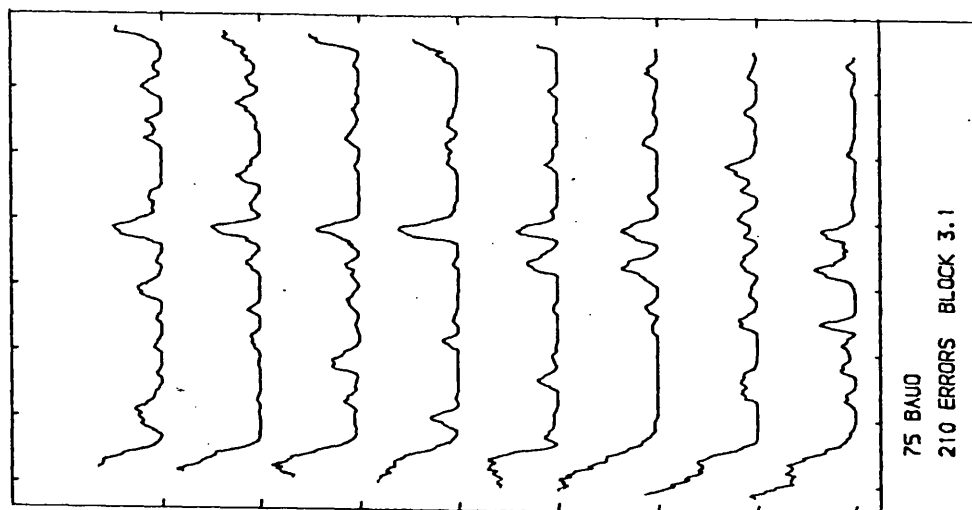
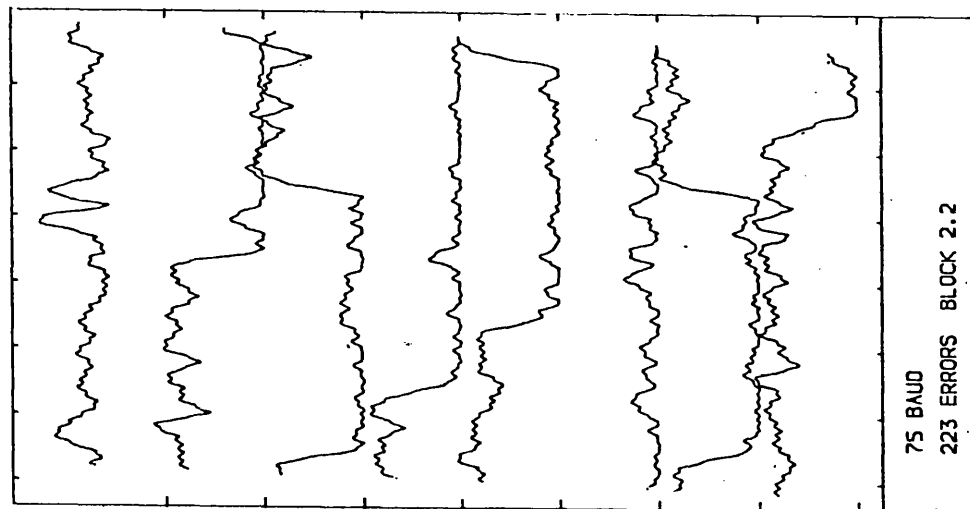
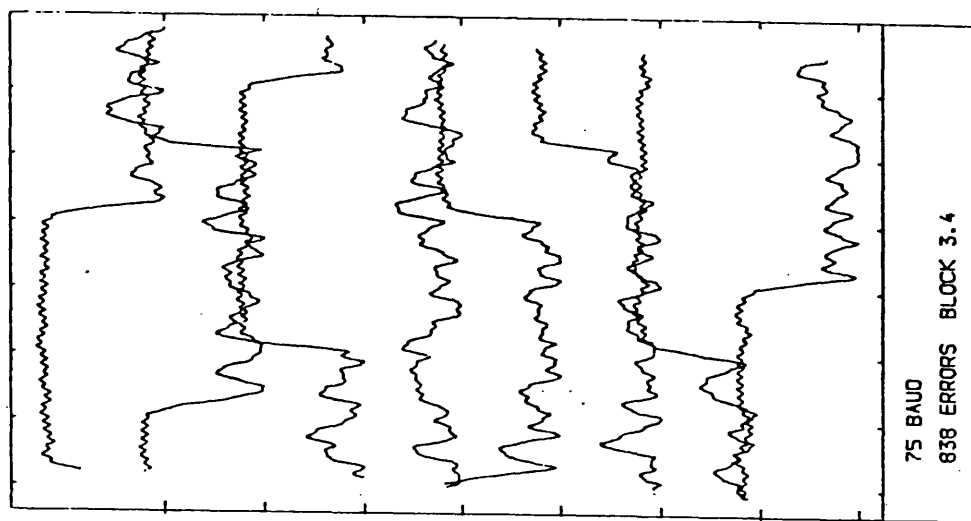


Fig 7.2.15



G9BLD ELGIN
13.1 GMT 07.04.81
4.792500 MHZ



G9BLD ELGIN
12.44 GMT 02.04.81
4.792500 MHZ

Fig 7.2.17

Fig 7.2.18

also present. In this case however the interference is so powerful that both the pulse logging routine and one of the PRS routines fail to correctly identify the wanted G9BLD signal. The second PRS data set was however found correctly but with a very high number of high errors, a large proportion of which are in bursts which is again a sign of man-made interference. These examples confirm the conclusion of section 7.2.4 that the sounding signal is of little benefit when the operating frequency is suffering from co-channel interference.

7.3 THE EFFECT OF IONOSPHERIC PROPAGATION ON PRS DATA

The effect of propagation conditions on the PRS data has been studied by means of a computer simulation technique (section 5.7.4). This program allows the various factors discussed in the previous section to be varied individually and their influence on the data evaluated. The results are presented in graphical form. The control conditions for this investigation are given below :-

Modes	Relative amplitude	Relative time of arrival
	A1 = 167	T1 = 0.0ms
Noise	(S/S+N) = 90%	
Bandwidth	3KHz	
Baudrate	75 baud	

The results obtained for these conditions are plotted out in fig 7.3.1 which displays the data sequence as it would

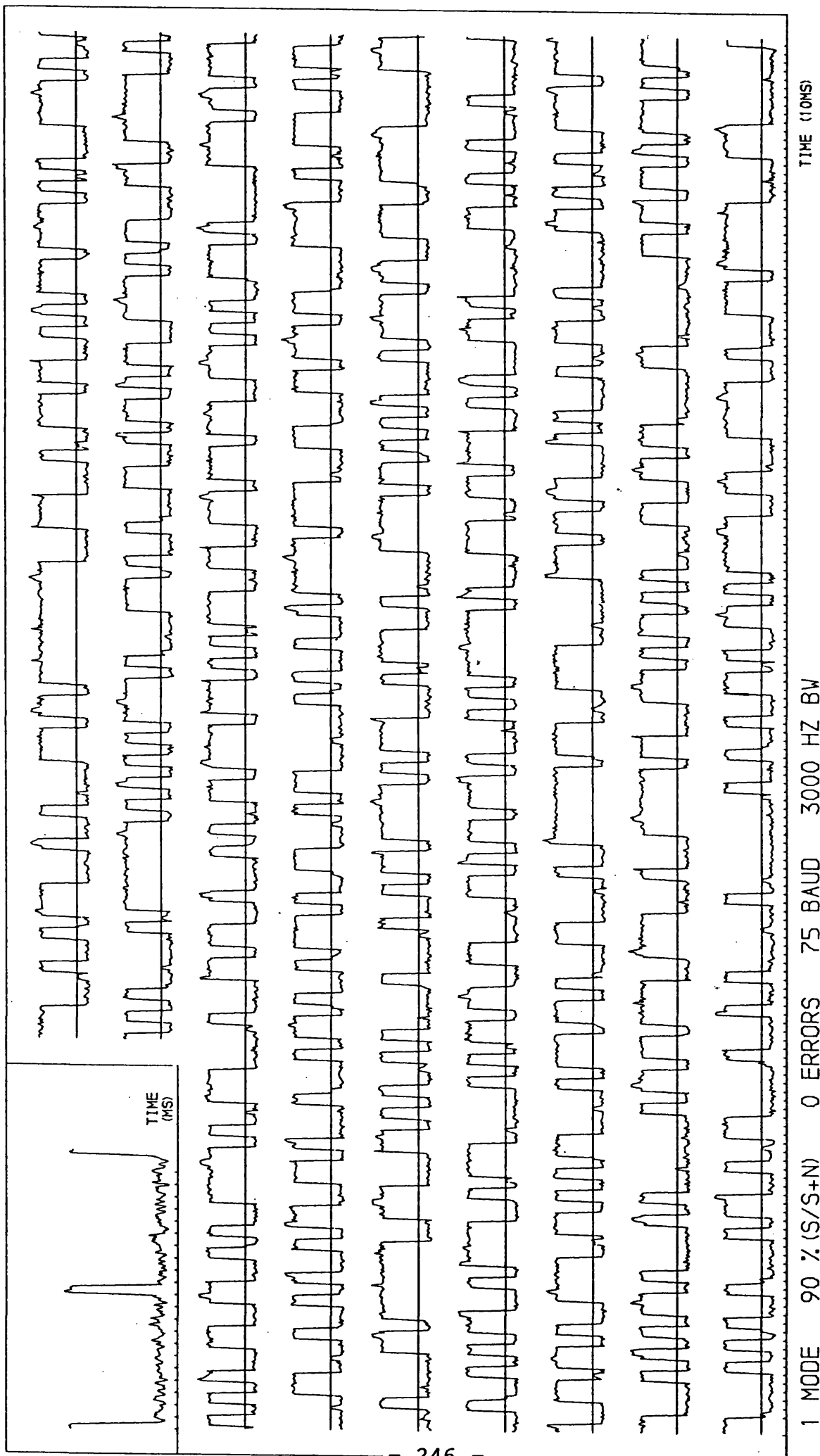


Fig 7.3.1 Single Mode Only

normally appear on the monitor oscilloscope and as it is presented to the analogue to digital converter. A small amount of noise is visible but this is not sufficient to cause errors. When a small second mode of amplitude 68 and relative time of arrival 2ms is added the resulting waveform is displayed as fig 7.3.2. Light fading is now evident on the PRS trace but not sufficient to cause any data errors. The following sub-sections will demonstrate the effect of altering the various control parameters to further clarify the causes of data errors.

7.3.1 Data Rate

As the data rate is increased from 75 baud, the multipath propagation allows a data bit travelling via a long path and the following bit travelling via a more direct path to arrive simultaneously thus causing a possible data error. Fig 7.3.3 presents an example for a 600 baud data stream under the same conditions as in fig 7.3.2. Here the multipath propagation has caused 256 errors (ie each time a '1' is followed by a '0', the '0' of the pair is converted into a '1' by the action of the longer path)

The program decides if a bit is high or low by comparing the signal level with a threshold over the centre third of the bit. Therefore the maximum data rate for these conditions, if multipath problems of this type are to be avoided, is about 180 baud. This subject is also mentioned in section 2.3.1 in connection with the multipath reduction factor.

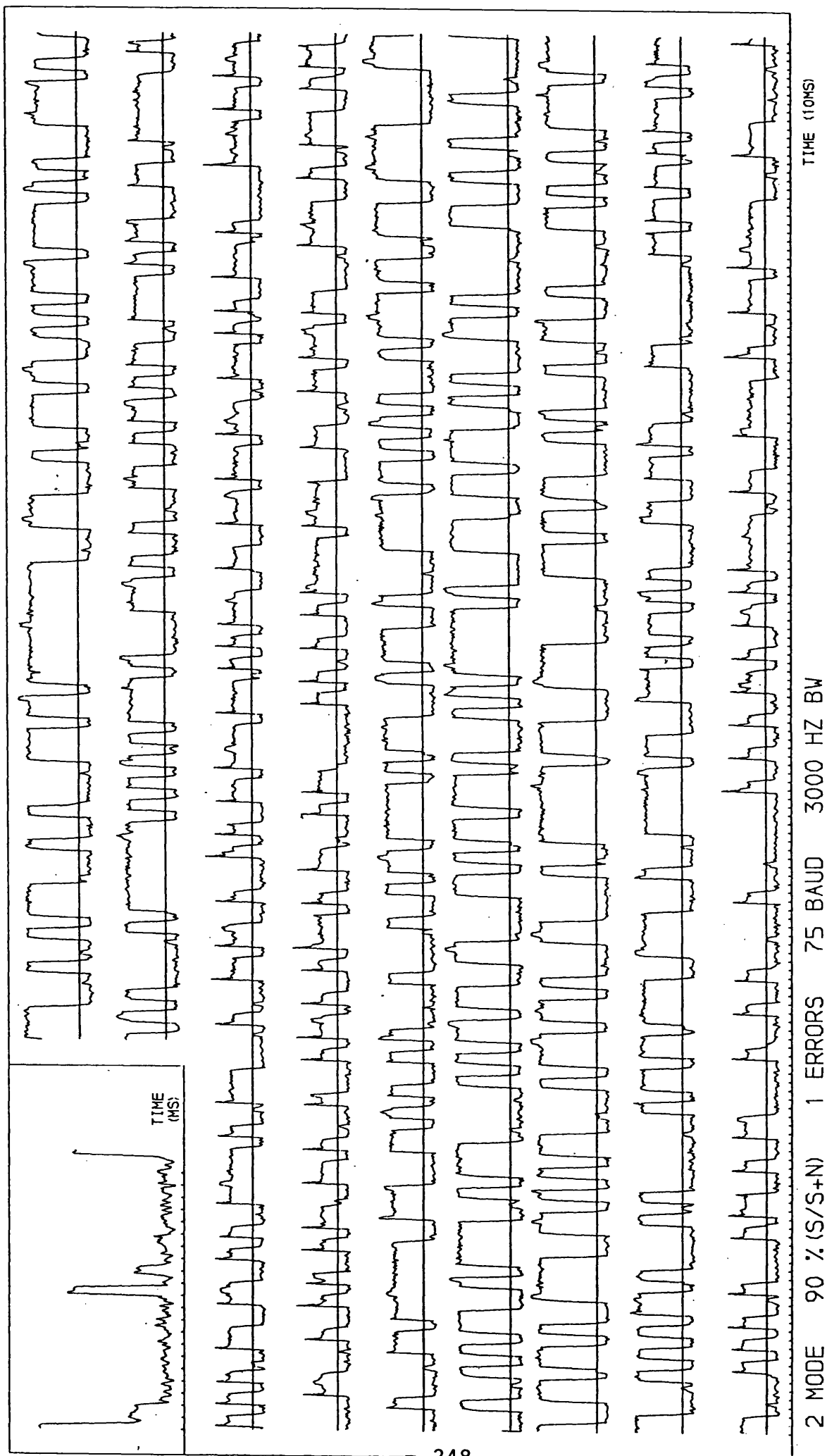
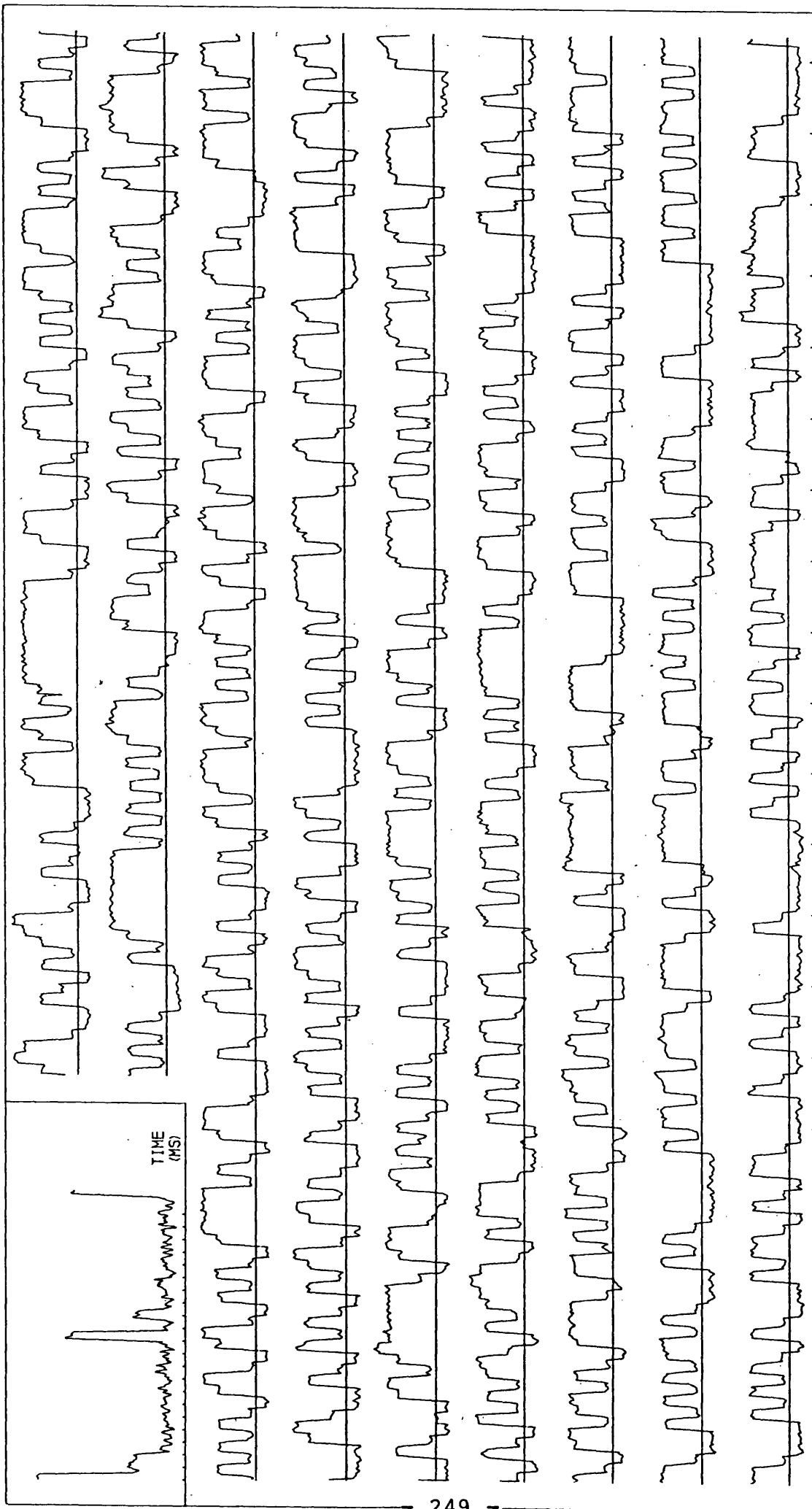


Fig 7.3.2



TIME (10NS)

2 MODE 90 % (S/S+N) 256 ERRORS 600 BAUD 3000 HZ BW

Fig 7.3.3 Fast Data Rate

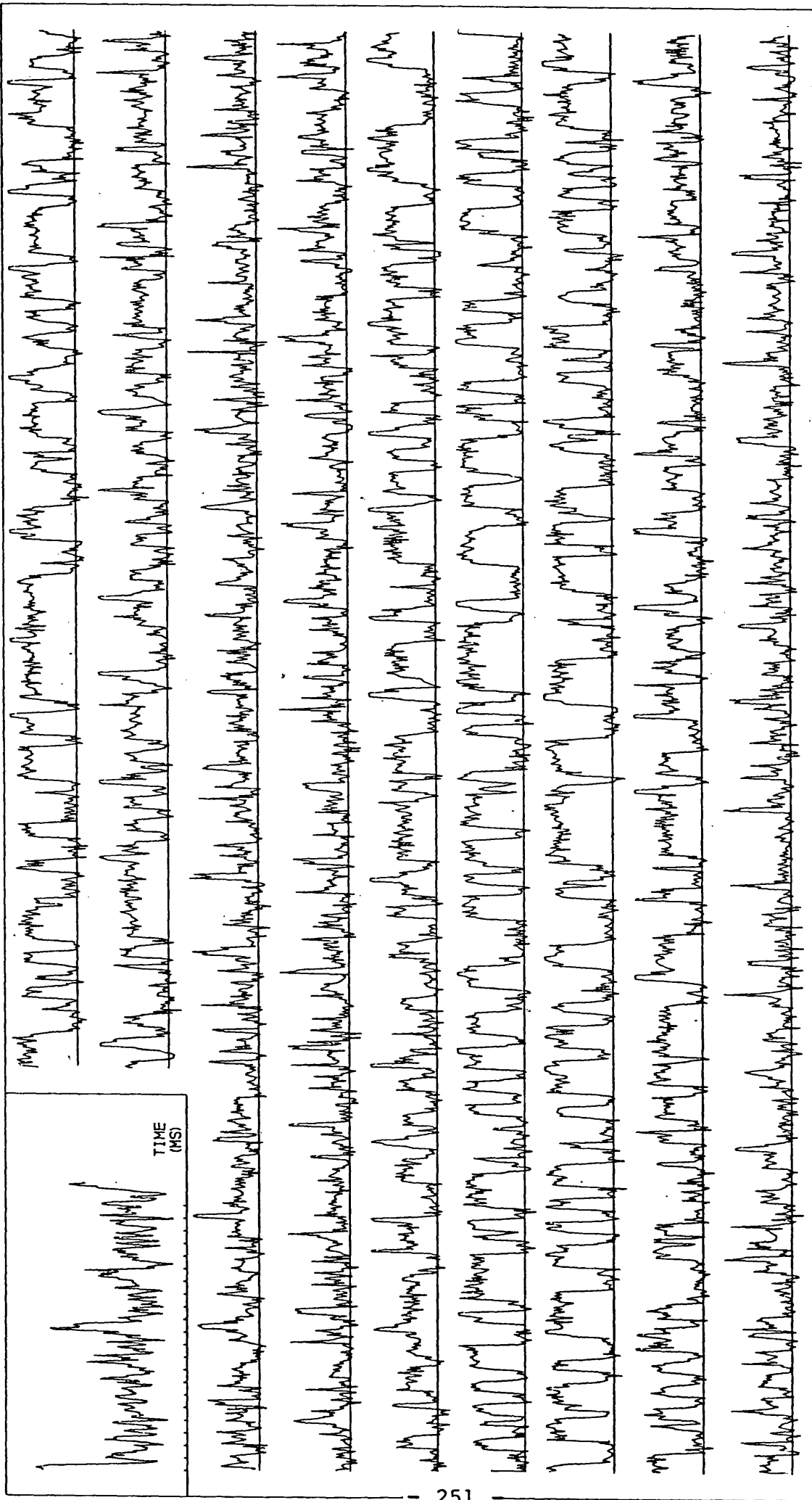
7.3.2 Noise

Noise has been a constant source of errors throughout the experiments. Noise factors of 70% and 50% (S/S+N) were added to fig 7.3.2 and the results are presented in fig 7.3.4 and 7.3.5 respectively. In fig 7.3.4 the sounding pulse echos and the PRS data can be clearly seen by inspection. The computer would have no difficulty in decoding the pulse sounding but the noise has raised much of the PRS data above the threshold level, hence causing an unnecessarily high number of data errors. This leads to the conclusion that for moderate levels of noise it would be useful to increase the threshold level as the (S/S+N) ratio decreases.

In the case of fig 7.3.5 the noise and signal levels are equal and even with a variable threshold, both the pulse sounding and PRS data would be incomprehensible. No data of this type has been recorded as the routines which usually recognise the sounding and PRS data are incapable of operating in such a high noise environment. For these conditions a change in operating frequency, or at least a reduction in bandwidth, would be required to reduce the noise level.

7.3.3 Bandwidth

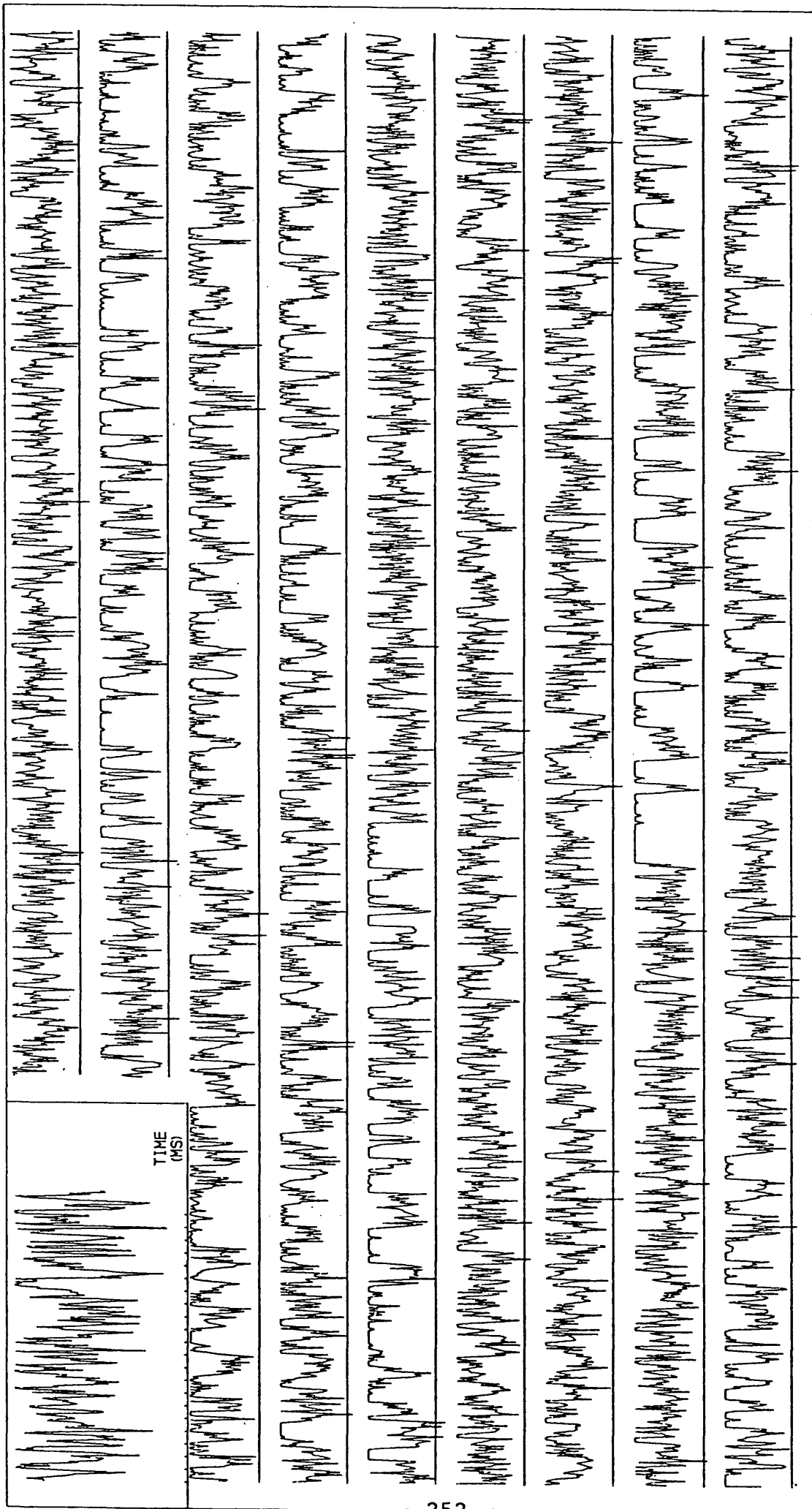
In the simulation program the receiver bandwidth was modeled by means of a simple running average filter. For a narrower bandwidth a greater number of points were included in the average. Filters of 1200Hz and 300Hz were applied to fig



TIME (10MS)

2 MODE 70 % (S/S+N) 358 ERRORS 75 BAUD 3000 HZ BW

Fig 7.3.4. Significant Noise



2 MODE 50 % (S/S+N) 511 ERRORS 75 BAUD 3000 HZ BW

Fig 7.3.5 Excessive Noise

7.3.2. The results are plotted out as fig 7.3.6 and 7.3.7 respectively. The major effects of reducing the bandwidth are all clearly visible in the pulse sounding record plots and are summarised below.

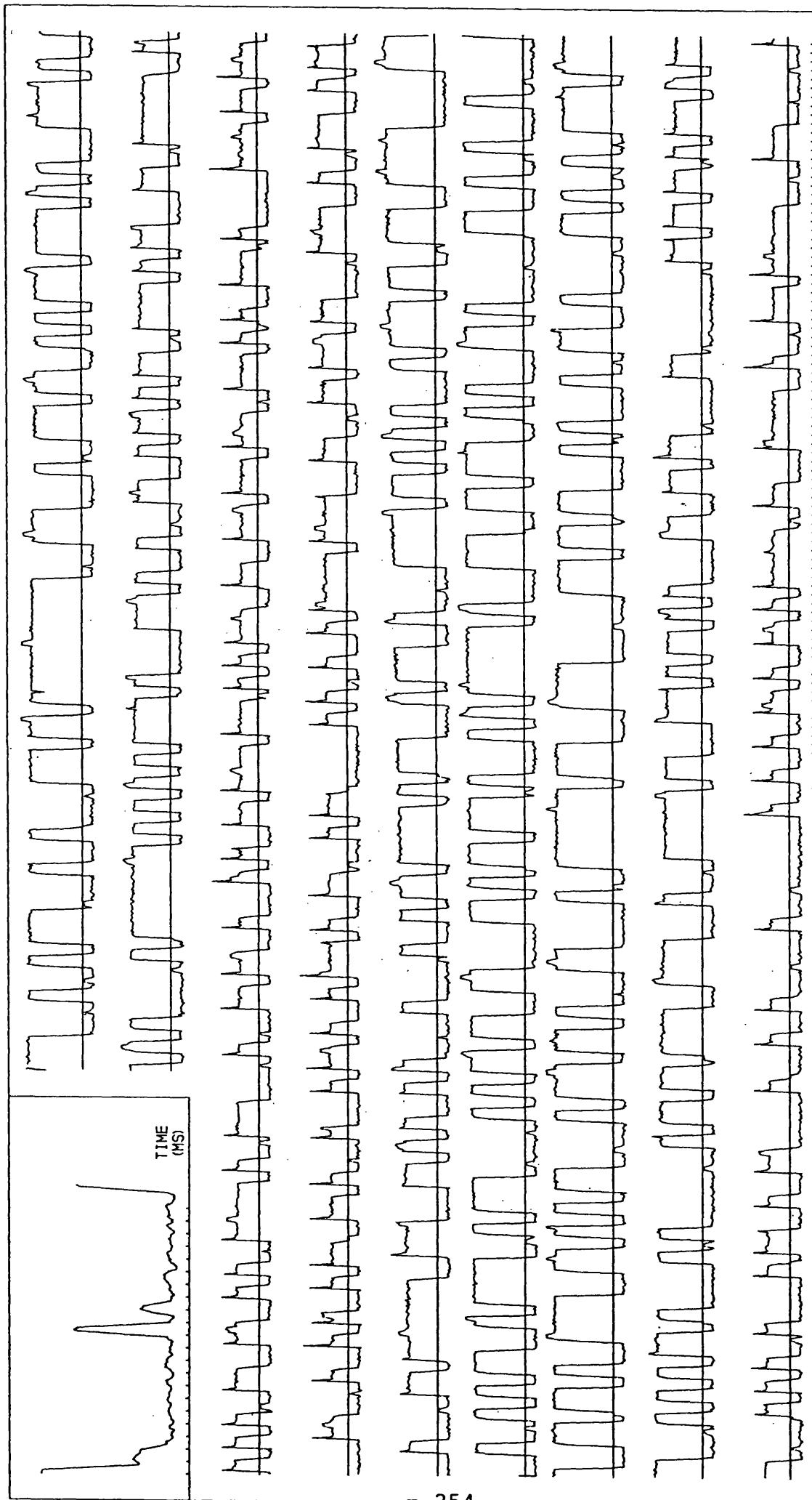
- a) The random noise is greatly reduced. This is most noticeable when comparing fig 7.3.2 and 7.3.6.
- b) The time resolution is reduced.
- c) The pulse amplitudes are reduced as can be seen by comparing the 1200Hz and 300Hz examples

Throughout the changes in bandwidth the PRS data remains almost unaffected, which agrees with the conclusions of section 7.2.4. The reason for the slightly unrealistic 'linear' appearance of the pulse record in fig 7.3.7 is the rather crude nature of the digital filter employed. An improved type such as a Butterworth low pass filter would have removed this unwanted effect.

7.3.4 Fading

The fading rate in the simulation was 10sec (ie 10 seconds from one fade to the next). This represents a doppler shift of 0.1Hz between the two paths. The measurements suggest that this is a realistic value for normal conditions and corresponds to the value given for quiet conditions by the CCIR (1974). The depth of fade is controlled by the relative amplitudes of the various modes of propagation.

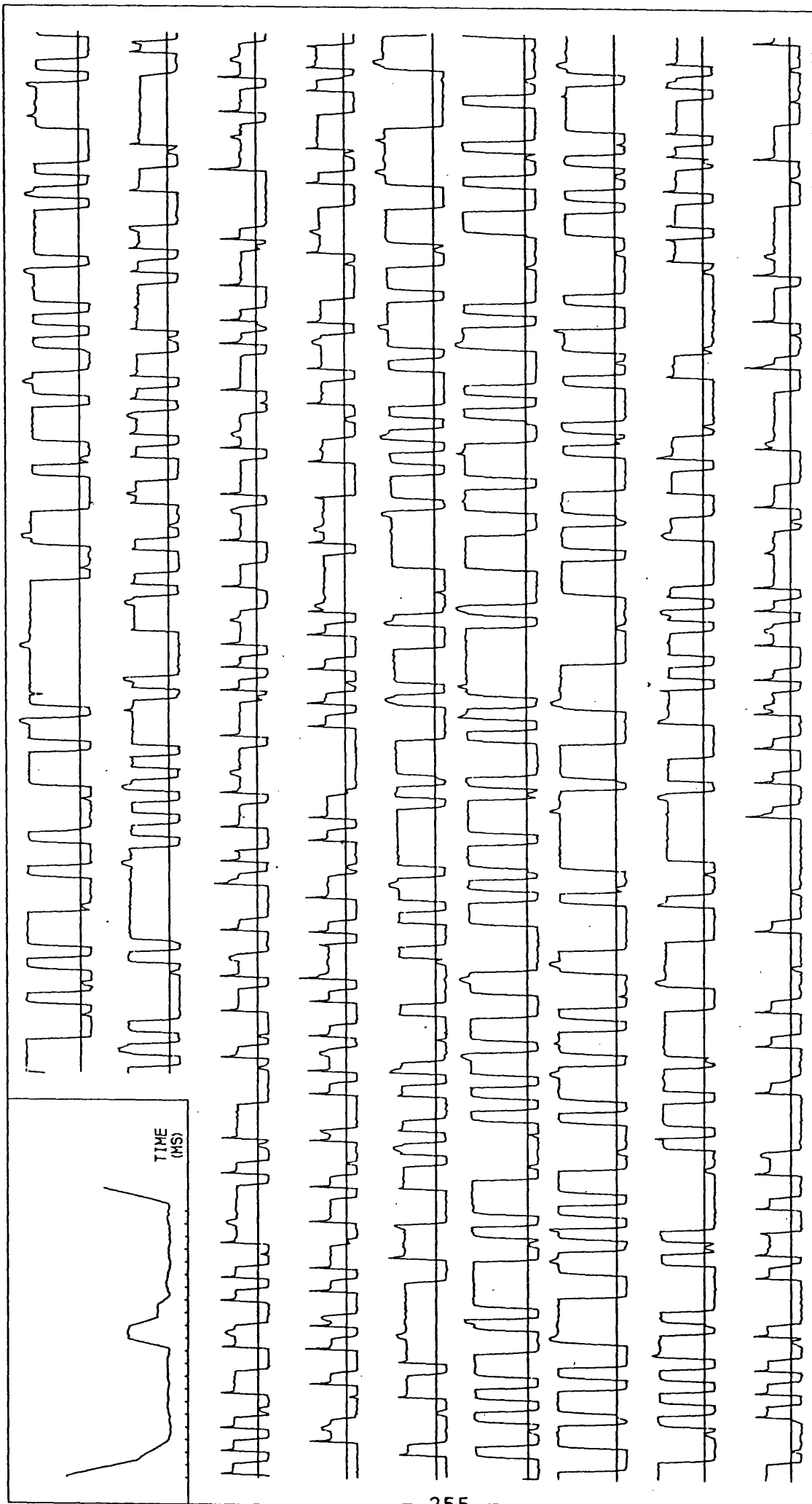
In fig 7.3.2 the relative amplitudes of 167 and 68 lead to fading but not of sufficient depth to cause data errors. In the



TIME (10NS)

2 MODE 90 % (S/S+N) 0 ERRORS 75 BAUD 1200 HZ BW

Fig 7.3.6 Medium Bandwidth



TIME (10MS)

2 MODE 90 % (S/S+N) 0 ERRORS 75 BAUD 300 HZ BW

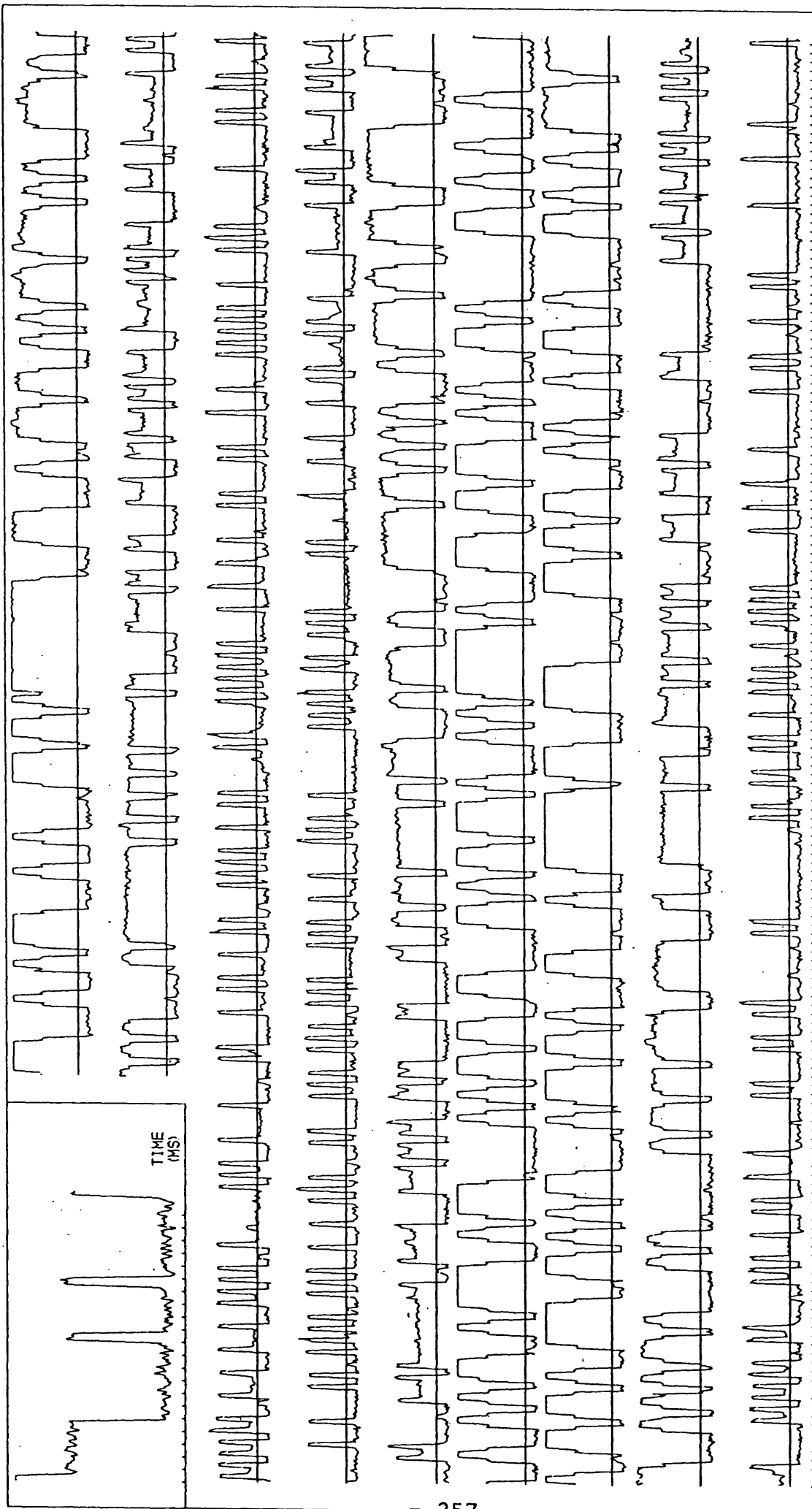
Fig 7.3.7 Very Narrow Bandwidth

extreme case (fig 7.3.8) of equal mode amplitudes, the PRS data fades out completely, leaving only spikes of signal at the start and end of a burst of high data bits where no multipath interference is possible. In this example when the signal fades below the threshold level many data errors are recorded.

7.3.5 Time Stability

The computer simulation proved to be a useful exercise in demonstrating how ionospheric and system properties affected both the pulse sounding and the PRS data. To cut down the number of variables it assumes that the conditions remain constant over the period considered. This is often the case as in fig 7.3.9 where the pulse sounding indicates one dominant mode of amplitude about 200 and a secondary one of amplitude about 60, joining together to give fading consistent with these levels.

In the majority of cases however, conditions change to some degree between logging the pulse data and logging the PRS data. Examples of this can be seen in fig 7.3.10 and 7.3.11. In fig 7.3.10 the pulse sounding exhibits only one mode, yet the PRS data contains definite signs of fading. In fig 7.3.11 two modes are present and yet there is no evidence of fading at all. These rapid changes account for many of the differences between the measured data errors and those predicted from the pulse sounding data.



2 MODE 90 % (S/S+N) 143 ERRORS 75 BAUD 3000 HZ BW

Fig 7.3.8 Two Equal Amplitude Modes

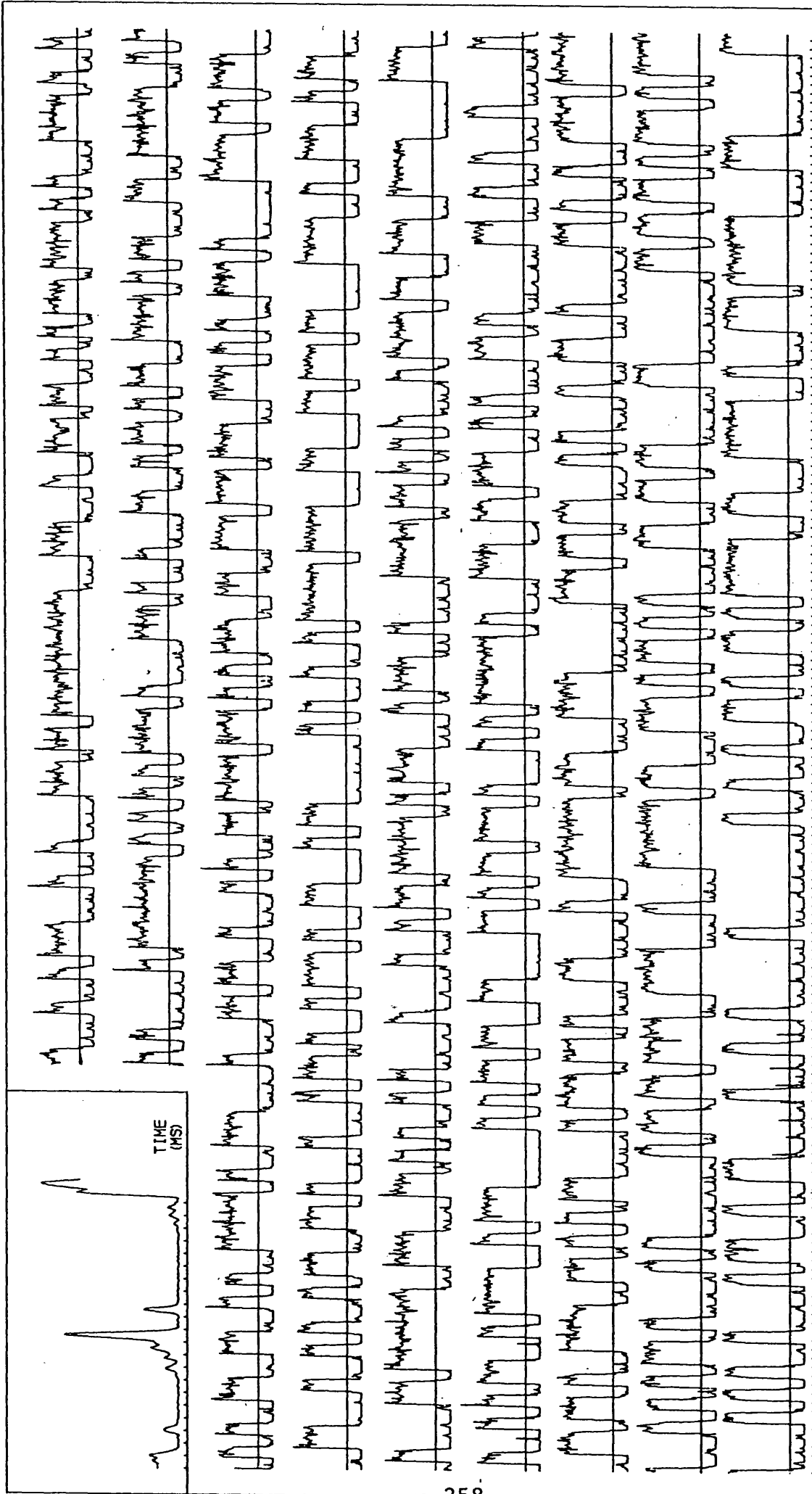


Fig 7.3.9 Received Data from Oadby 01.07.81 16.54 GMT

TIME (10MS)

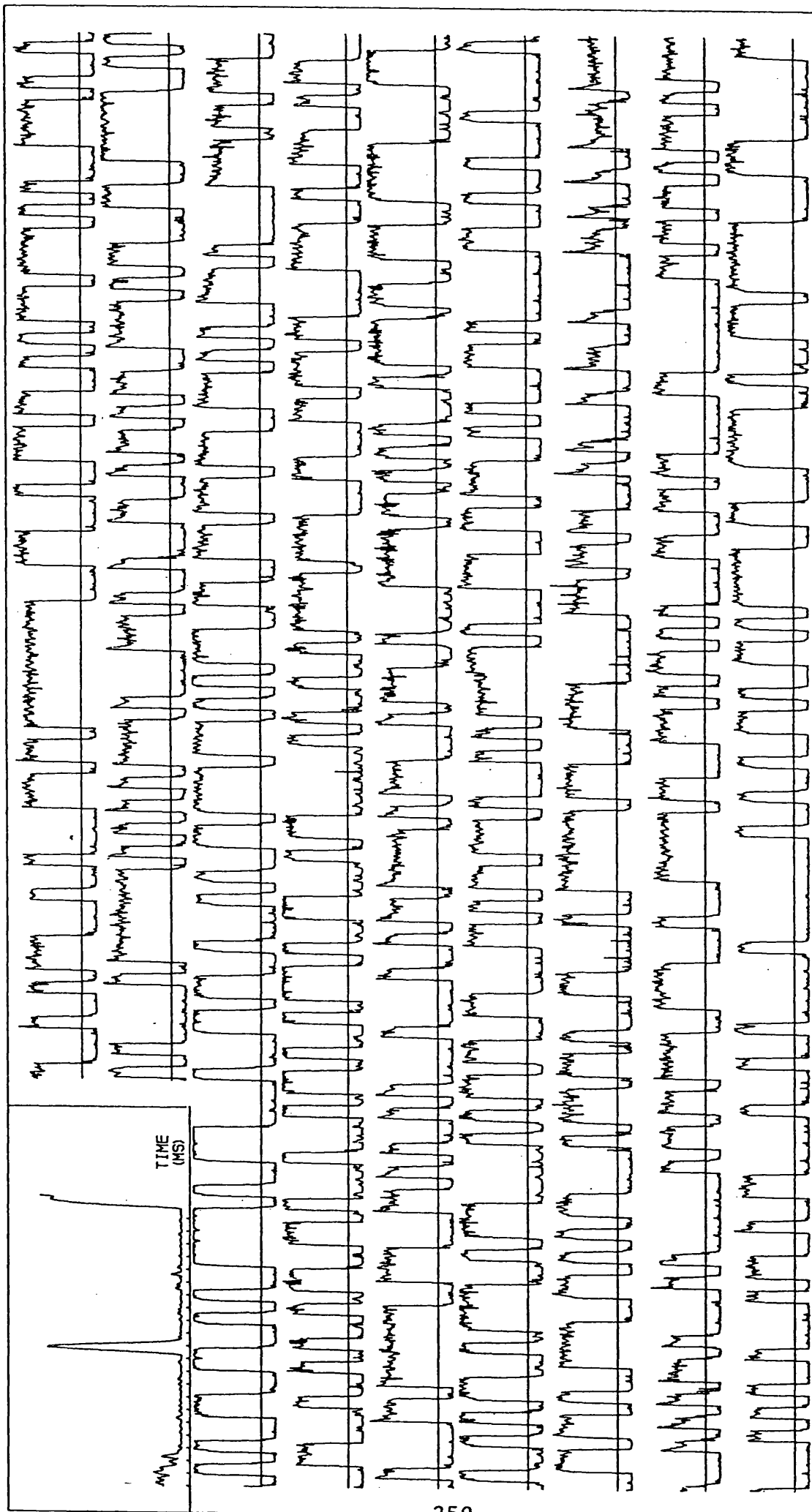


Fig 7.3.10 Received Data from Oadby 01.07.81 16.40 GMT

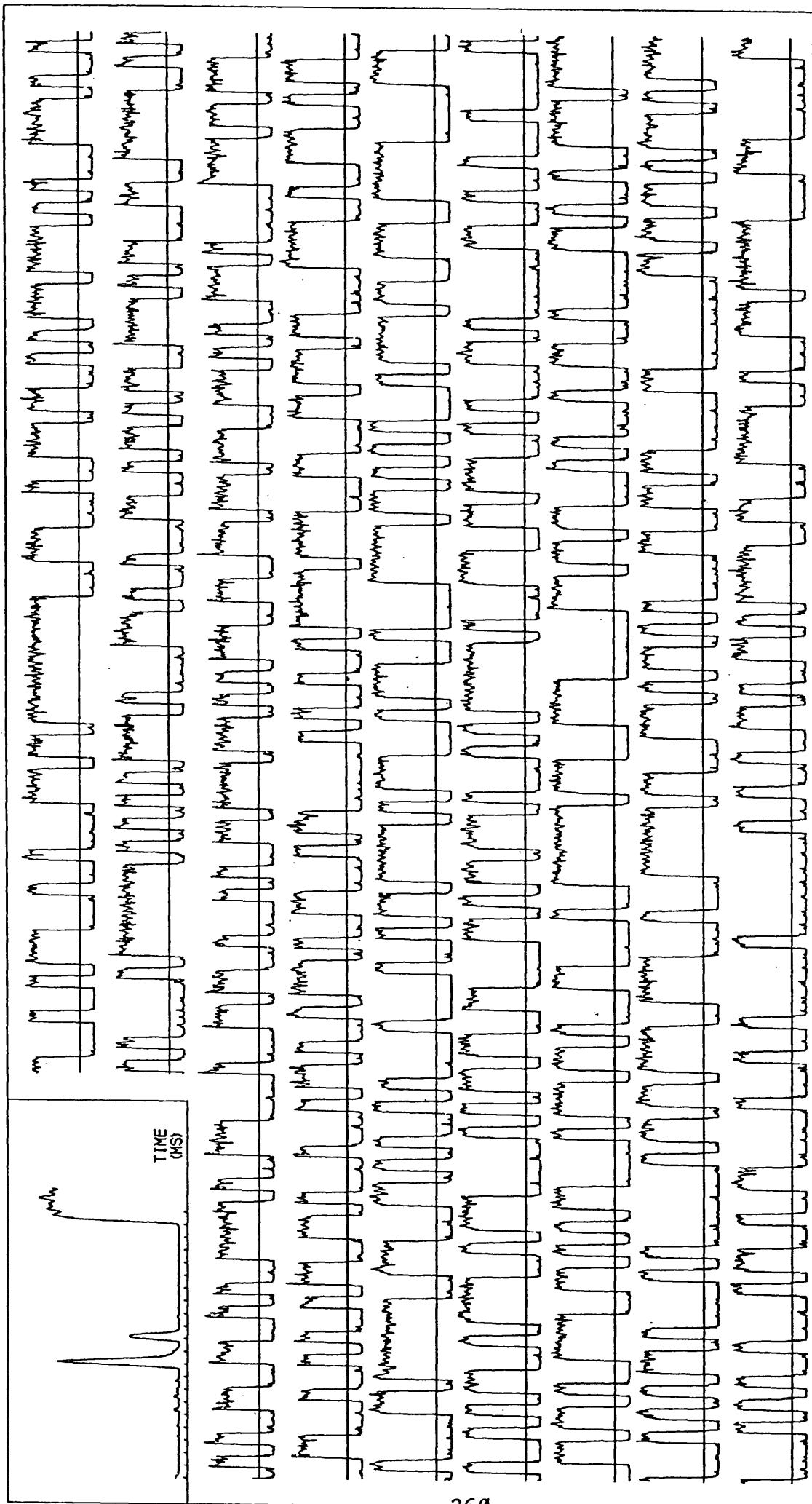


Fig 7.3.11 Received Data from Qadby 01.07.81 16.50 GMT

7.4 PULSE SOUNDING PREDICTIONS - PRS DATA CORRELATION

To be of practical use one of two characteristics of the pulse sounding system must be utilised. If a steerable antenna is available the mode content information will enable beams and nulls in the radiation pattern to be adjusted so as to reduce multipath interference. Secondly the estimate of the expected data errors for a given path and time of day would be helpful in a practical context. From this information the operator can decide how best to protect the data against errors for example, by adopting a slower data rate or error correcting codes. This section assesses the success of the system in providing accurate error rate predictions over the Elgin Leicester path during the spring of 1981.

The entire data set upon which this analysis is based is presented in fig 7.4.1 which displays the received error percentage against the ratio $(S/S+N)$ for every PRS data set. The points follow a general trend from the bottom right hand corner to the top left hand corner of the graph. This is expected since the greater the noise level the more errors would be present. The maximum percentage of error bits is about 50% as discussed in section 7.2.2.

The points running up the vertical axis are caused by a measured $(S/S+N)$ of zero which implies that the program was unable to recognise the pulse sounding signal and therefore could not find a value for S. The points running along the top of the graph represent error rates of approximately 50% and hence no correlation with the PRS. This situation is caused by

ERROR RATE (%)

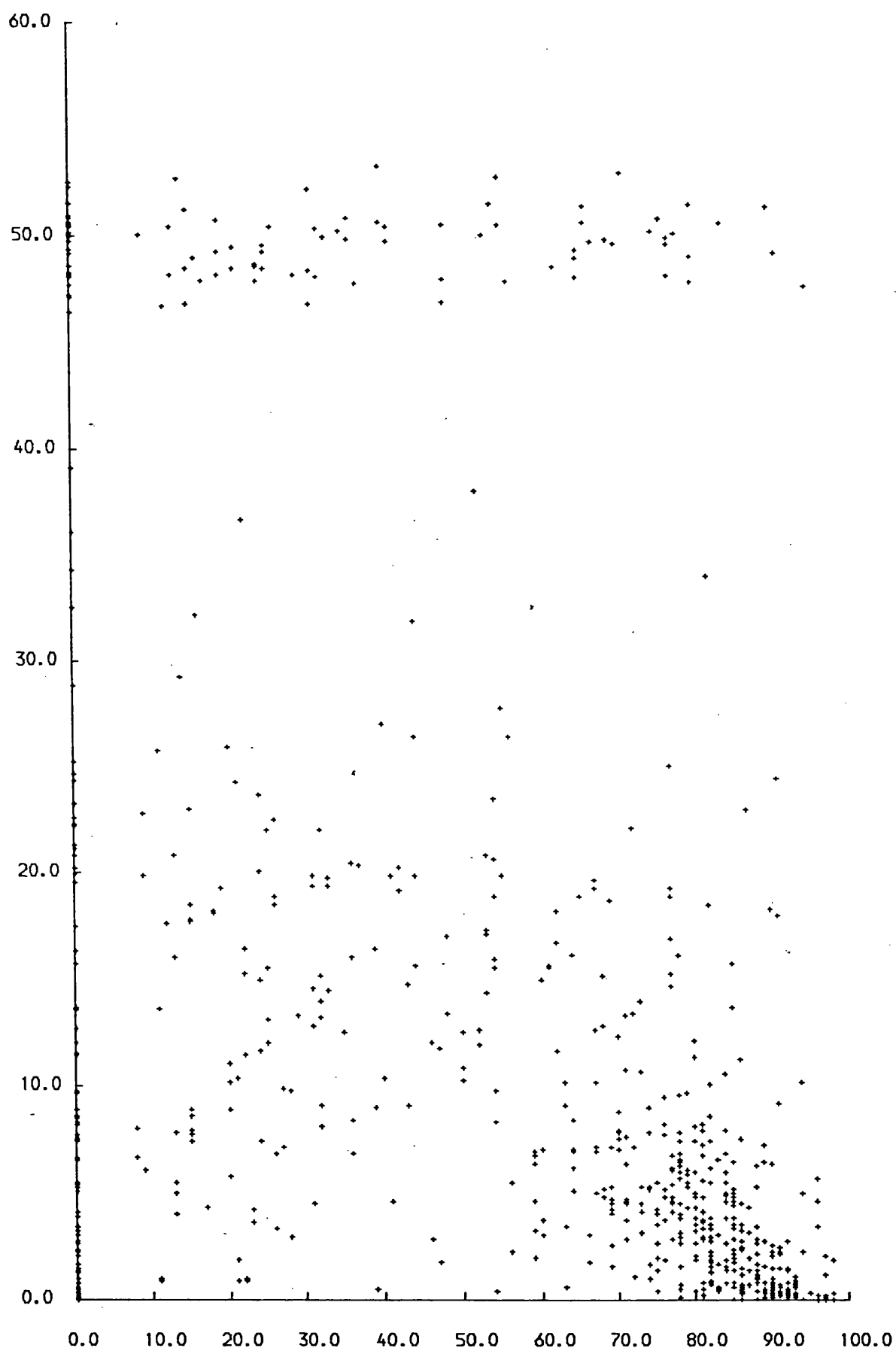


Fig 7.4.1 PRS Error Rate V Pulse S/S+N

a failure of the program to identify the Barker sequence. Both of these events indicate a system failure due to a rapid change in the propagation conditions between the reception of the pulse sounding and the PRS data (ie within 25 sec). This partially explains the wide spread of points around the general trend. It should also be noted that multipath fading will cause some spread in the data points.

The distribution of samples of both $(S/S+N)$ and error percentage are presented as histograms in fig 7.4.2. From these it is apparent that most of the samples collected have high $(S/S+N)$ and relatively low received errors which again confirms the correlation between these two measurements. The system errors appear as smaller peaks around 50% received errors and zero $(S/S+N)$.

A comparison with the measured values of fig 7.4.1, is presented in fig 7.4.3 where the predicted errors, are plotted as a function of $(S/S+N)$. This figure contains half as many points as fig 7.4.1 because only one error prediction is made from each period of pulse sounding. However the errors are measured twice during this period. When the two graphs are compared, the general trends are the same but as expected, the predicted errors do not contain the same spread of points caused by changes in propagation conditions found within the measured errors. Such spread as does exist in the predicted error graph is due to multipath effects. The controlling factor however is clearly noise, as measured by the ratio $(S/S+N)$.

The success or otherwise of the method can be judged by plotting out the predicted errors against the actual received

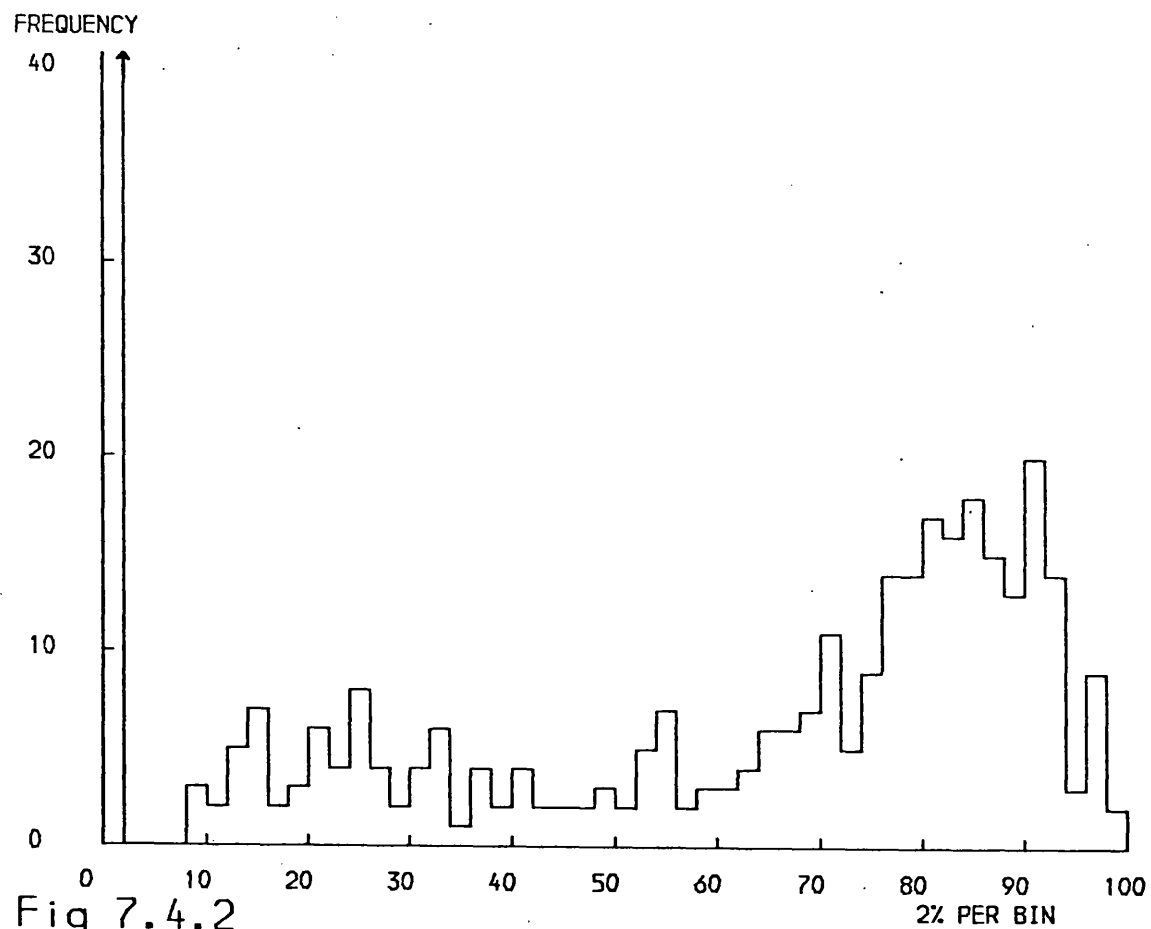
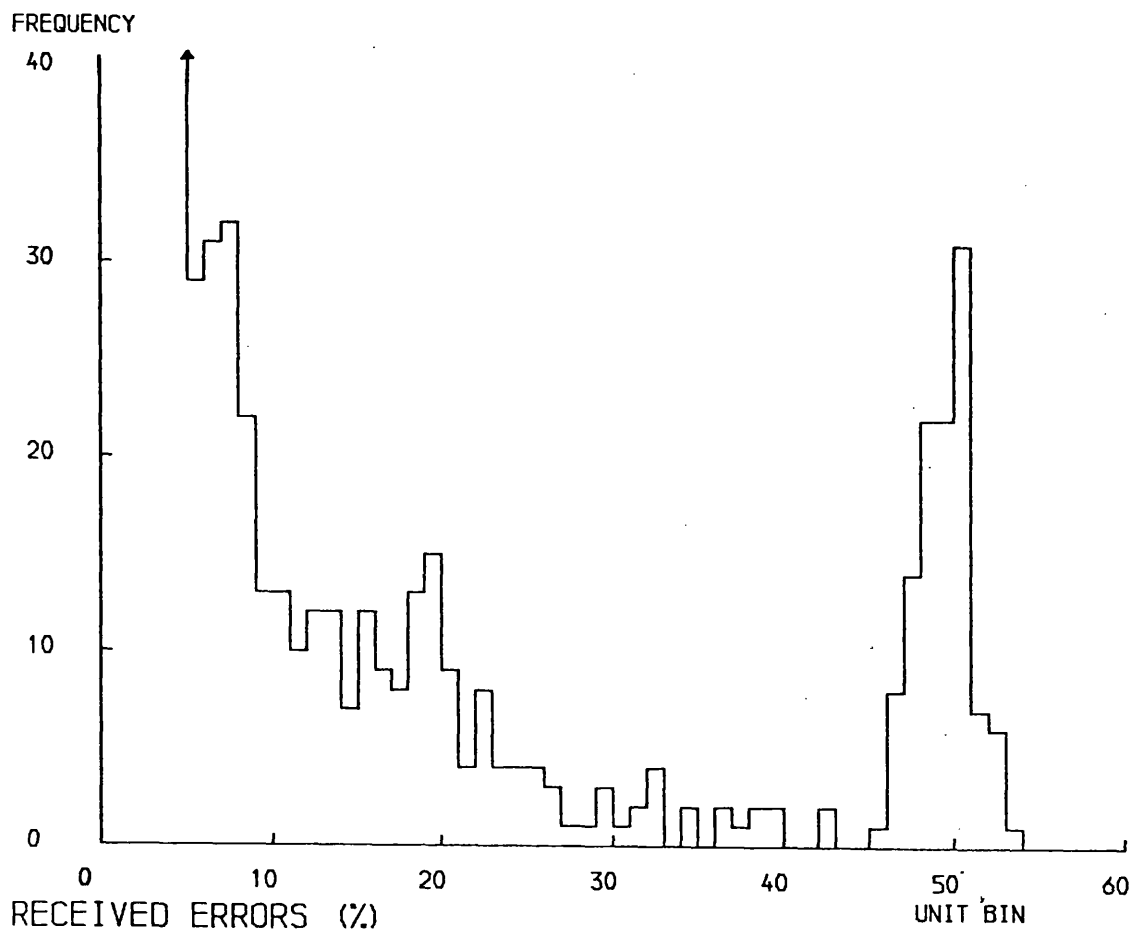


Fig 7.4.2

PREDICTED
ERROR RATE (%)

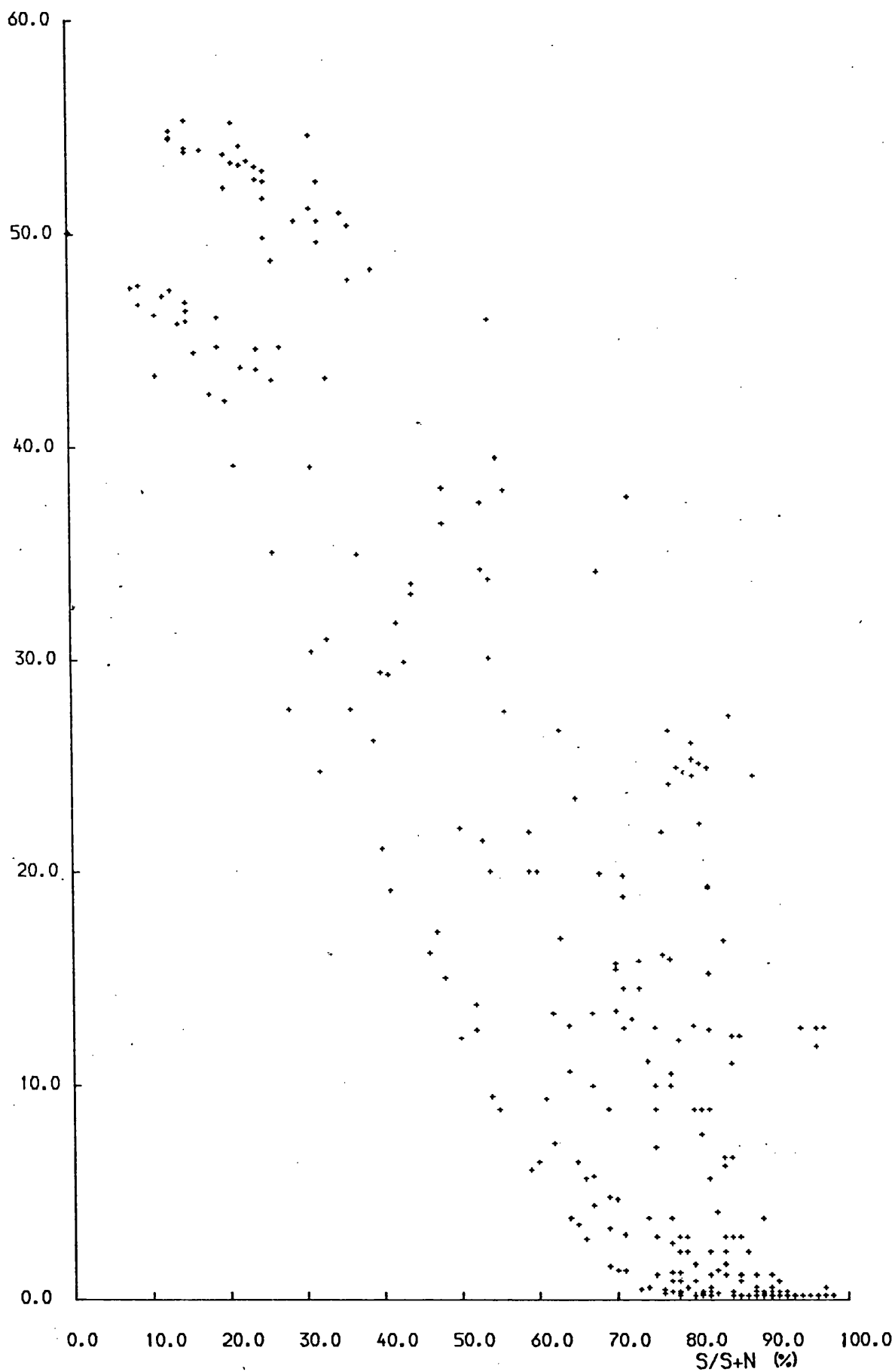


Fig 7.4.3 Gaussian Prediction V Pulse S/S+N

errors (fig 7.4.4). This graph displays the good agreement of predicted and measured results at low error rates. Also reasonable correlation exists for very high error rates with a cluster of data points around the coordinates (50,50). The normal spread due to the variability of ionospheric and local noise characteristics is apparent over the middle section of the graph. The most serious area of disagreement is the line of errors in the bottom right hand corner of the plot, caused by the program failing to recognise the sounding pulses.

If the pulse sounding signals are employed in real time under operational conditions, rather than being stored for later analysis as presented here, this problem would not arise. Under operational conditions the program would restart and try again, if a failure to recognise the pulse sounding was encountered, rather than simply reporting the failure as in the present situation

From fig 7.4.4 it is possible to calculate a confidence factor in the error prediction for a given error rate. The first method of displaying this function is given in fig 7.4.5. This plots out the average percentage error in the predicted error over the entire range of predictions. As expected from fig 7.4.4 a very low average error in the prediction is recorded for low error predictions (about 7%) gradually rising to about 30% for high predicted errors. It must be noted that due to a rather small number of data points in the centre section of the graph, these results are less reliable than those at the extreme values. In order to emphasise any general trends and reduce the fluctuations caused by this lack of data

RECEIVED ERRORS (%)

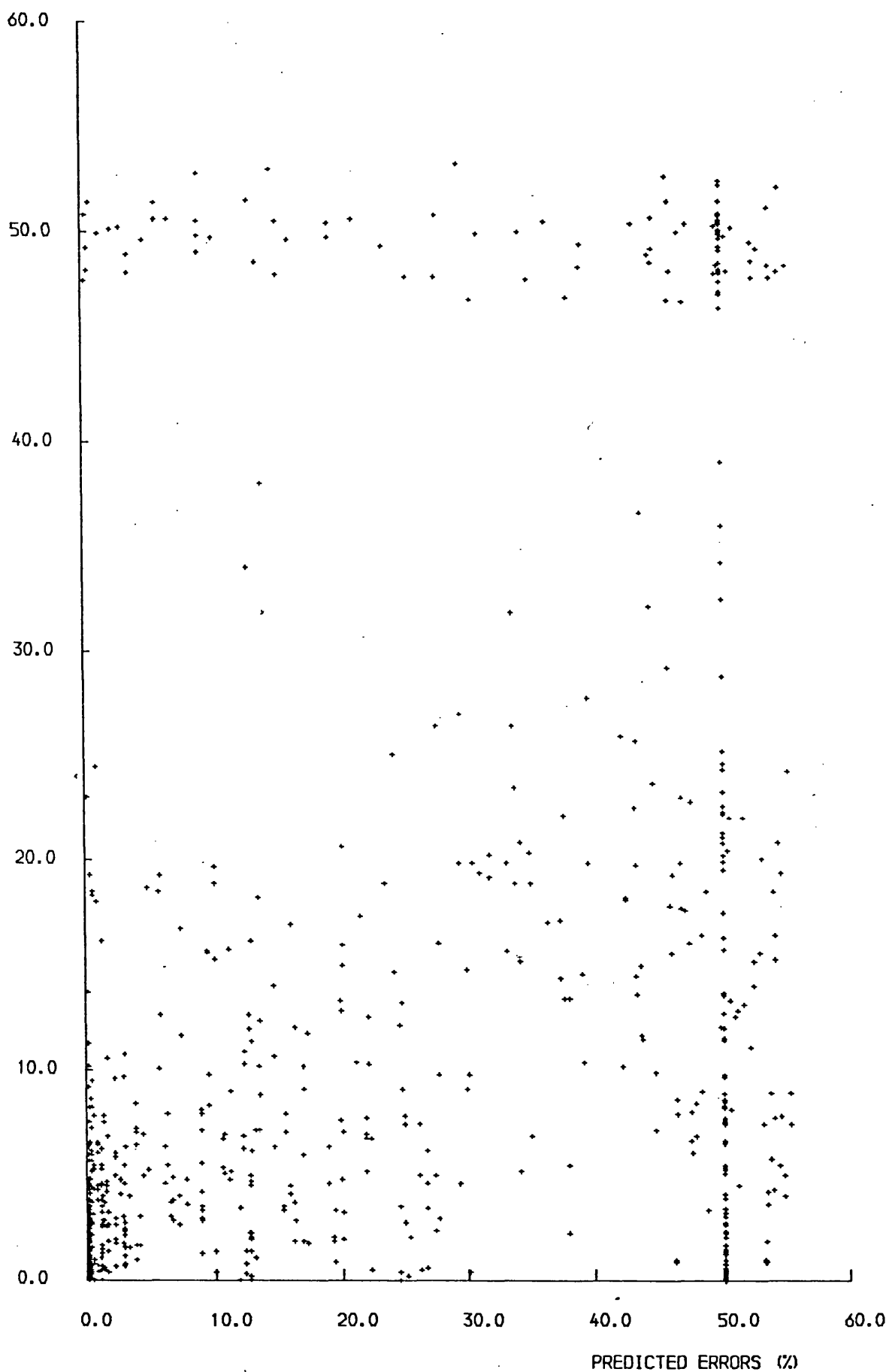


Fig 7.4.4 Gaussian Error Predictions

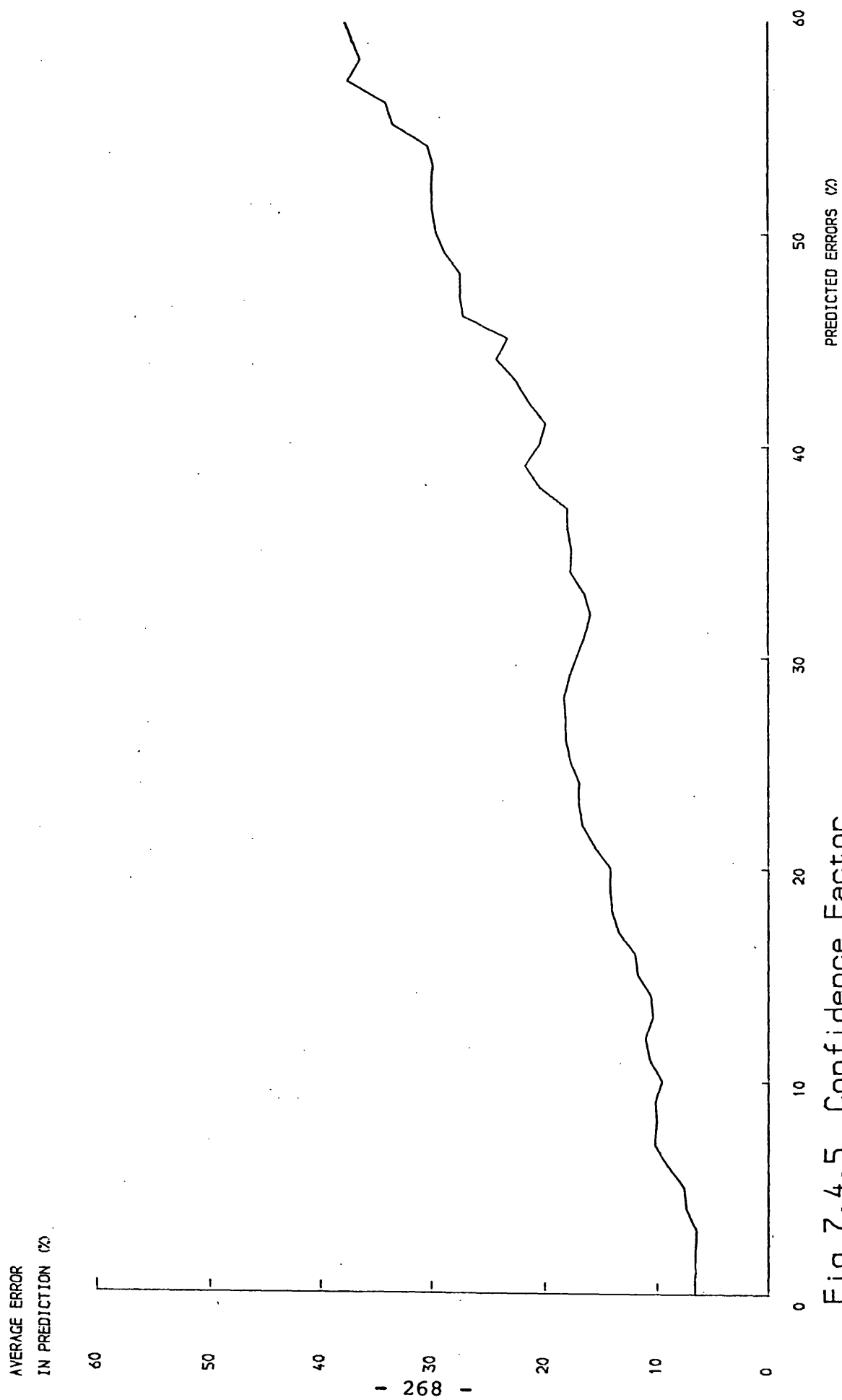


Fig 7.4.5 Confidence Factor

points averages were obtained from a running mean over eight percentage points.

A more meaningful method of displaying the potential accuracy of the system is to plot the proportion of the predictions which lie within a given percentage of the measured value. Fig 7.4.6 does this over the entire range of results for given percentages (5 to 30%). This indicates that the proportion of accurate predictions is greatest at low error rates, falls to a very low success rate around 30% and rises again towards the higher predicted errors. For a specific case, if the computer predicts an error rate of less than 5%, about 85% of such predictions would be within 10% of the measured value. It must be noted that such predictions only apply to this particular data transmission format. The longer the time separation between the pulse sounding and the data stream, the less accurate the predictions become.

FRACTION OF PREDICTIONS
WITHIN X% OF RESULT (%)

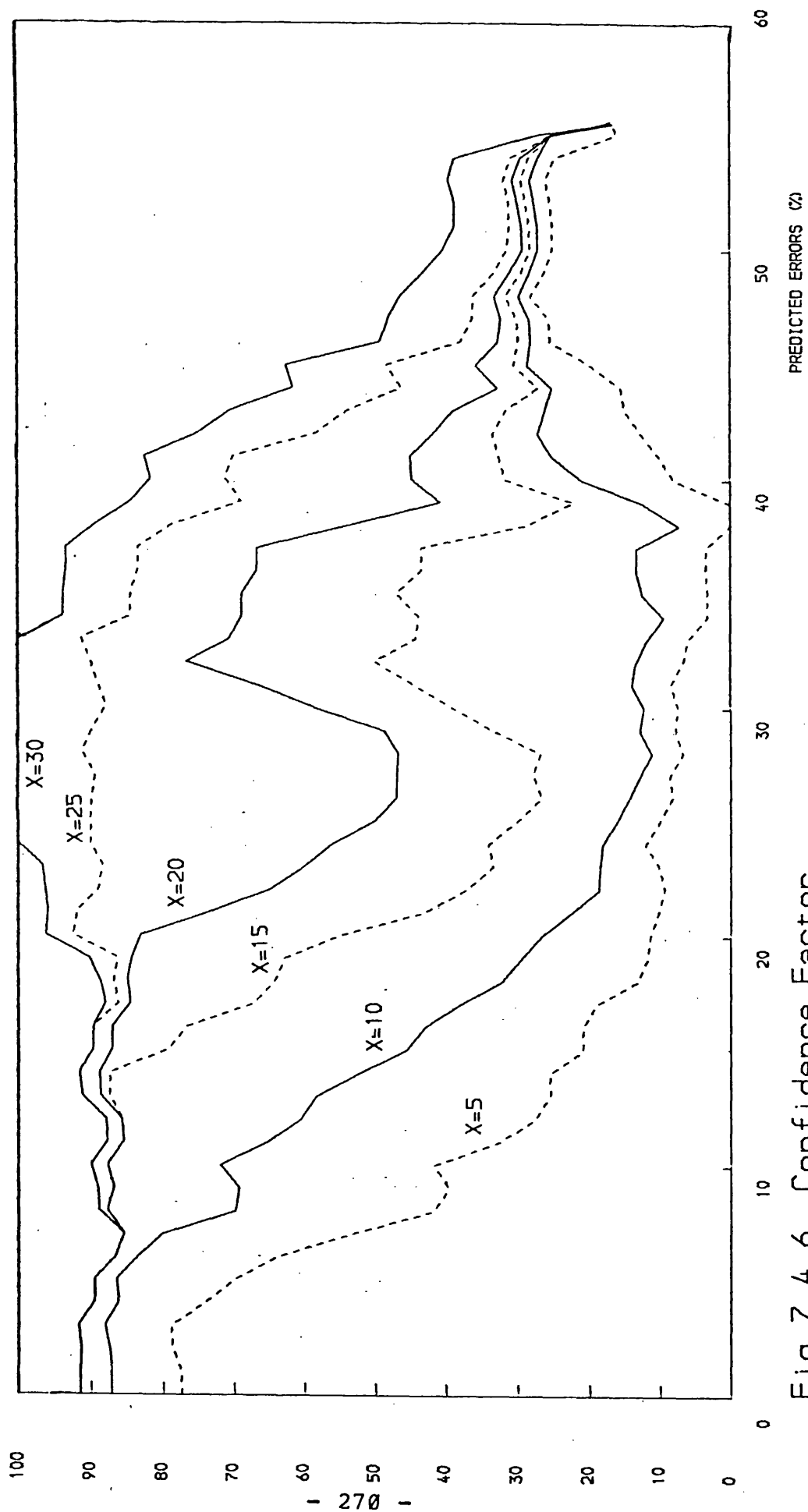


Fig 7.4.6 Confidence Factor

CHAPTER 8

SUMMARY AND CONCLUSIONS

8.1 SUMMARY OF THE SYSTEM DEVELOPED

The original aim of this investigation was to build a system capable of recognising the pulse sounding signal, from which the propagation modes could be identified. From this information a steerable antenna is to be controlled to reduce the effect of multipath interference on an HF data link.

The sounding signal was generated by a small computer which keyed the radio transmitter. After reflection in the ionosphere the signal was received, detected and converted into a digital form. It was then passed to the main computer to be stored for later analysis. The system was tested over a range of propagation paths of various lengths. With the exceptions of the commercial transmitter and receiver, all the equipment was constructed at Leicester.

The correlation between the ionospheric conditions and error rate in data communications was investigated by combining a pseudo random data message with the pulse sounding signal.

Pulse sounding experiments were undertaken over four paths of lengths from 4 to 2300 Km. The active modes were identified by means of the pulse sounding results and a very simple ionospheric model.

Measurements of the error rate in a pseudo random data

message were conducted over the Elgin-Leicester path. It proved possible to establish a correlation between the error rate and the pulse sounding measurements.

8.2 PULSE EXPERIMENT, CONCLUSIONS

The principal objectives of the pulse experiments were :-

- 1) To evaluate the pulse sounding signal with a view to mode detection and antenna steering.
- 2) To provide a low cost ionospheric sounder for paths on which sounding would otherwise be unavailable.

The investigations have shown that the pulse sounding procedure can reliably recognise propagation modes and hence could provide control for a steerable antenna to reduce multipath interference. Mode identification could however only take place within the following limits. The maximum time resolution of the system appears to be approximately 0.5ms between arriving pulses. Thus modes with nearly equal times of flight (eg 1E and 1F on paths longer than 500Km) are not easily resolved. It should however be borne in mind that modes with small differences in arrival times tend to have relatively small angular displacements and so are also difficult to separate with a steerable antenna. Further investigations are necessary to determine which of these factors will eventually limit the overall system performance. The present system can not provide an improvement during in- mode fading where relative time delays and angular separations are too small to be resolved.

For the time resolution required, there was virtually no difference between the predicted time delays calculated from a simple ionospheric model and those obtained by means of a ray tracing program. This lead to the decision to adopt the simpler model, which together with the measured time delays, gave reliable mode estimations.

The major practical limitations of the system are the twin evils of noise and interference. To achieve the best time resolution, a receiver bandwidth of at least 3KHz is required, which under normal circumstances, allows a significant amount of noise to enter the system. The compromise solution was to adopt a bandwidth of 1200Hz which reduced the noise by 50% and degraded the time resolution to about 0.7ms. This bandwidth was adequate for most of the experiments undertaken. It was not however possible to overcome co-channel interference within the 1200Hz pass band and this proved to be one of the system's major operational drawbacks. Under these conditions recourse must be made to predictions, or a new frequency selected.

The pulse sounding system can also be employed as a low cost aid in HF communications. The structure of the multipath propagation can provide an estimate of the expected fading induced error rate for a given data signal by comparing the relative amplitudes of the active modes. The measured relative time delays between modes can provide an indication of the maximum data rate possible in order to avoid multipath fading induced bit errors. Moreover the pulse sounding signal can provide the (S/N) ratio for a given channel upon which error rate estimates can be based. Finally the presence of

unpredicted modes such as sporadic E and Auroral propagation can be indicated to the operator thus enabling more efficient use to be made of propagation conditions for any given time.

8.3 DATA EXPERIMENT, CONCLUSIONS

If the sounding system is to be employed as a communications aid it is important to establish the dependence of the error rate over the link on the mode content as determined from the sounding pulses. An attempt was made to identify the causes of errors in the particular data test sequence employed, so that the error rates could be predicted from observations of the mode content.

In general the error rate increases with the number of modes present, and expected error rates could be predicted from this mode structure. The reliability of these predictions varied with the predicted error rate and the confidence factors discussed in section 7.4 must be applied. The low confidence values sometimes noted are thought to be due to rapid changes in ionospheric conditions between the pulse sounding and the data test sequence. For accurate error predictions the pulse sounding must therefore be closely integrated within the data stream. A possible scheme would involve 10 cycles of sounding every 100 characters, which would provide real time sounding once every 10 seconds, compared with every two minutes during the present study. This improvement in predictions would be at the expense of a 12% reduction in the overall data rate (at 75 baud). Even more accuracy would be gained by interleaving the

transmitted data within the carrier block portion of the pulse sounding signal. This would however involve major alterations to existing communications equipment and can therefore be rejected as impractical.

The majority of errors recorded during the experiment were due to random noise. These could be minimised by reducing the receiver bandwidth but this is detrimental to the pulse sounding. This highlights a major problem encountered when mixing sounding and data transmissions. The optimum available bandwidth for 75 baud data is 3000Hz, whereas for pulse sounding it is at least 12000Hz. For future experiments of this type it would be advantageous to have a variable pass band receiver which could be changed by the control computer to suit the type of signal being monitored at any instant. If equipment limitations make this impossible, a variable threshold level as proposed in section 7.3.2 would go some way to reduce the high percentage of data errors due to random noise caused by a wide receiver pass band.

8.4 FUTURE WORK

A proposed practical implementation of the sounding system together with some suggestions for further work are now described.

8.4.1 Practical Implementation

A block diagram of the proposed operational version of

this project is given in fig 8.4.1. A microcomputer similar to that described in section 4.10 drives a steerable antenna via the antenna control electronics. The system contains two receivers, one connected to the steerable antenna and the other to an omnidirectional antenna. 1200Hz bandwidth detected outputs from both receivers are fed through an analogue to digital converter and on to the control computer. The data output consists of a 300Hz bandwidth detected signal from the steerable antenna receiver. The computer is controlled from a VDU which also displays the system status. Two modes of operation would be available (fig 8.4.2).

Normally the transmitter latitude, longitude and operating frequency would be typed into the computer and the receivers would automatically tune to the correct frequency. The control program would then calculate the transmitter ground range and from that the expected modes and likely arrival angles. The sounding signal from receiver 2 would be examined and the strongest mode identified. The steerable antenna would then be directed to form a beam in the predicted direction together with nulls in the directions of any secondary modes. The sounding signal from receiver 1 would then be compared with that from receiver 2. If the secondary modes are not completely nulled out, the positions of the nulls would be changed slightly in a local search pattern until this is achieved. Finally the main beam position would also be changed in a local search for best (S/N) ratio from receiver 1. The system would then be tuned in and ready to receive data.

If the data signal strength starts to decrease the beam

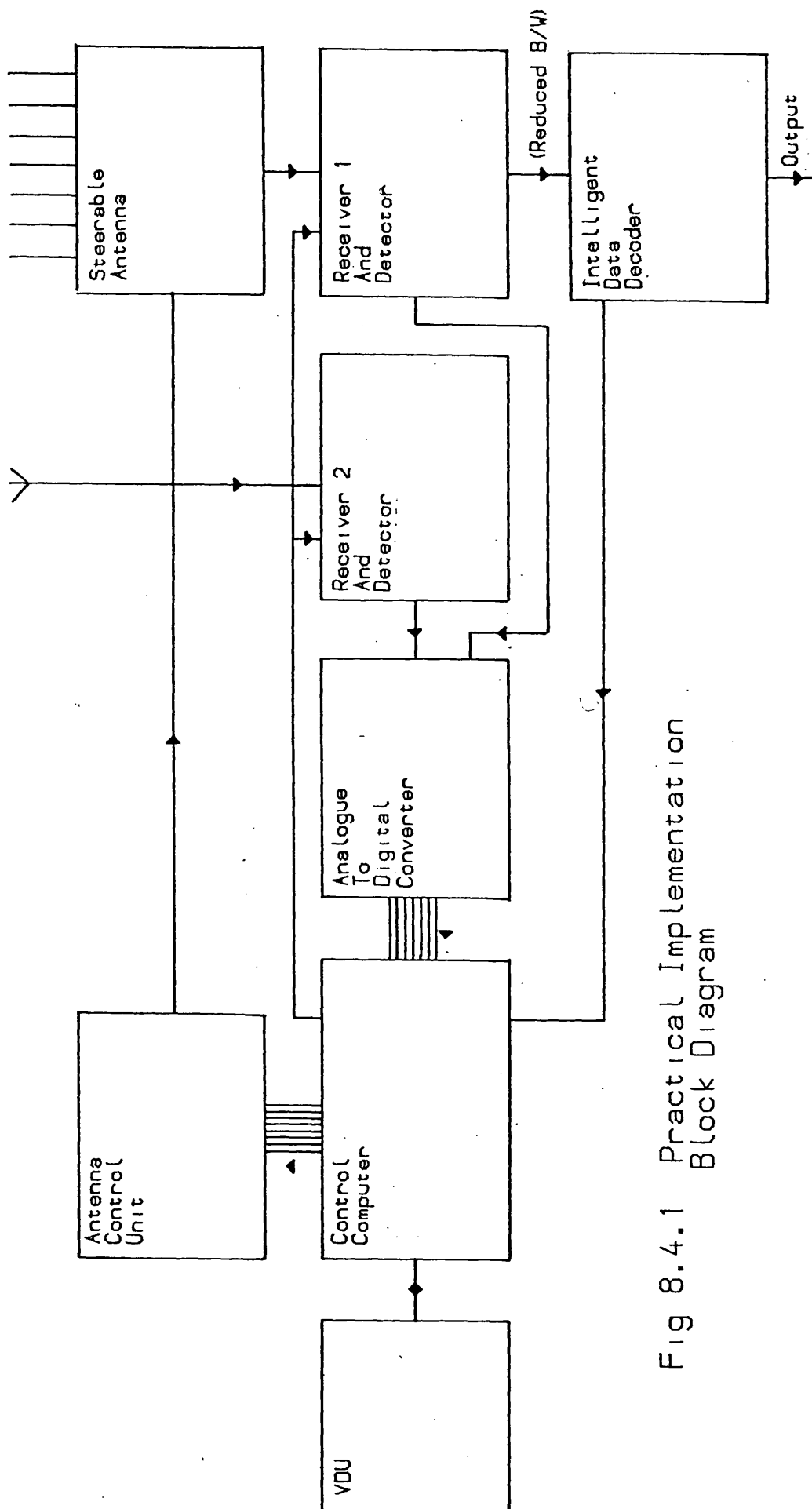


Fig 8.4.1 Practical Implementation
Block Diagram

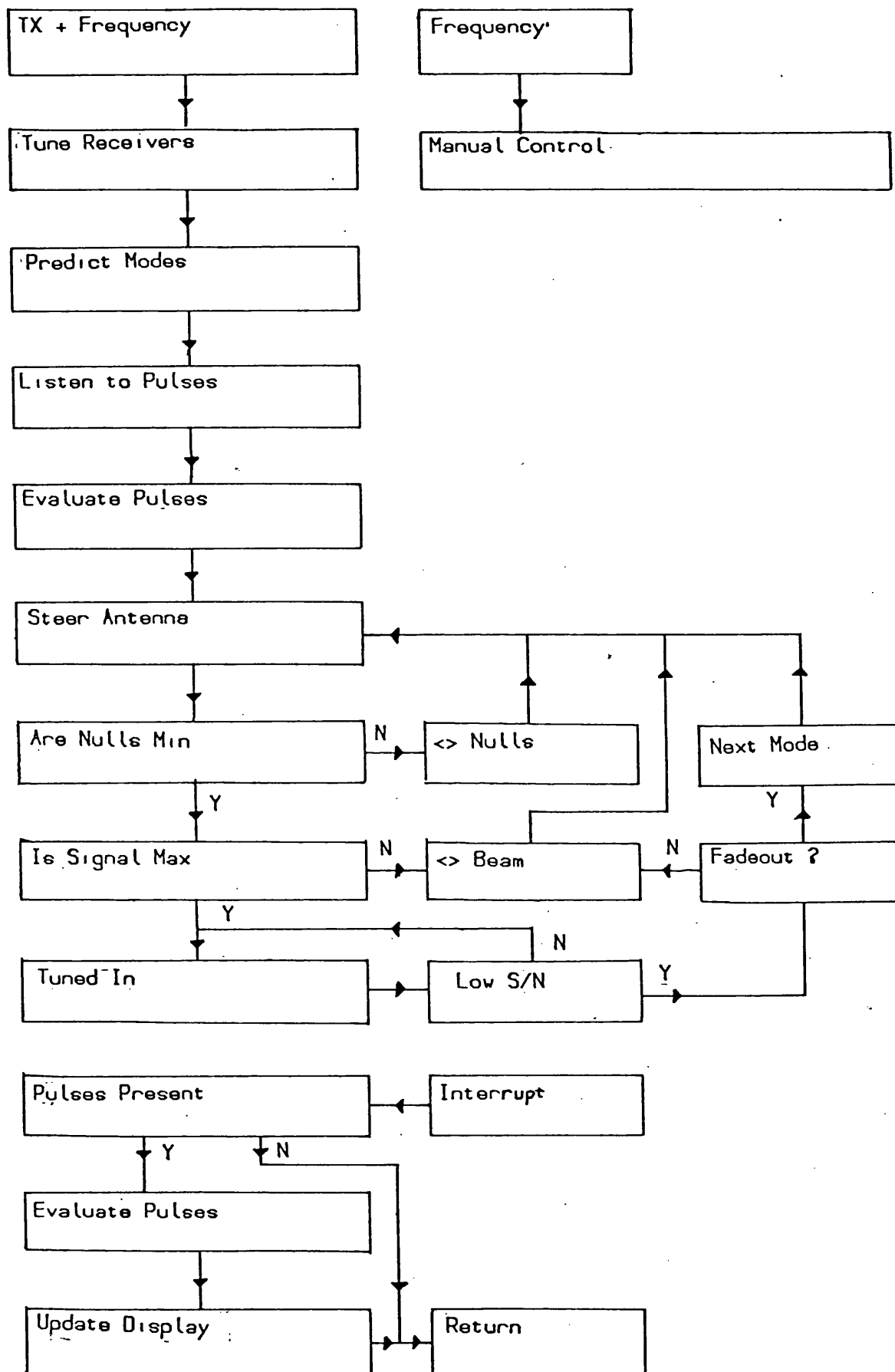


Fig 8.4.2 Practical Implementation

direction will be slightly changed in a search for maximum signal, hence tracking the incoming path. If the main mode fades out completely but a signal is still visible from receiver 2, the main beam will be redefined as the larger of the secondary modes (detected during the most recent period of pulse sounding), the antenna redirected and searched as before. The sounding signal would be repeated once every 30 seconds for about 5 seconds allowing the program to update its picture of the ionosphere. The most recent sounding information would be displayed on the VDU.

The data decoder is a separate unit allowing greater speed and freeing the control computer to maintain the optimum beam and null headings. Also note the input bandwidth of the data decoder is reduced (to 300Hz for 75 baud data).

An alternative mode of operation employs greater manual control. As the sounding frequency is monitored the antenna beam can be swept in elevation angle to provide a signal amplitude against arrival angle plot on the VDU. The system could then be instructed to use any particular mode specified by the operator. Finally if the signal from receiver 1 appears to be strong, reliable and single moded, an increase in the data rate could be requested to take advantage of the improved conditions.

8.4.2 Develop Predictions

Due to equipment limitations the only modulation method employed during this project was on-off keying. Further work

should expand the error rate predictions to FSK and PSK modulation schemes. These require different detection techniques and data errors may arise from different causes than in the present investigation. A new error prediction algorithm would be required.

8.4.3 Pseudo Error

The pseudo error, as described in section 2.2.9, should be investigated to enable the computer to determine how close to the decision threshold the system is operating. It would be particularly useful to have this information available as the pseudo error is more sensitive to ionospheric conditions than the actual error rate. Any control decision, such as antenna steering, could be based on this parameter thus minimising the loss of actual data.

8.4.4 Range Finding

As the transmitter is moved away from the receiver, the time taken for the signal to travel increases for all propagation modes. The propagation times for each mode do not change by the same amount for a given range change and therefore a unique time delay exists between the returned pulses for a given transmitter- receiver distance and ionospheric height. By measuring the various time delays and assuming a value for the reflection height, the range between the transmitter and the receiver can be estimated. To obtain an

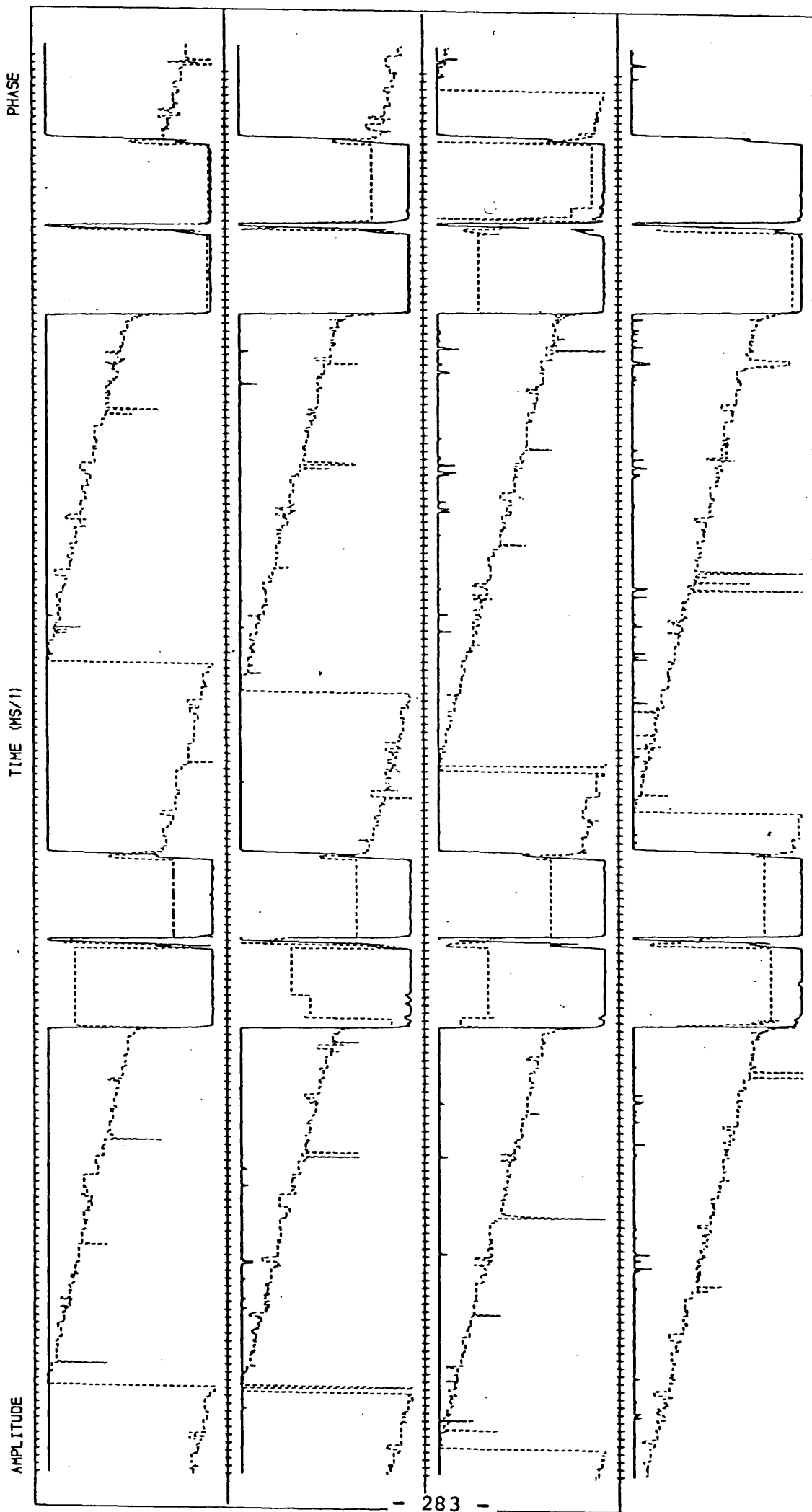
acceptable distance resolution the ionospheric height would have to be measured from ionograms and the sampling rate of the processor increased to its maximum of about 100KHz to provide more accurate pulse recognition. It is appreciated that this method is not capable of very high resolution but could still be of considerable value where no other range finding system is available.

8.4.5 Phase

During the experiments detailed in this thesis only the amplitude of the sounding signal was investigated. However the phase of the sounding pulses also contains valuable information regarding the propagation conditions. Measurement of the phase across a single pulse echo promises to provide a suitable method of distinguishing two modes with very similar times of flight. Although these modes could not be resolved with the steerable antenna their presence would indicate the likelihood of fading and therefore the desirability of steering towards a different mode if possible.

A phase measuring unit was designed, built and connected to the control computer during the course of the current investigation (section 4.7). This functioned correctly during the large blocks of carrier and was a useful aid in tuning the radio receiver. However, this particular detector was badly affected by noise superimposed on the sounding pulses and failed to produce any worthwhile information regarding the pulses. The project computer was only just fast enough to

record both phase and amplitude information simultaneously and this led to unreliability, which could be overcome by means of a faster computer. An example of one of the more satisfactory phase and amplitude plots is presented in fig 8.4.3. The beat in frequency between the received signal and the local standard is clearly evident. The information from the pulses themselves is ambiguous since it includes the phase- amplitude dependence of the detector. This factor would be corrected for during the calibration process. The phase measurements represent the most interesting area for future development of the pulse sounding system.



G9BLD OADBY 15.39 GMT 10.06.81 4.792500 MHZ (1)

Fig 8.4.3 Phase and Amplitude Plot

BIBLIOGRAPHY

- AGY, V.: (1959) National Bureau of Standards, 63D, 2.
- AMES, J.W. & Egan, R.D.: (1967) I.E.E.E. Trans. Ant. Prop.,
AP15, 3, p382.
- AMES, J.W.: (1969) I.E.E.E. Trans. Comm. Tech., COM17, 4, p438.
- APPELTON, E.V. & Barnett, M.A.F.: (1925) Nature, 115, p333.
- ARRENONDO, G.A. & Chriss, W.H.: (1973) I.E.E.E. Trans. Veh.
Tech., VT22, p241.
- BAILEY, D.K.: (1959) I.R.E. Trans. Ant. Prop., AP7, p397.
- BARCLAY, L.W.: (1970) Marconi Review, p61.
- BARCLAY, L.W.: (1973) Point to Point Comm., 17, 1, p25.
- BARKER, R.H.: (1953) Comm. Theory Sym, Butterworth, London,
p273.
- BARROW, B.B.: (1963) I.E.E.E. Comm. Sys., CS11, p73.
- BATES, H.F., Albee, P.R. & Hunsucker, R.D.: (1966) J. Geophys.
Res., 71, 5, p1413.
- BAULCH, R.N.E. & Butcher, E.C.: (1978) J. Atmos. Terr. Phys.,
40, p1235.
- BAYLEY, D. & Ralphs, J.D.: (1972) Proc. I.E.E., 119, 9, p1229.
- BECK, D. & Betts, J.A.: (1965) Elec. Eng., p74.
- BELLO, P.A.: (1965) I.E.E.E. Trans. Comm. Tech., COM13, 3, p320.
- BETTS, J.A. & Darnell, M.: (1975) Agard Conf., CP173, p18-1.
- BEYNON, W.J.G.: (1948) Wireless Eng., 25, p322.
- BIBL, K. & Reinisch, B.W.: (1978) Rad. Sci., 13, 3, p519.
- BOLTON, E.: (1971) Rev. Sci. Inst., 42, 5, p574.
- BOND, F.E.: (1957) Proc. I.R.E., 45, p636.

- BOOKER, H.G.: (1975) Rad. Sci., 10, p665.
- BOWMAN, G.G.: (1969) Planetary and Space Sci., 17, p777.
- BRADLEY, P.A.: (1975) Agard Conf., CP173, p11-1.
- BRADLEY, P.A. & Lockwood, M.: (1981) Agard Conf., CP295, p32-1.
- BRAYER, K. & Cardinale, O.: (1967) I.E.E.E. Trans. Comm. Tech.,
COM15, 3, p371.
- BRAYER, K.: (1971) I.E.E.E. Trans. Comm. Tech., COM19, p781.
- BREIT, G. & Tuve, M.A.: (1926) Phys. Rev., 28, p554.
- BRUCE, E.: (1931) Proc. I.R.E., 19, 8, p1406.
- BUSSGANG, J.J. Goldberg, B. & Getchell, E.: (1974)
Telecommunications, 8, 1, p17.
- CARLSON, A.B.: (1968) Comm. Sys., McGraw- Hill, Kogakasha, p397.
- C.C.I.R. : (1974) XIIIth Plenary Assembly, Geneva, 3, rep 549.
- C.I.R.A. : (1965) Cospar International Ref. Atmos., North-
Holland Pub., Amsterdam.
- CHAPMAN, J.H. Davies, K. & Littlewood, C.A.: (1955) Can. J. of
Phys., 33, p713.
- CHASE, D.: (1972) I.E.E.E. Trans. Info. Theory, IT18, p170.
- CLARKE, R.H. & Tibble, D.V.: (1978) Proc. I.E.E.E., 125, 1, p17.
- COLL, D.C. & Storey, J.R.: (1964) Rad. Sci. J. of Res. NBS/USNC
- URSI, 68D, 10, p1155.
- COLL, D.C.: (1968) Ionospheric Rad. Comm., Plenum, New York,
p341.
- COTTRELL, R.A.: (1979) I.E.E. Colloquium Dig., 1979/48, p57.
- COX, J.W. & Davies, K.: (1955) Wireless Eng., 2, p35.
- DAMBOLT, T.: (1979) Agard Conf., CP263, p7-1.

- DARNELL, M.: (1975a) Agard Conf., CP173, p16-1.
- DARNELL, M.: (1975b) Agard Conf., CP173, p23-1.
- DARNELL, M.: (1979a) N.A.T.O. Conf. Comm. Sys. and Random Process Theory, Darlington, p891.
- DARNELL, M.: (1979b) N.A.T.O. Conf. Comm. Sys. and Random Process Theory, Darlington, p425.
- DARNELL, M.: (1979c) I.E.E. Colloquium Dig., 1979/48, p50.
- DARNELL, M.: (1981) I.E.E. Conf. Pub., CP195(2), p254.
- DAVIES, K.: (1965) Ionospheric Rad. Prop., N.B.S monograph, 80.
- DAVIES, K.: (1981) Rad. Sci., 16, 6, p1407.
- DEVLIN, J.C. Dyson, P.L. & Hammer, P.R.: (1977) Rad. Sci., 12, 5, p767.
- DIEMINGER, W.: (1968) Radio Wave Propagation, Agard Summer School, Leicester, Ref 3.
- DOELZ, M.L., Heald, E.T. & Martin, D.L.: (1957) Proc. I.R.E., 45, p656.
- DOYLE, D.J. Ducharme, E.D. & Jull, G.W.: (1960) I.R.E. Trans. Ant. Prop., AP8, p449.
- DOWNING, A.M.: (1979) Rad. Sci., 14, 5, p863.
- DRIPPS, J.H. & Rosie, A.M.: (1979) I.E.E. Colloquium Dig., 1979/48, p8.
- EGAN, R.D. & Pratt, D.S.: (1963) Granger Associates, Palo Alto, California.
- EVANS, R.E. & Jones, T.B.: (1971) J. Atmos. Terr. Phys., 33, p627
- FARMER, F.T. & Ratcliffe, J.A.: (1936) Proc. Phys. Soc., 48, p839.

- FARRELL, P.G. & Monday, E.: (1979) I.E.E. Colloquium Dig.,
1979/48, p102.
- FARRELL, P.G.: (1979) N.A.T.O. Conf. Comm. Sys. and Random
Process Theory, Darlington, p181.
- FELDMAN, C.B.: (1939) Proc. I.R.E., 27, 10, p635.
- FENWICK, R.B. & Barry, G.H.: (1967) Conf. Ground Based Rad. Wave
Studies of the Lower Ionosphere, Ottawa, p532.
- FENWICK, R.B. & Woodhouse, T.J.: (1979) Agard Conf., CP263,
p5-1.
- FENWICK, R.C. & Villard, O.G.: (1960) J. Geophys. Res., 65, 10,
p3249.
- FILTER, J.H.J. Arazi, B. & Thomson, R.G.W.: (1978) I.E.E.E.
Trans. Comm., COM26, p913.
- FISCHER, W.H.: (1965) J. Atmos. Terr. Phys., 27, p475.
- FRICKER, R.: (1981) I.E.E. Conf., CP195(1), p237.
- FRIIS, H.T. Feldman, C.B. & Sharpless, W.M.S.: (1934) Proc.
I.R.E., 22, 1, p47.
- FRIIS, H.T. & Feldman, C.B.: (1937) Proc. I.R.E., 25, p841.
- FRITCHMAN, B.D. & Leonard, J.F.: (1965) I.E.E. Trans. Comm.
Tech., 13, p233.
- GABRIEL, W.F.: (1976) Proc. I.E.E.E., 76, p239.
- GEORGE, P.L. & Bradley, P.A.: (1973) Proc. I.E.E., 120, 11,
p1355.
- GETHING, P.J.D.: (1969) Proc. I.E.E., 116, 2, p185.
- GOLDBERG, B.: (1961) I.R.E. Trans. Comm. Sys., CS9, p21.
- GOLDBERG, B. Heyd, R.L. & Pochmerski, D.: (1965) I.E.E.E. 1st
Annual Conv. (Conf. Rep.), Boulder, Colorado, p619.
- GOLDBERG, B.: (1966) I.E.E.E. Trans. Comm., COM14, 6, p767.

- GOODING, D.J.: (1968) I.E.E.E. Trans. Comm. Tech. COM16, 3, p380.
- GOODMAN, R.M.F. & Farrell, P.G.: (1975) Proc. I.E.E., 122, 2, p113.
- GOODMAN, R.M.F. Green, A.D. & Winfield, A.F.T.: (1979) I.E.E. Colloquium Dig., 1979/48, p86.
- GOTT, G.F. & Stainforth, M.J.D.: (1978) Proc. I.E.E., 25, 11, p1208.
- GOTT, G.F. & Dutta, S.: (1979) I.E.E. Colloquium Dig., 1979/48, p110.
- JONES, J.J.: (1968) I.E.E.E. Trans. Comm., COM16, 6, p808.
- JONES, T.B. Spracklen, C.T. & Stewart, C.P.: (1978) Agard Conf., CP238, p17-1.
- JULL, G.W.: (1962) Proc. I.R.E., 50, 7, p1676.
- JULL, G.W.: (1967) Ionospheric Radio Communications, Plenum, New York, p225.
- HATTON, W.L.: (1961) I.R.E. Trans. Comm. Sys., CS9, 3, p275.
- HATTON, W.L.: (1968) Ionospheric Radio Communications, Plenum, New York, p209.
- HEAVISIDE, O.: (1902) Encyclopedia Britannica, 10th Ed, 33, p215.
- H.M.S.O.: (1938) The Admiralty Handbook of Wireless Telegraphy, para R54.
- HUMPHREY, J.A.: (1979) I.E.E. colloquium Dig., 1979/48, p68.
- HUNSUCKER, R.D. & Bates, H.F.: (1969) Rad. Sci., 4, 4, p347.
- INSTON, H.H.: (1969) Proc. I.E.E., 116, 11, p1789.
- KENNELLY, A.E.: (1902) Elec. World & Eng., 39, p473.
- KOEHLER, J.A.: (1976) Monitor Proc. I.R.E.E. Aust., 8, p253.

- KNUDTZON, N.H.: (1968) Ionospheric Radio Communications, Plenum,
New York, p384.
- LAW, H.B. Lee, F.J. Loser, R.C. & Levett, F.A.W.: (1957) Proc.
I.E.E. , B, p117.
- LEVINE, P.H. Rose, R.B. & Martin, J.N.: (1978) I.E.E. Conf.,
CP169(2), p161.
- MALAGA, A. & McIntosh, R.E.: (1979) Trans. Ant. Prop., AP27, 4,
p508.
- MARCONI, G.: (1901) The Times, Dec 21.
- MARTYN, D.F.: (1935) Proc. Phys. Soc., 47, p323.
- MASLIN, N.M.: (1979) Agard Conf., CP263, p6-1.
- MATELY, W. & Bywater, R.E.H.: (1977) The Rad. and Elec. Eng.,
47, 7, p305.
- MORGAN, D.R.: (1978) I.E.E.E. Trans. Comm., COM26, 9, p1380.
- MULDREW, D.B.: (1965) J. Geophys. Res., 70, 11, p2635.
- PALMER, L.C.: (1974) Modelling and Simulation, 5, pt2, p881.
- PENNINGTON, J.: (1979) I.E.E. Colloquium Dig., 1979/48, p79.
- PETERSON, A.M. Egam, R.D. & Pratt, D.S.: (1959) Proc. I.R.E.,
47, p300.
- PICKERING, L.W.: (1975) I.E.E.E. Trans. Comm., COM23, p526.
- PINNOCK, M.: (1981) To be Published
- PRICE, R. & Green, P.E.: (1958) Proc. I.R.E., 46, p555.
- PROBST, S.E.: (1968) Ionospheric Radio Communication, Plenum,
New York, p370.
- RALPHS, J.D.: (1971) Proc. I.E.E., 118, 3, p409.
- RALPHS, J.D. & Sladen, F.M.E.: (1976) Rad. and Elec. Eng., **,
p579.
- RAWER, K.: (1975) Rad. Sci., 10, p669.

REES, R.L.D. & Owen-Jones, E.S.: (1979) J. Atmos. Terr. Phys.,
39, 4, p475.

RIDOUT, P.N. & Wheeler, L.K.: (1963) Proc. I.E.E., 110, 8,
 p1402.

ROBIN, H.K. Bayley, D. Murray, T.L. & Ralphs, J.D.: (1963) Proc.
 I.R.E., 110, 9, p1554.

RUSH, C.M.: (1981) I.E.E. Conf., CP195(2), p229.

SALAMAN, R.K.: (1962) I.R.E. Trans. Comm. Sys., CS10, p220.

SHEARMAN, E.D.R. & Martin, L.T.J.: (1956) Wireless Eng.,
 p190.

SILBERSTEIN, R.: (1954) I.R.E. Trans. Ant. Prop., AP2, p56.

SLOGGETT, D.R.: (1979) I.E.E. Colloquium Dig., 1979/48, p74.

STANLEY, G.M.: (1966) J. Geophys. Res., 71, 21, p5067.

STEVENS, E.E.: (1968) Ionospheric Radio Communication, Plenum,
 New York, p359.

STRASSMAN, A.J.: (1961) I.R.E. Trans. Comm. Sys., CS9, p383.

STRUSSYNSKI, W. & Gott, G.F.: (1970) I.E.E.E. Conf., CP64, p74.

SULZER, P.G.: (1955) J. Geophys. Res., 60, 4, p409.

SUSANS, D.E.: (1979) I.E.E. Colloquium Dig., 1979/48, p116.

THRANE, E.V. & Bradley, P.A.: (1981) I.E.E. Conf., CP195(2),
 p258.

TVETEN, L.H. & Hunsucker, R.D.: (1969) Proc. I.E.E.E., 57, 4,
 p487.

VAN ZANDT, T.E. & Knecht, R.W.: (1964) Space Phys., John Wiley &
 Sons, New York.

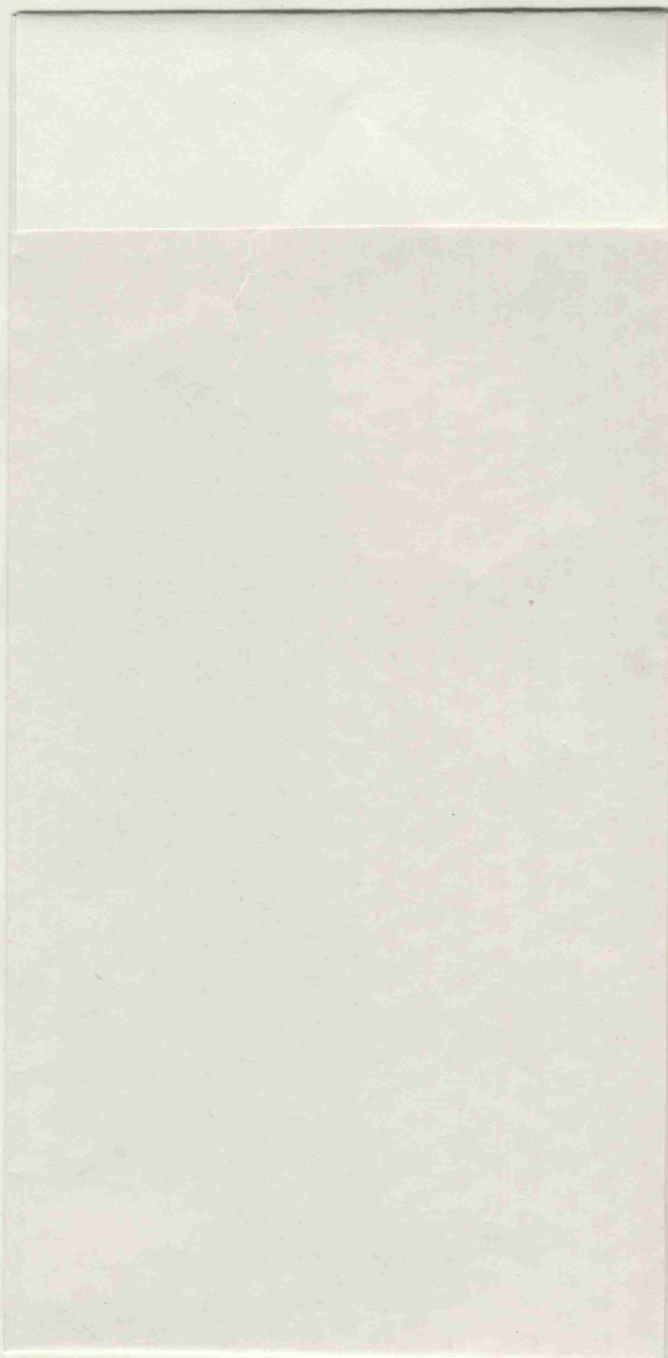
VOELCKER, H.B.: (1960) Proc. I.E.E. (B), 107, p31.

WAGNER, R.A. & Pike, C.P.: (1971) Agard Conf., CP97, p4-1.



MICROFICHE

APPENDIX I



APPENDIX II

APPENDIX III

APPENDIX IV

APPENDIX V

AN IONOSPHERIC MODE DETECTION SOUNDER FOR
HF DATA COMMUNICATIONS

P.L. HAYHURST

ABSTRACT

A major problem experienced in HF data communications is that of multipath interference. Interference between the components, of a transmitted signal, arriving at the receiver over different propagation paths can produce serious errors in data transmission.

A pulse sounding technique has been developed to resolve the interfering modes in the time domain. This signal consists of a 0.7ms pulse of radio wave energy sent within a 20ms break in transmission, repeated every 90ms. The sounding signal is generated by a small computer which keys the radio transmitter. After reflection in the ionosphere the signal was received and digitised. A second computer then analyses the digital record to discover the amplitude and time of arrival of any sounding pulses present. The results are then compared with predictions to identify the active modes.

Pulse sounding experiments were undertaken over four paths of lengths from 4 to 2156km. E, Es, F, 2F, 3F and auroral propagation paths were successfully recognised. This information could be used to advise on the likelihood of interference fading or more positively to control an elevation steerable antenna to adaptively cancel out this unwanted effect.

To investigate the relationship between ionospheric conditions and the error rate in data communications a pseudo random test data message was transmitted with the pulse sounding. Measurements in the error rate in the message were conducted over the 578km path from Elgin to Leicester. It proved possible to establish an approximate correlation between the recorded data errors and the ionospheric conditions derived from the pulse sounding. This allows error rates to be estimated from the sounding results.